



HAL
open science

Manganese oxides for degradation of organic contaminants in water

Daqing Jia

► **To cite this version:**

Daqing Jia. Manganese oxides for degradation of organic contaminants in water. Analytical chemistry. Université Clermont Auvergne, 2021. English. NNT : 2021UCFAC071 . tel-03652331

HAL Id: tel-03652331

<https://theses.hal.science/tel-03652331v1>

Submitted on 26 Apr 2022

HAL is a multi-disciplinary open access archive for the deposit and dissemination of scientific research documents, whether they are published or not. The documents may come from teaching and research institutions in France or abroad, or from public or private research centers.

L'archive ouverte pluridisciplinaire **HAL**, est destinée au dépôt et à la diffusion de documents scientifiques de niveau recherche, publiés ou non, émanant des établissements d'enseignement et de recherche français ou étrangers, des laboratoires publics ou privés.

ED SF n° d'ordre :

UNIVERSITE CLERMONT AUVERGNE
ECOLE DOCTORALE DES SCIENCES FONDAMENTALES

THESE

Présentée pour obtenir le grade de

DOCTEUR D'UNIVERSITE

Spécialité : Chimie théorique, physique, analytique

Par **Daqing JIA**

**MANGANESE OXIDES FOR DEGRADATION OF ORGANIC
CONTAMINANTS IN WATER**

Soutenue le « 26/11/2021 », devant la commission d'examen suivante :

Pr. Sonia GIL, Université Claude Bernard Lyon 1, France

Pr. María-José LOPEZ-MUNOZ, Université de Rey Juan Carlos, Espagne

Pr. Khalil HANNA, Ecole Nationale Supérieure de Chimie de Rennes, France

Directeurs de thèse :

Pr. Marcello BRIGANTE, Université Clermont Auvergne, France

DR. Gilles MAILHOT, CNRS, Université Clermont Auvergne, France

Table of contents

Introduction	1
Chapter I Bibliography	7
1.1 Advanced oxidation processes (AOPs)	8
1.1.1 General description of AOPs.....	8
1.1.2 The commonly used oxidants in AOPs	9
1.1.3 Transition metals-based AOPs	11
1.2 Manganese oxides	17
1.2.1 Oxidation states	17
1.2.2 Structures.....	19
1.3 Trivalent manganese oxides activating sulfur radical-AOPs	23
1.3.1 Effect of structure on the reactivity of Mn(III) (oxyhydr)oxides.....	24
1.3.2 Activation of PMS by Mn(III) (oxyhydr)oxides	28
1.3.3 Activation of PDS by Mn(III) (oxyhydr)oxides	35
1.3.4 Influence factors for Mn(III) (oxyhydr)oxides reactivity	41
1.4 Manganese dioxide activated AOPs	45
1.4.1 Activation of H ₂ O ₂ by MnO ₂	45
1.4.2 Activation of PMS and PDS by MnO ₂	48
1.5 Emerging pollutants	50
1.5.1 Source and harm of BPA, E2 and EE2	52
1.5.2 Source and harm of CAF.....	54
1.5.3 Treatment technologies for EDCs and CAF.....	56
Reference.....	57

Chapter II Materials and Methods	88
2.1 Chemicals and instruments.....	89
2.1.1 Chemicals.....	89
2.1.2 Instruments.....	91
2.2 Preparation of materials and solutions.....	91
2.2.1 Synthesis of acid birnessite.....	91
2.2.2 Synthesis of Mn(III) rich birnessite.....	92
2.2.3 Synthesis of manganite.....	92
2.2.4 Sewage treatment plant water collection.....	92
2.3 Reaction process.....	93
2.3.1 Acid birnessite reduction by H ₂ O ₂	93
2.3.2 PDS and PMS activation by Mn ₂ O ₃	93
2.3.3 PMS activation by γ -MnOOH.....	94
2.4 Analysis methods.....	94
2.4.1 Determination of target pollutants concentration.....	94
2.4.2 H ₂ O ₂ quantification.....	97
2.4.3 Determination of PDS and PMS concentration.....	98
2.4.4 Identification of caffeine byproducts.....	99
2.4.5 Identification of hydroxyl radicals.....	99
2.4.6 Identification of reactive oxygen species.....	99
2.4.7 Determination of Mn ²⁺ concentration.....	100
2.4.8 Determination of Mn average oxidation state.....	101
2.4.9 Characterization of manganese oxides.....	102
2.4.10 Determination of total organic carbon.....	103

Reference.....	105
Chapter III Impacts of environmental levels of hydrogen peroxide and oxyanions on the redox activity of MnO₂ particles	107
Motivation	108
1. Introduction	109
2. Materials and Methods	111
2.1. Chemicals	111
2.2. Synthesis and characterization of acid birnessite	111
2.3. Kinetics experiments and analyses.....	111
3. Results and Discussion.....	113
3.1. Effect of H ₂ O ₂ on the oxidative ability of birnessite.....	113
3.2. Effects of Mn(II) on the removal capacity of MnO ₂	119
3.3. Synergistic effects of anions and H ₂ O ₂ on the oxidative activity of MnO ₂	122
4. Conclusions	125
Acknowledgments	125
Reference.....	126
Supplementary Materials.....	134
Chapter IV Trivalent manganese oxides activation of peroxydisulfate and peroxymonosulfate for organic pollutants degradation in water	143
Motivation	144
Part 1: Caffeine degradation using peroxydisulfate and peroxymonosulfate in the presence of Mn₂O₃. Efficiency, reactive species formation and application in sewage treatment plant water	145
1. Introduction	146

2. Materials and Methods	148
2.1. Chemicals	148
2.2. Catalyst characterization	148
2.3. Experimental procedures	148
2.4. Chemical analysis and kinetics	149
3. Results and discussion.....	151
3.1. Reactivity of Mn ₂ O ₃ with PS and PMS.....	151
3.2. Effect of pH.....	158
3.3. Effects of Mn ₂ O ₃ and oxidant dosages.....	159
3.4. CAF degradation pathway and mineralization.....	161
3.5. Degradation efficiency in sewage treatment plant waters (STPW)	163
4. Conclusion.....	165
Acknowledgments	165
Reference.....	166
Supplementary Materials.....	173
Part 2: Efficient removal of estrogenic compounds in water by Mn^{III}-activated peroxymonosulfate: mechanisms and application in sewage treatment plant water.....	191
1. Introduction	192
2. Material and Methods.....	193
2.1. Chemicals and reagents	193
2.2. γ -MnOOH synthesis and characterization.....	194
2.3. Real water matrix	195
2.4. Experimental procedure	195
2.5. Analytical methods	195

3. Results and discussion.....	197
3.1. Effect of γ -MnOOH and PMS dosage.....	197
3.2. Activation pathway and reactive species formation.....	200
3.3. Degradation and mineralization of BPA, E2 and EE2	205
3.4. Effect of inorganic ions	207
3.5. Efficiency in the real water matrix	210
4. Conclusion.....	211
Acknowledgements	211
Reference.....	211
Supplementary Material	217
Chapter V General conclusion and outlook.....	226

Introduction

With the increase of urbanization, industrialization, and the number of people on Earth, a large number of chemical products are consumed and discharged, leading to the occurrence and increase of emerging pollutants (EPs) in various water compartments [1]. The concentration of EPs detected in waters ranges from ng/L to $\mu\text{g/L}$ [2]. The presence of EPs in the environment poses a threat to the safety of the ecosystem and the health of human beings [3,4]. However, the conventional wastewater treatment technologies (such as adsorption, precipitation, and filtration) have shown low efficiency on the removal of EPs [5]. EPs can enter the environment repeatedly through the discharging of the sewage treatment plants (STP), leading to the bioaccumulation of EPs in the various organism and water compartments [6]. Advanced oxidation processes (AOPs) have attracted much attention due to their high efficiency in the degradation of recalcitrant pollutants. AOPs are able to mineralize, through the generation of reactive radicals including sulfate and hydroxyl radicals, various organic pollutants [7].

The generation of reactive species in AOPs can be achieved through the activation of radical precursors (such as hydrogen peroxide (H_2O_2), peroxymonosulfate (PMS, HSO_5^-), and peroxydisulfate (PDS, $\text{S}_2\text{O}_8^{2-}$)) by various techniques including ultraviolet light (UV), heat, electrochemistry, ultra-sonication, and transition metals [8]. Among these methods, the transition metals-based AOPs have been widely used in the treatment of wastewater due to the advantage of simple implementation. Fenton reaction is one of the typical transition metals-based AOPs, which uses the Fe^{2+} to activate H_2O_2 for the generation of hydroxyl radicals. The latter is an high oxidant species and is able to degrade organic pollutants [9]. However, the strict reaction conditions of the Fenton reaction (such as low pH) limited its application in practical water treatment [10]. In comparison, manganese (Mn) has shown a good reactivity in transition metal-based AOPs due to its various valence states and wider pH stability [11].

In the natural environment, manganese species mainly exist in the oxidation states of Mn(II), Mn(III), and Mn(IV). The activation of radical precursors by various manganese oxides for the removal of organic pollutants have been widely reported. For example, Watts et al. reported the

degradation of carbon tetrachloride in the β -MnO₂ activated H₂O₂ system through the generation of reactively transient species [12]. Zhu et al. employed the β -MnO₂ nanorods to activate PDS for the removal of phenol. Efficient degradation of phenol was achieved in β -MnO₂/PDS system through the generation of singlet oxygen (¹O₂) [13]. Zhou et al. indicated the higher catalytic property of α -MnO₂ than δ -MnO₂ in PMS activation for 4-nitrophenol degradation because α -MnO₂ owns more active sites, larger Brunauer-Emmett-Teller (BET) area, faster electron transfer rate, and better adsorption performance [14]. Moreover, it was reported that the structure of manganese oxides and the contents of Mn(III) on the surface of manganese oxides play a critical role in the oxidative and catalytic reactivity of manganese oxides. For instance, Huang et al. investigated the activation of PMS by MnO₂ with different crystal phases (i.e. α -, β -, γ -, and δ -MnO₂) [15]. The results demonstrated the important role of crystalline structure and Mn(III) contents on the catalytic reactivity of MnO₂. Saputra et al. investigated the effect of Mn oxidation states (such as MnO, Mn₂O₃, Mn₃O₄, and MnO₂) on the activation of PMS for phenol degradation [16]. The results showed that Mn₂O₃ has the highest ability on PMS activation among these manganese oxides. He et al. also demonstrated the efficient degradation of 2,4-dichlorophenol in the Mn^{III}OOH activated PMS system [17].

Although the good activity of Mn(III/IV) oxides for radical precursors activation has been demonstrated, the underlying mechanisms of activation and generation of reactive species are not fully understood. Moreover, the previous studies focused on the elimination efficiency of pollutants, and overlooked the influence of oxidants (for example H₂O₂) on the oxidative activity of Mn(III/IV) oxides. Furthermore, most of the previous literature were conducted in the pure water. Indeed, the degradation efficiency of organic pollutants by manganese oxides-based AOPs in the real wastewaters need to be evaluated. Therefore, the purpose of this study was to 1) investigate the impacts of H₂O₂ and oxyanions on the reactivity of acid birnessite. 2) investigate the activation mechanism of various radical precursors by Mn₂O₃ at near-neutral pH solution. 3) investigate the reactivity of manganite (γ -MnOOH) in PMS activation and evaluate the efficiency of manganite/PMS system in the removal of multi-pollutants in the real wastewater.

In this work, different organic pollutants such as bisphenol A (BPA), caffeine (CAF), 17 β -estradiol (E2), and 17 α -ethinylestradiol (EE2) were used as the model pollutants to investigate the activation mechanism of various radical precursors by manganese (III/IV) oxides. The main experimental contents were summarized as follows:

In the first part of our work, the impacts of environmental levels of hydrogen peroxide and oxyanions on the redox activity of MnO₂ particles have been investigated. Specifically, the effect of different parameters such as the H₂O₂ concentration, pH values, Mn(II) contents, and oxyanion types (such as silicate, nitrate, and phosphate) on the reactivity of acid birnessite was evaluated.

In the second part of this manuscript, the degradation of caffeine by Mn₂O₃ activated peroxymonosulfate or peroxydisulfate system is described. In this study, the effects of solution pH, Mn₂O₃ dosages, PDS and PMS concentrations on the reactivity of Mn₂O₃ were reported. The primary reactive species generated in Mn₂O₃ activated PDS or PMS system were identified using chemical scavenging experiments and electron paramagnetic resonance (EPR) spectroscopy. The mineralization efficiency of Mn₂O₃ + PDS or PMS system was monitored by measuring the total organic carbon (TOC) decrease as a function of reaction time. Moreover, the performance of Mn₂O₃ activated PDS or PMS to degrade CAF in the real conditions was evaluated using sewage treatment plant (STP) water.

In the third part of our work, the removal of three estrogenic compounds (BPA, E2, and EE2) by manganite-activated peroxymonosulfate was investigated. The effect of manganite and PMS dosages on the degradation rate of selected pollutants was studied. The scavenging tests, EPR and X-ray photoelectron spectroscopy (XPS) experiments were conducted to identify the main reactive species generated in the reaction and Mn oxidation state changes. The influence of various inorganic ions on the system of manganite/PMS was also studied and application for the degradation of three pollutants in the STP water was reported.

Reference

- [1] T.K. Kasonga, M.A.A. Coetzee, I. Kamika, V.M. Ngole-Jeme, M.N. Benteke Momba, Endocrine-disruptive chemicals as contaminants of emerging concern in wastewater and surface water: A review, *Journal of Environmental Management*. 277 (2021) 111485. <https://doi.org/10.1016/j.jenvman.2020.111485>.
- [2] Y. Li, G. Zhu, W.J. Ng, S.K. Tan, A review on removing pharmaceutical contaminants from wastewater by constructed wetlands: Design, performance and mechanism, *Science of The Total Environment*. 468–469 (2014) 908–932. <https://doi.org/10.1016/j.scitotenv.2013.09.018>.
- [3] F. Riva, E. Zuccato, E. Davoli, E. Fattore, S. Castiglioni, Risk assessment of a mixture of emerging contaminants in surface water in a highly urbanized area in Italy, *Journal of Hazardous Materials*. 361 (2019) 103–110. <https://doi.org/10.1016/j.jhazmat.2018.07.099>.
- [4] E.R. Kabir, M.S. Rahman, I. Rahman, A review on endocrine disruptors and their possible impacts on human health, *Environmental Toxicology and Pharmacology*. 40 (2015) 241–258. <https://doi.org/10.1016/j.etap.2015.06.009>.
- [5] C.V.T. Rigueto, M.T. Nazari, C.F. De Souza, J.S. Cadore, V.B. Brião, J.S. Piccin, Alternative techniques for caffeine removal from wastewater: An overview of opportunities and challenges, *Journal of Water Process Engineering*. 35 (2020) 101231. <https://doi.org/10.1016/j.jwpe.2020.101231>.
- [6] S. Sauvé, M. Desrosiers, A review of what is an emerging contaminant, *Chemistry Central Journal*. 8 (2014) 15. <https://doi.org/10.1186/1752-153X-8-15>.
- [7] W.H. Glaze, J.-W. Kang, D.H. Chapin, The Chemistry of Water Treatment Processes Involving Ozone, Hydrogen Peroxide and Ultraviolet Radiation, *Ozone: Science & Engineering*. 9 (1987) 335–352. <https://doi.org/10.1080/01919518708552148>.
- [8] M. Muruganandham, R.P.S. Suri, S. Jafari, M. Sillanpää, G.-J. Lee, J.J. Wu, M. Swaminathan, Recent Developments in Homogeneous Advanced Oxidation Processes for Water and Wastewater Treatment, *International Journal of Photoenergy*. 2014 (2014) e821674. <https://doi.org/10.1155/2014/821674>.

- [9] H. Zhou, H. Zhang, Y. He, B. Huang, C. Zhou, G. Yao, B. Lai, Critical review of reductant-enhanced peroxide activation processes: Trade-off between accelerated $\text{Fe}^{3+}/\text{Fe}^{2+}$ cycle and quenching reactions, *Applied Catalysis B: Environmental*. 286 (2021) 119900. <https://doi.org/10.1016/j.apcatb.2021.119900>.
- [10] A.D. Bokare, W. Choi, Review of iron-free Fenton-like systems for activating H_2O_2 in advanced oxidation processes, *Journal of Hazardous Materials*. 275 (2014) 121–135. <https://doi.org/10.1016/j.jhazmat.2014.04.054>.
- [11] C.K. Remucal, M. Ginder-Vogel, A critical review of the reactivity of manganese oxides with organic contaminants, *Environmental Science: Processes and Impacts*. 16 (2014) 1247. <https://doi.org/10.1039/c3em00703k>.
- [12] R.J. Watts, J. Howsawkung, A.L. Teel, Destruction of a Carbon Tetrachloride Dense Nonaqueous Phase Liquid by Modified Fenton's Reagent, *Journal of Environmental Engineer*. 131 (2005) 1114–1119. [https://doi.org/10.1061/\(ASCE\)0733-9372\(2005\)131:7\(1114\)](https://doi.org/10.1061/(ASCE)0733-9372(2005)131:7(1114)).
- [13] S. Zhu, X. Li, J. Kang, X. Duan, S. Wang, Persulfate Activation on Crystallographic Manganese Oxides: Mechanism of Singlet Oxygen Evolution for Nonradical Selective Degradation of Aqueous Contaminants, *Environmental Science and Technology*. 53 (2019) 307–315. <https://doi.org/10.1021/acs.est.8b04669>.
- [14] Z.-G. Zhou, H.-M. Du, Z. Dai, Y. Mu, L.-L. Tong, Q.-J. Xing, S.-S. Liu, Z. Ao, J.-P. Zou, Degradation of organic pollutants by peroxymonosulfate activated by MnO_2 with different crystalline structures: Catalytic performances and mechanisms, *Chemical Engineering Journal*. 374 (2019) 170–180. <https://doi.org/10.1016/j.cej.2019.05.170>.
- [15] J. Huang, Y. Dai, K. Singewald, C.-C. Liu, S. Saxena, H. Zhang, Effects of MnO_2 of different structures on activation of peroxymonosulfate for bisphenol A degradation under acidic conditions, *Chemical Engineering Journal*. 370 (2019) 906–915. <https://doi.org/10.1016/j.cej.2019.03.238>.
- [16] E. Saputra, S. Muhammad, H. Sun, H.-M. Ang, M.O. Tadé, S. Wang, Manganese oxides at different oxidation states for heterogeneous activation of peroxymonosulfate for phenol

degradation in aqueous solutions, *Applied Catalysis B: Environmental*. 142–143 (2013) 729–735. <https://doi.org/10.1016/j.apcatb.2013.06.004>.

[17] D. He, Y. Li, C. Lyu, L. Song, W. Feng, S. Zhang, New insights into MnOOH/peroxymonosulfate system for catalytic oxidation of 2,4-dichlorophenol: Morphology dependence and mechanisms, *Chemosphere*. 255 (2020) 126961. <https://doi.org/10.1016/j.chemosphere.2020.126961>.

Chapter I

Bibliography

1.1 Advanced oxidation processes (AOPs)

1.1.1 General description of AOPs

The wide occurrence of emerging pollutants (EPs) in the aquatic environment has raised much concern about water security. It is suspected that the increase of some incidence and diseases (such as heart diseases, diabetes, and cancer) is related to the presence of EPs in the environment [1]. Due to the chemical stability of EPs and the low efficiency of conventional water treatment technologies (such as physicochemical adsorption, coagulation precipitation, and membrane filtration), EPs can be persistent in various waters and bioaccumulate through the biological cycles in different organisms [2]. Therefore, it is necessary to develop an efficient water treatment technology to efficiently remove EPs in waters. In the past decades, advanced oxidation processes (AOPs) have attracted much attention due to their excellent efficiency in the removal of refractory pollutants.

AOPs are defined as the processes involving the generation of highly reactive species which can degrade organic substances [3]. AOPs can remove and mineralize most of the organic contaminants into less toxic products (e.g. CO₂, H₂O) [4]. The mentioned processes also exhibit excellent performance in the treatment of multiple organic pollutants in simultaneous time. The good oxidation reactivity of AOPs is attributed to the generation of highly reactive oxygen or sulfur species (ROS/RSS), for example, hydroxyl radical (HO[•]) and sulfate radical (SO₄^{•-}). Hydroxyl radical has a high standard redox potential ($E_0 = 2.80$ V vs NHE) which can mineralize various organic pollutants without selectivity [5]. For sulfate radical, it exhibits high activity on the oxidation of various organic substances relying on its high standard reduction potential ($E_0 = 2.60$ V vs NHE) [5]. The pathways of organic pollutants degradation by HO[•] and SO₄^{•-} include hydrogen abstraction, electron transfer, carbon double bonds addition, and radical interaction [6,7].

The way of AOPs activation can be classified into homogeneous and heterogeneous processes based on the uniformity of substances which participating in the reaction. For example, Fenton reaction (Fe²⁺/H₂O₂), Fenton-like reaction (Fe³⁺/H₂O₂), H₂O₂ photolysis (UV/H₂O₂), ultrasonic irradiation, and ozonation (O₃) are all homogeneous processes [8]. In comparison,

heterogeneous catalysis usually refers to the radical generation processes which use transition metal oxides (such as Fe_3O_4 , Fe_2O_3 , Co_3O_4 , CuO , MnO_2 , and Mn_2O_3) as catalysts [4]. The efficiency of radical formation in homogeneous and heterogeneous processes can be improved by adding different radical precursors such as hydrogen peroxide (H_2O_2), peroxydisulfate (PDS, $\text{S}_2\text{O}_8^{2-}$), and peroxymonosulfate (PMS, HSO_5^-). To better understand the activation mechanism of oxidants in AOPs, the properties of H_2O_2 , PDS and PMS were summarized in the next section.

1.1.2 The commonly used oxidants in AOPs

In this section, the primary properties of H_2O_2 , PDS, and PMS are presented.

1.1.2.1 The chemical and physical properties of H_2O_2

Hydrogen peroxide is a colorless liquid, less volatile, and more viscous than water [9]. The primary physiochemical properties of H_2O_2 are listed in Table 1-1. H_2O_2 has a three-dimensional structure which is popularly known as an “open book” structure (Figure 1-1(a)) [10]. H_2O_2 is highly unstable and can be slowly decomposed in the presence of light. The decomposition of H_2O_2 into oxygen and water can be accelerated with the occurrence of metals [11]. Therefore, H_2O_2 is typically stored with a stabilizer in a weakly acidic solution in the plastic bottle. H_2O_2 exhibits different chemical properties in different pH environments, for example, H_2O_2 acts as an oxidizing agent ($E_0 = 1.77 \text{ V}$) in the acidic medium while in the basic environment, H_2O_2 acts as a reducing agent [12,13]. The application of H_2O_2 is diverse, for instance, oxidizer, bleaching agent, detergent, disinfectant, antiseptic, and propellant in the rocket [14]. In the study of pollutants removal by AOPs, H_2O_2 is usually used as the oxidant to promote the generation of radicals. However, it is important to realize that the wide occurrence of H_2O_2 in water may have impacts on the natural degradation processes of organic pollutants by oxidative minerals due to the reactions between H_2O_2 with natural metal oxides.

Table 1-1. The physical and chemical properties of H₂O₂, PDS, and PMS [14,15].

Priorities	H ₂ O ₂	PDS ¹	PMS ²
CAS number	7722-84-1	7775-27-1	70693-62-8
Chemical formula	H ₂ O ₂	Na ₂ S ₂ O ₈	KHSO ₅ • 0.5KHSO ₄ • 0.5K ₂ SO ₄
Molar weight (g mol ⁻¹)	34	238.1	307.28
Water Solubility ³ (g L ⁻¹)	miscible	730	298
Density (g cm ⁻³)	1.11 ⁴	2.59	1.15
pKa	11.75	-3.5	9.3

¹ PDS refers to sodium peroxydisulfate.

² PMS refers to Oxone (KHSO₅ • 0.5KHSO₄ • 0.5K₂SO₄).

³ The values of water solubility are achieved at 20°C.

⁴ The density is achieved in 20°C with 30% (w/w) H₂O₂ solution.

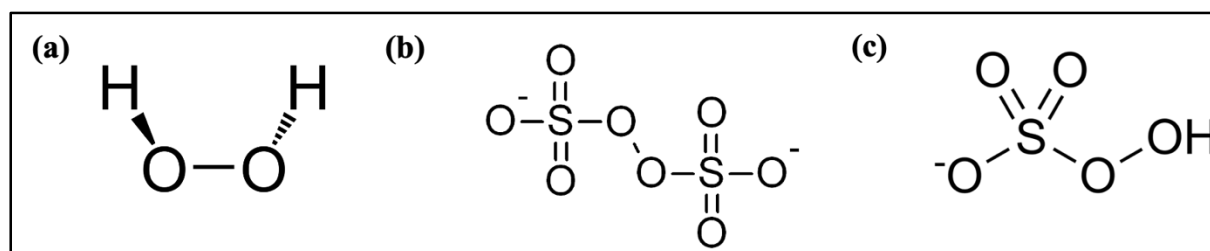


Figure 1-1. The chemical structures of H₂O₂ (a), PDS (b), and PMS (c).

1.1.2.2 The chemical and physical properties of PDS and PMS

Peroxydisulfate (PDS) can be associated with three different salts i.e. sodium (Na₂S₂O₈), potassium (K₂S₂O₈), and ammonia ((NH₄)₂S₂O₈). The application of K₂S₂O₈ and (NH₄)₂S₂O₈ in the *in situ* remediation has been restricted due to some disadvantages [15]. For example, K₂S₂O₈ has very low solubility, and the application of (NH₄)₂S₂O₈ can cause residual ammonia and secondary contamination. In comparison, Na₂S₂O₈ exhibits good performance for in situ chemical oxidation (ISCO) treatment. The main chemical and physical properties of PDS have been listed in Table 1-1. It is worth noting that PDS is composed of a symmetrical O-O bond (Figure 1-1(b)). The bond dissociation energy and bond length of O-O bond was respectively determined to be 92 kJ mol⁻¹ and 1.497 Å [15].

Peroxymonosulfate (PMS) originates from Caro's acid (H_2SO_5) but is difficult to handle owing to its reactive and explosive characteristics. HSO_5^- has been identified as the dominant species under neutral and weakly acidic conditions due to its high dissociation constants ($\text{pK}_a = 9.3$) [16]. To generate a more stable form, a triple salt was synthesized with a commercial name Oxone. The artificial Oxone contains three salts 2KHSO_5 , KHSO_4 , K_2SO_4 or KHSO_5 , 0.5KHSO_4 , $0.5\text{K}_2\text{SO}_4$. The physical and chemical properties of PMS have been listed in Table 1-1. As shown in Figure 1-1(c), PMS possesses unsymmetrical reactive O-O bond whose length (1.46 \AA) is shorter than PDS while the bond dissociation energy (377 kJ mol^{-1}) is higher than PDS [15]. Theoretically, PMS requires more energy to break the O-O bond, however, in the actual catalysis process, PMS is easier than PDS to be activated. This phenomenon might be related to the unsymmetrical structure of PMS. The standard oxidation-reduction potential for the reduction of PDS anion (Eq. (1-1)) equals 2.01 V, hence it is higher than that of PMS i.e. 1.4 V (Eq. (1-2)) [15].



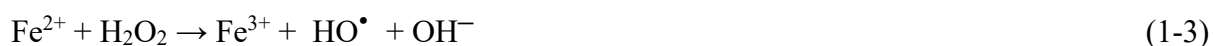
1.1.3 Transition metals-based AOPs

The application of transition metals-based AOPs (TMs-AOPs) in water or wastewater treatment has gained increasing attention due to their good performance on recalcitrant pollutants degradation. The excellent catalytic reactivity of transition metals is attributed to the presence of multiple oxidation states which is resulted from the special arrangement of electrons in the electric orbital of transition metal atoms [17]. The AOPs based on transition metals activation can be classified into two categories including homogeneous and heterogeneous TMs-AOPs according to the form of transition metals participated in the reaction [18]. The homogeneous TMs-AOPs employ transition metal ions such as Fe^{2+} , Fe^{3+} , Mn^{2+} , and Co^{2+} as the catalysts, while in heterogeneous TMs-AOPs, the transition metal oxides (e.g. Fe_2O_3 , Fe_3O_4 , MnO_2 , Co_3O_4 , and CuO) are usually used as the radical activators. The radical precursors commonly used in TMs-AOPs include H_2O_2 , PDS, and PMS. In this section, the introduction of TMs-

AOPs is presented by summarizing the mechanism of homogeneous and heterogeneous TMs-AOPs.

1.1.3.1 The homogeneous TMs-AOPs

The activation of radical precursors such as H₂O₂, PDS, and PMS by transition metal ions has been widely reported [19,20]. The transition metals commonly used in AOPs activation include iron (Fe), manganese (Mn), copper (Cu), cerium (Ce), chromium (Cr), cobalt (Co), silver (Ag), nickel (Ni), vanadium (V) and ruthenium (Ru). The representative homogeneous TMs-AOPs is Fenton reaction which employs ferrous ion (Fe²⁺) as the catalyst to activate H₂O₂ aiming to generate reactive hydroxyl radicals (Eq. (1-3)) [20]. Since the dual roles of H₂O₂, the formed Fe³⁺ can be reduced to Fe²⁺ by H₂O₂ realizing the cycle of iron ions (Eq. (1-4)) [20].



The mechanism of H₂O₂ activation by other transition metals such as Mn, Co, Cu, and V are similar to the Fenton reaction, thus one representative activation process has been proposed, as shown in Eqs. (1-5) - (1-6). It is worth noting that although the activation processes are uniform, the valence states of transition metals involved in the H₂O₂ activation are different, as example, Fe²⁺/Fe³⁺, Ce³⁺/Ce⁴⁺ and Co²⁺/Co³⁺. A list of valence states of transition metals that participated in the activation of oxidants (such as H₂O₂, PDS, and PMS) is presented in Table 1-2. The transition metals activated H₂O₂ processes have shown many advantages in the process of non-selective degradation of stubborn pollutants. However, the homogeneous TMs-AOPs still exists some disadvantages in the practical water treatment. For example, in the Fenton reaction, the narrow optimal pH range (2.5-3.5), the difficult recovery of iron catalysts, and the excess iron sludge generation restricts its application in the practical water treatment processes [21]. The application of the Cr⁶⁺/H₂O₂ system in wastewater treatment has been blocked by the risk of leaking harmful Cr⁶⁺ [20]. To minimize the influence of transition metal ions and broaden the application scope of solution pH, different alternatives have been developed. For example, the introduction of various energy resources (such as ultraviolet light (UV), solar light, ultrasound,

and electricity) and employing metal oxides (such as Fe₃O₄, Fe₂O₃, Mn₂O₃, MnO₂) as the catalysts [4]. In addition, the employment of PMS or PDS is also a good substitute for improving the efficiency of pollutants degradation.



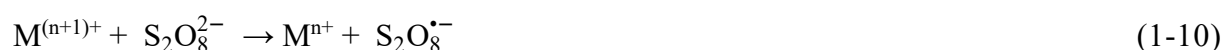
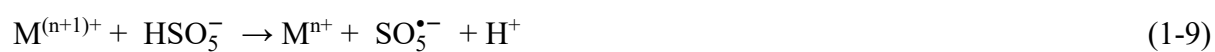
Table 1-2. The valence states of transition metals involved in oxidants activation.

Transition metals	Main oxidation state	Redox potential vs NHE	Reference
Fe	+2, +3	$E^0 (Fe^{3+}/Fe^{2+}) = 0.771 \text{ V}$	[22]
Ce	+3, +4	$E^0 (Ce^{4+}/Ce^{3+}) = 1.72 \text{ V}$	[20]
Ag	0, +1	$E^0 (Ag^+/Ag^0) = 0.799 \text{ V}$	[23]
Ru	+2, +3	$E^0 (Ru^{3+}/Ru^{2+}) = 1.29 \text{ V}$	[24]
Mn	+2, +3, +4	$E^0 (Mn^{3+}/Mn^{2+}) = 1.54 \text{ V}$ $E^0 (Mn^{4+}/Mn^{2+}) = 1.24 \text{ V}$	[25,26]
Cr	+3, +6	$E^0 (Cr^{6+}/Cr^{3+}) = 1.35 \text{ V}$	[27]
Cu	+1, +2	$E^0 (Cu^{2+}/Cu^+) = 0.153 \text{ V}$	[28]
Co	+2, +3	$E^0 (Co^{3+}/Co^{2+}) = 1.92 \text{ V}$	[29]
V	+3, +4	$E^0 (V^{4+}/V^{3+}) = 0.34 \text{ V}$	[19]

The activation of PDS and PMS by transition metals has provided one new way to degrade the organic pollutants in water. According to the previous literature, the activation mechanism of PDS and PMS by transition metals can be described by the equations (1-7)-(1-10) [7]. Generally, sulfate radical can be generated through the breaking of the O-O bonds of persulfate anions activated by transition metals with lower valence while higher valence of them can promote the formation of $SO_5^{\bullet-}$ and $S_2O_8^{\bullet-}$ radicals. The homogeneous activation of PDS and PMS by transition metals has been reported by previous studies [19]. For instance, Anipsitakis and Dionysiou investigated the activation of PDS and PMS by nine transition metal ions including Ag(I), Ce(III), Co(II), Fe(II), Fe(III), Mn(II), Ni(II), Ru(III), and V(III) [19]. It was found that Co(II) and Ru(III) are the best transition metal catalysts for the activation of PMS. Ag(I) showed

the best results toward activating PDS. In comparison, Mn(II) showed low efficiency in PMS activation for 2,4-dichlorophenol (2,4-DCP) degradation, and no 2,4-DCP removal was observed in the system of Mn(II)/PDS in the neutral pH. The results indicated that Mn(II) can activate PMS to generate reactive species while PDS is difficult to be catalyzed by Mn(II) at pH 7. This activation mechanism of PDS and PMS by Mn(II) has been verified in many related studies. For instance, Zhu et al. reported that the degradation of organic pollutants in crystallographic MnO₂/PDS system was not related to the leaching of Mn²⁺ since Mn²⁺ is not reactive for catalytic PDS activation [30]. Zhou et al. demonstrated that the increased degradation efficiency of 4-nitrophenol in the α -MnO₂/PMS system was attributed to the presence of Mn²⁺ and Mn³⁺ which can improve the generation of reactive radicals [31]. The different activation performance of Mn²⁺ on PDS and PMS might be attributed to the different chemical structures of oxidants as discussed in *section 1.1.2*.

In summary, the degradation efficiency of recalcitrant pollutants in homogeneous TMs-AOPs depends on the employed oxidants and transition metals. Fe(II) and Fe(III) are the most efficient transition metals for the activation of H₂O₂. Co(II) and Ru(III) show good performance on PMS activation while Ag(I) is the best activator for PDS decomposition. The concerned Mn(II) shows less reactivity in H₂O₂ and PDS activation but exhibited good ability for PMS activation.



1.1.3.2 The heterogeneous TMs-AOPs

The heterogeneous AOPs based on transition metal oxides have been widely applied in the treatment of recalcitrant pollutants due to their various advantages, for example, high efficiency, low cost, and environmental-friendly [32]. Moreover, the development of heterogeneous TMs-AOPs efficiently solves the drawbacks of the homogeneous TMs-AOPs, for example, the low recovery of metal ions, high cost, restrict pH condition, and secondary treatment for residual

metal ions. The high catalytic performance of transition metal oxides on oxidants can be attributed to the presence of more active sites on the surface of heterogeneous catalysts which can activate radical precursors to produce more reactive species. The amounts of active sites on the surface of transition metal oxides were believed to be related to the specific surface area and the crystal structure of catalysts [33]. Various transition metal oxides can activate oxidants (e.g. H₂O₂, PDS, and PMS) to produce the reactive oxidation species such as SO₄^{•-}, HO[•], and singlet oxygen (¹O₂). The commonly reported transition metal oxides used in radical precursors activation include iron oxides (such as Fe₃O₄, α-Fe₂O₃, α-FeOOH and FeS₂) [34,35], Copper oxide (such as CuO) [36,37], Cobalt oxide (such as Co₃O₄) [38], manganese oxides (such as MnO₂, Mn₂O₃, Mn₃O₄, and γ-MnOOH) [39,40].

Iron-based materials are widely employed for catalysis because they are cost-effective, eco-friendly, and efficient materials [32]. The activation of H₂O₂ by iron oxides (commonly named as Fenton-like reaction) has been widely used in the treatment of recalcitrant pollutants. For instance, Zhang et al. reported the efficient oxidation of phenolic and aniline compounds by nano-Fe₃O₄ activated Fenton-like reaction in the neutral solution [41]. Wang et al. demonstrated that α-FeOOH could efficiently degrade methyl orange through activating H₂O₂ [42]. Although iron is fixed in the catalyst and can effectively produce HO[•] by activating H₂O₂ without producing the iron hydroxide precipitation in heterogeneous Fenton-like reactions, there is still an iron leaching problem, especially when the catalyst is reused. Thus, some strategies were developed to improve the iron redox cycle in heterogeneous Fenton system catalyzed by iron materials, for example, introducing semiconductors, the modification with other elements, the application of carbon materials as carriers, the introduction of metal sulfides as co-catalysts, and the direct reduction with reducing substances [4].

As mentioned above, Co²⁺ exhibited good performance on PMS activation, thus the application of cobalt oxide such as Co₃O₄ in PMS activation for organic pollutants degradation has been reported. For example, Chen et al. reported that Co₃O₄ nano-spheres were most effective in the degradation of Acid Orange 7 and were more stable at the neutral condition with dissolved Co concentration below 0.05 mg L⁻¹ [38]. Saputra et al. also reported that Co₃O₄ nanoparticles

could completely remove phenol in about 20 min in the presence of PMS [43]. However, the undesirable Co leaching during the catalysis of PMS with cobalt oxides restricts its application in practical water treatment [44]. To reduce the Co leaching problem, Co_3O_4 has been decorated on various supports including inert 1/2/3-D materials [45], metal oxides [46], magnetic particles [47], and molecular sieves [48]. In addition, the activation of PMS by other common transition metal oxides such as CuO , Fe^0 , Fe_2O_3 , Fe_3O_4 , MnO_2 , and Mn_2O_3 for organic pollutants degradation are also reported [34,49–52].

In comparison with PMS, the redox recycling of the metal-based catalyst in the PDS system cannot be achieved easily due to the nature of PDS which cannot act as a reductant [19]. Among the transition metal catalysts, the zero-valent iron (Fe^0) is the most widely used heterogeneous catalyst for PDS activation due to its advantages such as low-cost, versatile, and eco-friendly [53]. The system of Fe^0/PDS has been reported in the elimination of various organic pollutants such as pharmaceuticals [54], phenolic compounds [55], arsenic [56], pesticides [57], and industrial waste [58]. Furthermore, the magnetic Fe_3O_4 [59], Co_3O_4 [60], MnO_2 [30], Zn^0 [61], and Ni^0 [62] have also been investigated as PDS activator. It is worth noting that except for the generation of reactive radicals, the non-radical species such as the catalyst surface activated PDS molecules and singlet oxygen were also identified in the system of transition metal oxides-activated PDS. For example, Zhang et al. reported the efficient degradation of 2,4-dichlorophenol by CuO -activated PDS under mild conditions with the formation of outer-sphere intermediates between PDS and CuO [63].

In conclusion, the common oxidants (i.e. H_2O_2 , PDS, and PMS) can be efficiently activated by most transition metal oxides to remove the organic pollutants in water. Moreover, both radical and non-radical mechanisms were involved in the activation of oxidants by transition metal oxides. The leaching of metal ions from heterogeneous catalysts has become one concerning problem in the application of heterogeneous TMs-AOPs on the treatment of wastewater. Thus, various substitute strategies were developed to control the release of metal ions and improve the catalytic efficiency of transition metal oxides.

1.2 Manganese oxides

1.2.1 Oxidation states

Manganese (Mn) is one of the most abundant elements on the earth. The average concentration of Mn in the Earth's crust is 11 g/kg [64]. Mn exists in different oxidation states from Mn(II) to Mn(VII). Among them, Mn(II), Mn(III) and Mn(IV) are the dominant Mn valences that are discovered in the natural environment [65]. Generally, Mn(II) ions are soluble in water and can be oxidized to form various manganese oxides (MnOx) on exposure to oxygen and moisture [66]. Mn(IV) oxides as the oxidation products of Mn(II) are always presented in solution with insoluble forms [64]. For Mn(III) species, the existing situation is more complicated than Mn(II) and (IV) species. On one hand, Mn(III) species are not stable in solution and can combine with other parts of Mn(III) species to generate Mn(II) and Mn(IV) [67]. On the other hand, the complex generated between Mn(III) and organic substances (for example, humic compound, pyrophosphate chemicals) can be dissolved and stable in solution [68].

In nature, MnOx can be obtained through the oxidation of Mn(II) species. The ways of Mn(II) oxidation can be classified into abiotic and biogenic processes [69]. Firstly, the formation of MnOx based on the abiotic processes was considered as a long-term formation procedure due to its strict reaction conditions such as the high activation energy, the suitable solution pH value, and Mn concentrations [70]. It was reported the half-life of Mn(II) in oxic seawater is 350 days in the absence of catalysts for its oxidation [71]. In addition, the oxidation of Mn(II) on the surface of minerals was also found to have a contribution to the formation of MnOx [72]. Although the speed of mineral surface-triggered Mn(II) oxidation is more rapid than the homogeneous Mn(II) oxidation, the rate is still slower than the biogenic Mn(II) oxidation in five orders of magnitude [64]. The biogenic processes are induced by widespread fungi and bacteria with multifunctional enzymes, which are the main pathways to the formation of natural MnOx [73]. In biogenic processes, the microorganisms serve as the primary catalysts for the oxidation of Mn(II). The formed MnOx further assists the oxidation of Mn(II) on its surface. Moreover, most of the low-crystalline MnOx formed by biogenic processes will be transferred to crystalline minerals during the aging process [74].

Previous literature reported that more than 30 kinds of crystalline and non-crystalline MnOx have been found on the Earth's surface or crust [64]. Some representative MnOx minerals and their chemical formulas are listed in Table 1-3. MnOx is ubiquitous in the natural environments and occurs in a wide range of environmental settings, for example, fine-grained aggregates, veins, marine, and fresh-water nodules and concretions, crusts, dendrites, ocean floors, soils, and sediments [64]. Owing to the variable redox states and unique tunnel/layer structures, MnOx has been applied in many areas, such as lithium-ion batteries, magnetic materials, chemical catalysts, and energy storage [75–77]. Moreover, to improve the oxidative and catalytic performance of MnOx, various nanostructures of MnOx have been synthesized through different artificial methods (i.e. hydrothermal, solvothermal, sol-gel, co-precipitation, electrochemical, and thermal annealing techniques) [78]. To better understand the reactivity of MnOx, their structures are introduced in the following section.

Table 1-3. Representative MnOx minerals [64].

Mineral name	Chemical formula	Mn valence
Manganosite	MnO	+II
Pyrochroite	Mn(OH) ₂	+II
Rhodocrosite	MnCO ₃	+II
Hausmannite	Mn ₃ O ₄	+II, +III
Bixbyite	Mn ₂ O ₃	+III
Groutite	α -MnOOH	+III
Feitknechte	β -MnOOH	+III
Manganite	γ -MnOOH	+III
Birnessite	(Na, K, Ca) ₄ Mn ₇ O ₁₄ · 2.8 H ₂ O	+II, +III, +IV
Vernadite	MnO ₂ · nH ₂ O	
Lithiophorite	LiAl ₂ (Mn ⁴⁺ Mn ³⁺)O ₆ (OH) ₆	+III, +IV
Manjiroite	Na _x (Mn ⁴⁺ , Mn ³⁺) ₈ O ₁₆	+III, +IV
Chalcophanite	ZnMn ₃ O ₇ · 3 H ₂ O	+II, +IV

Table 1-3 (continued)

Mineral name	Chemical formula	Mn valence
Todorokite	$(\text{Ca,Na,K})_x(\text{Mn}^{4+}, \text{Mn}^{3+})_6\text{O}_{12} \cdot 3.5 \text{H}_2\text{O}$	+III, +IV
Romanechite	$\text{Ba}_{0.66}(\text{Mn}^{4+}, \text{Mn}^{3+})_5\text{O}_{10} \cdot 1.34 \text{H}_2\text{O}$	+III, +IV
Coronadite	$\text{Pb}_x(\text{Mn}^{4+}, \text{Mn}^{3+})_8\text{O}_{16}$	+III, +IV
Cryptomelane	$\text{K}_x(\text{Mn}^{4+}, \text{Mn}^{3+})_8\text{O}_{16}$	+III, +IV
Hollandite	$\text{Ba}_x(\text{Mn}^{4+}, \text{Mn}^{3+})_8\text{O}_{16}$	+III, +IV
Nsutite	$\text{Mn}(\text{O},\text{OH})_2$	+II, +III, +IV
Ramsdellite	$\gamma\text{-MnO}_2$	+IV
Pyrolusite	$\beta\text{-MnO}_2$	+IV

1.2.2 Structures

It was reported that recalcitrant pollutants in wastewater can be efficiently removed by different MnOx due to their good oxidative and catalytic performance. However, the reactivity of MnOx can be substantially affected by its structure. The basic building block for most of the MnOx is the MnO₆ octahedral. The basic unit MnO₆ can be assembled through sharing edges and/or corners to construct tunnel or layer structure MnOx [64].

For the formation of tunnel MnOx, the MnO₆ octahedral units are firstly gathered via sharing edges, which leads to the generation of chains with different lengths (such as, single, double, and triple chains) [78]. Then the various chains can be linked by sharing the corners resulting in the fabrication of tunnel MnOx with distinct shapes including square, rectangular, and crossing shapes (Figure 1-2(A-C)). The scale of tunnel MnOx depends on the length of formed chains. Therefore, the size of tunnel MnOx ranges from 1×1 to 3×3 chains. Moreover, different metal ions or water molecules can be hosted in tunnels leading to the formation of different tunnel MnOx. The classical tunnel-type MnOx found in nature include ramsdellite, pyrolusite, nsutite, romanechite, hollandite, and todorokite [64].

Layer-type MnOx is widespread in the environment. It was reported that layer-type MnOx exhibits excellent oxidative reactivity in organic pollutants removal [79]. To construct layer-

type MnOx, the MnO₆ octahedral units are first arranged to form sheets through sharing the edges, then the formed sheets are stacked together with the insertion of different metal ions or water molecules in the interlayer (Figure 1-2D)[64]. The performance of layer-type MnOx can be influenced by various factors, such as the number of vacancy sites, the concentration of Mn(III) in layer and interlayer, and the type of insert metal ions. The commonly found layer-type MnOx include birnessite and birnessite-like minerals [65]. To better understand the structure of MnOx, some representative tunnel, and layer-type MnOx will be introduced in detail.

Pyrolusite. Pyrolusite (β -MnO₂) is the most stable and abundant Mn(IV) mineral compared with other MnO₂ such as ramsdellite and nsutite. In pyrolusite, a (1x1) tunnel structure was constructed by basic MnO₆ units through the way of sharing the corners between the formed single chains (Figure 1-2A) [64]. The tunnel size of pyrolusite is too small to host other chemical species leading to the composition of pyrolusite has high similarity with pure MnO₂. The existing forms of pyrolusite in nature are the low-temperature hydrothermal deposits or the replacements of other MnOx.

Ramsdellite. The crystal phase of ramsdellite is γ -MnO₂. Ramsdellite shows the (1x2) tunnel structure with a rectangular-shaped cross-section (Figure 1-2B) [64]. Minor amounts of water, Na, and Ca ions are detected in ramsdellite tunnels. Ramsdellite occurs as the low-temperature hydrothermal deposits and commonly transfers to pyrolusite.

Hollandite. Hollandite is a group of MnO₂ minerals that has the same chemical formula (R_{0.8-1.5}[Mn(IV), Mn(III)]₈O₁₆, R = Ba, Pb, K or Na). Hollandite has the crystal phase of α -MnO₂. In hollandite, double chains of edge-sharing MnO₆ octahedral are formed and construct a (2x2) tunnel structure with the square cross-section (Figure 1-2C) [64]. The tunnels of hollandite are filled with large uni- or divalent cations and some water molecules. The increase of hollandite charge with the introduction of cations can be balanced by the substitution of Mn(IV). Hollandite is mainly found in the oxidized zones of Mn deposits and ores.

Birnessite. Birnessite and birnessite-like minerals are ubiquitous in the environment and widely used in the elimination of organic pollutants [65]. In birnessite, the basic MnO₆ octahedral are

assembled to form sheets by sharing the edges. Then the sheets are stacked to construct the layer-type structure (Figure 1-2D) [64]. The interlayers are filled with various cations and water molecules. Various terms such as birnessite, acid birnessite, δ -MnO₂, and busserite are used interchangeably in referring to the layered Mn(IV) oxides that contain small contents of Mn(III) in layers and Na⁺ as the interlayer cation [80].

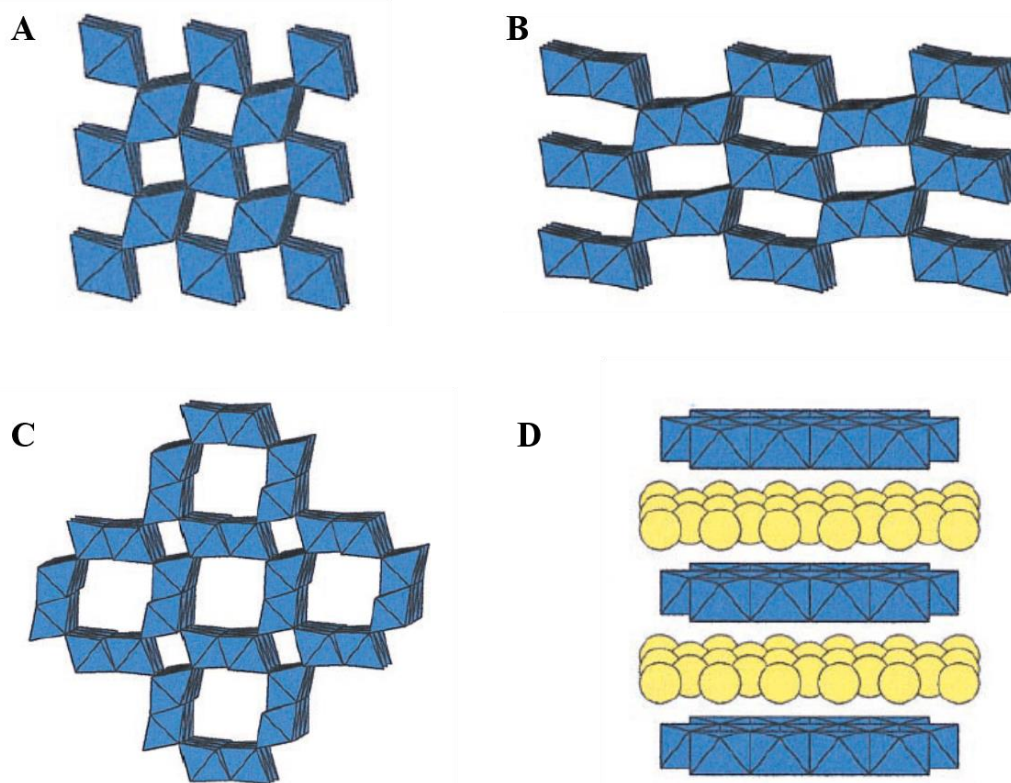


Figure 1-2. The crystal structures of (A) pyrolusite, (B) ramsdellite, (C) hollandite, (D) birnessite, stacked layers of MnO₆ are blue and the yellow balls represent the disordered H₂O or Na⁺ [64].

MnOOH. MnOOH has three different crystal phases including groutite (α -MnOOH), feitknechite (β -MnOOH), and manganite (γ -MnOOH). Among these three MnOOH, γ -MnOOH is the most stable and abundant mineral. γ -MnOOH possesses a (1 \times 1) tunnel structure which is constructed by the single chains sharing the corners. The structure of γ -MnOOH is analogous to that of pyrolusite but all of the Mn is trivalent and one-half of the O atoms are replaced by hydroxyl anions (Figure 1-3A) [64]. γ -MnOOH occurs in hydrothermal vein deposits as acicular or prismatic crystals, or as an alteration product of other Mn-bearing minerals.

Mn(III) oxide and hausmannite. The structure of Mn(III) oxide (α - Mn_2O_3) has been recognized as the body-centered cubic bixbyite phase (Figure 1-3B) [81], whereas the hausmannite (Mn_3O_4) exhibits a normal spinel structure with the formula $\text{Mn}^{2+}(\text{Mn}^{3+})_2\text{O}_4$ where the Mn^{2+} and Mn^{3+} ions occupy the tetrahedral and octahedral sites, respectively (Figure 1-3C) [64].

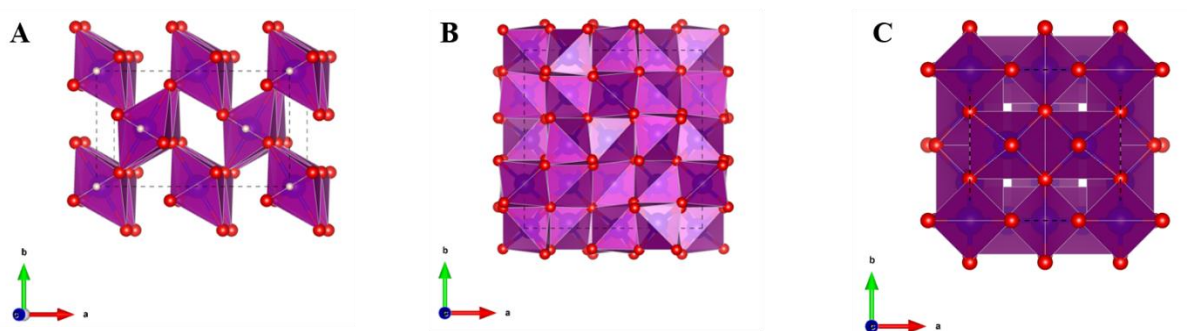


Figure 1-3. The crystal structures of (A) γ - MnOOH , (B) α - Mn_2O_3 and (C) Mn_3O_4 . The red, blue and white balls represent oxygen, manganese and hydrogen atoms, respectively. The black dashed lines represent the single unit cell. The crystalline parameters of Mn(III) (oxyhydr)oxides were taken from the crystallography open database (COD), and the COD ID of α - Mn_2O_3 , γ - MnOOH , and Mn_3O_4 are 2105791, 1011012, and 1514121, separately.

In addition to crystal phases, the morphology and crystal facets also can affect the reactivity of MnOx . It was reported that MnOx can present in different dimensions including one-dimensional (1D) tunnel structures, two-dimensional (2D) layered phases, and three-dimensional (3D) spinels [78]. The dimensional effects of MnOx not only impact the porous structure and specific surface areas (SSA), but also regulate the surface-atom arrangement, redox capacity of Mn species, and exposed facets [32]. The morphologies of α -, β -, δ - MnO_2 are identified as nanowires, nanorods, and layers by high-resolution scanning electron microscopy (SEM) (as shown in Figure 1-4) [82]. In addition, the SEM images of synthesized Mn_2O_3 with different facets are also demonstrated in previous literature. Figure 1-5 shows that α - Mn_2O_3 -octahedral (Mn_2O_3 -O), α - Mn_2O_3 -cubic (Mn_2O_3 -C), and α - Mn_2O_3 -truncated octahedral (Mn_2O_3 -T) have the facets of (111), (001) and the mixture of (111) and (001), separately [83].

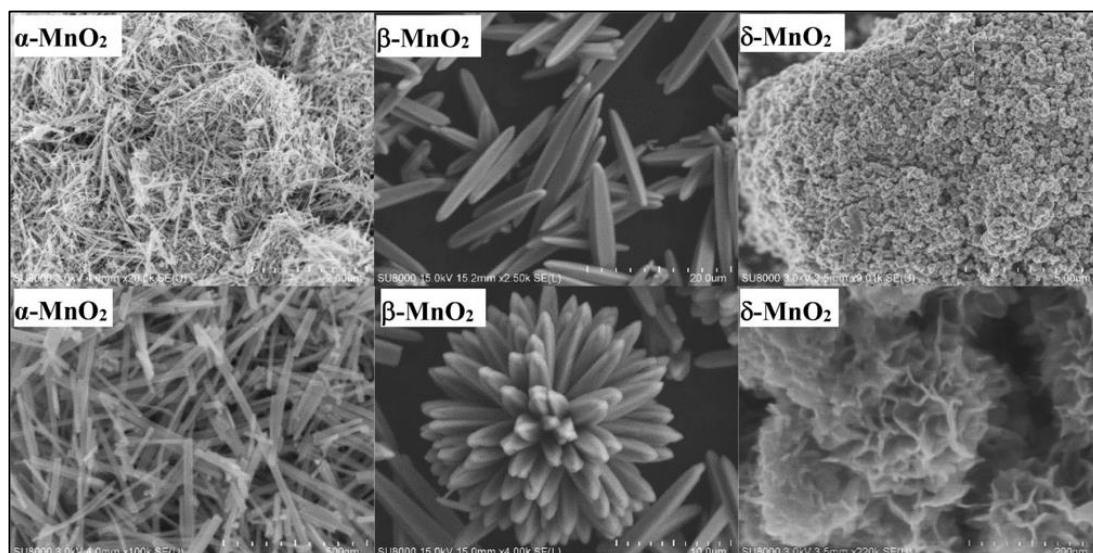


Figure 1-4. The SEM images of the α -, β -, and δ - MnO_2 [82].

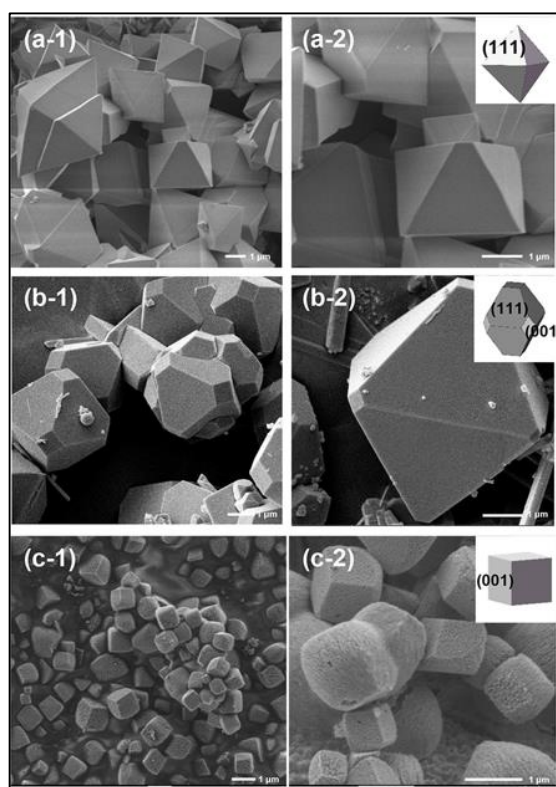


Figure 1-5. The SEM images of the (a) $\text{Mn}_2\text{O}_3\text{-O}$, (b) $\text{Mn}_2\text{O}_3\text{-T}$, and (c) $\text{Mn}_2\text{O}_3\text{-C}$ [83].

1.3 Trivalent manganese oxides activating sulfur radical-AOPs

Sulfur radical-based advanced oxidation processes (SR-AOPs) have attracted increasing attention due to their high efficiency in organic pollutants degradation. Mn(III) species have been proved to play an important role in the oxidative and catalytic reactivity of manganese

oxides. The commonly used Mn(III) (oxyhydr)oxides in the activation of peroxydisulfate (PDS) and peroxymonosulfate (PMS) include α -Mn₂O₃, γ -MnOOH, and Mn₃O₄. In this section, the effect of structure on the reactivity of Mn(III) (oxyhydr)oxides is presented. Then, the mechanisms of PMS and PDS activation by different single or combined Mn(III) (oxyhydr)oxides are discussed in detail. Both radicals (sulfate and hydroxyl radicals) and non-radical (singlet oxygen and surface activated complex) mechanisms are presented. Finally, the effect of solution pH and inorganic ions on the catalytic performance of Mn(III) (oxyhydr)oxides are discussed.

1.3.1 Effect of structure on the reactivity of Mn(III) (oxyhydr)oxides

The oxidative and catalytic performance of manganese oxides can be affected by various structural factors including crystal phases, morphologies, crystal facets, and structural dimensionalities [84]. For instance, Huang et al. reported that δ -MnO₂ showed higher oxidative activity than α -, β -, γ -, λ -MnO₂ on bisphenol A (BPA) oxidation due to the occurrence of more accessible active sites in layered δ -MnO₂ than other tunnel structured MnO₂ [85]. The authors also demonstrated the effects of structured MnO₂ on peroxymonosulfate (PMS) activation, and the low reactivity of δ -MnO₂ was attributed to its less crystallinity [40].

The influence of structures in the reactivity of common Mn(III) (oxyhydr)oxides was summarized in Table 1-4. For instance, Saputra et al. investigated the effect of morphology on the oxidation of phenol by Mn₂O₃ activated PMS. The results showed that cubic-Mn₂O₃ has the highest reactivity on PMS activation in comparison with octahedral- and truncated octahedral-Mn₂O₃ and it was due to the high surface area and distinct surface atoms arrangement of cubic-Mn₂O₃ [86]. Similarly, Cheng et al. successfully prepared three α -Mn₂O₃ in cubic-, truncated octahedral- and octahedral- structure and investigated the effect of crystal facets on the combustion of soot [87]. The results show that the soot combustion efficiency followed the order of α -Mn₂O₃-cubic > α -Mn₂O₃-truncated octahedral > α -Mn₂O₃-octahedral. The enhanced reactivity of α -Mn₂O₃-cubic was explained by the fact that the exposed (001) surface facets of α -Mn₂O₃-cubic have higher amounts of low-coordinated surface oxygen sites which are capable of facilitating the oxygen activation and improving the surface redox properties.

In addition to α - Mn_2O_3 , the oxidative and catalytic performances of Mn_3O_4 and γ - MnOOH were also reported to be affected by their structures. For example, Ji et al. reported that hexagonal nanoplate Mn_3O_4 exhibited superior catalytic performance on diesel soot combustion compared to the octahedral and nanoparticle Mn_3O_4 , and the finding was explained by the improved amount of surface Mn^{4+} species and surface reactive oxygen species due to the increased fraction of exposed (112) facets in hexagonal nanoplate Mn_3O_4 [88]. The effect of morphology was also discovered by Liu et al. which demonstrated that the nanoflake Mn_3O_4 (exposure of (001) facet) has the highest oxygen reduction reactivity in comparison with nanoparticle Mn_3O_4 and nanorod Mn_3O_4 (exposure of (101) facet) [89]. In addition, He et al. investigated the activation of PMS by γ - MnOOH with different shapes, and the results showed that the catalytic activity of γ - MnOOH followed the order of nanowires > multi-branches > nanorods [90]. Different physicochemical parameters such as specific surface area, Lewis sites, zeta-potential, and redox potential were measured to study the reason for the different catalytic performances of γ - MnOOH with distinct morphologies. It was found that the charge density on the surface played a crucial role in the interfacial reactivity between PMS and γ - MnOOH . In summary, the reactivity of Mn(III) (oxyhydr)oxides on radical precursors activation and pollutants oxidation can be deeply affected by their structures. The desirable morphologies and facets (such as cubic structure with (001) facet exposure) can improve the reactivity of Mn(III) (oxyhydr)oxides.

Table 1-4. The effect of structures on the reactivity of Mn(III) (oxyhydr)oxides.

Catalysts	Structure	Initial conditions	Reactivity	Mechanism	Ref.
α -Mn ₂ O ₃	cubic	[Catalyst] = 0.4 g/L	100% of phenol removal by cubic-Mn ₂ O ₃ in 60 min	high surface area and surface atoms arrangement of cubic-Mn ₂ O ₃	[86]
	octahedral	[PMS] = 2 g/L			
	truncated octahedral	[Phenol] = 25 ppm			
α -Mn ₂ O ₃	cubic	[Catalyst] = 4 g/L	high catalytic activity (0.87 mmol/ (h m ²)) and high selectivity for glycerol (52.6 %) was achieved by α -Mn ₂ O ₃ -truncated octahedral	co-exposed (001) and (111) facets of α -Mn ₂ O ₃ -truncated octahedral	[83]
	octahedral	[Glycerol] = 20 g/L			
	truncated octahedral				
α -Mn ₂ O ₃		180 mg of catalysts	high NO turnover frequency ((3.6 ± 0.1) × 10 ⁻³ s ⁻¹) was achieved by α -Mn ₂ O ₃ -truncated octahedral at 513K	the exposure of a small fraction of (001) facets in α -Mn ₂ O ₃ -truncated octahedral	[91]
		500 ppm of NO			
	octahedral	500 ppm of NH ₃			
	truncated octahedral	5% v/v of O ₂			
		N ₂ as balance gas			
		36000 h ⁻¹ of GSHV			

Table 1-4 (continued)

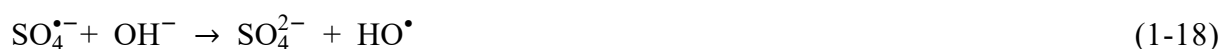
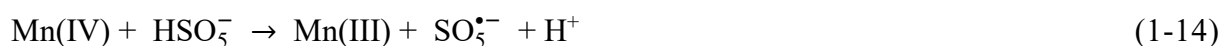
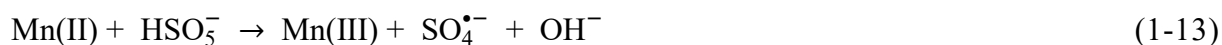
Catalysts	Structure	Initial conditions	Reactivity	Mechanism	Ref.
α -Mn ₂ O ₃	cubic octahedral truncated octahedral	100 mg of catalysts	96.3, 89.7 and 85.2% of soot combustion efficiencies were observed with the catalysis of α -Mn ₂ O ₃ -cubic, -truncated octahedral, -octahedral	the exposed (001) facet of cubic Mn ₂ O ₃	[87]
		10 mg of soot			
		5% v/v of O ₂			
		0.25% v/v of NO			
γ -MnOOH	nanowires multi-branches nanorods	N ₂ as balance gas	98%, 88%, and 55% removal of 2,4-DCP was achieved in γ -MnOOH nanowires, multi-branches, and nanorods activated PMS systems, separately	higher zeta-potential value of nanowires γ -MnOOH	[90]
		9990 h ⁻¹ of GSHV			
		[Catalyst] = 0.3 g/L			
		[PMS] = 12 mM			
Mn ₃ O ₄	nano-cubic nano-plate nano-octahedral	[2,4-DCP*] = 100 mg/L	100% CIP removal in 80 min by Mn ₃ O ₄ nano-octahedral	lager surface Mn(IV) contents of Mn ₃ O ₄ nano-octahedral	[92]
		Initial pH = 7			
		[Catalyst] = 0.2 g/L			
		[PMS] = 0.65 mM			
		[CIP*] = 10 mg/L			
		pH = 7.7			

* CIP: ciprofloxacin.

*2,4-DCP: 2,4-dichlorophenol

1.3.2 Activation of PMS by Mn(III) (oxyhydr)oxides

The Mn(III) (oxyhydr)oxides/PMS system has been applied for the removal of various contaminants, such as phenol, bisphenol A, 2,4-dichlorophenol, ciprofloxacin, and organic dyes [92–97]. Different studies involving PMS activation by Mn(III) (oxyhydr)oxides are gathered in Table 1-5. According to the literature, the efficient degradation of organic pollutants is generally attributed to the generation of active species such as $\text{SO}_4^{\bullet-}$, HO^\bullet , and $^1\text{O}_2$. The activation mechanisms of PMS by Mn(III) (oxyhydr)oxides are proposed as shown in Eqs. (1-11)-(1-14) [52]. The simultaneous formation of Mn(II) and Mn(IV) and the conversion of Mn ions with different oxidation states explained well the good performance of Mn(III) (oxyhydr)oxides on PMS activation. Except for the above-mentioned processes, the direct generation of HO^\bullet by Mn(III) activation of PMS was also reported by some researchers (Eq. (1-15)) [92,94,96,98–100]. In comparison with $\text{SO}_4^{\bullet-}$, $\text{SO}_5^{\bullet-}$ has been regarded as a low oxidative activity for organic pollutants removal due to its low reduction potential ($E_0 = 1.10$ V vs NHE) [5]. Nevertheless, the transformation from $\text{SO}_5^{\bullet-}$ to $\text{SO}_4^{\bullet-}$ in Mn(III)Ox/PMS system still makes some contribution to the degradation of organic pollutants (Eq. (1-16)) [101]. In addition, the conversion from $\text{SO}_4^{\bullet-}$ to HO^\bullet in water should not be neglected (Eq. (1-17)), especially, when the solution is in the alkaline environment (Eq. (1-18)) [39].



In addition to the active radicals, the generation of non-radical species (such as $^1\text{O}_2$) in the Mn(III) (oxyhydr)oxides-activated PMS system was also reported. For example, He et al.

demonstrated the contribution of $^1\text{O}_2$ for the degradation of 2,4-dichlorophenol in the γ -MnOOH/PMS system. The generation of $^1\text{O}_2$ was attributed to two pathways including the decomposition of PMS and the reaction of $\text{O}_2^{\bullet-}$ with HO^\bullet (Eqs. (1-19)-(1-24)) [90,102,103]. Chen et al. synthesized one new Mn_3O_4 nanodots-g- C_3N_4 nanosheet ($\text{Mn}_3\text{O}_4/\text{CNNS}$) and investigated its performance on PMS activation for 4-chlorophenol (4-CP) degradation [104]. The chemical scavenging tests and electron spin resonance (ESR) experiments confirmed the contribution of $^1\text{O}_2$ for the removal of 4-CP.



Currently, the Mn-based oxide composites have attracted increasing attention due to their various advantages such as more oxygen vacancies, higher surface oxygen mobility, and enforced synergistic effects. For instance, Chen et al. prepared the $\text{Fe}_2\text{O}_3/\text{Mn}_2\text{O}_3$ composite and studied its activity on PMS activation for tartrazine (TTZ) degradation. The results showed that 97.3% removal of TTZ was achieved in 30 min in the $\text{Fe}_2\text{O}_3/\text{Mn}_2\text{O}_3/\text{PMS}$ system. The efficient degradation of TTZ originated from the generation of active species (e.g. $\text{SO}_4^{\bullet-}$, HO^\bullet) and the synergistic effect between iron and manganese ions [105]. γ -MnOOH coated nylon membrane was synthesized and applied in the activation of PMS towards the removal of 2,4-dichlorophenol (2,4-DCP). The deep removal of 2,4-DCP was explained by the synergetic “trap-and-zap” process which improved the stability and catalytic reactivity of γ -MnOOH [93]. In conclusion, the activation of PMS by Mn(III) (oxyhydr)oxides including pure Mn(III) oxides and Mn(III) containing composites is favorable. The degradation of various pollutants in the Mn(III) (oxyhydr)oxides/PMS system can be achieved through the generation of active radicals and non-radical species.

Table 1-5. Summary of PMS activation by Mn(III) (oxyhydr)oxides.

Catalyst	Pollutant	Initial conditions	Reactivity	Active species	Ref.
Mn ₂ O ₃	Phenol	[Catalyst] = 0.4 g/L [PMS] = 2 g/L [Phenol] = 25 mg/L	100% removal of phenol in 60 min	SO ₄ ^{•-}	[52]
Mn ₃ O ₄	Phenol	[Catalyst] = 0.4 g/L [PMS] = 2 g/L [Phenol] = 25 mg/L	100% removal of phenol in 20 min	SO ₄ ^{•-}	[43]
Mn ₃ O ₄ nanoparticle	Methylene blue (MB)	[Catalyst] = 0.12 g/L [PMS] = 0.94 g/L [MB] = 62 mg/L pH = 4	86.71% removal of MB in 20 min	SO ₄ ^{•-}	[94]
Mn ₃ O ₄ nano-octahedral	Ciprofloxacin (CIP)	[Catalyst] = 0.2 g/L [PMS] = 0.65 mM [CIP] = 10 mg/L pH = 7.7	100% removal of CIP in 80 min	SO ₄ ^{•-} HO [•]	[92]

Table 1-5 (continued)

Catalyst	Pollutant	Initial conditions	Reactivity	Active species	Ref.
yolk-shell Mn ₃ O ₄	Bisphenol A (BPA)	[Catalyst] = 0.1 g/L [PMS] = 0.3 g/L [BPA] = 10 mg/L pH = 5.3	87.7% of removal of BPA in 60 min	SO ₄ ^{•-} HO [•]	[97]
3D hierarchical Mn ₃ O ₄	Phenol	[Catalyst] = 0.2 g/L [PMS] = 6.5 mM [Phenol] = 20 ppm pH = 6.8	100% removal of phenol in 60 min	SO ₄ ^{•-} HO [•]	[96]
dumbbell-like Mn ₂ O ₃	Rhodamine B (RhB)	[Catalyst] = 0.25 g/L [PMS] = 0.75 g/L [RhB] = 10 mg/L	100% of removal of RhB in 30 min	SO ₄ ^{•-} HO [•] O ₂ ^{•-} ¹ O ₂	[95]
α-Mn ₂ O ₃ -cubic	Phenol	[Catalyst] = 0.4 g/L [PMS] = 2 g/L [Phenol] = 25 ppm	100% removal of phenol in 1 h	SO ₄ ^{•-}	[86]

Table 1-5 (continued)

Catalyst	Pollutant	Initial conditions	Reactivity	Active species	Ref.
γ -MnOOH nanowire	2,4-dichlorophenol (2,4-DCP)	[Catalyst] = 0.3 g/L [PMS] = 12 mM [2,4-DCP] = 100 mg/L pH = 7	98% removal of 2,4-DCP in 6 h	$\text{SO}_4^{\bullet-}$ HO^\bullet $\text{O}_2^{\bullet-}$ $^1\text{O}_2$	[90]
Ce-Mn ₂ O ₃	2,4-dichlorophenol (2,4-DCP)	[Catalyst] = 0.2 g/L [PMS] = 1.0 g/L [2,4-DCP] = 50 mg/L pH = 7	100% removal of 2,4-DCP in 90 min	$\text{SO}_4^{\bullet-}$ HO^\bullet $^1\text{O}_2$	[106]
Mn ₃ O ₄ -GO	Orange II	[Catalyst] = 50 mg/L [PMS] = 1.5 g/L [Orange II] = 30 mg/L	100% removal of Orange II in 120 min under neutral pH	$\text{SO}_4^{\bullet-}$	[107]
MnOOH@nylon	2,4-dichlorophenol (2,4-DCP)	[Catalyst]=0.76 mg/cm ² [PMS] = 138 mg/L [2,4-DCP] = 25 mg/L pH = 6.0-6.4	97.9% removal of 2,4-DCP in 2 h	$\text{SO}_4^{\bullet-}$ HO^\bullet $\text{O}_2^{\bullet-}$ $^1\text{O}_2$	[93]

Table 1-5 (continued)

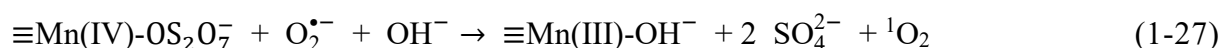
Catalyst	Pollutant	Initial conditions	Reactivity	Active species	Ref.
γ -MnOOH-rGO	Bentazone	[Catalyst] = 0.075 g/L [PMS] = 0.615 g/L [Bentazone] = 10 mg/L pH = 7, sunlight	96.1% removal of Bentazone in 90 min	HO [•] ¹ O ₂	[108]
Fe ₂ O ₃ /Mn ₂ O ₃	Tartrazine (TTZ)	[Catalyst] = 0.6 g/L [PMS] = 0.8 g/L [TTZ] = 10 mg/L pH = 6.89	97.3% removal of TTZ in 30 min	SO ₄ ^{•-} HO [•]	[105]
Mn ₂ O ₃ @Mn ₅ O ₈	4-chlorophenol (4-CP)	[Catalyst] = 0.3 g/L [PMS] = 1.5 mM [4-CP] = 80 ppm	100% removal of 4-CP in 60 min	SO ₄ ^{•-} HO [•] O ₂ ^{•-} / ¹ O ₂	[109]
Mn ₃ O ₄ -MnO ₂	Ciprofloxacin (CIP)	[Catalyst] = 0.1 g/L [PMS] = 1 mM [CIP] = 50 μ M pH = 7.0 \pm 0.1	97.6% removal of CIP in 25 min	SO ₄ ^{•-} HO [•]	[98]

Table 1-5 (continued)

Catalyst	Pollutant	Initial conditions	Reactivity	Active species	Ref.
Mn ₃ O ₄ /MOF	Rhodamine B (RhB)	[Catalyst] = 0.4 g/L [PMS] = 0.3 g/L [RhB] = 10 mg/L pH = 5.18	98% removal of RhB in 60 min	SO ₄ ^{•-} HO [•]	[99]
Fe ₃ O ₄ /Mn ₃ O ₄ /GO	Methylene Blue (MB)	[Catalyst] = 100 mg/L [PMS] = 0.3 g/L [MB] = 50 mg/L pH = 7	98.8% removal of MB in 30 min	SO ₄ ^{•-} HO [•]	[110]
α-Mn ₂ O ₃ @α-MnO ₂ -350	Phenol	[Catalyst] = 0.4 g/L [PMS] = 2.0 g/L [Phenol] = 25 mg/L pH = 3-3.5	100% removal of phenol in 25 min	SO ₄ ^{•-} HO [•]	[111]
α-Mn ₂ O ₃ @α-MnO ₂ -500	Phenol	[Catalyst] = 0.15 g/L [PMS] = 1 mM [Phenol] = 25 ppm	100% removal of phenol in 70 min	SO ₄ ^{•-} HO [•] ¹ O ₂	[112]

1.3.3 Activation of PDS by Mn(III) (oxyhydr)oxides

Single or combined Mn(III) (oxyhydr)oxides have been employed to activate PDS to remove different organic pollutants, such as phenol, p-chloroaniline (PCA), 2,4-dichlorophenol (2,4-DCP), and organic dyes (Table 1-6). The activation pathway of PDS varies with the different types of Mn(III) (oxyhydr)oxides. For example, Shabanloo et al. reported the generation of active $\text{SO}_4^{\bullet-}$ radicals in the nano- Mn_3O_4 /PDS system [113]. Since both Mn(II) and Mn(III) species are identified in the Mn_3O_4 structure, the formation of $\text{SO}_4^{\bullet-}$ was mainly attributed to the activation of PDS by Mn(II) (Eq. (1-25)). In contrast, the persulfate radical ($\text{S}_2\text{O}_8^{\bullet-}$) was produced by the reaction of PDS and Mn(III) (Eq. (1-26)). For the system of Mn_2O_3 /PDS, it is believed that the singlet oxygen was the primary active species that was responsible for the degradation of organic pollutants [114]. As demonstrated by Khan et al., one complex $\equiv\text{Mn(III/IV)-OS}_2\text{O}_7^-$ was formed between PDS and Mn_2O_3 through the inner-sphere interaction. Then, another $\text{S}_2\text{O}_8^{2-}$ was decomposed by $\equiv\text{Mn(III/IV)-OS}_2\text{O}_7^-$ to generate $\text{HO}_2^{\bullet}/\text{O}_2^{\bullet-}$ radicals. The $^1\text{O}_2$ was finally formed from the direct oxidation of $\text{O}_2^{\bullet-}$ by $\equiv\text{Mn(IV)-OS}_2\text{O}_7^-$ or the recombination of HO_2^{\bullet} and $\text{O}_2^{\bullet-}$ (Eqs. (1-27)). The pathway of $^1\text{O}_2$ formation in the system of A- Mn_2O_3 /PDS is comparable to the approach of producing $^1\text{O}_2$ in the β - MnO_2 /PDS system in which the important metastable manganese intermediate was first formed through the complex reaction between the hydroxyl group (-OH) and cleavage $\text{S}_2\text{O}_8^{2-}$ [30]. Therefore, the hydroxyl group on the surface of manganese oxides plays a significant role in PDS activation.



In comparison with Mn_3O_4 and Mn_2O_3 , γ - MnOOH presents more -OH groups on the surface leading to the high efficiency in PDS activation. For instance, Li et al. reported that γ - MnOOH exhibited higher reactivity in PDS activation for phenol oxidation in comparison with Mn_2O_3 and Mn_3O_4 [115]. The authors reported that the degradation efficiency of phenol in the γ -

MnOOH/PDS system was pH-dependent. Under the basic condition (pH 11), phenol was efficiently removed due to the generation of $\text{SO}_4^{\bullet-}$ and HO^{\bullet} radicals. However, at pH 3 and 7, the oxidative intermediate ($\equiv\text{Mn(III)}-\text{OSOOSO}_3^-$) was believed to be responsible for the removal of phenol. Although the mentioned report explained well the oxidation performance of γ -MnOOH/PMS for phenol removal, the information regarding the mechanism of PDS activation on the surface of γ -MnOOH was not given in detail. Considering this, Xu et al. conducted a further investigation focusing on the catalytic mechanism of PDS by γ -MnOOH [116]. Based on the results of chemical scavenging and ESR experiments, a non-radical mechanism was proposed. Generally, the non-radical mechanism in PDS activation was attributed to three aspects including the generation of $^1\text{O}_2$, the electron transfer process, and the catalyst surface-activated intermediates [117–121]. However, the $^1\text{O}_2$ production and electron transfer process mechanism were excluded according to the results of ESR and linear sweep voltammetry (LSV) experiments. Therefore, the γ -MnOOH surface-activated PDS molecule was verified as the main active species for the degradation of PCA. The corresponding diagram of PDS activation on the γ -MnOOH surface was shown in Figure 1-6.

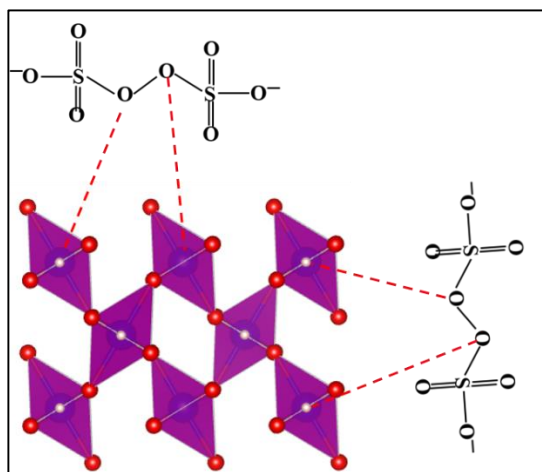


Figure 1-6. The picture of PDS activation on the surface of γ -MnOOH. The red, blue, and white balls represent oxygen, manganese, and hydrogen atoms, respectively [116].

The activation of PDS by Mn(III) (oxyhydr)oxides composites for pollutants degradation has also been reported [122–124]. For instance, Liu et al. synthesized the carbon-coated Mn_3O_4 composite ($\text{Mn}_3\text{O}_4/\text{C}$) and investigated the reactivity in the presence of PDS for 2,4-

dichlorophenol (2,4-DCP) degradation [122]. The results showed that 95 % of 2,4-DCP removal was reached in 140 min and the enhanced degradation was attributed to the existence of the defective edges of the carbon layer which facilitated the attraction and activation of PDS. The diagram of PDS activation by $\text{Mn}_3\text{O}_4/\text{C}$ composite towards 2,4-DCP degradation was shown in Figure 1-7. Rizal et al. prepared $\text{Ag}/\text{Mn}_3\text{O}_4$ and $\text{Ag}/\text{Mn}_3\text{O}_4/\text{graphene}$ composites and studied the degradation efficiency of methylene blue (MB) by synthesized catalysts activated PDS in the presence of visible light [123]. The results showed that 40 mg/L of MB was completely removed in 30 min by the system of $\text{Ag}/\text{Mn}_3\text{O}_4/\text{graphene} + \text{PDS}$ under visible light. The enhanced degradation of MB was attributed to the hampered electron-hole recombination due to the loading of Ag and graphene. Furthermore, the studies regarding the application of modified Mn_2O_3 in oxidants (such as PMS, H_2O_2) activation for contaminants removal were also reported [111,125–127]. For example, Saputra et al. prepared an egg-shaped core/shell $\alpha\text{-Mn}_2\text{O}_3@ \alpha\text{-MnO}_2$ catalyst via a hydrothermal process and investigated the catalytic activity of $\alpha\text{-Mn}_2\text{O}_3@ \alpha\text{-MnO}_2$ in heterogeneous Oxone[®] activation for phenol degradation [111]. The loaded $\alpha\text{-MnO}_2$ improved the generation of Mn(III) species through the reaction with PMS. The amount of $\text{SO}_4^{\bullet -}$ and HO^\bullet was then increased leading to the enhanced degradation of phenol. The efficient degradation of organic dye pollutants (such as Rhodamine B (RB) and Congo Red (CR)) by bimetallic $\text{Mn}_2\text{O}_3\text{-Co}_3\text{O}_4/\text{carbon}$ catalyst activated Fenton-like reaction was also reported [126]. The superior reactivity of $\text{Mn}_2\text{O}_3\text{-Co}_3\text{O}_4/\text{C}$ catalyst in H_2O_2 activation for RB and CR degradation was attributed to the good synergistic effect between Co_3O_4 and Mn_2O_3 as well as the interaction between metal oxides and carbon. However, the investigation regarding the activation of PDS by modified $\alpha\text{-Mn}_2\text{O}_3$ has been less reported. The same effect was also observed for the $\gamma\text{-MnOOH}$ -based composites. This might be attributed to the distinct activation way of PDS by $\alpha\text{-Mn}_2\text{O}_3$ or $\gamma\text{-MnOOH}$ compared with Mn_3O_4 .

In summary, Mn_3O_4 can activate PDS to generate $\text{SO}_4^{\bullet -}$ through radical mechanisms, while the activation of PDS by $\alpha\text{-Mn}_2\text{O}_3$ and $\gamma\text{-MnOOH}$ is processed in a non-radical mechanism with the generation of $^1\text{O}_2$ and catalyst surface-activated PDS substances. For the activation of PDS by Mn(III) (oxyhydr)oxides composites, the Mn_3O_4 -based composites have shown good

catalytic performance in PDS activation for pollutants degradation. In comparison, the activation of PDS by modified α - Mn_2O_3 or γ - MnOOH catalysts needs to be further investigated.

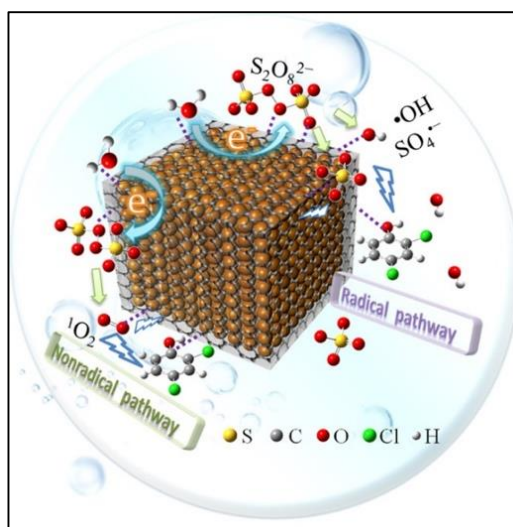


Figure 1-7. The diagram of PDS activation by $\text{Mn}_3\text{O}_4/\text{C}$ composite towards 2,4-D degradation [122].

Table 1-6. Summary of PDS activation by Mn(III) (oxyhydr)oxides.

Catalyst	Pollutant	Initial conditions	Reactivity	Active species	Ref.
γ -MnOOH	P-chloroaniline (PCA)	[Catalyst] = 0.4 g/L [PDS] = 2.5 mM [PCA] = 0.5 mM pH = 4.2	100% removal of PCA in 180 min	γ -MnOOH-PDS complex	[116]
γ -MnOOH	Phenol	[Catalyst] = 1 g/L [PDS] = 2 g/L [Phenol] = 100 mg/L	91.86% removal of phenol in 360 min under neutral pH	γ -MnOOH-PDS complex	[115]
α -Mn ₂ O ₃	Phenol	[Catalyst] = 0.2 g/L [PDS] = 2 mM [Phenol] = 12 ppm pH = 3.2	100% removal of phenol in 70 min	¹ O ₂	[114]
Nano-Mn ₃ O ₄	Furfural	[Catalyst] = 1.2 g/L [PDS] = 6.34 mM [Furfural] = 50 mg/L pH = 4.82	91.14% of furfural removal in 60 min	SO ₄ ^{•-}	[113]

Table 1-6 (continued)

Catalyst	Pollutant	Initial conditions	Reactivity	Active species	Ref.
Ag/Mn ₃ O ₄ -5 G	Methylene Blue (MB)	[Catalyst] = 0.5 g/L [PDS] = 12 mM [MB] = 40 mg/L pH = 3, visible-light	100% of MB removal in 30 min	SO ₄ ^{•-} HO [•]	[123]
Mn ₂ O ₃ /Mn ₃ O ₄ /MnO ₂	Orange II	[Catalyst] = 0.4 g/L [PDS] = 2 g/L [Orange II] = 20 mg/L	95% removal of Orange II in 50 min	SO ₄ ^{•-} HO [•]	[128]
0.5-Mn ₃ O ₄ /C-T4	2,4-dichlorophenol (2,4-DCP)	[Catalyst] = 0.2 g/L [PDS] = 2 g/L [2,4-DCP] = 100 mg/L pH = 6.37	95% removal of 2,4-DCP in 140 min	SO ₄ ^{•-} HO [•] ¹ O ₂	[122]
γ-Fe ₂ O ₃ /Mn ₃ O ₄	Rhodamine B (RhB)	[Catalyst] = 50 mg/L [PDS] = 50 mg/L [RhB] = 10 mg/L pH = 4.5	97.5% removal of RhB in 150 min	SO ₄ ^{•-} HO [•]	[124]

1.3.4 Influence factors for Mn(III) (oxyhydr)oxides reactivity

1.3.4.1 The effect of pH

The Mn(III) (oxyhydr)oxides -mediated activation of PDS/PMS can be affected by solution pH in different ways. For example, influencing the property of charge on the surface of catalysts, changing the ionic forms of PDS/PMS and pollutants molecules, as well as altering the reduction potential of active radicals.

First, the solution pH can affect the interaction between catalyst and PDS/PMS and pollutants through changing the electrostatic effect. The point of zero charges (PZC) of catalyst and the acid dissociation constant (pKa) of radical precursors and contaminants are two important parameters that are used to recognize the charge type on the surface of catalysts and the ionic situation of oxidants and pollutants in solution. For instance, when the solution pH is equal to the PZC value of catalyst, the amounts of positive and negative charges on the surface of catalyst are equal (i.e. the surface charge of catalyst is zero). When the solution pH is higher than the PZC value of catalyst, the surface charges of catalyst are negative. On the contrary, if the solution pH is lower than catalyst PZC value, the surface of catalyst will be positively charged [129]. The same situation is suitable for the analysis of the ionic form of oxidants and pollutants. The PZC values of commonly used Mn(III) (oxyhydr)oxides and the pKa values of PMS/PDS and some typical pollutants are summarized in Table 1-7. The impacts of solution pH on the interaction between Mn(III) (oxyhydr)oxides and PDS/PMS and pollutants have been reported. For example, Zhao et al. reported that the adsorption and degradation of ciprofloxacin (CIP) by synthesized Mn_3O_4 - MnO_2 composite were facilitated at neutral pH solution [98]. The results were explained by the enhanced electrostatic attraction between Mn_3O_4 - MnO_2 and CIP. The PZC value of Mn_3O_4 - MnO_2 composite was measured at 2.5, thus, in the solution pH 7, the surface of the catalyst was negatively charged. In comparison, the pKa of CIP was 8.7-10.58 leading to the formation of positively charged CIP ions in the neutral pH solution. Therefore, the electrostatic attraction between the negative catalyst and the positive CIP was improved

resulting in a facilitating degradation of CIP. The same phenomenon was also reported in the studies of PDS activation by γ -MnOOH/ α -Mn₂O₃ for pollutants degradation [114,116].

Second, the transformation of radicals also influenced the reactivity of Mn(III) (oxyhydr)oxides for pollutants degradation. For instance, the reported conversion of $\text{SO}_4^{\bullet-}$ to HO^\bullet under the basic solution (as shown in (Eq. (1-18))) can have a significant impact. Since the reduction potential value of HO^\bullet under natural pH is lower than that in acidic solution (1.8 vs 2.7V) [130], and the lifetime of HO^\bullet is shorter than $\text{SO}_4^{\bullet-}$ (20 ns vs 30-40 μ s) [131], thus the transformation from $\text{SO}_4^{\bullet-}$ ($E = 2.6$ V) to HO^\bullet under alkaline solution might lead to a decrease of pollutants degradation. In addition, the leaching of Mn^{2+} from Mn(III) (oxyhydr)oxides in an acidic condition also should be taken into consideration for the activation of sulfate compounds (PMS/PDS).

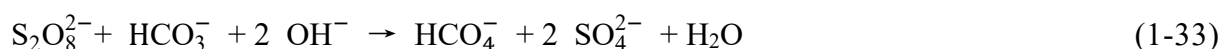
Table 1-7. The PZC values of Mn(III) (oxyhydr)oxides and pKa values of PMS/PDS and pollutants.

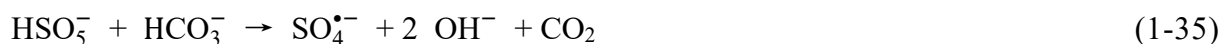
Catalysts	PZC	Reference
α -Mn ₂ O ₃	4.7	[114,132]
γ -MnOOH	3.4	[116]
Mn ₃ O ₄	5.6-7.34	[98,113,133]
Oxidants	pKa	Reference
PMS	9.4	[134]
PDS	-3.5	[135]
Pollutants	pKa	Reference
Phenol	9.98	[136]
Bisphenol A	9.6-10.2	[137]
2,4-dichlorophenol	9.4	[109]
Ciprofloxacin	8.70-10.58	[98,138]
p-Chloroaniline	4.2	[116,139]
4-Chlorophenol	9.29	[140]
Orange II	11.4	[128]

1.3.4.2 The effect of inorganic anions

Inorganic anions are ubiquitous in various aquatic compartments. It is reported that inorganic anions can suppress the degradation of pollutants in Mn(III) (oxyhydr)oxides activated PMS/PDS systems through competing with pollutants for radicals' reactivity. Thus, to evaluate the applicability of the Mn(III) (oxyhydr)oxides + PMS/PDS system in different water matrices, the influence of inorganic anions on the removal of pollutants has been investigated by many researchers [93,108,114,123,141]. In this section, the effect of inorganic anions such as carbonate/bicarbonate ions ($\text{CO}_3^{2-}/\text{HCO}_3^-$), chloride ions (Cl^-), and nitrate (NO_3^-)/nitrite ions (NO_2^-) on the reactivity of Mn(III) (oxyhydr)oxides was summarized.

Carbonate (CO_3^{2-})/bicarbonate (HCO_3^-) can react with $\text{SO}_4^{\bullet-}$ and HO^\bullet to generate less reactive carbonate radical ($\text{CO}_3^{\bullet-}$) and bicarbonate radical (HCO_3^\bullet) (Eqs. (1-28)-(1-32)) leading to the inhibited degradation of pollutants [142]. However, although the redox potential of $\text{CO}_3^{\bullet-}$ is low (1.59V vs NHE), it can still selectively degrade some organic pollutants with a reaction rate of 10^3 - $10^9 \text{ M}^{-1}\text{s}^{-1}$ [143,144]. In addition, the presence of carbonate and bicarbonate ions can affect the stability of oxidants. For example, PDS can be activated by HCO_3^- to generate peroxymonocarbonate (HCO_4^-) (Eq. (1-33)) [145]. Similarly, PMS can be catalyzed by both CO_3^{2-} and HCO_3^- to form active radicals and HCO_4^- (Eqs. (1-34)-(1-36)). Furthermore, the solution pH can be changed in the presence of carbonate/bicarbonate ions, which can affect the reactivity of Mn(III) (oxyhydr)oxides in PMS/PDS activation as discussed in *section 1.3.4.1*.





Chloride ion (Cl^-) exists widely in various water bodies including surface water, groundwater, and industrial wastewater [146]. The influence of Cl^- on the degradation of organic pollutants by sulfate radical-based AOPs (SR-AOP) was reported by previous studies [147–150]. Generally, Cl^- can react with $\text{SO}_4^{\bullet-}$ to generate Cl^\bullet which can react with another Cl^- to form $\text{Cl}_2^{\bullet-}$ (Eqs. (1-37)-(1-38)) [149]. Both Cl^\bullet and $\text{Cl}_2^{\bullet-}$ have low reduction potentials ($E_0 = 2.4$ & 2.0 V) in comparison with $\text{SO}_4^{\bullet-}$, thus the consumption of $\text{SO}_4^{\bullet-}$ by Cl^- leads to the decrease of organic pollutants degradation [151,152]. However, Cl^\bullet was believed to own higher selectivity on electron-rich compounds than nonselective $\text{SO}_4^{\bullet-}$, which can offset the negative effect of Cl^- on $\text{SO}_4^{\bullet-}$ [153]. Therefore, the conflicting effect of Cl^- on organic pollutants in SR-AOP might be attributed to the different reactivity of pollutants with Cl^\bullet and $\text{Cl}_2^{\bullet-}$. In addition, the reactivity of HO^\bullet can also be suppressed by Cl^- due to the formation of low active radical $\text{ClOH}^{\bullet-}$ (Eq.(1-39)) [154].



Nitrate (NO_3^-) and nitrite (NO_2^-) can be commonly found in various water matrices [146]. Both NO_3^- and NO_2^- can react with $\text{SO}_4^{\bullet-}$ to generate low reactive NO_3^\bullet ($E_0 = 2.3$ - 2.5 V) and NO_2^\bullet radicals ($E_0 = 1.03$ V) (Eqs. (1-40)-(1-41)) [7]. The reaction rate constants of $\text{SO}_4^{\bullet-}$ with NO_3^- and NO_2^- are $5 \times 10^4 \text{ M}^{-1} \text{ s}^{-1}$ and $8.8 \times 10^8 \text{ M}^{-1} \text{ s}^{-1}$, respectively [155]. Thus, NO_2^- , compared with NO_3^- , has higher reactivity with $\text{SO}_4^{\bullet-}$ and increased its consumption. In addition and in a similar way, NO_2^- was also reported as the sink of HO^\bullet radicals (Eq. (1-42)) [156].



Given the conducted summary, some further perspectives are proposed. First, the activation mechanism of PDS by α - Mn_2O_3 needs to be further investigated. Although the previous study already identified the generation of $^1\text{O}_2$ in α - Mn_2O_3 /PDS system using the ESR and quenching experiments, the detailed catalytic process of PDS on the surface of Mn_2O_3 was not reported. Second, the application of α - Mn_2O_3 or γ - MnOOH based composites in PDS activation can be investigated to understand the synergistic performance of α - Mn_2O_3 or γ - MnOOH with other loaded materials (such as active carbon, graphene, and transition metals) and improve the reactivity of α - Mn_2O_3 / γ - MnOOH in PDS activation.

1.4 Manganese dioxide activated AOPs

The activation of radical precursors (e.g. H_2O_2 , PDS, and PMS) by manganese dioxides (MnO_2) for recalcitrant pollutants degradation has been widely reported. MnO_2 possesses different structures (such as 1D, 2D, 3D- MnO_2), crystal phases (such as α -, β -, γ -, δ - MnO_2), morphologies (such as rod, wire, tube, and flower) and crystal facets (such as 100, 110 and 310) [78]. The reactivity of MnO_2 is affected by a combination of several structural factors, including surface area, crystallinity, crystal facets, and the fraction of $\text{Mn}^{3+}/\text{Mn}^{4+}$ [155]. Therefore, in this section, the activation mechanism of different oxidants (i.e. H_2O_2 , PDS, and PMS) by various MnO_2 will be discussed. Moreover, the limitation and prospective of MnO_2 -activated AOPs will be presented.

1.4.1 Activation of H_2O_2 by MnO_2

Manganese oxides with various surface and crystal morphologies exhibit high activities for H_2O_2 decomposition to degrade recalcitrant organic contaminants under mild conditions. Moreover, due to the wide existence of manganese oxides in the natural environment, the understanding of H_2O_2 decomposition by manganese oxides toward organic pollutants degradation is of crucial significance.

The mechanism of H_2O_2 activation by MnO_2 has been investigated by many researchers. Watts et al. studied the primary reactive species generated in the system of pyrolusite (β - MnO_2)/ H_2O_2 using carbon tetrachloride (CT) as the chemical probe [157]. The high degradation of CT

in the system of β -MnO₂/H₂O₂ suggested that a transient species other than hydroxyl radical was generated in the reaction, because CT was unreactive with hydroxyl radical. The transient species generated in β -MnO₂/H₂O₂ system was further identified as the reductants including superoxide (O₂^{•-}) and hydroperoxide anion (HO₂⁻) at a near neutral pH [158]. The same activation mechanism of H₂O₂ by β -MnO₂ was also reported by Do et al., and the application of the β -MnO₂/H₂O₂ system for the oxidation of toluene sorbed on activated carbon (AC) was also investigated [159,160]. He et al. employed the β -MnO₂/H₂O₂ system to efficiently clean the fouled ultrafiltration membranes through simultaneously generating reactive free radicals and oxygen [161]. In addition to β -MnO₂, γ -MnO₂ also exhibited the reactivity on H₂O₂ activation. For instance, Mitchell et al. reported the efficient degradation of perfluorooctanoic acid (PFOA) in the γ -MnO₂ activated H₂O₂ system at neutral pH, and the dominate reactive species were identified as O₂^{•-} and HO₂⁻ [162]. Furman et al. reported that γ -MnO₂-catalyzed decomposition of H₂O₂ promoted the degradation of the superoxide probe hexachloroethane (HCA), and the electron spin resonance spectroscopy (ESR) confirmed that superoxide was the dominant reactive species generated in γ -MnO₂/H₂O₂ system.

As discussed before, the reactivity of manganese oxides on oxidants activation was influenced by their crystal structures. Kim et al. investigated the degradation of methylene blue (MB) dye by various manganese oxide nanorods (α -, β -, γ -, δ -MnO₂) activated H₂O₂ [163]. The results showed that the catalytic activity of MnO₂ nanorods followed the order of γ -MnO₂ > β -MnO₂ > α -MnO₂ > δ -MnO₂. The high reactivity of γ -MnO₂ was assigned to its largest surface area and pore volume which facilitating more efficient mass transport and reactants diffusion. However, the catalytic reactivity of MnO₂ is not simply function of the surface area. The crystallinity of catalyst was considered as the key factor of affecting the reactivity of MnO₂. For example, the crystalline β -MnO₂ with lowest surface area ($9.2 \pm 0.8 \text{ m}^2\text{g}^{-1}$) showed the greater activity than amorphous δ -MnO₂ with the surface area of $47.8 \pm 2.9 \text{ m}^2\text{g}^{-1}$. Therefore, the reactivity of MnO₂ in the activation of H₂O₂ is highly dependent on their crystal structures. In addition, Sabri et al. investigated the effect of structure and disorder on the oxidative and catalytic reactivity of manganese (III/IV) oxides against three substrates including methylene blue, hydrogen

peroxide and water [164]. The results showed that disorder destabilizes the materials thermodynamically, making them stronger chemical oxidants but not necessarily better catalysts. The schematic diagram of the reaction of H_2O_2 and MnO_2 was presented in Figure 1-8. In summary of these studies, it can get one clear conclusion that the crystal structure of MnO_2 plays a vital role in the activation of H_2O_2 . Specifically, the crystal MnO_2 has the good ability in catalyzing H_2O_2 , while the disordered MnO_2 is a good oxidant in H_2O_2 oxidation. This conclusion was also verified by other studies. For instance, Huang et al. reported that in comparison to α -, β -, γ -, λ - MnO_2 , δ - MnO_2 showed the highest efficiency in bisphenol A oxidation [85].

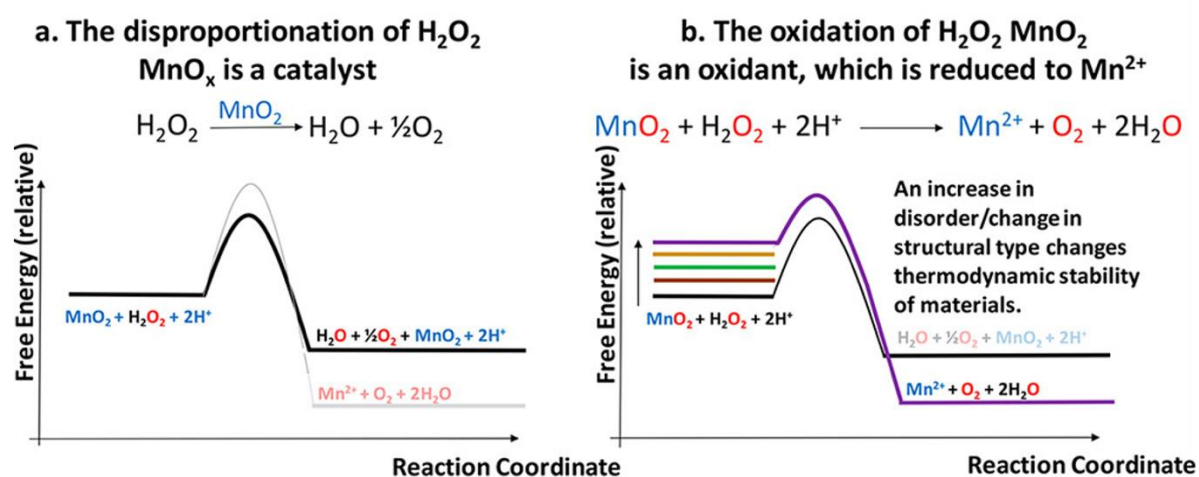


Figure 1-8. The schematic diagram of the reaction of H_2O_2 with MnO_2 . (a) disproportionation of H_2O_2 in which MnO_2 acts as a catalyst and (b) oxidation H_2O_2 in which MnO_2 acts as a sacrificial oxidant that is concomitantly reduced to Mn^{2+} .

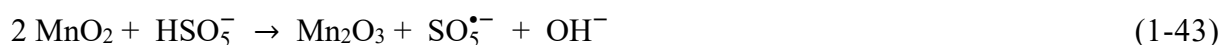
Natural H_2O_2 can be formed in oceanic and atmospheric systems as well as the subsurface environment with the assistance of light, natural organic matter, and biological-mediated processes [165–167]. The concentration of H_2O_2 in aquatic environments ranges from nM to μM [167–170]. Natural manganese oxides such as birnessite have highly catalytic and oxidative reactivity in the degradation of organic pollutants. Despite the catalyzed decomposition of hydrogen peroxide by MnO_2 has been well investigated [158,171,172], knowledge is very limited on the effect of H_2O_2 on the reactivity of birnessite at environmental levels of H_2O_2 .

Thus, the influence of H₂O₂ on the reactivity of birnessite under environmentally relevant conditions was investigated in this thesis using bisphenol A as the model pollutant.

1.4.2 Activation of PMS and PDS by MnO₂

In the past two decades, the sulfate radical-based advanced oxidation processes (SR-AOPs) have drawn increasing attention, and manganese oxides have been proven to be effective catalysts for activating PMS and PDS to degrade various recalcitrant organic pollutants. This section focuses on the discussion of the activation mechanism of PDS and PMS by various MnO₂. Both radical and nonradical mechanisms are presented, and the influence factors of the catalytic and oxidative reactivity of MnO₂ are also discussed.

Manganese dioxides have been used to activate PMS to remove various contaminants, such as bisphenol A, phenol, ibuprofen, and organic dyes [40,173,174]. It is generally considered that sulfate and hydroxyl radicals were generated in the system of MnO₂/PMS, as shown in Eqs. (1-43)-(1-44) and Eqs. (1-17)-(1-18) [39]. The presence of SO₄^{•-} and HO[•] was not verified in the early study of the activation process of PMS by MnO₂ [174,175]. However, with the development of technology, the identification of reactive radicals (such as SO₄^{•-} and HO[•]) and non-radical species (such as singlet oxygen and reactive surface complex) were achieved in various MnO₂/PMS systems [176,177]. For instance, Huang et al. reported the generation of SO₄^{•-}, HO[•], and ¹O₂ in the activation of PMS by α-, β-, γ-, δ-MnO₂ under acidic pH [40]. Wang et al. demonstrated that the degradation of BPA by amorphous MnO₂-activated PMS was not attributed to the generation of SO₄^{•-}, HO[•], and ¹O₂. On the contrary, the formed reactive complexes between amorphous MnO₂ and PMS was believed to be responsible for BPA degradation [137].

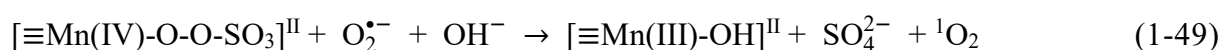
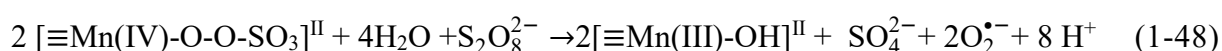
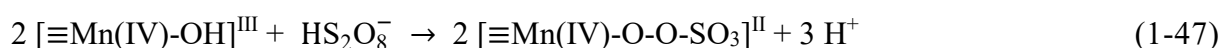


The catalytic and oxidative reactivity of MnO₂ can be influenced by several factors, such as the crystalline structure, morphology, and dimension. For example, Saputra et al. reported that α-MnO₂ exhibited higher activity than β- and γ-MnO₂ in PMS activation for phenol degradation[175]. The differences in polymorphs were attributed to the distinct tunnel sizes,

oxygen liability, and MnO_6 edges. A similar conclusion was observed by Huang et al. that showed the reactivity of MnO_2 in PMS activation followed a decreased order: $\alpha\text{-MnO}_2 > \gamma\text{-MnO}_2 > \beta\text{-MnO}_2 > \delta\text{-MnO}_2$ [40]. To reveal the different reactivity of MnO_2 in PMS activation, some physicochemical properties of MnO_2 were investigated. The results showed that the catalytic reactivity of MnO_2 was linearly correlated with the Mn(III) content, Mn average oxidation state (AOS) and conductivity. MnO_2 morphologies also affected the exposed crystal facets and specific surface areas (SSA), which further impacted the PMS activation activity. Wang et al. compared the catalytic reactivity of $\alpha\text{-MnO}_2$ with different shapes (i.e. nanowire, nanorod and nanotube) in PMS activation [176]. The results showed that the $\alpha\text{-MnO}_2$ in the shape of nanowire exhibited a better catalytic performance in PMS activation than $\alpha\text{-MnO}_2$ in nanorod and nanotube shape, which can be ascribed to the higher surface areas and exposed high-energy facet (001) of $\alpha\text{-MnO}_2$ (nanowire). The nanostructures of MnO_2 in different dimensions also exerted a considerable effect on the catalytic activity. For instance, Deng et al. synthesized different dimensional $\alpha\text{-MnO}_2$ including 0D nanoparticle, 1D nanorod, and 3D nanoflower and investigated the reactivity of $\alpha\text{-MnO}_2$ in PMS activation for ciprofloxacin (CIP) degradation [178]. The result showed that the catalytic activity of $\alpha\text{-MnO}_2$ followed an order of $\alpha\text{-MnO}_2$ nanoflowers $>$ $\alpha\text{-MnO}_2$ nanorods $>$ $\alpha\text{-MnO}_2$ nanoparticles $>$ commercial MnO_2 . The variances were explained by the difference in surface area and crystallinity. Based on the above studies, one short conclusion can be provided that the catalytic activity of MnO_2 in PMS activation relies on various physicochemical properties including the morphology of nanostructures, crystal structure, exposed crystal facets, surface area, Mn(III) content, and oxygen species.

The activation of PDS by MnO_2 for organic pollutants degradation was reported by a few papers. For example, Zhao et al. investigated the degradation of 2,4-dichlorophenol in an aqueous solution by $\alpha\text{-MnO}_2$ nanowire-activated PDS. The results of quenching tests and ESR experiments showed that the $\text{SO}_4^{\bullet-}$ and HO^\bullet were responsible for the removal of 2,4-dichlorophenol in the system of $\alpha\text{-MnO}_2$ /PDS. The activation mechanism is as shown in Eqs. (1-45)-(1-46) and Eqs. (1-17)-(1-18). Zhu et al. reported the efficient degradation of phenol by

β -MnO₂-activated PDS, and the primary reactive oxygen species was identified as singlet oxygen [30]. The generation of ¹O₂ was originated from the direct oxidation or recombination of superoxide ions (Eqs. (1-47)-(1-50)). However, in comparison to PMS, the investigation of PDS activation by MnO₂ was less reported. To better understand the catalytic activity of various MnO₂ in PDS activation, more experiments should be conducted.



In summary, the common oxidants (i.e. H₂O₂, PDS, and PMS) can be activated by various MnO₂ to generate reactive species for the removal of organic pollutants. The oxidative and catalytic activity of MnO₂ can be influenced by various factors, such as the crystalline structure, morphology, and exposed crystal facets. With the increase of H₂O₂ concentration in the natural environment, the influence of H₂O₂ on the reactivity of MnO₂ for organic pollutant removal should be considered. Moreover, more investigation regarding the activation of PDS by different structural MnO₂ should be conducted to improve the understanding of the PDS activation mechanism.

1.5 Emerging pollutants

Emerging pollutants (EPs) have been defined as a group of natural or synthetic chemicals occurring in water bodies throughout the globe, which are potential to cause environmental problems and pose a threat to the safety of the ecosystem and the health of human beings [179]. The EPs reported in previous literature include different types of organic pollutants, for example, disinfection by-products, pesticides, pharmaceuticals and personal care products (PPCPs), endocrine-disrupting compounds (EDCs), industrial chemicals, artificial sweeteners and food additives, sunscreens, and flame retardants [180]. With the progress of urbanization,

industrialization, and number of people, a large number of EPs-containing products were consumed and discharged. The concentration of EPs detected in waters ranges from ng/L to $\mu\text{g/L}$ [181]. However, the conventional treatment technologies in wastewater treatment plants (WWTPs) cannot completely degrade these recalcitrant pollutants leading to the occurrence and increase of EPs in waters [182]. Among the EPs, the PPCPs and EDCs have attracted increasing attention due to their close connection with the daily life of humans.

PPCPs represent a diverse array of chemical materials which are used for therapeutic purposes in humans and animals and used in personal hygiene and for make-up [2]. Common PPCPs include caffeine (CAF), carbamazepine, diclofenac, ibuprofen, iopamidol, musk, clofibrac acid, triclosan, and phthalates [2]. PPCPs can be released from various anthropogenic activities such as industry, agriculture, farm, and domestic life [183]. The ubiquitous presence and ecological risk of PPCPs have attracted growing attention from environmental research. The widespread of PPCPs in the environment can be attributed to the overuse of PPCPs, the low removal efficiency of WWTPs, and the stable structures of PPCPs [184]. Although the amount of PPCPs detected in water is in trace range, the detrimental effect of PPCPs has been reported through the toxic tests in fishes and plants [185,186].

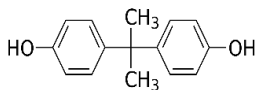
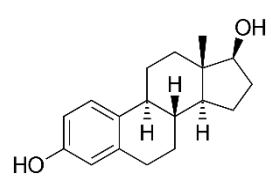
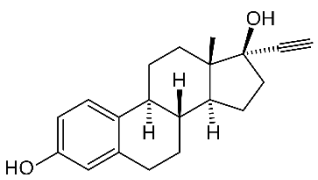
Endocrine-disrupting compounds (EDCs) are defined by the Environmental Protection Agency (EPA, U.S.) as a series of chemical substances which can interfere with the normal hormone function in bodies of aquatic organisms and human beings [187]. Trace concentrations of EDCs have been detected in various waters including wastewater, sediments, drinking water, groundwater, and surface water [188,189]. The persistence of EDCs in water poses a high risk to the security of the environment, especially to aquatic organisms and humans [190]. It was reported that the increase of some incidence and diseases (such as heart diseases, diabetes, metabolic disorders, and cancer) was related to the presence of EDCs in the environment [183]. The EDCs can be divided into natural substances, synthetic substances, and heavy metals [189]. The sources of EDCs are attributed to various ways including (1) food contact materials and diet; (2) cosmetics and personal care products; (3) consumer goods and cleaning products; (4) pesticides; (5) drugs [191].

1.5.1 Source and harm of BPA, E2 and EE2

BPA, E2, and EE2 as the representative EDCs were largely adopted as the model contaminants for the investigation of catalysts' reactivity. The physicochemical properties of these three EDCs are listed in Table 1-8. BPA has been widely used as an industrial additive and raw material to fabricate polymer materials such as polycarbonates, epoxy resins, and polysulfone resins [192]. All of these polymer materials are further used to produce industrial products including beverage containers, drink bottles, baby bottles, food cans, food containers, dental sealants, thermal paper, flame retardants, building materials, electronic products, and medical equipments [193]. The produced BPA-containing products greatly improve the life quality of humans. However, with the rise of anthropogenic activities, the consumption and discharging of BPA products was increased leading to the widespread distribution of BPA in the natural environment. The concentrations of BPA detected in surface waters, groundwaters, and drinking waters were listed in Table 1-9. It was reported that BPA may cause different diseases, such as human breast cancer, hormonal disorder, metabolic imbalance, diabetes, and abnormal reproductive and developmental behavior [194]. The exposure route of humans to EDC is summarized in Figure 1-9.

E2 and EE2 are natural and synthetic estrogens separately with strong estrogenic activity even at very low concentrations [195]. Natural E2 plays an important role in the development of female secondary sex characteristics and reproduction. Synthetic EE2 and E2 are widely used to produce oral contraceptives [196]. The occurrence of E2 and EE2 has been identified in various waters including wastewater, surface water, underground water, and drinking water (Table 1-9) [197]. The presence of E2 and EE2 in water poses a high risk to the health of humans due to their strongly adverse effects. It was reported that the sexuality of fish can be changed on the exposure of E2, even at a very low concentration (0.5 ng/L) [198]. EE2 was also reported to have detrimental effects on fishes, for example, hormonal imbalance, intersex, increased egg mortality, and infertility [199]. To avoid the potential harm of EE2 to humans, EE2 has been listed in the latest Japanese Drinking Water Quality Standard [200].

Table 1-8. The physicochemical properties of BPA, E2, and EE2 [189].

Priorities	Bisphenol A (BPA)	17 β -estradiol (E2)	17 α -Ethinylestradiol (EE2)
CAS number	80-05-7	50-28-2	57-63-6
Chemical formula	C ₁₅ H ₁₆ O ₂	C ₁₈ H ₂₄ O ₂	C ₂₀ H ₂₄ O ₂
Chemical structure			
Molar weight	228.9 g mol ⁻¹	272.4 g mol ⁻¹	296.4 g mol ⁻¹
Water Solubility ¹	120 mg L ⁻¹	3.6 mg L ⁻¹	11 mg L ⁻¹
Log Kow ²	3.32	4.01	3.67
pKa	9.6	10.71	10.4

¹The values of water solubility are achieved at 25°C.

²Log Kow: Octanol-water partition coefficient.

Table 1-9. The occurrence of EDCs in various water systems.

Target EDCs	Concentration (ng L ⁻¹)		
	Surface water	Groundwater	Drinking water
BPA	< 8.8-1000 [201]	n.d-7 [202]	0.5-2.0 [203]
	0.5-14 [203]	n.d-930 [204]	5.0 [205]
	65-295 [205]		
E2	< 0.3-5.5 [206]	n.d-45 [207]	0.2-2.1 [203]
	0.6-1.0 [208]	6-66 [209]	2.6 [210]
	< 0.8-1.0 [201]	13-80 [211]	n.d-2.6 [212]
EE2	< 0.1-4.3 [206]	n.d-0.94 [204]	0.15-0.5 [203]
	< 0.3-0.4 [201]		
	0.1-5.1 [203]		

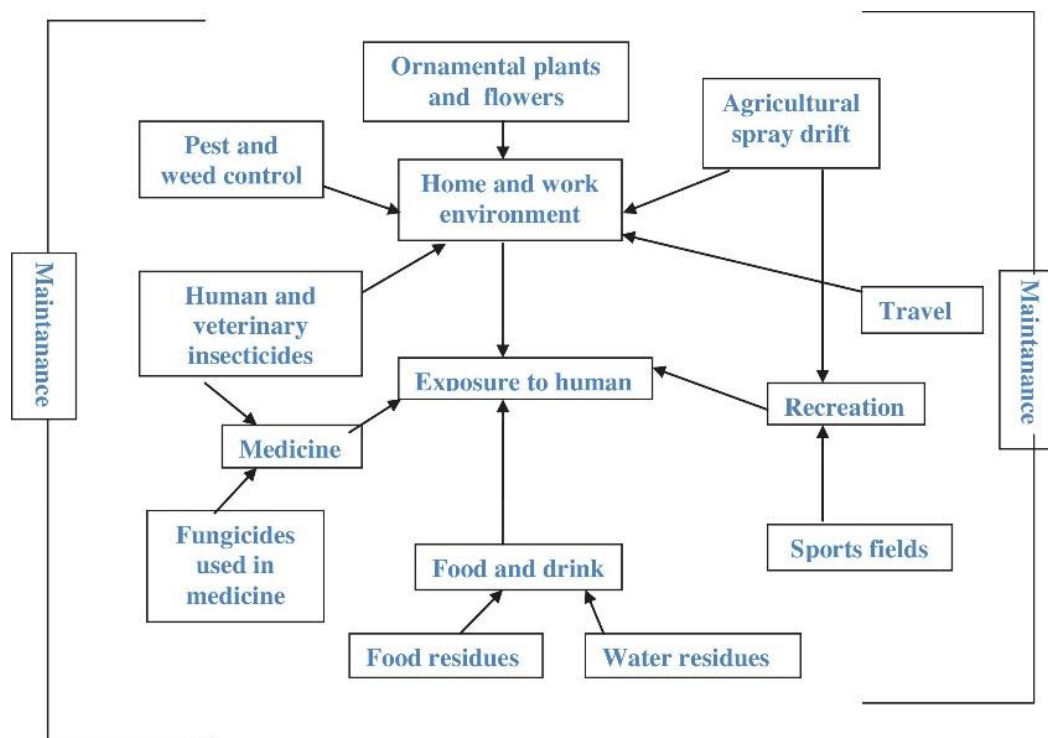


Figure 1-9. Different exposure routes of humans to EDCs [191].

1.5.2 Source and harm of CAF

Caffeine (CAF) is a substance that belongs to the methylxanthines class of drugs [213]. The physicochemical properties of CAF are listed in Table 1-10. CAF can be found in various beverages (e.g. coffee, cocoa, tea, chocolate, soft drinks, and energy drinks) and prescription or over-the-counter drugs (e.g. cold medicines, analgesics, stimulants, and illegal drugs) [213]. It was evaluated that the average caffeine consumption is around 70 mg per person in the world [213]. Over 90% of adults are regular consumers of CAF, with a mean daily intake of 227 mg [214]. However, it is worth noting that approximately 5% of ingested caffeine cannot be digested and absorbed by human bodies and eventually excreted in urine [213]. Given the above, with the increase in the consumption of caffeinated products, a large of CAF has been discharged into the waters. The concentration of CAF detected in different water matrices ranges from ng/L to $\mu\text{g/L}$ (Table1-11). The adverse effects of CAF on aquatic organisms and human beings have been widely reported, such as depression, cardiovascular disorders, and hyperactivity [215]. An appropriate CAF intake for adults recommended by the European Food Safety Authority (EFSA) is 400 mg per day [216].

Table 1-10. The physicochemical properties of CAF [213].

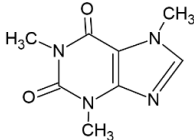
Priorities	Caffeine (CAF)
CAS number	58-08-2
Chemical formula	C ₈ H ₁₀ N ₄ O ₂
Chemical structure	
Density	1.23 g cm ⁻³
Molar weight	194.19 g mol ⁻¹
Water Solubility	20 g L ⁻¹
Log Kow	-0.04 to 0.01
Melting point	235 to 238°C
pKa	10.4

Table 1-11. CAF concentration in different water matrices.

Waters	CAF concentration	Reference
Rivers and lakes	130-370 ng L ⁻¹ (USA)	[217]
	median 530 ng L ⁻¹ , up to 880 ng L ⁻¹ (Germany)	[218]
	up to 171 ng L ⁻¹ (Netherlands)	[219]
	160 ng L ⁻¹ (Greece)	[220]
Groundwater	10-80 ng L ⁻¹ , median 30 ng L ⁻¹ (USA)	[221]
	<40 ng L ⁻¹ (wells deeper than 10 m, USA)	[222]
Seawater	2-16 ng L ⁻¹ (North Sea)	[223]
	5-71 ng L ⁻¹ (Massachusetts Bay)	[217]
	140-1600 ng L ⁻¹ (Boston Harbor)	[217]
WWTPs, influent water	20 µg L ⁻¹ (USA)	[217]
	147 µg L ⁻¹ (Germany)	[218]
WWTPs, effluent water	6.7 µg L ⁻¹ (USA)	[217]
	0.19 ± 0.09 µg L ⁻¹ , up to 1.9 µg L ⁻¹ (Germany)	[218]
	2 µg L ⁻¹ (Sweden)	[224]

1.5.3 Treatment technologies for EDCs and CAF

The occurrence of EDCs and CAF in water has attracted considerable research attention owing to the potential safety risks they posed to the ecosystem and human beings. To improve the removal efficiency of EDCs and CAF in waters, various water treatment technologies have been developed as shown in Table 1-12. The efficient degradation of EDCs and CAF by these technologies demonstrated the potential of AOPs in the treatment of wastewater. Moreover, EDCs and CAF are proved to be good probes for testing the efficiency of various wastewater treatment technologies.

Table 1-12 Technologies for EDCs and CAF degradation.

Pollutants	Technologies	Reference
BPA	UV/TiO ₂	[225]
	MnO ₂ /PMS	[40]
	CuFe ₂ O ₄ /PMS	[226]
	Electro-Fenton	[227]
	Fe(III)-EDDS*/H ₂ O ₂	[228]
E2/EE2	Fenton	[229]
	Ozonation	[230]
	UV/H ₂ O ₂	[231]
	UV/PDS	[232]
	Photo-Fenton	[233]
	Bio-electro-Fenton	[234]
CAF	O ₃ /UV	[235]
	UV/H ₂ O ₂	[236]
	UVC/PDS	[237]
	Solar/TiO ₂	[238]
	Photo-Fenton	[239]
	Solar/Fe/H ₂ O ₂ /EDDS	[240]

*EDDS: Ethylene diamine-*N,N'*-disuccinic acid

Reference

- [1] T.K. Kasonga, M.A.A. Coetzee, I. Kamika, V.M. Ngole-Jeme, M.N. Benteke Momba, Endocrine-disruptive chemicals as contaminants of emerging concern in wastewater and surface water: A review, *Journal of Environmental Management*. 277 (2021) 111485. <https://doi.org/10.1016/j.jenvman.2020.111485>.
- [2] S. Hena, L. Gutierrez, J.-P. Croué, Removal of pharmaceutical and personal care products (PPCPs) from wastewater using microalgae: A review, *Journal of Hazardous Materials*. 403 (2021) 124041. <https://doi.org/10.1016/j.jhazmat.2020.124041>.
- [3] W.H. Glaze, J.-W. Kang, D.H. Chapin, The Chemistry of Water Treatment Processes Involving Ozone, Hydrogen Peroxide and Ultraviolet Radiation, *Ozone: Science & Engineering*. 9 (1987) 335–352. <https://doi.org/10.1080/01919518708552148>.
- [4] C. Lai, X. Shi, L. Li, M. Cheng, X. Liu, S. Liu, B. Li, H. Yi, L. Qin, M. Zhang, N. An, Enhancing iron redox cycling for promoting heterogeneous Fenton performance: A review, *Science of The Total Environment*. 775 (2021) 145850. <https://doi.org/10.1016/j.scitotenv.2021.145850>.
- [5] W.-D. Oh, Z. Dong, T.-T. Lim, Generation of sulfate radical through heterogeneous catalysis for organic contaminants removal: Current development, challenges and prospects, *Applied Catalysis B: Environmental*. 194 (2016) 169–201. <https://doi.org/10.1016/j.apcatb.2016.04.003>.
- [6] G. Boczkaj, A. Fernandes, Wastewater treatment by means of advanced oxidation processes at basic pH conditions: A review, *Chemical Engineering Journal*. 320 (2017) 608–633. <https://doi.org/10.1016/j.cej.2017.03.084>.
- [7] S. Giannakis, K.-Y.A. Lin, F. Ghanbari, A review of the recent advances on the treatment of industrial wastewaters by Sulfate Radical-based Advanced Oxidation Processes (SR-AOPs), *Chemical Engineering Journal*. 406 (2021) 127083. <https://doi.org/10.1016/j.cej.2020.127083>.
- [8] M. Muruganandham, R.P.S. Suri, S. Jafari, M. Sillanpää, G.-J. Lee, J.J. Wu, M. Swaminathan, Recent Developments in Homogeneous Advanced Oxidation Processes for Water and Wastewater Treatment, *International Journal of Photoenergy*. 2014 (2014) e821674. <https://doi.org/10.1155/2014/821674>.

- [9] G. Goor, J. Glenneberg, S. Jacobi, J. Dadabhoy, E. Candido, Hydrogen Peroxide, in: Ullmann's Encyclopedia of Industrial Chemistry, Wiley-VCH Verlag GmbH & Co. KGaA, Weinheim, Germany, 2019: pp. 1–40. https://doi.org/10.1002/14356007.a13_443.pub3.
- [10] P.A. Giguère, Molecular association and structure of hydrogen peroxide, *Journal of Chemical Education*. 60 (1983) 399. <https://doi.org/10.1021/ed060p399>.
- [11] A.B. Laursen, I.C. Man, O.L. Trinhammer, J. Rossmeisl, S. Dahl, The Sabatier Principle Illustrated by Catalytic H₂O₂ Decomposition on Metal Surfaces, *Journal of Chemical Education*. 88 (2011) 1711–1715. <https://doi.org/10.1021/ed101010x>.
- [12] J.O. Bockris, L.F. Oldfield, The oxidation-reduction reactions of hydrogen peroxide at inert metal electrodes and mercury cathodes, *Transactions of the Faraday Society*. 51 (1955) 249. <https://doi.org/10.1039/tf9555100249>.
- [13] T. Poux, A. Bonnefont, A. Ryabova, G. Kéranguéven, G. A. Tsirlina, E. R. Savinova, Electrocatalysis of hydrogen peroxide reactions on perovskite oxides: experiment versus kinetic modeling, *Physical Chemistry Chemical Physics*. 16 (2014) 13595–13600. <https://doi.org/10.1039/C4CP00341A>.
- [14] M. Abdollahi, A. Hosseini, Hydrogen Peroxide, in: P. Wexler (Ed.), *Encyclopedia of Toxicology (Third Edition)*, Academic Press, Oxford, 2014: pp. 967–970. <https://doi.org/10.1016/B978-0-12-386454-3.00736-3>.
- [15] S. Waclawek, H.V. Lutze, K. Grübel, V.V.T. Padil, M. Černík, Dionysios.D. Dionysiou, Chemistry of persulfates in water and wastewater treatment: A review, *Chemical Engineering Journal*. 330 (2017) 44–62. <https://doi.org/10.1016/j.cej.2017.07.132>.
- [16] Y.-Y. Ahn, E. Yun, Heterogeneous metals and metal-free carbon materials for oxidative degradation through persulfate activation: A review of heterogeneous catalytic activation of persulfate related to oxidation mechanism, *Korean Journal of Chemical Engineering*. 36 (2019) 1767–1779. <https://doi.org/10.1007/s11814-019-0398-4>.
- [17] Y. Li, H. Dong, L. Li, L. Tang, R. Tian, R. Li, J. Chen, Q. Xie, Z. Jin, J. Xiao, S. Xiao, G. Zeng, Recent advances in waste water treatment through transition metal sulfides-based

advanced oxidation processes, *Water Research*. 192 (2021) 116850. <https://doi.org/10.1016/j.watres.2021.116850>.

[18] S. Guerra-Rodríguez, E. Rodríguez, D.N. Singh, J. Rodríguez-Chueca, Assessment of Sulfate Radical-Based Advanced Oxidation Processes for Water and Wastewater Treatment: A Review, *Water*. 10 (2018) 1828. <https://doi.org/10.3390/w10121828>.

[19] G.P. Anipsitakis, D.D. Dionysiou, Radical Generation by the Interaction of Transition Metals with Common Oxidants, *Environmental Science and Technology*. 38 (2004) 3705–3712. <https://doi.org/10.1021/es035121o>.

[20] A.D. Bokare, W. Choi, Review of iron-free Fenton-like systems for activating H₂O₂ in advanced oxidation processes, *Journal of Hazardous Materials*. 275 (2014) 121–135. <https://doi.org/10.1016/j.jhazmat.2014.04.054>.

[21] A.N. Soon, B.H. Hameed, Heterogeneous catalytic treatment of synthetic dyes in aqueous media using Fenton and photo-assisted Fenton process, *Desalination*. 269 (2011) 1–16. <https://doi.org/10.1016/j.desal.2010.11.002>.

[22] H. Zhou, H. Zhang, Y. He, B. Huang, C. Zhou, G. Yao, B. Lai, Critical review of reductant-enhanced peroxide activation processes: Trade-off between accelerated Fe³⁺/Fe²⁺ cycle and quenching reactions, *Applied Catalysis B: Environmental*. 286 (2021) 119900. <https://doi.org/10.1016/j.apcatb.2021.119900>.

[23] J.J. Lingane, W.D. Larson, The Standard Electrode Potential of Silver, *Journal of the American Chemical Society*. 58 (1936) 2647–2648. <https://doi.org/10.1021/ja01303a503>.

[24] Z. Hu, C.-F. Leung, Y.-K. Tsang, H. Du, H. Liang, Y. Qiu, T.-C. Lau, A recyclable polymer-supported ruthenium catalyst for the oxidative degradation of bisphenol A in water using hydrogen peroxide, *New Journal of Chemistry*. 35 (2011) 149–155. <https://doi.org/10.1039/C0NJ00583E>.

[25] K.S. Yamaguchi, D.T. Sawyer, The Redox Chemistry of Manganese(III) and -(IV) Complexes, *Israel Journal of Chemistry*. 25 (1985) 164–176. <https://doi.org/10.1002/ijch.198500026>.

- [26] R.J. Watts, J. Sarasa, F.J. Loge, A.L. Teel, Oxidative and Reductive Pathways in Manganese-Catalyzed Fenton's Reactions, *Journal of Environmental Engineering*. 131 (2005) 158–164. [https://doi.org/10.1061/\(ASCE\)0733-9372\(2005\)131:1\(158\)](https://doi.org/10.1061/(ASCE)0733-9372(2005)131:1(158)).
- [27] A.D. Bokare, W. Choi, Chromate-Induced Activation of Hydrogen Peroxide for Oxidative Degradation of Aqueous Organic Pollutants, *Environmental Science and Technology*. 44 (2010) 7232–7237. <https://doi.org/10.1021/es903930h>.
- [28] K. Chen, D. Xue, Reaction Route to the Crystallization of Copper Oxides, *Applied Science and Convergence Technology*. 23 (2014) 14–26. <https://doi.org/10.5757/ASCT.2014.23.1.14>.
- [29] S.K. Ling, S. Wang, Y. Peng, Oxidative degradation of dyes in water using $\text{Co}^{2+}/\text{H}_2\text{O}_2$ and Co^{2+} /peroxymonosulfate, *Journal of Hazardous Materials*. 178 (2010) 385–389. <https://doi.org/10.1016/j.jhazmat.2010.01.091>.
- [30] S. Zhu, X. Li, J. Kang, X. Duan, S. Wang, Persulfate Activation on Crystallographic Manganese Oxides: Mechanism of Singlet Oxygen Evolution for Nonradical Selective Degradation of Aqueous Contaminants, *Environmental Science and Technology*. 53 (2019) 307–315. <https://doi.org/10.1021/acs.est.8b04669>.
- [31] Z.-G. Zhou, H.-M. Du, Z. Dai, Y. Mu, L.-L. Tong, Q.-J. Xing, S.-S. Liu, Z. Ao, J.-P. Zou, Degradation of organic pollutants by peroxymonosulfate activated by MnO_2 with different crystalline structures: Catalytic performances and mechanisms, *Chemical Engineering Journal*. 374 (2019) 170–180. <https://doi.org/10.1016/j.cej.2019.05.170>.
- [32] R. Xiao, Z. Luo, Z. Wei, S. Luo, R. Spinney, W. Yang, D.D. Dionysiou, Activation of peroxymonosulfate/persulfate by nanomaterials for sulfate radical-based advanced oxidation technologies, *Current Opinion in Chemical Engineering*. 19 (2018) 51–58. <https://doi.org/10.1016/j.coche.2017.12.005>.
- [33] Y. Yao, C. Xu, J. Qin, F. Wei, M. Rao, S. Wang, Synthesis of Magnetic Cobalt Nanoparticles Anchored on Graphene Nanosheets and Catalytic Decomposition of Orange II, *Industrial & Engineering Chemistry Research*. 52 (2013) 17341–17350. <https://doi.org/10.1021/ie401690h>.

- [34] C. Tan, N. Gao, Y. Deng, J. Deng, S. Zhou, J. Li, X. Xin, Radical induced degradation of acetaminophen with Fe_3O_4 magnetic nanoparticles as heterogeneous activator of peroxymonosulfate, *Journal of Hazardous Materials*. 276 (2014) 452–460. <https://doi.org/10.1016/j.jhazmat.2014.05.068>.
- [35] J. Liu, J. Zhou, Z. Ding, Z. Zhao, X. Xu, Z. Fang, Ultrasound irradiation enhanced heterogeneous activation of peroxymonosulfate with Fe_3O_4 for degradation of azo dye, *Ultrasonics Sonochemistry*. 34 (2017) 953–959. <https://doi.org/10.1016/j.ultsonch.2016.08.005>.
- [36] S. Wang, S. Gao, J. Tian, Q. Wang, T. Wang, X. Hao, F. Cui, A stable and easily prepared copper oxide catalyst for degradation of organic pollutants by peroxymonosulfate activation, *Journal of Hazardous Materials*. 387 (2020) 121995. <https://doi.org/10.1016/j.jhazmat.2019.121995>.
- [37] Y.-C. Cho, R.-Y. Lin, Y.-P. Lin, Degradation of 2,4-dichlorophenol by CuO-activated peroxydisulfate: Importance of surface-bound radicals and reaction kinetics, *Science of The Total Environment*. 699 (2020) 134379. <https://doi.org/10.1016/j.scitotenv.2019.134379>.
- [38] X. Chen, J. Chen, X. Qiao, D. Wang, X. Cai, Performance of nano- Co_3O_4 /peroxymonosulfate system: Kinetics and mechanism study using Acid Orange 7 as a model compound, *Applied Catalysis B: Environmental*. 80 (2008) 116–121. <https://doi.org/10.1016/j.apcatb.2007.11.009>.
- [39] F. Ghanbari, M. Moradi, Application of peroxymonosulfate and its activation methods for degradation of environmental organic pollutants: Review, *Chemical Engineering Journal*. 310 (2017) 41–62. <https://doi.org/10.1016/j.cej.2016.10.064>.
- [40] J. Huang, Y. Dai, K. Singewald, C.-C. Liu, S. Saxena, H. Zhang, Effects of MnO_2 of different structures on activation of peroxymonosulfate for bisphenol A degradation under acidic conditions, *Chemical Engineering Journal*. 370 (2019) 906–915. <https://doi.org/10.1016/j.cej.2019.03.238>.
- [41] S. Zhang, X. Zhao, H. Niu, Y. Shi, Y. Cai, G. Jiang, Superparamagnetic Fe_3O_4 nanoparticles as catalysts for the catalytic oxidation of phenolic and aniline compounds, *Journal of Hazardous Materials*. 167 (2009) 560–566. <https://doi.org/10.1016/j.jhazmat.2009.01.024>.

- [42] Y. Wang, Y. Gao, L. Chen, H. Zhang, Goethite as an efficient heterogeneous Fenton catalyst for the degradation of methyl orange, *Catalysis Today*. 252 (2015) 107–112. <https://doi.org/10.1016/j.cattod.2015.01.012>.
- [43] E. Saputra, S. Muhammad, H. Sun, H.-M. Ang, M.O. Tadé, S. Wang, A comparative study of spinel structured Mn_3O_4 , Co_3O_4 and Fe_3O_4 nanoparticles in catalytic oxidation of phenolic contaminants in aqueous solutions, *Journal of Colloid and Interface Science*. 407 (2013) 467–473. <https://doi.org/10.1016/j.jcis.2013.06.061>.
- [44] G.P. Anipsitakis, E. Stathatos, D.D. Dionysiou, Heterogeneous Activation of Oxone Using Co_3O_4 , *The Journal of Physical Chemistry B*. 109 (2005) 13052–13055. <https://doi.org/10.1021/jp052166y>.
- [45] P. Shi, R. Su, S. Zhu, M. Zhu, D. Li, S. Xu, Supported cobalt oxide on graphene oxide: Highly efficient catalysts for the removal of Orange II from water, *Journal of Hazardous Materials*. 229–230 (2012) 331–339. <https://doi.org/10.1016/j.jhazmat.2012.06.007>.
- [46] Q. Yang, H. Choi, Y. Chen, D.D. Dionysiou, Heterogeneous activation of peroxymonosulfate by supported cobalt catalysts for the degradation of 2,4-dichlorophenol in water: The effect of support, cobalt precursor, and UV radiation, *Applied Catalysis B: Environmental*. 77 (2008) 300–307. <https://doi.org/10.1016/j.apcatb.2007.07.020>.
- [47] Y.B. Wang, P.T. Wu, B.A. Engel, S.K. Sun, Application of water footprint combined with a unified virtual crop pattern to evaluate crop water productivity in grain production in China, *Science of The Total Environment*. 497–498 (2014) 1–9. <https://doi.org/10.1016/j.scitotenv.2014.07.089>.
- [48] P. Shukla, H. Sun, S. Wang, H.M. Ang, M.O. Tadé, Co-SBA-15 for heterogeneous oxidation of phenol with sulfate radical for wastewater treatment, *Catalysis Today*. 175 (2011) 380–385. <https://doi.org/10.1016/j.cattod.2011.03.005>.
- [49] F. Ji, C. Li, L. Deng, Performance of CuO/Oxone system: Heterogeneous catalytic oxidation of phenol at ambient conditions, *Chemical Engineering Journal*. 178 (2011) 239–243. <https://doi.org/10.1016/j.cej.2011.10.059>.

- [50] F. Ghanbari, M. Moradi, M. Manshour, Textile wastewater decolorization by zero valent iron activated peroxymonosulfate: Compared with zero valent copper, *Journal of Environmental Chemical Engineering*. 2 (2014) 1846–1851. <https://doi.org/10.1016/j.jece.2014.08.003>.
- [51] F. Ji, C. Li, X. Wei, J. Yu, Efficient performance of porous Fe₂O₃ in heterogeneous activation of peroxymonosulfate for decolorization of Rhodamine B, *Chemical Engineering Journal*. 231 (2013) 434–440. <https://doi.org/10.1016/j.cej.2013.07.053>.
- [52] E. Saputra, S. Muhammad, H. Sun, H.-M. Ang, M.O. Tadé, S. Wang, Manganese oxides at different oxidation states for heterogeneous activation of peroxymonosulfate for phenol degradation in aqueous solutions, *Applied Catalysis B: Environmental*. 142–143 (2013) 729–735. <https://doi.org/10.1016/j.apcatb.2013.06.004>.
- [53] B.D. Yirsaw, M. Megharaj, Z. Chen, R. Naidu, Environmental application and ecological significance of nano-zero valent iron, *Journal of Environmental Sciences*. 44 (2016) 88–98. <https://doi.org/10.1016/j.jes.2015.07.016>.
- [54] C.-C. Lin, Y.-H. Chen, Feasibility of using nanoscale zero-valent iron and persulfate to degrade sulfamethazine in aqueous solutions, *Separation and Purification Technology*. 194 (2018) 388–395. <https://doi.org/10.1016/j.seppur.2017.10.073>.
- [55] R. Li, X. Jin, M. Megharaj, R. Naidu, Z. Chen, Heterogeneous Fenton oxidation of 2,4-dichlorophenol using iron-based nanoparticles and persulfate system, *Chemical Engineering Journal*. 264 (2015) 587–594. <https://doi.org/10.1016/j.cej.2014.11.128>.
- [56] Y.-G. Kang, H. Yoon, W. Lee, E. Kim, Y.-S. Chang, Comparative study of peroxide oxidants activated by nZVI: Removal of 1,4-Dioxane and arsenic(III) in contaminated waters, *Chemical Engineering Journal*. 334 (2018) 2511–2519. <https://doi.org/10.1016/j.cej.2017.11.076>.
- [57] C. Zhu, G. Fang, D.D. Dionysiou, C. Liu, J. Gao, W. Qin, D. Zhou, Efficient transformation of DDTs with Persulfate Activation by Zero-valent Iron Nanoparticles: A Mechanistic Study, *Journal of Hazardous Materials*. 316 (2016) 232–241. <https://doi.org/10.1016/j.jhazmat.2016.05.040>.

- [58] L. Zhao, Y. Ji, D. Kong, J. Lu, Q. Zhou, X. Yin, Simultaneous removal of bisphenol A and phosphate in zero-valent iron activated persulfate oxidation process, *Chemical Engineering Journal*. 303 (2016) 458–466. <https://doi.org/10.1016/j.cej.2016.06.016>.
- [59] D. Ding, C. Liu, Y. Ji, Q. Yang, L. Chen, C. Jiang, T. Cai, Mechanism insight of degradation of norfloxacin by magnetite nanoparticles activated persulfate: Identification of radicals and degradation pathway, *Chemical Engineering Journal*. 308 (2017) 330–339. <https://doi.org/10.1016/j.cej.2016.09.077>.
- [60] J. Zhang, R. Zhang, B. Wang, L. Ling, Insight into the adsorption and dissociation of water over different CuO(111) surfaces: The effect of surface structures, *Applied Surface Science*. 364 (2016) 758–768. <https://doi.org/10.1016/j.apsusc.2015.12.211>.
- [61] H. Li, J. Guo, L. Yang, Y. Lan, Degradation of methyl orange by sodium persulfate activated with zero-valent zinc, *Separation and Purification Technology*. 132 (2014) 168–173. <https://doi.org/10.1016/j.seppur.2014.05.015>.
- [62] Y. Yao, J. Zhang, M. Gao, M. Yu, Y. Hu, Z. Cheng, S. Wang, Activation of persulfates by catalytic nickel nanoparticles supported on N-doped carbon nanofibers for degradation of organic pollutants in water, *Journal of Colloid and Interface Science*. 529 (2018) 100–110. <https://doi.org/10.1016/j.jcis.2018.05.077>.
- [63] T. Zhang, Y. Chen, Y. Wang, J. Le Roux, Y. Yang, J.-P. Croué, Efficient Peroxydisulfate Activation Process Not Relying on Sulfate Radical Generation for Water Pollutant Degradation, *Environmental Science and Technology*. 48 (2014) 5868–5875. <https://doi.org/10.1021/es501218f>.
- [64] J.E. Post, Manganese oxide minerals: Crystal structures and economic and environmental significance, *Proceedings of the National Academy of Sciences*. 96 (1999) 3447–3454. <https://doi.org/10.1073/pnas.96.7.3447>.
- [65] C.K. Remucal, M. Ginder-Vogel, A critical review of the reactivity of manganese oxides with organic contaminants, *Environmental Science: Processes and Impacts*. 16 (2014) 1247. <https://doi.org/10.1039/c3em00703k>.

- [66] C.R. Myers, K.H. Nealson, Bacterial manganese reduction and growth with manganese oxide as the sole electron acceptor, *Science*. 240 (1988) 1319–1321. <https://doi.org/10.1126/science.240.4857.1319>.
- [67] J.J. Morgan, Manganese in natural waters and earth's crust: its availability to organisms, *Metal Ions in Biological Systems*. 37 (2000) 1–34.
- [68] S. Madison, B.M. Tebo, A. Mucci, B. Sundby, G.W. Luther, Abundant porewater Mn(III) is a major component of the sedimentary redox system, *Science*. 341 (2013) 875–878. <https://doi.org/10.1126/science.1241396>.
- [69] D.R. Learman, B.M. Voelker, A.I. Vazquez-Rodriguez, C.M. Hansel, Formation of manganese oxides by bacterially generated superoxide, *Nature Geoscience*. 4 (2011) 95–98. <https://doi.org/10.1038/ngeo1055>.
- [70] W.G. Sunda, S.A. Huntsman, G.R. Harvey, Photoreduction of manganese oxides in seawater and its geochemical and biological implications, *Nature*. 301 (1983) 234–236. <https://doi.org/10.1038/301234a0>.
- [71] J.J. Morgan, Kinetics of reaction between O₂ and Mn(II) species in aqueous solutions, *Geochimica et Cosmochimica Acta*. 69 (2005) 35–48. <https://doi.org/10.1016/j.gca.2004.06.013>.
- [72] R.J. Gilkes, R.M. McKenzie, *Geochemistry and Mineralogy of Manganese in Soils, Manganese in Soils and Plants*. (1988) 23–35. https://doi.org/10.1007/978-94-009-2817-6_3.
- [73] N. Miyata, Y. Tani, K. Maruo, H. Tsuno, M. Sakata, K. Iwahori, Manganese(IV) Oxide Production by *Acremonium* sp. Strain KR21-2 and Extracellular Mn(II) Oxidase Activity, *Applied and Environmental Microbiology*. 72 (2006) 6467–6473. <https://doi.org/10.1128/AEM.00417-06>.
- [74] A. Manceau, M.A. Marcus, S. Grangeon, M. Lanson, B. Lanson, A.-C. Gaillot, S. Skanthakumar, L. Soderholm, Short-range and long-range order of phyllo-manganate nanoparticles determined using high-energy X-ray scattering, *Journal of Applied Crystallography*. 46 (2013) 193–209. <https://doi.org/10.1107/S0021889812047917>.

- [75] A. Perner, K. Holl, D. Ilic, M. Wohlfahrt-Mehrens, A New MnO_x Cathode Material for Rechargeable Lithium Batteries, *European Journal of Inorganic Chemistry*. 2002 (2002) 1108–1114. [https://doi.org/10.1002/1099-0682\(200205\)2002:5<1108:AID-EJIC1108>3.0.CO;2-0](https://doi.org/10.1002/1099-0682(200205)2002:5<1108:AID-EJIC1108>3.0.CO;2-0).
- [76] C. Zener, Interaction Between the *d* Shells in the Transition Metals, *Phys. Rev.* 81 (1951) 440–444. <https://doi.org/10.1103/PhysRev.81.440>.
- [77] J.M. Ko, K.M. Kim, Electrochemical properties of MnO₂/activated carbon nanotube composite as an electrode material for supercapacitor, *Materials Chemistry and Physics*. 114 (2009) 837–841. <https://doi.org/10.1016/j.matchemphys.2008.10.047>.
- [78] S. Zhu, S.-H. Ho, C. Jin, X. Duan, S. Wang, Nanostructured manganese oxides: natural/artificial formation and their induced catalysis for wastewater remediation, *Environmental Science: Nano*. 7 (2020) 368–396. <https://doi.org/10.1039/C9EN01250H>.
- [79] K. Lin, W. Liu, J. Gan, Oxidative Removal of Bisphenol A by Manganese Dioxide: Efficacy, Products, and Pathways, *Environmental Science and Technology*. 43 (2009) 3860–3864. <https://doi.org/10.1021/es900235f>.
- [80] I. Saratovsky, P.G. Wightman, P.A. Pastén, J.-F. Gaillard, K.R. Poepelmeier, Manganese oxides: parallels between abiotic and biotic structures, *Journal of the American Chemical Society*. 128 (2006) 11188–11198. <https://doi.org/10.1021/ja062097g>.
- [81] S.K. Ghosh, Diversity in the Family of Manganese Oxides at the Nanoscale: From Fundamentals to Applications, *ACS Omega*. 5 (2020) 25493–25504. <https://doi.org/10.1021/acsomega.0c03455>.
- [82] Q. Li, X. Huang, G. Su, M. Zheng, C. Huang, M. Wang, C. Ma, D. Wei, The Regular/Persistent Free Radicals and Associated Reaction Mechanism for the Degradation of 1,2,4-Trichlorobenzene over Different MnO₂ Polymorphs, *Environmental Science and Technology*. 52 (2018) 13351–13360. <https://doi.org/10.1021/acs.est.8b03789>.
- [83] H. Yan, Q. Shen, Y. Sun, S. Zhao, R. Lu, M. Gong, Y. Liu, X. Zhou, X. Jin, X. Feng, X. Chen, D. Chen, C. Yang, Tailoring Facets of α -Mn₂O₃ Microcrystalline Catalysts for Enhanced Selective Oxidation of Glycerol to Glycolic Acid, *ACS Catalysis*. (2021) 6371–6383. <https://doi.org/10.1021/acscatal.1c01566>.

- [84] P. Wu, X. Jin, Y. Qiu, D. Ye, Recent Progress of Thermocatalytic and Photo/Thermocatalytic Oxidation for VOCs Purification over Manganese-based Oxide Catalysts, *Environmental Science and Technology*. 55 (2021) 4268–4286. <https://doi.org/10.1021/acs.est.0c08179>.
- [85] J. Huang, S. Zhong, Y. Dai, C.-C. Liu, H. Zhang, Effect of MnO₂ Phase Structure on the Oxidative Reactivity toward Bisphenol A Degradation, *Environmental Science and Technology*. 52 (2018) 11309–11318. <https://doi.org/10.1021/acs.est.8b03383>.
- [86] E. Saputra, S. Muhammad, H. Sun, H.-M. Ang, M.O. Tadé, S. Wang, Shape-controlled activation of peroxymonosulfate by single crystal α -Mn₂O₃ for catalytic phenol degradation in aqueous solution, *Applied Catalysis B: Environmental*. 154–155 (2014) 246–251. <https://doi.org/10.1016/j.apcatb.2014.02.026>.
- [87] L. Cheng, Y. Men, J. Wang, H. Wang, W. An, Y. Wang, Z. Duan, J. Liu, Crystal facet-dependent reactivity of α -Mn₂O₃ microcrystalline catalyst for soot combustion, *Applied Catalysis B: Environmental*. 204 (2017) 374–384. <https://doi.org/10.1016/j.apcatb.2016.11.041>.
- [88] F. Ji, Y. Men, J. Wang, Y. Sun, Z. Wang, B. Zhao, X. Tao, G. Xu, Promoting diesel soot combustion efficiency by tailoring the shapes and crystal facets of nanoscale Mn₃O₄, *Applied Catalysis B: Environmental*. 242 (2019) 227–237. <https://doi.org/10.1016/j.apcatb.2018.09.092>.
- [89] J. Liu, L. Jiang, T. Zhang, J. Jin, L. Yuan, G. Sun, Activating Mn₃O₄ by Morphology Tailoring for Oxygen Reduction Reaction, *Electrochimica Acta*. 205 (2016) 38–44. <https://doi.org/10.1016/j.electacta.2016.04.103>.
- [90] D. He, Y. Li, C. Lyu, L. Song, W. Feng, S. Zhang, New insights into MnOOH/peroxymonosulfate system for catalytic oxidation of 2,4-dichlorophenol: Morphology dependence and mechanisms, *Chemosphere*. 255 (2020) 126961. <https://doi.org/10.1016/j.chemosphere.2020.126961>.
- [91] Z. Fan, Z. Wang, J.-W. Shi, C. Gao, G. Gao, B. Wang, Y. Wang, X. Chen, C. He, C. Niu, Charge-redistribution-induced new active sites on (0 0 1) facets of α -Mn₂O₃ for significantly enhanced selective catalytic reduction of NO_x by NH₃, *Journal of Catalysis*. 370 (2019) 30–37. <https://doi.org/10.1016/j.jcat.2018.12.001>.

- [92] F. Wang, M. Xiao, X. Ma, S. Wu, M. Ge, X. Yu, Insights into the transformations of Mn species for peroxymonosulfate activation by tuning the Mn_3O_4 shapes, *Chemical Engineering Journal*. 404 (2021) 127097. <https://doi.org/10.1016/j.cej.2020.127097>.
- [93] H. Zhang, X. Wang, Y. Li, K. Zuo, C. Lyu, A novel $MnOOH$ coated nylon membrane for efficient removal of 2,4-dichlorophenol through peroxymonosulfate activation, *Journal of Hazardous Materials*. 414 (2021) 125526. <https://doi.org/10.1016/j.jhazmat.2021.125526>.
- [94] R. Shokoohi, M. Khazaei, K. Godini, G. Azarian, Z. Latifi, L. Javadimanesh, H. Zolghadr Nasab, Degradation and mineralization of methylene blue dye by peroxymonosulfate/ Mn_3O_4 nanoparticles using central composite design: Kinetic study, *Inorganic Chemistry Communications*. 127 (2021) 108501. <https://doi.org/10.1016/j.inoche.2021.108501>.
- [95] Y. Li, D. Li, S. Fan, T. Yang, Q. Zhou, Facile template synthesis of dumbbell-like Mn_2O_3 with oxygen vacancies for efficient degradation of organic pollutants by activating peroxymonosulfate, *Catalysis Science & Technology*. 10 (2020) 864–875. <https://doi.org/10.1039/C9CY01849B>.
- [96] Q. Wang, Y. Li, Z. Shen, X. Liu, C. Jiang, Facile synthesis of three-dimensional Mn_3O_4 hierarchical microstructures for efficient catalytic phenol oxidation with peroxymonosulfate, *Applied Surface Science*. 495 (2019) 143568. <https://doi.org/10.1016/j.apsusc.2019.143568>.
- [97] L. Zhang, T. Tong, N. Wang, W. Ma, B. Sun, J. Chu, K.A. Lin, Y. Du, Facile Synthesis of Yolk–Shell Mn_3O_4 Microspheres as a High-Performance Peroxymonosulfate Activator for Bisphenol A Degradation, *Industrial & Engineering Chemistry Research*. 58 (2019) 21304–21311. <https://doi.org/10.1021/acs.iecr.9b03814>.
- [98] Z. Zhao, J. Zhao, C. Yang, Efficient removal of ciprofloxacin by peroxymonosulfate/ Mn_3O_4 - MnO_2 catalytic oxidation system, *Chemical Engineering Journal*. 327 (2017) 481–489. <https://doi.org/10.1016/j.cej.2017.06.064>.
- [99] L. Hu, G. Deng, W. Lu, Y. Lu, Y. Zhang, Peroxymonosulfate activation by Mn_3O_4 /metal-organic framework for degradation of refractory aqueous organic pollutant rhodamine B, *Chinese Journal of Catalysis*. 38 (2017) 1360–1372. [https://doi.org/10.1016/S1872-2067\(17\)62875-4](https://doi.org/10.1016/S1872-2067(17)62875-4).

- [100] R. Shokoohi, M. Foroughi, Z. Latifi, H. Goljani, A. Ansari, M.R. Samarghandi, D. Nematollahi, Comparing the performance of the peroxymonosulfate/ Mn_3O_4 and three-dimensional electrochemical processes for methylene blue removal from aqueous solutions: Kinetic studies, *Colloid and Interface Science Communications*. 42 (2021) 100394. <https://doi.org/10.1016/j.colcom.2021.100394>.
- [101] A.N. Yermakov, B.M. Zhitomirsky, G.A. Poskrebyshv, D.M. Sozurakov, The branching ratio of peroxomonosulfate radicals (SO_5^-) self-reaction aqueous solution, *The Journal of Physical Chemistry*. 97 (1993) 10712–10714. <https://doi.org/10.1021/j100143a031>.
- [102] D.F. Evans, M.W. Upton, Studies on singlet oxygen in aqueous solution. Part 3. The decomposition of peroxy-acids, *Journal of the Chemical Society, Dalton Transactions*. (1985) 1151–1153. <https://doi.org/10.1039/DT9850001151>.
- [103] D.L. Ball, J.O. Edwards, The Kinetics and Mechanism of the Decomposition of Caro's Acid. I, *Journal of the American Chemical Society*. 78 (1956) 1125–1129. <https://doi.org/10.1021/ja01587a011>.
- [104] C. Chen, M. Xie, L. Kong, W. Lu, Z. Feng, J. Zhan, Mn_3O_4 nanodots loaded g- C_3N_4 nanosheets for catalytic membrane degradation of organic contaminants, *Journal of Hazardous Materials*. 390 (2020) 122146. <https://doi.org/10.1016/j.jhazmat.2020.122146>.
- [105] G. Chen, L.-C. Nengzi, Y. Gao, G. Zhu, J. Gou, X. Cheng, Degradation of tartrazine by peroxymonosulfate through magnetic $\text{Fe}_2\text{O}_3/\text{Mn}_2\text{O}_3$ composites activation, *Chinese Chemical Letters*. (2020) S1001841720300930. <https://doi.org/10.1016/j.cclet.2020.02.033>.
- [106] N. Tian, X. Tian, Y. Nie, C. Yang, Z. Zhou, Y. Li, Enhanced 2, 4-dichlorophenol degradation at pH 3–11 by peroxymonosulfate via controlling the reactive oxygen species over Ce substituted 3D Mn_2O_3 , *Chemical Engineering Journal*. 355 (2019) 448–456. <https://doi.org/10.1016/j.cej.2018.08.183>.
- [107] Y. Yao, C. Xu, S. Yu, D. Zhang, S. Wang, Facile Synthesis of Mn_3O_4 -Reduced Graphene Oxide Hybrids for Catalytic Decomposition of Aqueous Organics, *Industrial & Engineering Chemistry Research*. 52 (2013) 3637–3645. <https://doi.org/10.1021/ie303220x>.

- [108] N. Li, R. Li, Y. Yu, J. Zhao, B. Yan, G. Chen, Efficient degradation of bentazone via peroxymonosulfate activation by 1D/2D γ -MnOOH-rGO under simulated sunlight: Performance and mechanism insight, *Science of The Total Environment*. 741 (2020) 140492. <https://doi.org/10.1016/j.scitotenv.2020.140492>.
- [109] A. Khan, S. Zou, T. Wang, J. Ifthikar, A. Jawad, Z. Liao, A. Shahzad, A. Ngambia, Z. Chen, Facile synthesis of yolk shell $\text{Mn}_2\text{O}_3@ \text{Mn}_5\text{O}_8$ as an effective catalyst for peroxymonosulfate activation, *Physical Chemistry Chemical Physics*. 20 (2018) 13909–13919. <https://doi.org/10.1039/C8CP02080A>.
- [110] B. Yang, Z. Tian, B. Wang, Z. Sun, L. Zhang, Y. Guo, H. Li, S. Yan, Facile synthesis of Fe_3O_4 /hierarchical- Mn_3O_4 /graphene oxide as a synergistic catalyst for activation of peroxymonosulfate for degradation of organic pollutants, *RSC Advances*. 5 (2015) 20674–20683. <https://doi.org/10.1039/C4RA15873C>.
- [111] E. Saputra, H. Zhang, Q. Liu, H. Sun, S. Wang, Egg-shaped core/shell α - $\text{Mn}_2\text{O}_3@ \alpha$ - MnO_2 as heterogeneous catalysts for decomposition of phenolics in aqueous solutions, *Chemosphere*. 159 (2016) 351–358. <https://doi.org/10.1016/j.chemosphere.2016.06.021>.
- [112] A. Khan, H. Wang, Y. Liu, A. Jawad, J. Ifthikar, Z. Liao, T. Wang, Z. Chen, Highly efficient α - $\text{Mn}_2\text{O}_3@ \alpha$ - MnO_2 -500 nanocomposite for peroxymonosulfate activation: comprehensive investigation of manganese oxides, *Journal of Materials Chemistry A*. 6 (2018) 1590–1600. <https://doi.org/10.1039/C7TA07942G>.
- [113] A. Shabanloo, M. Salari, N. Shabanloo, M.H. Dehghani, C.U. Pittman, D. Mohan, Heterogeneous persulfate activation by nano-sized Mn_3O_4 to degrade furfural from wastewater, *Journal of Molecular Liquids*. 298 (2020) 112088. <https://doi.org/10.1016/j.molliq.2019.112088>.
- [114] A. Khan, K. Zhang, P. Sun, H. Pan, Y. Cheng, Y. Zhang, High performance of the α - Mn_2O_3 nanocatalyst for persulfate activation: Degradation process of organic contaminants via singlet oxygen, *Journal of Colloid and Interface Science*. 584 (2021) 885–899. <https://doi.org/10.1016/j.jcis.2020.10.021>.

- [115] Y. Li, L.-D. Liu, L. Liu, Y. Liu, H.-W. Zhang, X. Han, Efficient oxidation of phenol by persulfate using manganite as a catalyst, *Journal of Molecular Catalysis A: Chemical*. 411 (2016) 264–271. <https://doi.org/10.1016/j.molcata.2015.10.036>.
- [116] X. Xu, Y. Zhang, S. Zhou, R. Huang, S. Huang, H. Kuang, X. Zeng, S. Zhao, Activation of persulfate by MnOOH: Degradation of organic compounds by nonradical mechanism, *Chemosphere*. 272 (2021) 129629. <https://doi.org/10.1016/j.chemosphere.2021.129629>.
- [117] T. Zhang, Y. Chen, Y. Wang, J.L. Roux, Y. Yang, J.-P. Croué, Efficient Peroxydisulfate Activation Process Not Relying on Sulfate Radical Generation for Water Pollutant Degradation, *Environmental Science and Technology*. 2014, 48, 10, 5868–5875.
- [118] X. Wang, Y. Qin, L. Zhu, H. Tang, Nitrogen-Doped Reduced Graphene Oxide as a Bifunctional Material for Removing Bisphenols: Synergistic Effect between Adsorption and Catalysis, *Environmental Science and Technology*. 49 (2015) 6855–6864. <https://doi.org/10.1021/acs.est.5b01059>.
- [119] H. Lee, H.-J. Lee, J. Jeong, J. Lee, N.-B. Park, C. Lee, Activation of persulfates by carbon nanotubes: Oxidation of organic compounds by nonradical mechanism, *Chemical Engineering Journal*. 266 (2015) 28–33. <https://doi.org/10.1016/j.cej.2014.12.065>.
- [120] Y.-Y. Ahn, E.-T. Yun, J.-W. Seo, C. Lee, S.H. Kim, J.-H. Kim, J. Lee, Activation of Peroxymonosulfate by Surface-Loaded Noble Metal Nanoparticles for Oxidative Degradation of Organic Compounds, *Environmental Science and Technology*. 50 (2016) 10187–10197. <https://doi.org/10.1021/acs.est.6b02841>.
- [121] X. Cheng, H. Guo, Y. Zhang, X. Wu, Y. Liu, Non-photochemical production of singlet oxygen via activation of persulfate by carbon nanotubes, *Water Research*. 113 (2017) 80–88. <https://doi.org/10.1016/j.watres.2017.02.016>.
- [122] Y. Liu, J. Luo, L. Tang, C. Feng, J. Wang, Y. Deng, H. Liu, J. Yu, H. Feng, J. Wang, Origin of the Enhanced Reusability and Electron Transfer of the Carbon-Coated Mn₃O₄ Nanocube for Persulfate Activation, *ACS Catalysis*. 10 (2020) 14857–14870. <https://doi.org/10.1021/acscatal.0c04049>.

- [123] M.Y. Rizal, R. Saleh, A. Taufik, S. Yin, Photocatalytic decomposition of methylene blue by persulfate-assisted Ag/Mn₃O₄ and Ag/Mn₃O₄/graphene composites and the inhibition effect of inorganic ions, *Environmental Nanotechnology, Monitoring & Management*. 15 (2021) 100408. <https://doi.org/10.1016/j.enmm.2020.100408>.
- [124] Q. Ma, X. Zhang, R. Guo, H. Zhang, Q. Cheng, M. Xie, X. Cheng, Persulfate activation by magnetic γ -Fe₂O₃/Mn₃O₄ nanocomposites for degradation of organic pollutants, *Separation and Purification Technology*. 210 (2019) 335–342. <https://doi.org/10.1016/j.seppur.2018.06.060>.
- [125] W. Yang, Y. Peng, Y. Wang, Y. Wang, H. Liu, Z. Su, W. Yang, J. Chen, W. Si, J. Li, Controllable redox-induced in-situ growth of MnO₂ over Mn₂O₃ for toluene oxidation: Active heterostructure interfaces, *Applied Catalysis B: Environmental*. 278 (2020) 119279. <https://doi.org/10.1016/j.apcatb.2020.119279>.
- [126] K.K. Hazarika, H. Talukdar, P. Sudarsanam, S.K. Bhargava, P. Bharali, Highly dispersed Mn₂O₃–Co₃O₄ nanostructures on carbon matrix as heterogeneous Fenton - like catalyst, *Applied Organometallic Chemistry*. 34 (2020). <https://doi.org/10.1002/aoc.5512>.
- [127] Y. Wang, L. Chen, H. Cao, Z. Chi, C. Chen, X. Duan, Y. Xie, F. Qi, W. Song, J. Liu, S. Wang, Role of oxygen vacancies and Mn sites in hierarchical Mn₂O₃/LaMnO₃- δ perovskite composites for aqueous organic pollutants decontamination, *Applied Catalysis B: Environmental*. 245 (2019) 546–554. <https://doi.org/10.1016/j.apcatb.2019.01.025>.
- [128] D. Liu, Q. Li, J. Hou, H. Zhao, Mixed-valent manganese oxide for catalytic oxidation of Orange II by activation of persulfate: heterojunction dependence and mechanism, *Catalysis Science & Technology*. (2021) 10.1039/D1CY00087J. <https://doi.org/10.1039/D1CY00087J>.
- [129] Z. Dong, Q. Zhang, B.-Y. Chen, J. Hong, Oxidation of bisphenol A by persulfate via Fe₃O₄- α -MnO₂ nanoflower-like catalyst: Mechanism and efficiency, *Chemical Engineering Journal*. 357 (2019) 337–347. <https://doi.org/10.1016/j.cej.2018.09.179>.
- [130] G.V. Buxton, C.L. Greenstock, W.P. Helman, A.B. Ross, Critical Review of rate constants for reactions of hydrated electrons, hydrogen atoms and hydroxyl radicals (\cdot OH/ \cdot O⁻ in Aqueous

Solution, *Journal of Physical and Chemical Reference Data*. 17 (1988) 513–886. <https://doi.org/10.1063/1.555805>.

[131] J. Wang, S. Wang, Activation of persulfate (PS) and peroxymonosulfate (PMS) and application for the degradation of emerging contaminants, *Chemical Engineering Journal*. 334 (2018) 1502–1517. <https://doi.org/10.1016/j.cej.2017.11.059>.

[132] M. Kosmulski, Compilation of PZC and IEP of sparingly soluble metal oxides and hydroxides from literature, *Advances in Colloid and Interface Science*. 152 (2009) 14–25. <https://doi.org/10.1016/j.cis.2009.08.003>.

[133] R. Shokoohi, M. Salari, A. Shabanloo, N. Shabanloo, S. Marofi, H. Faraji, M.V. Tabar, M. Moradnia, Catalytic activation of persulphate with Mn_3O_4 nanoparticles for degradation of acid blue 113: process optimisation and degradation pathway, *International Journal of Environmental Analytical Chemistry*. 0 (2020) 1–20. <https://doi.org/10.1080/03067319.2020.1773810>.

[134] Y.-H. Guan, J. Ma, X.-C. Li, J.-Y. Fang, L.-W. Chen, Influence of pH on the Formation of Sulfate and Hydroxyl Radicals in the UV/Peroxymonosulfate System, *Environmental Science and Technology*. 45 (2011) 9308–9314. <https://doi.org/10.1021/es2017363>.

[135] Z. Chen, X. Li, S. Zhang, J. Jin, X. Song, X. Wang, P.G. Tratnyek, Overlooked Role of Peroxides as Free Radical Precursors in Advanced Oxidation Processes, *Environmental Science and Technology*. 53 (2019) 2054–2062. <https://doi.org/10.1021/acs.est.8b05901>.

[136] D. He, H. Niu, S. He, L. Mao, Y. Cai, Y. Liang, Strengthened Fenton degradation of phenol catalyzed by core/shell Fe–Pd@C nanocomposites derived from mechanochemically synthesized Fe-Metal organic frameworks, *Water Research*. 162 (2019) 151–160. <https://doi.org/10.1016/j.watres.2019.06.058>.

[137] L. Wang, J. Jiang, S.-Y. Pang, Y. Zhou, J. Li, S. Sun, Y. Gao, C. Jiang, Oxidation of bisphenol A by nonradical activation of peroxymonosulfate in the presence of amorphous manganese dioxide, *Chemical Engineering Journal*. 352 (2018) 1004–1013. <https://doi.org/10.1016/j.cej.2018.07.103>.

- [138] S.P. Sun, T.A. Hatton, T.-S. Chung, Hyperbranched Polyethyleneimine Induced Cross-Linking of Polyamide-imide Nanofiltration Hollow Fiber Membranes for Effective Removal of Ciprofloxacin, *Environmental Science and Technology*. 45 (2011) 4003–4009. <https://doi.org/10.1021/es200345q>.
- [139] X. Du, Y. Zhang, I. Hussain, S. Huang, W. Huang, Insight into reactive oxygen species in persulfate activation with copper oxide: Activated persulfate and trace radicals, *Chemical Engineering Journal*. 313 (2017) 1023–1032. <https://doi.org/10.1016/j.cej.2016.10.138>.
- [140] Y. Shih, Y. Su, R. Ho, P. Su, C. Yang, Distinctive sorption mechanisms of 4-chlorophenol with black carbons as elucidated by different pH, *Science of The Total Environment*. 433 (2012) 523–529. <https://doi.org/10.1016/j.scitotenv.2012.06.050>.
- [141] Y. Huang, L. Nengzi, X. Zhang, J. Gou, Y. Gao, G. Zhu, Q. Cheng, X. Cheng, Catalytic degradation of ciprofloxacin by magnetic CuS/Fe₂O₃/Mn₂O₃ nanocomposite activated peroxymonosulfate: Influence factors, degradation pathways and reaction mechanism, *Chemical Engineering Journal*. 388 (2020) 124274. <https://doi.org/10.1016/j.cej.2020.124274>.
- [142] N.S. Shah, J. Ali Khan, M. Sayed, Z. Ul Haq Khan, H. Sajid Ali, B. Murtaza, H.M. Khan, M. Imran, N. Muhammad, Hydroxyl and sulfate radical mediated degradation of ciprofloxacin using nano zerovalent manganese catalyzed S₂O₈²⁻, *Chemical Engineering Journal*. 356 (2019) 199–209. <https://doi.org/10.1016/j.cej.2018.09.009>.
- [143] R.E. Huie, C.L. Clifton, P. Neta, Electron transfer reaction rates and equilibria of the carbonate and sulfate radical anions, *International Journal of Radiation Applications and Instrumentation. Part C. Radiation Physics and Chemistry*. 38 (1991) 477 – 481. [https://doi.org/10.1016/1359-0197\(91\)90065-A](https://doi.org/10.1016/1359-0197(91)90065-A).
- [144] S.-N. Chen, M.Z. Hoffman, G.H. Parsons, Reactivity of the carbonate radical toward aromatic compounds in aqueous solution, *The Journal of Physical Chemistry*. 79 (1975) 1911–1912. <https://doi.org/10.1021/j100585a004>.
- [145] M. Jiang, J. Lu, Y. Ji, D. Kong, Bicarbonate-activated persulfate oxidation of acetaminophen, *Water Research*. 116 (2017) 324–331. <https://doi.org/10.1016/j.watres.2017.03.043>.

- [146] G.-D. Fang, D.D. Dionysiou, Y. Wang, S.R. Al-Abed, D.-M. Zhou, Sulfate radical-based degradation of polychlorinated biphenyls: Effects of chloride ion and reaction kinetics, *Journal of Hazardous Materials*. 227–228 (2012) 394–401. <https://doi.org/10.1016/j.jhazmat.2012.05.074>.
- [147] C. Qi, X. Liu, Y. Li, C. Lin, J. Ma, X. Li, H. Zhang, Enhanced degradation of organic contaminants in water by peroxydisulfate coupled with bisulfite, *Journal of Hazardous Materials*. 328 (2017) 98–107. <https://doi.org/10.1016/j.jhazmat.2017.01.010>.
- [148] Y. Lei, C.-S. Chen, Y.-J. Tu, Y.-H. Huang, H. Zhang, Heterogeneous Degradation of Organic Pollutants by Persulfate Activated by CuO-Fe₃O₄: Mechanism, Stability, and Effects of pH and Bicarbonate Ions, *Environmental Science and Technology*. 49 (2015) 6838–6845. <https://doi.org/10.1021/acs.est.5b00623>.
- [149] C. Liang, Z.-S. Wang, N. Mohanty, Influences of carbonate and chloride ions on persulfate oxidation of trichloroethylene at 20 °C, *Science of The Total Environment*. 370 (2006) 271–277. <https://doi.org/10.1016/j.scitotenv.2006.08.028>.
- [150] J. Zhou, J. Xiao, D. Xiao, Y. Guo, C. Fang, X. Lou, Z. Wang, J. Liu, Transformations of chloro and nitro groups during the peroxymonosulfate-based oxidation of 4-chloro-2-nitrophenol, *Chemosphere*. 134 (2015) 446–451. <https://doi.org/10.1016/j.chemosphere.2015.05.027>.
- [151] Y. Yang, J.J. Pignatello, J. Ma, W.A. Mitch, Comparison of Halide Impacts on the Efficiency of Contaminant Degradation by Sulfate and Hydroxyl Radical-Based Advanced Oxidation Processes (AOPs), *Environmental Science and Technology*. 48 (2014) 2344–2351. <https://doi.org/10.1021/es404118q>.
- [152] J.E. Grebel, J.J. Pignatello, W.A. Mitch, Effect of Halide Ions and Carbonates on Organic Contaminant Degradation by Hydroxyl Radical-Based Advanced Oxidation Processes in Saline Waters, *Environmental Science and Technology*. 44 (2010) 6822–6828. <https://doi.org/10.1021/es1010225>.
- [153] Y. Yang, J.J. Pignatello, J. Ma, W.A. Mitch, Effect of matrix components on UV/H₂O₂ and UV/S₂O₈²⁻ advanced oxidation processes for trace organic degradation in reverse osmosis

brines from municipal wastewater reuse facilities, *Water Research*. 89 (2016) 192–200. <https://doi.org/10.1016/j.watres.2015.11.049>.

[154] D. Minakata, D. Kamath, S. Maetzold, Mechanistic Insight into the Reactivity of Chlorine-Derived Radicals in the Aqueous-Phase UV–Chlorine Advanced Oxidation Process: Quantum Mechanical Calculations, *Environmental Science and Technology*. 51 (2017) 6918–6926. <https://doi.org/10.1021/acs.est.7b00507>.

[155] J. Huang, H. Zhang, Mn-based catalysts for sulfate radical-based advanced oxidation processes: A review, *Environment International*. 133 (2019) 105141. <https://doi.org/10.1016/j.envint.2019.105141>.

[156] J. Wang, S. Wang, Effect of inorganic anions on the performance of advanced oxidation processes for degradation of organic contaminants, *Chemical Engineering Journal*. 411 (2021) 128392. <https://doi.org/10.1016/j.cej.2020.128392>.

[157] R.J. Watts, J. Howsawkeng, A.L. Teel, Destruction of a Carbon Tetrachloride Dense Nonaqueous Phase Liquid by Modified Fenton's Reagent, *Journal of Environmental Engineering*. 131 (2005) 1114–1119. [https://doi.org/10.1061/\(ASCE\)0733-9372\(2005\)131:7\(1114\)](https://doi.org/10.1061/(ASCE)0733-9372(2005)131:7(1114)).

[158] R.J. Watts, J. Sarasa, F.J. Loge, A.L. Teel, Oxidative and Reductive Pathways in Manganese-Catalyzed Fenton's Reactions, *Journal of Environmental Engineering*. 131 (2005) 158–164. [https://doi.org/10.1061/\(ASCE\)0733-9372\(2005\)131:1\(158\)](https://doi.org/10.1061/(ASCE)0733-9372(2005)131:1(158)).

[159] S.-H. Do, B. Batchelor, H.-K. Lee, S.-H. Kong, Hydrogen peroxide decomposition on manganese oxide (pyrolusite): Kinetics, intermediates, and mechanism, *Chemosphere*. 75 (2009) 8–12. <https://doi.org/10.1016/j.chemosphere.2008.11.075>.

[160] S.-H. Do, S.-H. Kong, The oxidation of toluene sorbed on activated carbon in the presence of H₂O₂ and manganese oxide, *Water Science and Technology*. 66 (2012) 2349–2354. <https://doi.org/10.2166/wst.2012.467>.

[161] X. He, B. Li, P. Wang, J. Ma, Novel H₂O₂–MnO₂ system for efficient physico-chemical cleaning of fouled ultrafiltration membranes by simultaneous generation of reactive free

radicals and oxygen, *Water Research*. 167 (2019) 115111. <https://doi.org/10.1016/j.watres.2019.115111>.

[162] S.M. Mitchell, M. Ahmad, A.L. Teel, R.J. Watts, Degradation of Perfluorooctanoic Acid by Reactive Species Generated through Catalyzed H₂O₂ Propagation Reactions, *Environmental Science and Technology Letter*. 1 (2014) 117–121. <https://doi.org/10.1021/ez4000862>.

[163] E.-J. Kim, D. Oh, C.-S. Lee, J. Gong, J. Kim, Y.-S. Chang, Manganese oxide nanorods as a robust Fenton-like catalyst at neutral pH: Crystal phase-dependent behavior, *Catalysis Today*. 282 (2017) 71–76. <https://doi.org/10.1016/j.cattod.2016.03.034>.

[164] M. Sabri, H.J. King, R.J. Gummow, X. Lu, C. Zhao, M. Oelgemöller, S.L.Y. Chang, R.K. Hocking, Oxidant or Catalyst for Oxidation? A Study of How Structure and Disorder Change the Selectivity for Direct versus Catalytic Oxidation Mediated by Manganese(III, IV) Oxides, *Chemistry of Materials*. 30 (2018) 8244–8256. <https://doi.org/10.1021/acs.chemmater.8b03661>.

[165] J.D. Begg, M. Zavarin, A.B. Kersting, Plutonium desorption from mineral surfaces at environmental concentrations of hydrogen peroxide, *Environmental Science and Technology*. 48 (2014) 6201–6210. <https://doi.org/10.1021/es500984w>.

[166] W.J. Cooper, D.R.S. Lean, Hydrogen peroxide concentration in a northern lake: photochemical formation and diel variability, *Environmental Science and Technology*. 23 (1989) 1425–1428. <https://doi.org/10.1021/es00069a017>.

[167] S. Garg, A.L. Rose, T.D. Waite, Photochemical production of superoxide and hydrogen peroxide from natural organic matter, *Geochimica et Cosmochimica Acta*. 75 (2011) 4310–4320. <https://doi.org/10.1016/j.gca.2011.05.014>.

[168] X. Yuan, P.S. Nico, X. Huang, T. Liu, C. Ulrich, K.H. Williams, J.A. Davis, Production of Hydrogen Peroxide in Groundwater at Rifle, Colorado, *Environmental Science and Technology*. 51 (2017) 7881–7891. <https://doi.org/10.1021/acs.est.6b04803>.

[169] K.L. Roe, R.J. Schneider, C.M. Hansel, B.M. Voelker, Measurement of dark, particle-generated superoxide and hydrogen peroxide production and decay in the subtropical and temperate North Pacific Ocean, *Deep Sea Research Part I: Oceanographic Research Papers*. 107 (2016) 59–69. <https://doi.org/10.1016/j.dsr.2015.10.012>.

- [170] W.J. Cooper, J.K. Moegling, R.J. Kieber, J.J. Kiddle, A chemiluminescence method for the analysis of H₂O₂ in natural waters, *Marine Chemistry*. 70 (2000) 191–200. [https://doi.org/10.1016/S0304-4203\(00\)00025-6](https://doi.org/10.1016/S0304-4203(00)00025-6).
- [171] A.L.-T. Pham, F.M. Doyle, D.L. Sedlak, Inhibitory Effect of Dissolved Silica on H₂O₂ Decomposition by Iron(III) and Manganese(IV) Oxides: Implications for H₂O₂ -Based In Situ Chemical Oxidation, *Environmental Science and Technology*. 46 (2012) 1055–1062. <https://doi.org/10.1021/es203612d>.
- [172] M. Kamagate, M. Pasturel, M. Brigante, K. Hanna, Mineralization Enhancement of Pharmaceutical Contaminants by Radical-Based Oxidation Promoted by Oxide-Bound Metal Ions, *Environmental Science and Technology*. 54 (2020) 476–485. <https://doi.org/10.1021/acs.est.9b04542>.
- [173] C. Liu, D. Pan, X. Tang, M. Hou, Q. Zhou, J. Zhou, Degradation of Rhodamine B by the α -MnO₂/Peroxymonosulfate System, *Water Air Soil Pollution*. 227 (2016) 92. <https://doi.org/10.1007/s11270-016-2782-6>.
- [174] E. Saputra, S. Muhammad, H. Sun, A. Patel, P. Shukla, Z.H. Zhu, S. Wang, α -MnO₂ activation of peroxymonosulfate for catalytic phenol degradation in aqueous solutions, *Catalysis Communications*. 26 (2012) 144–148. <https://doi.org/10.1016/j.catcom.2012.05.014>.
- [175] E. Saputra, S. Muhammad, H. Sun, H.M. Ang, M.O. Tadé, S. Wang, Different Crystallographic One-dimensional MnO₂ Nanomaterials and Their Superior Performance in Catalytic Phenol Degradation, *Environmental Science and Technology*. 47 (2013) 5882–5887. <https://doi.org/10.1021/es400878c>.
- [176] Y. Wang, S. Indrawirawan, X. Duan, H. Sun, H.M. Ang, M.O. Tadé, S. Wang, New insights into heterogeneous generation and evolution processes of sulfate radicals for phenol degradation over one-dimensional α -MnO₂ nanostructures, *Chemical Engineering Journal*. 266 (2015) 12–20. <https://doi.org/10.1016/j.cej.2014.12.066>.
- [177] Y. Wang, H. Sun, H.M. Ang, M.O. Tadé, S. Wang, 3D-hierarchically structured MnO₂ for catalytic oxidation of phenol solutions by activation of peroxymonosulfate: Structure

dependence and mechanism, *Applied Catalysis B: Environmental*. 164 (2015) 159–167. <https://doi.org/10.1016/j.apcatb.2014.09.004>.

[178] J. Deng, Y. Ge, C. Tan, H. Wang, Q. Li, S. Zhou, K. Zhang, Degradation of ciprofloxacin using α -MnO₂ activated peroxymonosulfate process: Effect of water constituents, degradation intermediates and toxicity evaluation, *Chemical Engineering Journal*. 330 (2017) 1390–1400. <https://doi.org/10.1016/j.cej.2017.07.137>.

[179] F. Riva, E. Zuccato, E. Davoli, E. Fattore, S. Castiglioni, Risk assessment of a mixture of emerging contaminants in surface water in a highly urbanized area in Italy, *Journal of Hazardous Materials*. 361 (2019) 103–110. <https://doi.org/10.1016/j.jhazmat.2018.07.099>.

[180] V. Geissen, H. Mol, E. Klumpp, G. Umlauf, M. Nadal, M. van der Ploeg, S.E.A.T.M. van de Zee, C.J. Ritsema, Emerging pollutants in the environment: A challenge for water resource management, *International Soil and Water Conservation Research*. 3 (2015) 57–65. <https://doi.org/10.1016/j.iswcr.2015.03.002>.

[181] Y. Li, G. Zhu, W.J. Ng, S.K. Tan, A review on removing pharmaceutical contaminants from wastewater by constructed wetlands: Design, performance and mechanism, *Science of The Total Environment*. 468–469 (2014) 908–932. <https://doi.org/10.1016/j.scitotenv.2013.09.018>.

[182] S. Sauvé, M. Desrosiers, A review of what is an emerging contaminant, *Chemistry Central Journal*. 8 (2014) 15. <https://doi.org/10.1186/1752-153X-8-15>.

[183] G. Korekar, A. Kumar, C. Ugale, Occurrence, fate, persistence and remediation of caffeine: a review, *Environmental Science and Pollution Research*. 27 (2020) 34715–34733. <https://doi.org/10.1007/s11356-019-06998-8>.

[184] R.P. Deo, Pharmaceuticals in the Surface Water of the USA: A Review, *Current Environmental Health Reports*. 1 (2014) 113–122. <https://doi.org/10.1007/s40572-014-0015-y>.

[185] S.D. Melvin, D.R. Buck, L.D. Fabbro, Diurnal activity patterns as a sensitive behavioural outcome in fish: effect of short-term exposure to treated sewage and a sub-lethal PPCP mixture, *Journal of Applied Toxicology*. 36 (2016) 1173–1182. <https://doi.org/10.1002/jat.3284>.

- [186] C. Sun, S. Dudley, J. Trumble, J. Gan, Pharmaceutical and personal care products-induced stress symptoms and detoxification mechanisms in cucumber plants, *Environ Pollution*. 234 (2018) 39–47. <https://doi.org/10.1016/j.envpol.2017.11.041>.
- [187] R.J. Kavlock, G.R. Daston, C. DeRosa, L.E. Gray, S. Kaattari, G. Lucier, M. Luster, M.J. Mac, C. Maczka, R. Miller, R. Rolland, M. Sheehan, T. Sinks, H.A. Tilson, Research needs for the risk assessment of health and environmental effects of endocrine disruptors: a report of the U.S. EPA-sponsored workshop., *Environmental Health Perspectives*. 104 (1996) 26.
- [188] M.P. Fernandez, M.G. Ikonou, I. Buchanan, An assessment of estrogenic organic contaminants in Canadian wastewaters, *Science of the Total Environment*. 373 (2007) 250–269. <https://doi.org/10.1016/j.scitotenv.2006.11.018>.
- [189] Z. Liu, Y. Kanjo, S. Mizutani, Removal mechanisms for endocrine disrupting compounds (EDCs) in wastewater treatment — physical means, biodegradation, and chemical advanced oxidation: A review, *Science of The Total Environment*. 407 (2009) 731–748. <https://doi.org/10.1016/j.scitotenv.2008.08.039>.
- [190] C.G. Campbell, S.E. Borglin, F.B. Green, A. Grayson, E. Wozzi, W.T. Stringfellow, Biologically directed environmental monitoring, fate, and transport of estrogenic endocrine disrupting compounds in water: A review, *Chemosphere*. 65 (2006) 1265–1280. <https://doi.org/10.1016/j.chemosphere.2006.08.003>.
- [191] E.R. Kabir, M.S. Rahman, I. Rahman, A review on endocrine disruptors and their possible impacts on human health, *Environmental Toxicology and Pharmacology*. 40 (2015) 241–258. <https://doi.org/10.1016/j.etap.2015.06.009>.
- [192] Y. Yang, Y. Yang, J. Zhang, B. Shao, J. Yin, Assessment of bisphenol A alternatives in paper products from the Chinese market and their dermal exposure in the general population, *Environmental Pollution*. 244 (2019) 238–246. <https://doi.org/10.1016/j.envpol.2018.10.049>.
- [193] C.A. Staples, P.B. Dome, G.M. Klecka, S.T. Oblock, L.R. Harris, A review of the environmental fate, effects, and exposures of bisphenol A, *Chemosphere*. 36 (1998) 2149–2173. [https://doi.org/10.1016/S0045-6535\(97\)10133-3](https://doi.org/10.1016/S0045-6535(97)10133-3).

- [194] J.R. Rochester, Bisphenol A and human health: A review of the literature, *Reproductive Toxicology*. 42 (2013) 132–155. <https://doi.org/10.1016/j.reprotox.2013.08.008>.
- [195] Z. Tang, Z. Liu, H. Wang, Z. Dang, Y. Liu, Occurrence and removal of 17 α -ethynylestradiol (EE2) in municipal wastewater treatment plants: Current status and challenges, *Chemosphere*. 271 (2021) 129551. <https://doi.org/10.1016/j.chemosphere.2021.129551>.
- [196] A.Z. Aris, A.S. Shamsuddin, S.M. Praveena, Occurrence of 17 α -ethynylestradiol (EE2) in the environment and effect on exposed biota: a review, *Environment International*. 69 (2014) 104–119. <https://doi.org/10.1016/j.envint.2014.04.011>.
- [197] K. Lei, C.-Y. Lin, Y. Zhu, W. Chen, H.-Y. Pan, Z. Sun, A. Sweetman, Q. Zhang, M.-C. He, Estrogens in municipal wastewater and receiving waters in the Beijing-Tianjin-Hebei region, China: Occurrence and risk assessment of mixtures, *Journal of Hazardous Materials*. 389 (2020) 121891. <https://doi.org/10.1016/j.jhazmat.2019.121891>.
- [198] J. Hu, S. Cheng, T. Aizawa, Y. Terao, S. Kunikane, Products of Aqueous Chlorination of 17 β -Estradiol and Their Estrogenic Activities, *Environmental Science and Technol.* 37 (2003) 5665–5670. <https://doi.org/10.1021/es034324+>.
- [199] T.-S. Chen, T.-C. Chen, K.-J.C. Yeh, H.-R. Chao, E.-T. Liaw, C.-Y. Hsieh, K.-C. Chen, L.-T. Hsieh, Y.-L. Yeh, High estrogen concentrations in receiving river discharge from a concentrated livestock feedlot, *Science of The Total Environment*. 408 (2010) 3223–3230. <https://doi.org/10.1016/j.scitotenv.2010.03.054>.
- [200] S. Yuan, Z. Liu, H. Lian, C. Yang, Q. Lin, H. Yin, Z. Lin, Z. Dang, Fast trace determination of nine odorant and estrogenic chloro- and bromo-phenolic compounds in real water samples through automated solid-phase extraction coupled with liquid chromatography tandem mass spectrometry, *Environmental Science and Pollution Research*. 25 (2018) 3813–3822. <https://doi.org/10.1007/s11356-017-0816-2>.
- [201] A.D. Vethaak, J. Lahr, S.M. Schrap, A.C. Belfroid, G.B.J. Rijs, A. Gerritsen, J. de Boer, A.S. Bulder, G.C.M. Grinwis, R.V. Kuiper, J. Legler, T.A.J. Murk, W. Peijnenburg, H.J.M. Verhaar, P. de Voogt, An integrated assessment of estrogenic contamination and biological

effects in the aquatic environment of The Netherlands, *Chemosphere*. 59 (2005) 511–524. <https://doi.org/10.1016/j.chemosphere.2004.12.053>.

[202] A. Laganà, A. Bacaloni, I. De Leva, A. Faberi, G. Fago, A. Marino, Analytical methodologies for determining the occurrence of endocrine disrupting chemicals in sewage treatment plants and natural waters, *Analytica Chimica Acta*. 501 (2004) 79–88. <https://doi.org/10.1016/j.aca.2003.09.020>.

[203] H.M. Kuch, K. Ballschmiter, Determination of Endocrine-Disrupting Phenolic Compounds and Estrogens in Surface and Drinking Water by HRGC–(NCI)–MS in the Picogram per Liter Range, *Environmental Science and Technology*. 35 (2001) 3201–3206. <https://doi.org/10.1021/es010034m>.

[204] P. Hohenblum, O. Gans, W. Moche, S. Scharf, G. Lorbeer, Monitoring of selected estrogenic hormones and industrial chemicals in groundwaters and surface waters in Austria, *Science of The Total Environment*. 333 (2004) 185–193. <https://doi.org/10.1016/j.scitotenv.2004.05.009>.

[205] S. Rodriguez-Mozaz, M.J.L. de Alda, D. Barceló, Monitoring of estrogens, pesticides and bisphenol A in natural waters and drinking water treatment plants by solid-phase extraction-liquid chromatography-mass spectrometry, *Journal of Chromatography A*. 1045 (2004) 85–92. <https://doi.org/10.1016/j.chroma.2004.06.040>.

[206] A.C. Belfroid, A. Van der Horst, A.D. Vethaak, A.J. Schäfer, G.B. Rijs, J. Wegener, W.P. Cofino, Analysis and occurrence of estrogenic hormones and their glucuronides in surface water and waste water in The Netherlands, *Science of The Total Environment*. 225 (1999) 101–108. [https://doi.org/10.1016/s0048-9697\(98\)00336-2](https://doi.org/10.1016/s0048-9697(98)00336-2).

[207] C.H. Swartz, S. Reddy, M.J. Benotti, H. Yin, L.B. Barber, B.J. Brownawell, R.A. Rudel, Steroid Estrogens, Nonylphenol Ethoxylate Metabolites, and Other Wastewater Contaminants in Groundwater Affected by a Residential Septic System on Cape Cod, MA, *Environmental Science and Technology*. 40 (2006) 4894–4902. <https://doi.org/10.1021/es052595+>.

[208] T. Isobe, H. Shiraishi, M. Yasuda, A. Shinoda, H. Suzuki, M. Morita, Determination of estrogens and their conjugates in water using solid-phase extraction followed by liquid

chromatography–tandem mass spectrometry, *Journal of Chromatography A*. 984 (2003) 195–202. [https://doi.org/10.1016/S0021-9673\(02\)01851-4](https://doi.org/10.1016/S0021-9673(02)01851-4).

[209] E.W. Peterson, R.K. Davis, H.A. Orndorff, 17 β -Estradiol as an Indicator of Animal Waste Contamination in Mantled Karst Aquifers, *Journal of Environmental quality*. 29 (2000) 826–834.

[210] P. Roefer, S. Snyder, R.E. Zegers, D.J. Rexing, J.L. Fronk, Endocrine-disrupting chemicals in a source water, *Journal - American Water Works Association*. 92 (2000) 52–58. <https://doi.org/10.1002/j.1551-8833.2000.tb08992.x>.

[211] C. Wicks, C. Kelley, E. Peterson, Estrogen in a karstic aquifer, *Ground Water*. 42 (2004) 384–389. <https://doi.org/10.1111/j.1745-6584.2004.tb02686.x>.

[212] G. Morteani, P. Möller, A. Fuganti, T. Paces, Input and fate of anthropogenic estrogens and gadolinium in surface water and sewage plants in the hydrological basin of Prague (Czech Republic), *Environmental Geochem & Health*. 28 (2006) 257–264. <https://doi.org/10.1007/s10653-006-9040-6>.

[213] C.V.T. Riguetto, M.T. Nazari, C.F. De Souza, J.S. Cadore, V.B. Brião, J.S. Piccin, Alternative techniques for caffeine removal from wastewater: An overview of opportunities and challenges, *Journal of Water Process Engineering*. 35 (2020) 101231. <https://doi.org/10.1016/j.jwpe.2020.101231>.

[214] A. Nehlig, Interindividual Differences in Caffeine Metabolism and Factors Driving Caffeine Consumption, *Pharmacological Reviews*. 70 (2018) 384–411. <https://doi.org/10.1124/pr.117.014407>.

[215] I.J. Buerge, T. Poiger, M.D. Müller, H.-R. Buser, Caffeine, an Anthropogenic Marker for Wastewater Contamination of Surface Waters, *Environmental Science and Technol.* 37 (2003) 691–700. <https://doi.org/10.1021/es020125z>.

[216] Outcome of a public consultation on the draft Scientific Opinion of the EFSA Panel on Dietetic Products, Nutrition and Allergies (NDA) on the essential composition of infant and follow-on formulae, *EFSA Supporting Publications*. 11 (2014) 633E. <https://doi.org/10.2903/sp.efsa.2014.EN-633>.

- [217] R. Siegener, R.F. Chen, Caffeine in Boston Harbor seawater, *Marine Pollution Bulletin*. 44 (2002) 383–387. [https://doi.org/10.1016/s0025-326x\(00\)00176-4](https://doi.org/10.1016/s0025-326x(00)00176-4).
- [218] T. Ternes, M. Bonerz, T. Schmidt, Determination of neutral pharmaceuticals in wastewater and rivers by liquid chromatography–electrospray tandem mass spectrometry, *Journal of Chromatography A*. 938 (2001) 175–185. [https://doi.org/10.1016/S0021-9673\(01\)01205-5](https://doi.org/10.1016/S0021-9673(01)01205-5).
- [219] A.J. Hendriks, J.L. Maas-Diepeveen, A. Noordsij, M.A. Van der Gaag, Monitoring response of XAD-concentrated water in the rhine delta: A major part of the toxic compounds remains unidentified, *Water Research*. 28 (1994) 581–598. [https://doi.org/10.1016/0043-1354\(94\)90009-4](https://doi.org/10.1016/0043-1354(94)90009-4).
- [220] J. Patsias, E. Papadopoulou-Mourkidou, Development of an automated on-line solid-phase extraction–high-performance liquid chromatographic method for the analysis of aniline, phenol, caffeine and various selected substituted aniline and phenol compounds in aqueous matrices, *Journal of Chromatography A*. 904 (2000) 171–188. [https://doi.org/10.1016/S0021-9673\(00\)00927-4](https://doi.org/10.1016/S0021-9673(00)00927-4).
- [221] M.R. Burkhardt, P.P. Soliven, S.L. Werner, D.G. Vaught, Determination of Submicrogram-per-Liter Concentrations of Caffeine in Surface Water and Groundwater Samples by Solid-Phase Extraction and Liquid Chromatography, *Journal of AOAC INTERNATIONAL*. 82 (1999) 161–166. <https://doi.org/10.1093/jaoac/82.1.161>.
- [222] R.L. Seiler, S.D. Zaugg, J.M. Thomas, D.L. Howcroft, Caffeine and Pharmaceuticals as Indicators of Waste Water Contamination in Wells, *Groundwater*. 37 (1999) 405–410. <https://doi.org/10.1111/j.1745-6584.1999.tb01118.x>.
- [223] S. Weigel, J. Kuhlmann, H. Hühnerfuss, Drugs and personal care products as ubiquitous pollutants: occurrence and distribution of clofibric acid, caffeine and DEET in the North Sea, *Science of The Total Environment*. 295 (2002) 131–141. [https://doi.org/10.1016/S0048-9697\(02\)00064-5](https://doi.org/10.1016/S0048-9697(02)00064-5).

- [224] N. Paxéus, Organic pollutants in the effluents of large wastewater treatment plants in Sweden, *Water Research*. 30 (1996) 1115–1122. [https://doi.org/10.1016/0043-1354\(95\)00278-2](https://doi.org/10.1016/0043-1354(95)00278-2).
- [225] A.O. Kondrakov, A.N. Ignatev, F.H. Frimmel, S. Bräse, H. Horn, A.I. Revelsky, Formation of genotoxic quinones during bisphenol A degradation by TiO₂ photocatalysis and UV photolysis: A comparative study, *Applied Catalysis B: Environmental*. 160–161 (2014) 106–114. <https://doi.org/10.1016/j.apcatb.2014.05.007>.
- [226] X. Dong, B. Ren, Z. Sun, C. Li, X. Zhang, M. Kong, S. Zheng, D.D. Dionysiou, Monodispersed CuFe₂O₄ nanoparticles anchored on natural kaolinite as highly efficient peroxymonosulfate catalyst for bisphenol A degradation, *Applied Catalysis B: Environmental*. 253 (2019) 206–217. <https://doi.org/10.1016/j.apcatb.2019.04.052>.
- [227] R.C. Burgos-Castillo, I. Sirés, M. Sillanpää, E. Brillas, Application of electrochemical advanced oxidation to bisphenol A degradation in water. Effect of sulfate and chloride ions, *Chemosphere*. 194 (2018) 812–820. <https://doi.org/10.1016/j.chemosphere.2017.12.014>.
- [228] W. Huang, M. Brigante, F. Wu, C. Mousty, K. Hanna, G. Mailhot, Assessment of the Fe(III)–EDDS Complex in Fenton-Like Processes: From the Radical Formation to the Degradation of Bisphenol A, *Environmental Science and Technology*. 47 (2013) 1952–1959. <https://doi.org/10.1021/es304502y>.
- [229] Y. Li, A. Zhang, Removal of steroid estrogens from waste activated sludge using Fenton oxidation: Influencing factors and degradation intermediates, *Chemosphere*. 105 (2014) 24–30. <https://doi.org/10.1016/j.chemosphere.2013.10.043>.
- [230] S. Esplugas, D.M. Bila, L.G.T. Krause, M. Dezotti, Ozonation and advanced oxidation technologies to remove endocrine disrupting chemicals (EDCs) and pharmaceuticals and personal care products (PPCPs) in water effluents, *Journal of Hazardous Materials*. 149 (2007) 631–642. <https://doi.org/10.1016/j.jhazmat.2007.07.073>.
- [231] X. Ma, C. Zhang, J. Deng, Y. Song, Q. Li, Y. Guo, C. Li, Simultaneous Degradation of Estrone, 17 β -Estradiol and 17 α -Ethinyl Estradiol in an Aqueous UV/H₂O₂ System,

International Journal of Environmental Research and Public Health. 12 (2015) 12016–12029. <https://doi.org/10.3390/ijerph121012016>.

[232] A. Gabet, H. Métivier, C. de Brauer, G. Mailhot, M. Brigante, Hydrogen peroxide and persulfate activation using UVA-UVB radiation: Degradation of estrogenic compounds and application in sewage treatment plant waters, *Journal of Hazardous Materials*. 405 (2021) 124693. <https://doi.org/10.1016/j.jhazmat.2020.124693>.

[233] X. Feng, S. Ding, J. Tu, F. Wu, N. Deng, Degradation of estrone in aqueous solution by photo-Fenton system, *Science of The Total Environment*. 345 (2005) 229–237. <https://doi.org/10.1016/j.scitotenv.2004.11.008>.

[234] N. Xu, Y. Zhang, H. Tao, S. Zhou, Y. Zeng, Bio-electro-Fenton system for enhanced estrogens degradation, *Bioresource Technology*. 138 (2013) 136–140. <https://doi.org/10.1016/j.biortech.2013.03.157>.

[235] F.S. Souza, L.A. Féris, Degradation of Caffeine by Advanced Oxidative Processes: O₃ and O₃/UV, *Ozone: Science & Engineering*. 37 (2015) 379–384. <https://doi.org/10.1080/01919512.2015.1016572>.

[236] E. Kudlek, Decomposition of Contaminants of Emerging Concern in Advanced Oxidation Processes, *Proceedings*. 2 (2017) 180. <https://doi.org/10.3390/ecws-2-04949>.

[237] M.C.V.M. Starling, P.P. Souza, A. Le Person, C.C. Amorim, J. Criquet, Intensification of UV-C treatment to remove emerging contaminants by UV-C/H₂O₂ and UV-C/S₂O₈²⁻: Susceptibility to photolysis and investigation of acute toxicity, *Chemical Engineering Journal*. 376 (2019) 120856. <https://doi.org/10.1016/j.cej.2019.01.135>.

[238] M. Ghosh, K. Manoli, X. Shen, J. Wang, A.K. Ray, Solar photocatalytic degradation of caffeine with titanium dioxide and zinc oxide nanoparticles, *Journal of Photochemistry and Photobiology A: Chemistry*. 377 (2019) 1–7. <https://doi.org/10.1016/j.jphotochem.2019.03.029>.

[239] S. Miralles-Cuevas, D. Darowna, A. Wanag, S. Mozia, S. Malato, I. Oller, Comparison of UV/H₂O₂, UV/S₂O₈²⁻, solar/Fe(II)/H₂O₂ and solar/Fe(II)/S₂O₈²⁻ at pilot plant scale for the elimination of micro-contaminants in natural water: An economic assessment, *Chemical Engineering Journal*. 310 (2017) 514–524. <https://doi.org/10.1016/j.cej.2016.06.121>.

[240] S. Miralles-Cuevas, I. Oller, A. Ruíz-Delgado, A. Cabrera-Reina, L. Cornejo-Ponce, S. Malato, EDDS as complexing agent for enhancing solar advanced oxidation processes in natural water: Effect of iron species and different oxidants, *Journal of Hazardous Materials*. 372 (2019) 129–136. <https://doi.org/10.1016/j.jhazmat.2018.03.018>.

Chapter II

Materials and Methods

2.1 Chemicals and instruments

2.1.1 Chemicals

Table 2-1. Chemical reagents.

Reagent name	Chemical formula	CAS number	Grade	Company
Hydrogen peroxide	H ₂ O ₂	7722-84-1	30 wt.% in H ₂ O	Sigma-Aldrich*
Sodium persulfate	Na ₂ S ₂ O ₈	7775-27-1	98%	Sigma-Aldrich
Oxone	KHSO ₅ ·0.5KHSO ₄ ·0.5K ₂ SO ₄	70693-62-8	–	Sigma-Aldrich
Sodium bisulfite	NaHSO ₃	7631-90-5	ACS reagent	Sigma-Aldrich
Manganese(III) oxide	Mn ₂ O ₃	1317-34-6	99%	Sigma-Aldrich
Manganese chloride	MnCl ₂	7773-01-5	99%	Riedel-de Haen
Perchloric acid	HClO ₄	7601-90-3	72%	Sigma-Aldrich
Sodium hydroxide	NaOH	1310-73-2	97%	Sigma-Aldrich
Hydrochloric acid	HCl	7647-01-0	37%	Sigma-Aldrich
2-propanol	C ₃ H ₈ O	67-63-0	99%	Sigma-Aldrich
<i>tert</i> -butanol	C ₄ H ₁₀ O	75-65-0	99%	Acros organics
Ethanol	C ₂ H ₆ O	64-17-5	96%	VWRchemicals
Furfuryl alcohol	C ₅ H ₆ O ₂	98-00-0	98%	Sigma-Aldrich
Sodium chloride	NaCl	7647-14-5	99%	Sigma-Aldrich
Sodium bicarbonate	NaHCO ₃	144-55-8	99.7%	Sigma-Aldrich
Sodium nitrite	NaNO ₂	7632-00-0	97%	Sigma-Aldrich
Sodium nitrate	NaNO ₃	7631-99-4	99%	Fluka
Sodium phosphate	NaH ₂ PO ₄	7558-80-7	99%	Sigma-Aldrich
Sodium metasilicate	Na ₂ SiO ₃	6834-92-0	–	Sigma-Aldrich
Phosphoric acid	H ₃ PO ₄	7664-38-2	85%	Sigma-Aldrich

*Sigma-Aldrich refers to the Sigma-Aldrich company located in France.

Table 2-1 (continued)

Reagent name	Chemical formula	CAS number	Grade	Company
Acetonitrile	C ₂ H ₃ N	75-05-8	HPLC grade	Carlo Erba Reagents
Potassium permanganate	KMnO ₄	7722-64-7	99%	Sigma-Aldrich
HEPES	C ₈ H ₁₈ N ₂ O ₄ S	7365-45-9	99%	Sigma-Aldrich
Oxalic acid	H ₂ C ₂ O ₄	144-62-7	–	Sigma-Aldrich
Sulfuric acid	H ₂ SO ₄	7664-93-9	98%	Sigma-Aldrich
Hydroxylamine hydrochloride	NH ₂ OH·HCl	5470-11-1	98%	Sigma-Aldrich
Terephthalic acid	C ₈ H ₆ O ₄	100-21-0	98%	Sigma-Aldrich
Potassium iodide	KI	7681-11-0	99%	Sigma-Aldrich
2-hydroxy-terephthalic acid	C ₈ H ₆ O ₅	636-94-2	97%	Sigma-Aldrich
4-hydroxyphenylacetic acid	C ₈ H ₈ O ₃	156-38-7	98%	Sigma-Aldrich
Peroxidase	–	9003-99-0	–	Sigma-Aldrich
Nitric acid	HNO ₃	7697-37-2	65%	Sigma-Aldrich
Caffeine (CAF)	C ₈ H ₁₀ N ₄ O ₂	58-08-2	–	Sigma-Aldrich
Bisphenol A (BPA)	C ₁₅ H ₁₆ O ₂	80-05-7	99%	Sigma-Aldrich
17β-estradiol (E2)	C ₁₈ H ₂₄ O ₂	50-28-2	–	Sigma-Aldrich
17α-ethinylestradiol (EE2)	C ₂₀ H ₂₄ O ₂	57-63-6	98%	Sigma-Aldrich
DMPO ¹	C ₆ H ₁₁ NO	3317-61-1	–	Sigma-Aldrich
TEMP ²	C ₉ H ₁₉ NO	2403-88-5	98%	Sigma-Aldrich

¹DMPO: 5,5-dimethyl-1-pyrroline N-oxide;

²TEMP: 2,2,6,6-tetramethyl-4-piperidinol;

2.1.2 Instruments

Table 2-2. Equipment and instruments.

Instruments	Brand and model
pH meter	Cyberscan 510, Thermo Scientific
Total organic carbon (TOC)	TOC-L CPH CN200, SHIMADZU
X-ray Powder diffraction (XRD)	Bruker AXS D8 Advance
Fluorescence spectrophotometer	Varian Cary Eclipse
Atomic absorption spectrometer (AAS)	Perkin Elmer PinAAcle 900F
Scanning electron microscopy (SEM)	JEOL JSM-7100F
X-ray photoelectron spectroscopy (XPS)	OMICRON EA125, Germany
Ultraviolet visible spectrophotometer (UV-Vis)	Varian Cary 300
High performance liquid chromatography (HPLC)	Waters Alliance 2695
Electron paramagnetic resonance spectroscopy (EPR)	Bruker Xenon
Ultrapformance liquid chromatography-tandem Mass spectrometry (UPLC-MS/MS)	Acquity UPLC waters
High-resolution transmission electron microscopy (HRTEM)	JOEL 2100 LaB ₆

2.2 Preparation of materials and solutions

2.2.1 Synthesis of acid birnessite

Acid birnessite (AB) was prepared following the procedures of McKenzie [1]. 166 mL of concentrated HCl was added dropwise to 2.5 L of 0.4 M KMnO₄. The suspension was stirred vigorously and kept at 90°C during the HCl addition. The reaction was maintained at 90 °C for a further 10 min. Then, the obtained slurry was stirred vigorously at room temperature for 15 h. The precipitate was collected by centrifugation, washed with ultrapure water repeatedly until the conductivity was close to 0.6 μS cm⁻¹. The suspensions were stored in polypropylene containers at 4 °C for further use.

2.2.2 Synthesis of Mn(III) rich birnessite

Mn(III)-rich birnessite was synthesized according to previous published methods [2,3]. Briefly, about 2 g of acid birnessite was incubated with 80 mL of 10 mM sodium 4-(2-hydroxyethyl) piperazine-1-ethanesulfonate (HEPES) and 10 mM NaCl solutions at pH 6.5 ± 0.05 at a temperature of 25 °C for 48 h. The precipitate was collected by centrifugation and washed with ultrapure water.

2.2.3 Synthesis of manganite

Manganite (γ -MnOOH) particles were synthesized as described by Yu and co-workers [4]. Manganite was synthesized by adding 300 mL of 0.2 M NH_3 to a solution of 20.4 mL 30% H_2O_2 and 1000 mL 0.06 M MnSO_4 . The mixture was heated and kept at 95 °C for 6 h under constant stirring. Thereafter, the hot suspension was filtered through a G4 glass filter, washed with equal amounts (with respect to the initial solution) of hot deionized water, collected on watch glass and dried at room temperature under rough vacuum (10^{-3} Torr) in presence of P_2O_5 for 48 h. The manganite crystals dispersed well in suspensions, although they formed aggregates when dried.

2.2.4 Sewage treatment plant water collection

The sewage treatment plant water (STPW) was collected from the urban treatment plant named “3 rivières” in Clermont-Ferrand, France in December 2019. Prior to use, the STP water was filtered using a syringe filter (CHROMAFIL® Xtra RC-45/25) and then use for experiments. The main physico-chemical parameters relevant to this study are reported in Table 2-3.

Table 2-3. Characteristics of the sewage treatment plant water (STPW).

Parameters	Values
pH	8.5
TOC*	8.2 mgC L ⁻¹
IC*	30.35 mgC L ⁻¹
Cl ⁻	0.77 mM
NO ₃ ⁻	0.41 mM
SO ₄ ²⁻	0.29 mM
PO ₄ ³⁻	0.09 mM

*TOC: Total organic carbon; *IC: inorganic carbon.

2.3 Reaction process

2.3.1 Acid birnessite reduction by H₂O₂

BPA degradation was tested in this system. BPA kinetic experiments were carried out in a 150 mL serum bottle in aerated solution at 293 K. Reactivity change assessment was investigated as following: 100 mL aqueous suspension of acid birnessite corresponding to an initial concentration of 345 μM (30 mg L⁻¹) was first prepared and then an appropriate amounts of stock solutions of H₂O₂, BPA, and/or Mn(II) were added to start the reaction. The pH was adjusted to the desired value (6.5, unless otherwise indicated) using a pH meter by adding 0.1 M NaOH and/or HCl. The suspension was stirred with a speed of 350 rpm. At predetermined time interval, 1 mL of aqueous sample was withdrawn and filtered through 0.22 μm PTFE filter and immediately mixed with 200 μL of methanol to quench the reaction, and then analyzed. The same batch experiments were carried out in the presence of silicate or phosphate to evaluate the combined effects of anions and H₂O₂ on BPA oxidation.

2.3.2 PDS and PMS activation by Mn₂O₃

The chemical reactions were performed in a borosilicate brown bottle in which 100 mL of solution was kept at room temperature (298 ± 2 K) under stirring (700 rpm) to ensure

homogeneity. 25 μM of CAF was added to the 100 mL reaction solution containing a certain concentration of Mn_2O_3 , then a predetermined amount of oxidants (*i.e.* H_2O_2 , PS, PMS, or HSO_3^-) was added to start the reaction. The solution pH was fixed by adding 0.1 M NaOH and/or HClO_4 . 2 mL of samples were withdrawn at the predetermined interval times and were filtered (0.20 μm PTFE filter) to remove Mn_2O_3 particles. The reaction was stopped by the addition of 100 μL of methanol (HPLC grade, Sigma-Aldrich) and then the samples were analyzed by HPLC.

2.3.3 PMS activation by $\gamma\text{-MnOOH}$

PMS was added to the solution containing selected ECDs and $\gamma\text{-MnOOH}$ just before reaction starting. All reactions were performed in a brown glass bottle (125 mL) at room temperature (293 ± 2 K) and under stirring to ensure the homogeneity. Unless otherwise stated, experiments were performed at $\text{pH } 6.5 \pm 0.2$. For HPLC analysis, 2 mL of solution were withdrawn at fixed time intervals, filtered using (0.20 μm PTFE filter) and reaction was immediately quenched with addition of 20% methanol (HPLC grade, Sigma-Aldrich). Sample solution were kept at 277 K and analysis were performed within 4 hours. Furthermore, to identify the generated radicals, EtOH, TBA and FFA were added to the solution before PMS addition and a kinetic approach based on the second-order rate constants and pseudo-first order decay determination was used to assess the radical species involvement.

2.4 Analysis methods

2.4.1 Determination of target pollutants concentration

The concentration of target pollutants (*i.e.* BPA, CAF, E2 and EE2) were identified using the High-Performance Liquid Chromatography system (HPLC, Alliance 2695 Waters) equipped with Diode Array Detector (DAD) and multi λ Fluorescence Detector (FD). An Agilent Eclipse XDB C18 column (250×4.6 mm, 5 μm particle size) was adapted to analyze CAF, E2, EE2 and BPA (using FD detector). Another analytic column Macherey Nagel Nucleodur 100-5 C18 column (150×4.6 mm, 5 μm particle size) was used to analyze BPA (using DAD detector).

The temperatures of column and sample were set at 30 and 15 °C, respectively. The injection volume was set at 50 µL. Isocratic and gradient elution modes with different mobile phase compositions were used for the chromatographic separation. The parameters of flow rate and mobile phase compositions are presented in Table 2-4. For the measurement of E2, EE2 and BPA using the fluorescence detector, the excitation and emission wavelengths were set at 280 and 305 nm, respectively. The calibration curves of target compounds with different concentration were presented in Figure 2-1. According to the achieved calibration curves, the concentration of remaining pollutants in different reaction time can be obtained, and the corresponding degradation efficiency (DE) can be calculated using the equation of $\frac{C_0 - C_t}{C_0} \times 100$, where C_0 and C_t represent the initial and the residual concentration of the pollutants at time t, respectively.

Table 2-4. Parameters used for chromatographic separation of compounds on HPLC.

Chemicals	Detector	Flow rate	¹ DW	Elution mode & Mobile phase		
BPA	DAD	0.8 mL min ⁻¹	277 nm	Gradient elution mode		
					² MeOH	Water
				0 min	70%	30%
				7 min	90%	10%
				9 min	90%	10%
			9.5 min	70%	30%	
CAF	DAD	0.8 mL min ⁻¹	272 nm	Gradient elution mode		
					³ ACN	Water (0.1% H ₃ PO ₄)
				0 min	20%	80%
				6 min	70%	30%
				8 min	70%	30%
			8.5 min	20%	80%	
⁴ E2/EE2	FD	1.0 mL min ⁻¹	280 nm	isocratic	ACN (50%)	Water (50%)
BPA	FD	1.0 mL min ⁻¹	277 nm	isocratic	ACN (50%)	Water (50%)

¹DW: detection wavelength. ²MeOH: methanol. ³ACN: acetonitrile. ⁴E2/EE2: The retention time of E2 and EE2 are 6.2 and 7.3 min, respectively.

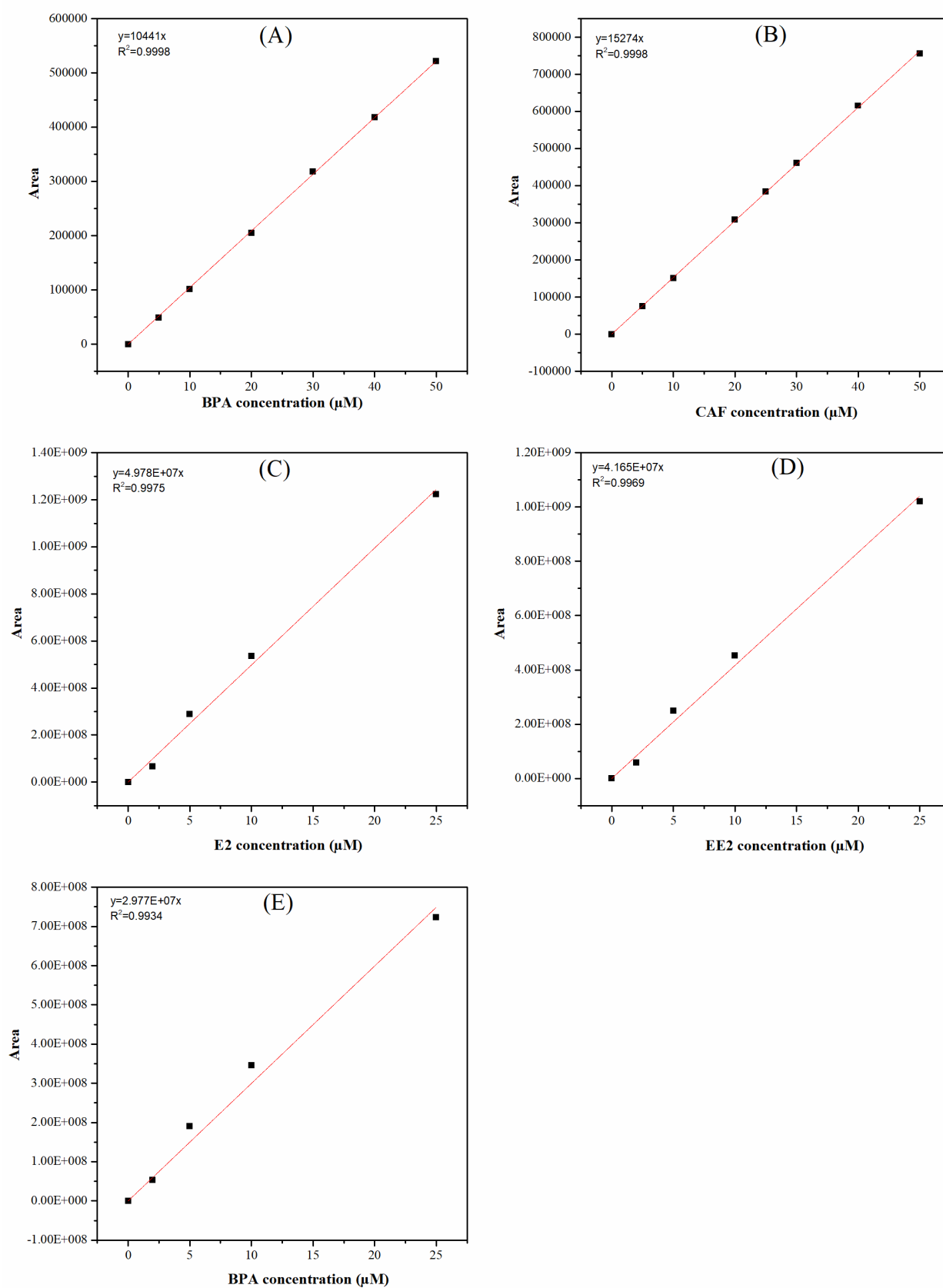


Figure 2-1. The calibration curves of target compounds. (A) BPA; (B) CAF; (C) E2; (D) EE2; and (E) for BPA using fluorescence detector.

2.4.2 H₂O₂ quantification

H₂O₂ concentration was determined using spectrofluorimetric detection [5]. The analysis is based on the reaction between H₂O₂ and 4-hydroxyphenylacetic acid which form the a stable 4-hydroxyphenyl acetic acid dimer in the presence of peroxidase (Figure 2-2) [6]. 4-hydroxyphenylacetic acid dimer is highly fluorescence compound with a maximum of excitation wavelength at 320 nm and emission at 420 nm. The calibration curve of H₂O₂ was obtained using different concentrations of H₂O₂ (Figure 2-3).

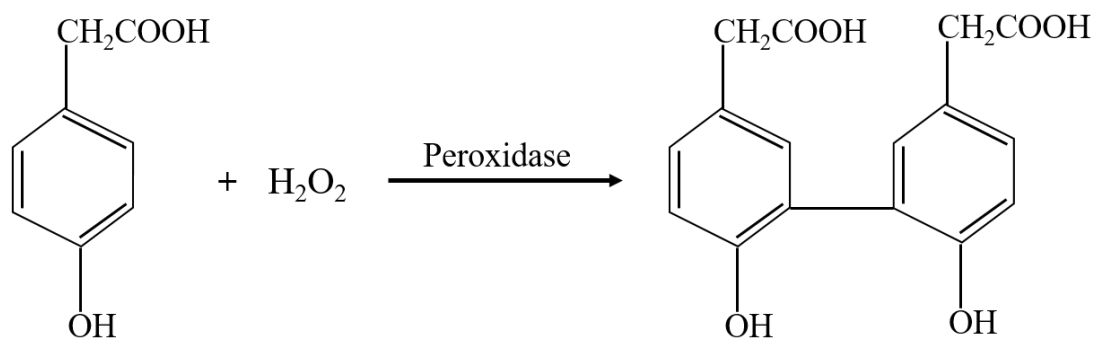


Figure 2-2. Enzyme peroxidase catalyzing reduction of H₂O₂.

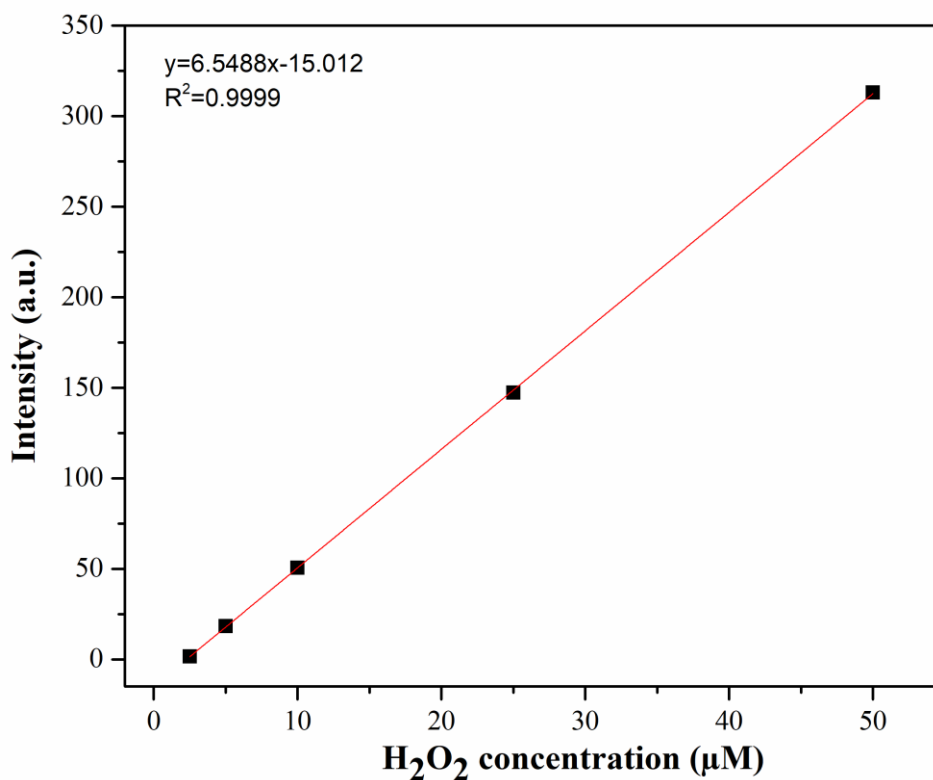


Figure 2-3. Calibration curve of H₂O₂ quantifications.

2.4.3 Determination of PDS and PMS concentration

The concentrations of PDS and PMS can be measured using a modified iodometric titration method [7]. The reaction mechanisms are as follow: PDS or PMS reacts with potassium iodide (KI) in the presence of sodium bicarbonate (NaHCO_3) to generate iodine (I_2). Then, I_2 further reacts with iodide (I^-) leading to the formation of triiodide (I_3^-). I_3^- can be quantified using a UV-visible spectrophotometer.

Specifically, 100 μL of sample containing PDS or PMS were transferred into 5 mL of a solution containing KI (0.6 M) and HCO_3^- (0.06 M). The absorption of solution at 348 nm was measured after 10 min of reaction and PDS/PMS concentration ($C_{\text{PDS/PMS}}$, (mM)) was determined as $C_{\text{PDS/PMS}} = \frac{V_{\text{tot}}}{V_{\text{PDS/PMS}}} \times \frac{\text{Abs}_{348 \text{ nm}}}{S}$. Where $V_{\text{PDS/PMS}}$ and V_{tot} are the volume of sample (100 μL) and total volume (5.1 mL), S was the slope of the linear correlation between the PDS/PMS concentration and value of absorption at 348 nm. In this study, S_{PDS} and S_{PMS} were 0.56 and 0.50, respectively. Calibration curves of PDS and PMS were performed using different PDS and PMS concentrations as shown in Figure 2-4.

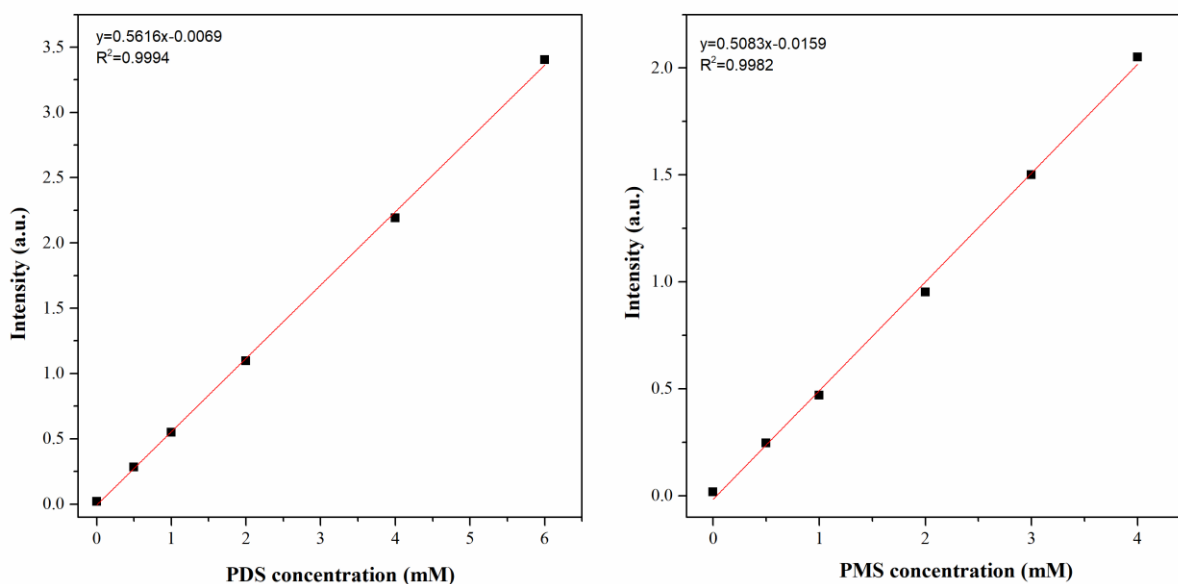


Figure 2-4. Calibration curve of PDS and PMS concentrations.

2.4.4 Identification of caffeine byproducts

The identification of CAF transformation intermediates was obtained by UPLC-MS system coupled with an ESI ion source (MSD VL). The column was a Phenomenex Kinetex C18 column (100 mm × 2.1 mm, particle and pore sizes 2.6 μm × 100 Å) using an initial gradient of 5% acetonitrile and 95% water acidified with 1% formic acid, followed by a linear gradient to 95% acetonitrile within 15 min and kept constant during 10 min. The flow rate was 0.2 mL min⁻¹ and the injection volume was 10 μL.

2.4.5 Identification of hydroxyl radicals

Terephthalic acid (TA) was reported to have the ability to trap hydroxyl radicals (HO•) leading to the formation of 2-hydroxyterephthalic acid (TAOH) (Figure 2-5). [8]. TAOH is a fluorescent product with an excitation wavelength at 320 nm and an emission wavelength at 425 nm, while TA cannot give any fluorescence. Therefore, the HO• generated in reactions can be quantified through detecting the product of HO• samples with TA using a fluorescence spectrophotometer.

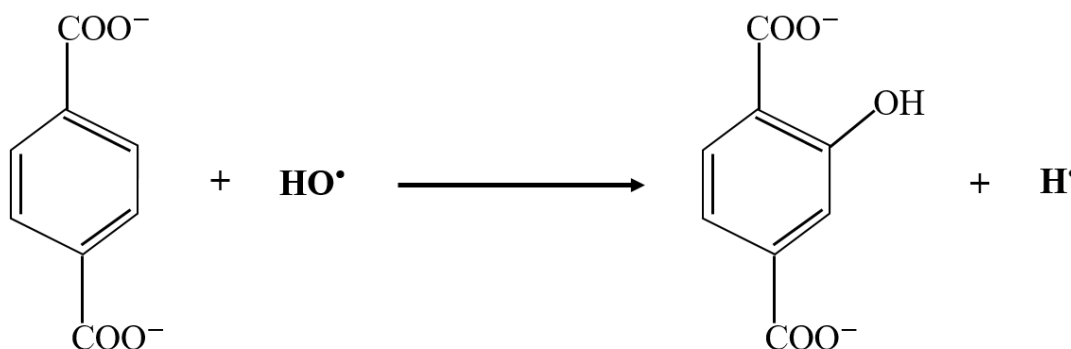


Figure 2-5. Reaction between TA and hydroxyl radicals.

2.4.6 Identification of reactive oxygen species

The common reactive oxygen species (such as sulfate radical, hydroxyl radical and singlet oxygen) can be identified using the electron paramagnetic resonance spectroscopy (EPR) with 5,5-dimethyl-1-pyrroline *N*-oxide (DMPO) or 2,2,6,6-tetramethyl-4-piperidinol (TEMP) as the spin trapping agents. DMPO is commonly used as the spin traps for sulfate and hydroxyl radicals. The typical hyperfine splitting constants of DMPO-HO• are $a_N = a_H = 14.9$ G. For

DMPO-SO₄^{•-}, the hyperfine splitting constants are $a_N = 13.2$ G, $a_H = 9.6$ G, $a_H = 1.48$ G, and $a_H = 0.78$ G [9]. TEMP is a commonly used spin trap for singlet oxygen. The characteristic peaks of TEMP-¹O₂ are the triplet signals (1:1:1) [9]. The procedure operated in the measurement were as follow, 375 μL of sample was withdrawn and immediately mixed with 125 μL of DMPO (100 mM) or TEMP (100 mM), then the mixture was transferred into an EPR quartz capillary tube (0.5 mm, 100 mm) for measurement. The EPR spectrometer was set as following: modulation frequency, ~100 kHz; microwave frequency, ~9.87 GHz; microwave power, ~6.87 mW; center field, ~352.7 mT; sweep width, 20 mT; sweep time, 30 s; sample g-factors, 2.0; modulation amplitude, 1.0 G.

2.4.7 Determination of Mn²⁺ concentration

The concentration of dissolved Mn²⁺ in solution was measured using an Atomic absorption spectroscopy (AAS). The parameters were settled as follows: the signal was set at AA (atomic absorption) with corrected background signal; the slit was set at 1.8 mm (width) / 2.3 mm (height); the detection wavelength was set at 279.48 nm; The lamp was installed for analysing Mn element with a courant of 30 mA; oxygen and acetylene flows were 10 and 2.5 L/min; integration time was 3s. Mn²⁺ standard solution for AAS (TraceCERT®, 1000 mg L⁻¹ Mn in 2% nitric acid) was used for making calibration curve of Mn²⁺ (Figure 2-6). The detection rages of Mn²⁺ in AAS was 0.2 to 5 mg L⁻¹. In the study, all the Mn²⁺ containing samples were first filtered through a 0.2 μm PTFE filter, then were acidified with the addition of 2% nitric acid (65%).

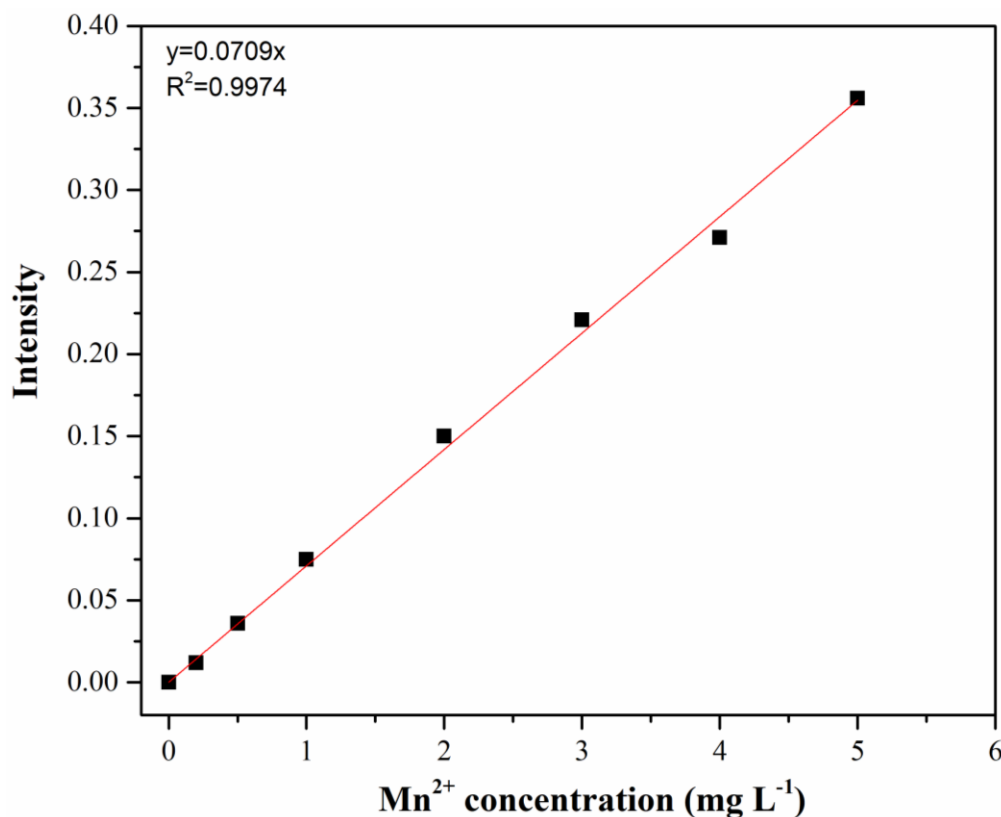
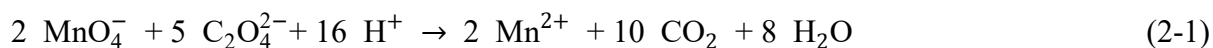


Figure 2-6. Calibration curve of Mn²⁺ concentrations.

2.4.8 Determination of Mn average oxidation state

A. Determination of Mn AOS using oxalic acid-permanganate back-titration method

The oxalic acid-permanganate back-titration method was employed to measure the average oxidation state (AOS) of acid birnessite [10]. The process was conducted as follow: 0.1 g of the acid birnessite were dissolved in 2.5 mL of 0.5 M H₂C₂O₄ and 5 mL of 1 M H₂SO₄ to reduce all highly charged manganese (such as Mn³⁺ and Mn⁴⁺) to Mn²⁺. The excess C₂O₄²⁻ was then back titrated with standardized 0.02 M KMnO₄ solution at 75-85 °C until the color of solution turned into reddish and lasted for 30 seconds without fading, to obtain the oxidation number of Mn (n_{Mn}) (see Eqs. (2-1) and (2-2)). Then, 0.1 g of the acid birnessite sample was dissolved in 20 mL of 0.25 M hydroxylamine hydrochloride and was diluted to 2 L with ultrapure water. AAS was used to determine the total Mn content (m_{Mn}). After that, according to the titration result and total Mn content, the AOS of acid birnessite was calculated (Eq. (2-3)).



$$n_{\text{Mn}} = 2 \times (\text{C}_{\text{H}_2\text{C}_2\text{O}_4} \times V_{\text{H}_2\text{C}_2\text{O}_4} - 2.5 \text{C}_{\text{KMnO}_4} \times V_{\text{KMnO}_4}) \times 10^{-3} \quad (2-2)$$

$$\text{AOS} = 2 + 54.94 \times \frac{n_{\text{Mn}}(\text{mol})}{m_{\text{Mn}}(\text{g})} \quad (2-3)$$

B. Determination of Mn AOS using X-ray photoelectron spectroscopy method

The determination of Mn AOS using x-ray photoelectron spectroscopy (XPS) can be achieved through analyzing the Mn 3s multiplet splitting spectra. The equation used for the calculation of Mn AOS is shown in Eq. (2-4) [11]. The ΔE_s can be obtained from the energy difference between the main peak and its satellite in Mn 3s.

$$\text{AOS} = 8.95 - 1.13 \Delta E_s \quad (2-4)$$

In addition, the Mn 2p spectrum can be used to obtain the abundance of Mn(II), Mn(III), and Mn(IV) on the surface of manganese oxides. The binding energy of Mn(II), Mn(III), and Mn(IV) in Mn 2p spectrum are 639, 640, and 643eV, separately. It is worth noting the binding energy of Mn ions may shift in a small scale due to the different reactions.

Data analysis, curve fitting and quantification of the Mn XPS spectra were performed using the CasaXPS and xpsPEAK4 software. The binding energy (BE) scale was referenced to the adventitious C1s peak at 284.8 eV. High-resolution XPS spectra were processed using Shirley back-ground subtraction. After background subtraction, the spectra were smoothed and fitted by using of Gaussian-Lorentzian peak shape. For each sample, fitting parameters (FWHM, the full width at half maximum; H, the peak height; E, the peak position center) were adjusted to minimize the value of residual standard deviation (STD).

2.4.9 Characterization of manganese oxides

A. Brunauer-Emmett-Teller (BET) surface measurement

The surface area of manganese oxide was measured using the BET method. Specifically, it allows the determination of the overall specific external and internal surface area of nano- or porous solids by measuring the amount of physically absorbed gas according to the BET method. A micrometrics ASAP 2010 instrument was employed to measure the adsorption of nitrogen. Prior to adsorption, the electrode materials were out-gassed under vacuum at room temperature.

B. X-ray diffraction (XRD) analysis

X-ray powder diffraction can provide the detailed information about the crystallographic structure, chemical composition, and physical properties of materials. In the study, the solid was characterized using XRD spectra obtained with the Bruker AXS D8 Advance diffractometer (θ - 2θ Bragg-Brentano geometry). The monochromatized $\text{CuK}\alpha 1$ (1.54\AA) was used to irradiate over the range of 10° - 100° 2θ at a step size of 0.02° . Phases were determined according to PDF database in Jade 6 software.

C. Microscopy-based techniques

Scanning electron microscopy (SEM) can provide a high-quality image of the material surface. Thus, the morphology of materials (such as rod, flower, and wire) can be identified using the SEM. The High-resolution transmission electron microscopy (HRTEM) provides more information about the internal structure of materials. The presented SEM and TEM images of this thesis were obtained using 1) SEM (JEOL JSM-7100F) and 2) HRTEM (JOEL 2100 LaB₆).

2.4.10 Determination of total organic carbon

The total organic carbon (TOC) is an important parameter to estimate the mineralization efficiency of organic pollutants. The TOC value can be determined as the difference between the total carbon (TC) and the inorganic carbon (IC) values. In the treatment process, the decreasing of TOC value indicates that the organic pollutant has been converted into carbon dioxide and carbonates ions. In this study, the TOC was determined using a TOC-L CPH CN200, SHIMADZU instrument. All the samples were filtered using the $0.45\ \mu\text{m}$ PTFE filter. The detection range of TC was 0 - $15\ \text{mgC L}^{-1}$. For the IC, the detection range was 0 - $4\ \text{mgC L}^{-1}$. The calibration curve of TC and IC with $50\ \mu\text{L}$ injection volume were shown in Figure 2-7.

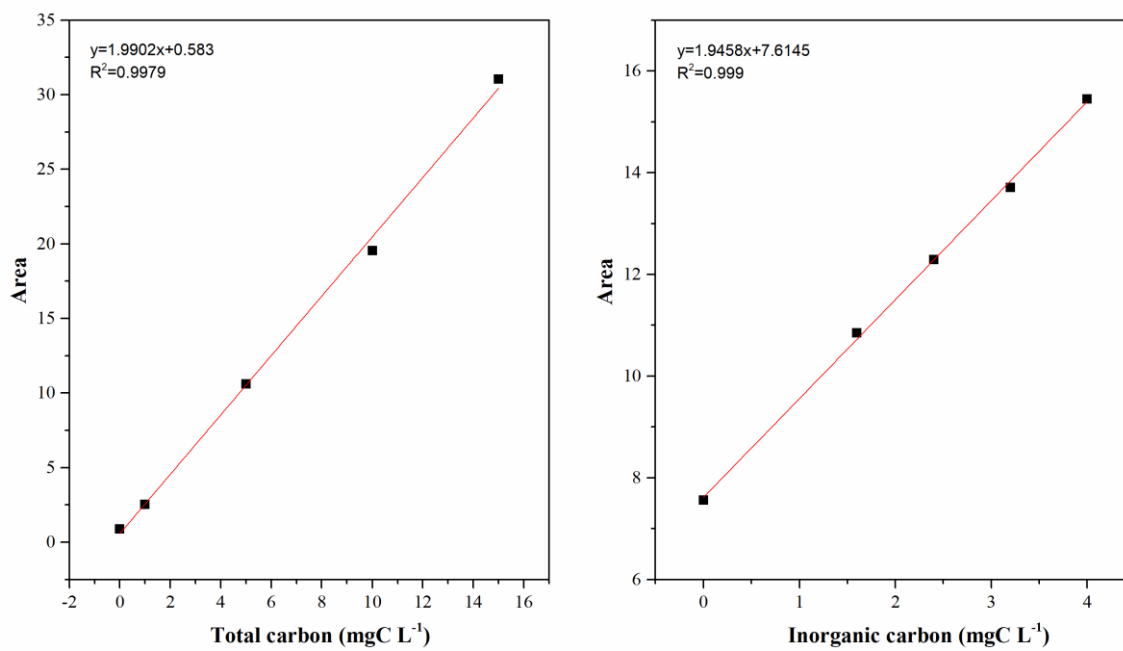


Figure 2-7. Calibration curves of total carbon and inorganic carbon.

Reference

- [1] R.M. McKenzie, The synthesis of birnessite, cryptomelane, and some other oxides and hydroxides of manganese, *Mineral. Mag.* 38 (1971) 493–502. <https://doi.org/10.1180/minmag.1971.038.296.12>.
- [2] A.A. Simanova, K.D. Kwon, S.E. Bone, J.R. Bargar, K. Refson, G. Sposito, J. Peña, Probing the sorption reactivity of the edge surfaces in birnessite nanoparticles using nickel(II), *Geochimica et Cosmochimica Acta.* 164 (2015) 191–204. <https://doi.org/10.1016/j.gca.2015.04.050>.
- [3] Q. Sun, P.-X. Cui, T.-T. Fan, S. Wu, M. Zhu, M.E. Alves, D.-M. Zhou, Y.-J. Wang, Effects of Fe(II) on Cd(II) immobilization by Mn(III)-rich δ -MnO₂, *Chemical Engineering Journal.* 353 (2018) 167–175. <https://doi.org/10.1016/j.cej.2018.07.120>.
- [4] C. Yu, J.-F. Boily, A. Shchukarev, H. Drake, Z. Song, K.J. Hogmalm, M.E. Åström, A cryogenic XPS study of Ce fixation on nanosized manganite and vernadite: Interfacial reactions and effects of fulvic acid complexation, *Chemical Geology.* 483 (2018) 304–311. <https://doi.org/10.1016/j.chemgeo.2018.02.033>.
- [5] Y. Wu, M. Passananti, M. Brigante, W. Dong, G. Mailhot, Fe(III)–EDDS complex in Fenton and photo-Fenton processes: from the radical formation to the degradation of a target compound, *Environ Sci Pollut Res.* 21 (2014) 12154–12162. <https://doi.org/10.1007/s11356-014-2945-1>.
- [6] A.L. Lazrus, G.L. Kok, S.N. Gitlin, J.A. Lind, S.E. McLaren, Automated fluorimetric method for hydrogen peroxide in atmospheric precipitation, *Anal. Chem.* 57 (1985) 917–922. <https://doi.org/10.1021/ac00281a031>.
- [7] S. Waclawek, K. Grübel, M. Černík, Simple spectrophotometric determination of monopersulfate, *Spectrochimica Acta Part A: Molecular and Biomolecular Spectroscopy.* 149 (2015) 928–933. <https://doi.org/10.1016/j.saa.2015.05.029>.
- [8] T. Charbouillot, M. Brigante, G. Mailhot, P.R. Maddigapu, C. Minero, D. Vione, Performance and selectivity of the terephthalic acid probe for OH as a function of temperature, pH and composition of atmospherically relevant aqueous media, *Journal of Photochemistry and*

Photobiology A: Chemistry. 222 (2011) 70–76. <https://doi.org/10.1016/j.jphotochem.2011.05.003>.

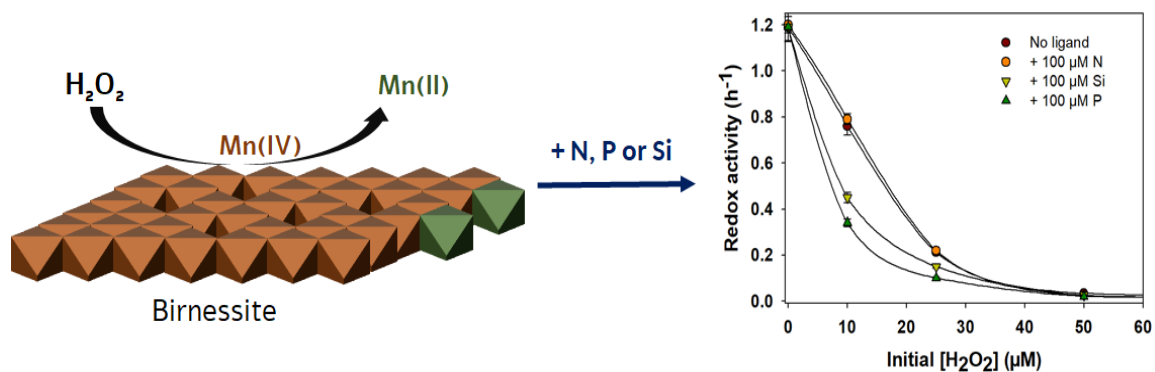
[9] J. Huang, H. Zhang, Mn-based catalysts for sulfate radical-based advanced oxidation processes: A review, *Environment International*. 133 (2019) 105141. <https://doi.org/10.1016/j.envint.2019.105141>.

[10] Y. Zhu, X. Liang, H. Zhao, H. Yin, M. Liu, F. Liu, X. Feng, Rapid determination of the Mn average oxidation state of Mn oxides with a novel two-step colorimetric method, *Anal. Methods*. 9 (2016) 103–109. <https://doi.org/10.1039/C6AY02472F>.

[11] J. Wan, L. Zhou, H. Deng, F. Zhan, R. Zhang, Oxidative degradation of sulfamethoxazole by different MnO₂ nanocrystals in aqueous solution, *Journal of Molecular Catalysis A: Chemical*. 407 (2015) 67–74. <https://doi.org/10.1016/j.molcata.2015.06.026>

Chapter III

Impacts of environmental levels of hydrogen peroxide and oxyanions on the redox activity of MnO₂ particles



Published journal: Environmental Science Processes & Impacts

Accepted date: 5th July, 2021

Motivation

Hydrogen peroxide (H_2O_2) was commonly used as the radical precursors in various AOPs. For instance, the classical Fenton reaction employs H_2O_2 as the oxidant to generate hydroxyl radicals in the presence ferrous ions (Fe^{2+}). Manganese dioxide (MnO_2) exhibited high performance in activation of various radical precursors and in oxidation of organic pollutants. For example, Huang et al reported the oxidation of bisphenol A by various MnO_2 (α -, β -, γ -, δ -, and λ - MnO_2). Liu et al. demonstrated the efficient degradation of DDT (1,1,1-trichloro-2,2-bis(p-chlorophenyl) ethane) by different MnO_2 (α -, β -, γ - MnO_2) activated PMS. The catalyzed decomposition of H_2O_2 by MnO_2 has been also investigated. For example, Kim et al. reported the removal of methylene blue (MB) dye using α -, β -, γ - and δ - MnO_2 activated H_2O_2 . Do et al. investigated the degradation of toluene sorbed on activated carbon in the system of β - $\text{MnO}_2/\text{H}_2\text{O}_2$. However, the previous studies focused on the elimination efficiency of pollutants, and overlooked the influence of H_2O_2 on the oxidative activity of MnO_2 . H_2O_2 has an ambivalent redox activity and has been commonly found in aquatic environments at concentration ranging from nM to μM . Birnessite-type MnO_2 play a key role in the global carbon cycle as well as pollutant dynamics. Therefore, it is significant to investigate the impact of environmental levels of H_2O_2 and oxyanions on the oxidative reactivity of acid birnessite.

1. Introduction

Layered structure manganese oxides (*e.g.* birnessite) are ubiquitous in a wide range of aquatic and terrestrial environments [1]. The presence of exchangeable hydrated cations within the interlayers combined with a high content of vacancy sites and variable oxidation states of manganese make them powerful sorbents and oxidants [2,3]. As a result, birnessite-type manganese oxides play a significant role in controlling the cycles of several key nutrients as well as the fate and mobility of inorganic and organic contaminants [4–9]. Acid birnessite has been widely investigated because it is structurally similar to biogenic “natural” manganese oxides [10–13]. The birnessite reactivity is mainly affected by solution pH, surface properties and composition of MnO₂ and structural characteristics of redox-active contaminants [4–6,12]. It can also be influenced by the presence of naturally occurring compounds, *e.g.* cations, anions, natural organic matter and other redox-active compounds. Among the latter, hydrogen peroxide (H₂O₂) has an ambivalent redox activity and is commonly found in aquatic environments at concentration ranging from nM to μM [14–26].

In environmental systems, photodependent reactions mediated by natural organic matter and biological-mediated processes dominate H₂O₂ production [26]. Sunlight-induced photochemical reactions mediated by organic ligands and/or biochemical metabolic processes can result in amounts of H₂O₂ up to 20 μM [14–18]. Input from rainwater can reach up to 40 μM [20,21], while hydrogen peroxide production has been often observed in irradiated seawater [19–21]. Light-independent generation of H₂O₂ has been recently reported in river sediments and in groundwater of an alluvial aquifer, which is likely to occur in transitional redox environments where reduced elements react with oxygen [22,23]. For example, natural hydroquinones or hydroquinone moieties ubiquitously present in reduced organic matter can donate electrons to O₂ to generate H₂O₂ [24,25]. H₂O₂ production through microbial mechanism has also been shown to enhance iodide oxidation and organo-iodine formation in soils and sediments [27]. All these studies suggested that H₂O₂ can be formed not only in oceanic and atmospheric systems but also in the subsurface environment. Finally, higher concentrations (up

to 1 mM) have been reported in nuclear waste repository scenarios when ionizing radiation of groundwater adjacent to spent nuclear fuel result in H₂O₂ production [28].

Despite the catalyzed decomposition of hydrogen peroxide by MnO₂ has been well investigated [29–31], knowledge is very limited on the effect of H₂O₂ on the reactivity of birnessite at environmental levels of H₂O₂. In engineering applications, metal oxides such as MnO₂ are generally investigated for catalytic decomposition of H₂O₂ and then formation of reactive transient species using very high concentrations of hydrogen peroxide (H₂O₂) (≥ 0.5 mM) [29–31]. While these remediation studies aimed to eliminate pollution in contaminated systems, they overlooked the influence of H₂O₂ on the electron transfer heterogeneous reaction and then the oxidative activity of birnessite. In addition, little is known about the influence of H₂O₂ on the birnessite composition and interactions of redox products (*e.g.* Mn(II)) with MnO₂ surfaces. In this study, we examine how H₂O₂ affects the reactivity of birnessite under environmentally relevant conditions. To monitor H₂O₂-induced changes in birnessite reactivity, we used Bisphenol A (BPA) as a model compound because it has a strong reactivity with the birnessite (δ -MnO₂), with a well-documented underlying redox mechanism [32–35]. Acid birnessite, a well-established laboratory synthesized analog of layered birnessite mineral, was chosen as a representative manganese dioxide mineral. The removal kinetics of BPA have been assessed in presence of variable amounts of H₂O₂ under a wide range of pH (4, 6.5 and 8) under aerobic and anaerobic conditions. Alteration of birnessite structure and composition was monitored using XRD and titration experiments under different conditions (H₂O₂/MnO₂ molar ratio, dissolved Mn(II) amount and pH value). To check whether the impact of H₂O₂ can persist in natural waters, changes in birnessite reactivity were investigated in presence of commonly found anionic ligands such as phosphate, nitrate and silicate. We notably demonstrated that at H₂O₂ concentrations as low as 10 μ M or with H₂O₂/MnO₂ molar ratio as low as 0.03, the reactivity of acid birnessite can be affected, which could alter biogeochemical cycles as well as pollutant dynamics.

2. Materials and Methods

2.1. Chemicals

KMnO₄, HCl, NaCl, NaOH, HEPES, H₂C₂O₄, H₂SO₄, hydroxylamine hydrochloride, H₂O₂, BPA, HNO₃, terephthalic acid, 2-hydroxyterephthalic acid, Na₂SiO₃, NaNO₃, NaH₂PO₄ and MnCl₂ were purchased from Sigma-Aldrich and were all AR grade. All chemicals were used as received without further purification. All solutions were prepared in ultrapure water obtained from a water purification system (Millipore, resistivity 18.2 MΩ cm).

2.2. Synthesis and characterization of acid birnessite

Acid birnessite was prepared following the procedure of McKenzie [36], and Mn(III)-rich MnO₂ was synthesized according to previous published methods [37,38]. More details are provided in the Supporting Information (SI). The solid was characterized using X-ray powder diffraction (XRD) using the Bruker AXS D8 Advance diffractometer (θ -2 θ Bragg-Brentano geometry) using monochromatized CuK α 1 (1.54Å) radiation over the range of 10°-100° 2 θ at a step size of 0.02°. X-ray diffraction (XRD) confirmed that the only product of the synthesis was poorly-crystalline hexagonal birnessite. The Brunauer–Emmett–Teller (BET) specific surface area of the synthetic birnessite measured by multipoint N₂ adsorption was 60 ± 2.5 (SD) m² g⁻¹. The Average Oxidation State (AOS= 3.98 (±0.02)) of synthetic birnessite and (AOS= 3.65 (±0.02)) of Mn(III)-rich MnO₂ were measured using the oxalic acid-permanganate back-titration method (more details are provided in SI). Scanning Electron Microscope (SEM; JEOL JSM-7100F) and High-resolution Transmission Electron Microscope (HRTEM; JEOL 2100 LaB₆) images showed a nanoflower-shaped birnessite consisting of nanoflakes aggregations (see Figure S1).

2.3. Kinetics experiments and analyses

Reactivity changes assessment were investigated as following: 100 mL aqueous suspension of acid birnessite (AB) corresponding to an initial concentration of 345 μM was first prepared and then an appropriate amount of stock solutions of H₂O₂, BPA, and/or Mn(II) were added to start

the reaction at room temperature. Since the involved reactions can consume protons (see below), the pH was adjusted to the desired value and then kept constant throughout the reaction using a pH meter (Cyberscan 510, Thermo Scientific) by adding 0.1 M NaOH or HCl. The suspension was stirred with a speed of 350 rpm. 1 mL of aqueous sample was withdrawn at different time interval, filtered through 0.22 μm PTFE filter, and then analyzed. The same batch experiments were carried out in the presence of silicate or phosphate to evaluate the combined effects of anions and H_2O_2 on BPA oxidation.

Potential generation of hydroxyl radical was monitored through the fluorescence emission spectrum of 2-hydroxyterephthalic acid (λ_{ex} 320 nm, λ_{em} 425 nm) using a spectrofluorometer (Shimadzu RF-5301PC) (more information is given in the SI).

The BPA concentration was determined by a high-performance liquid chromatography system (HPLC, Waters Alliance) equipped with a diode array detector (DAD). Chromatographic separation was performed using a Nucleodur 100-5 C18 column (150×4.6 mm, 5 μm of particle size, Macherey Nagel). The detection wavelength of BPA was set at 277 nm and the column temperature was kept at 30 $^\circ\text{C}$. Methanol and water were mixed as the mobile phase under a gradient eluent mode, and the percentage of methanol changed with time was as follows: from 0 to 7 min was increased from 70 to 90% and kept constant up to 9 min. The flow rate was set at 0.8 mL min^{-1} . The byproducts of BPA oxidation were identified using Ultraperformance Liquid Chromatography-tandem Mass Spectrometry (UPLC-MS/MS) system. An electrospray interface was used for the MS measurements in positive ionisation mode and full scan acquisition.

H_2O_2 concentration was determined using a spectrofluorometric detection as described in our previous work [39]. Briefly, samples containing H_2O_2 were mixed with 4-hydroxyphenylacetic acid to form the stable 4-hydroxyphenyl acetic acid dimer in the presence of peroxidase (POD, Sigma-Aldrich). The 4-hydroxyphenylacetic acid dimer was quantified using a Cary Eclipse fluorescence spectrophotometer. The excitation wavelength was set at 320 nm and emission wavelength maximum was determined at 420 nm. Concentration was calculated using calibration curve obtained using different concentrations of H_2O_2 [40].

Dissolved Mn(II) concentration in aqueous solution was determined by Atomic Absorption Spectroscopy (AAS, PerkinElmer). All the samples were first filtered using a PTFE 0.22 μm filter and then mixed with 2% nitric acid (HNO_3 , 65%, Sigma- Aldrich) prior for analyses. Dissolved Mn(II) standard solution for AAS (TraceCERT®, 1000 mg L^{-1} Mn(II) in 2% nitric acid, Sigma-Aldrich) was used for the calibration curve. The detection wavelength was set at 279 nm and the AAS detection limit lied at 0.02 μM . Mn(II) removal was calculated as the difference between the initial and final Mn(II) solution concentrations.

The impact of anions on reactivity changes was investigated as mentioned above, but with addition of the chosen anion with BPA or Mn(II) to the AB suspension. Silicate concentration was determined by the molybdenum-blue colorimetric method ⁴¹ while phosphate and nitrate concentrations by ion chromatography [42]. XRD was performed to determine the possible transformation of solids upon Mn(II) sorption.

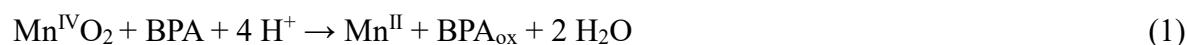
Since Mn(II) oxidation by molecular oxygen may take place, particularly at alkaline pH values, we compared the removal kinetics under aerobic (open atmosphere) vs anaerobic conditions (glove box $\text{N}_2:\text{H}_2$ 98:2). Prior for anoxic experiments, all solutions were sparged with nitrogen to remove oxygen. These preliminary tests showed that there is no effect of oxic conditions on the BPA removal in presence of H_2O_2 or Mn(II). Great attention has also been paid to the pH adjustment in all experiments, since the involved reactions are sensitive to pH value (see below). All experiments were conducted in triplicates and the standard deviation was calculated for all experimental series, and given in the caption of each figure.

3. Results and Discussion

3.1. Effect of H_2O_2 on the oxidative ability of birnessite

BPA removal was monitored in the presence of acid birnessite (AB) at different H_2O_2 concentrations at pH 6.5 (Figure 1). In the absence of H_2O_2 , almost complete removal of BPA was observed after 24 h of reaction time. Mass balance showed that the oxidation reaction was mainly involved in the removal of BPA in presence of MnO_2 , while adsorption was very low under our experimental conditions (*i.e.* less than 5% of initial BPA), which is consistent with

previous investigations [6,32,33]. Indeed, BPA containing two hydroxyphenyl functionalities is known to weakly interact with mineral surfaces, resulting in lower adsorption affinity to metal-oxides [32]. As previously reported [6,33,43], binding to birnessite is followed by an electron transfer process resulting in the concomitant oxidation of sorbed compound and reduction of surface-bound Mn(IV) to yield Mn(III) that can be further reduced to give Mn(II).



Electron exchange of BPA with MnO₂ forms a radical, followed by a series of reactions including radical coupling, fragmentation, substitution and elimination to form multiple byproducts [6,32,33]. LC/MS analysis identified one predominant species of mass-to-charge ratio of $m/z = 135$ as the most dominant byproduct of BPA over the first reaction time (90 min), which likely corresponds to 4-hydroxycumyl alcohol according to previous investigations [44].

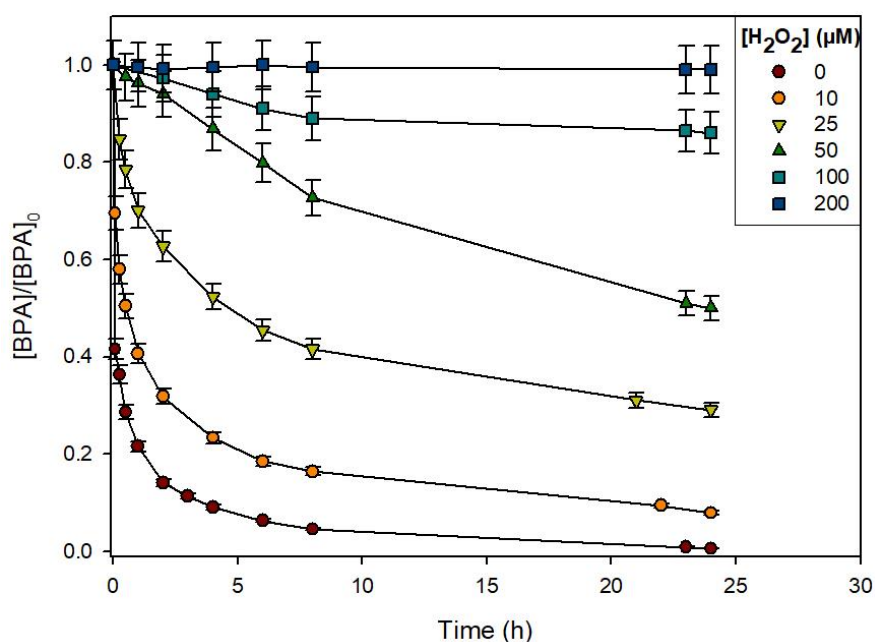


Figure 1. Effect of H₂O₂ concentration on the BPA removal at pH 6.5 at room temperature. Experimental conditions: [AB] = 345 μM, [BPA] = 25 μM. H₂O₂/MnO₂ ratio = 0 - 0.6. The relative experimental error lied at 5 % for BPA.

In the presence of hydrogen peroxide, the oxidative removal of BPA gradually decreased with increasing in H₂O₂ concentration, and completely suppressed at higher dose of H₂O₂ (200 μM equivalent to a H₂O₂/MnO₂ molar ratio ~ 0.6). In these experiments, the H₂O₂ decomposition

is relatively fast whatever the investigated pH, since complete decomposition of H₂O₂ was achieved after 15 min of reaction, even for the highest H₂O₂ dose (See Figure S2 and S3). Monitoring of fluorescence emission spectra of suspensions using a terephthalate as a chemical probe indicated that no hydroxyl radical was generated under the experimental conditions of this study. Additional experiments using 1-propanol (1 mM) or t-butanol (1 mM) as hydroxyl-radical scavengers confirmed that the BPA removal is a no radical-based oxidation process regardless of the presence or absence of H₂O₂.

The suppressive effect of H₂O₂ on the removal rate of BPA was then confirmed at two other pH values (4 and 8). The removal kinetics could not be properly described by simple equations that include classical exponential functions (*e.g.*, first- or second- order model), probably due to the complexity of involved reactions in the investigated system. Instead, we calculated the initial rate constant (k , h⁻¹) by linear regression of $\ln [BPA] / [BPA]_0$ versus time over the first stage of reaction (see example in Figure S4). The initial rate constants for all investigated H₂O₂ amounts exhibited the same order, pH 4 > pH 6.5 > pH 8 (Figure 2). In the absence of H₂O₂, k was decreased almost 20-fold when pH increased from 4 to 8. This suggests that acidic conditions favored BPA removal, a trend also observed for other organic compounds reacting with MnO₂ [33,34,45]. We attribute this to variability in two pH-dependent factors: 1) speciation of BPA that affects binding to MnO₂ surfaces and then oxidation (Figure S5), and 2) redox-potential of MnO₂ that decreases when the pH increased from 4 to 8 [46]. At relatively low pH, favorable electrostatic interactions between neutral BPA molecules and the negatively charged surface of MnO₂ (PZC of MnO₂ is ~ 2.3-2.9) may exist. On the other hand, reductive conversion of MnO₂ into Mn(II) is dependent on the amount of protons, which would result in increase in BPA removal rate when the pH decreases (Eq. 1). In the presence of H₂O₂, the removal rate constants of BPA sharply decreased with increasing in H₂O₂ amount whatever the investigated pH value (Figure 2).

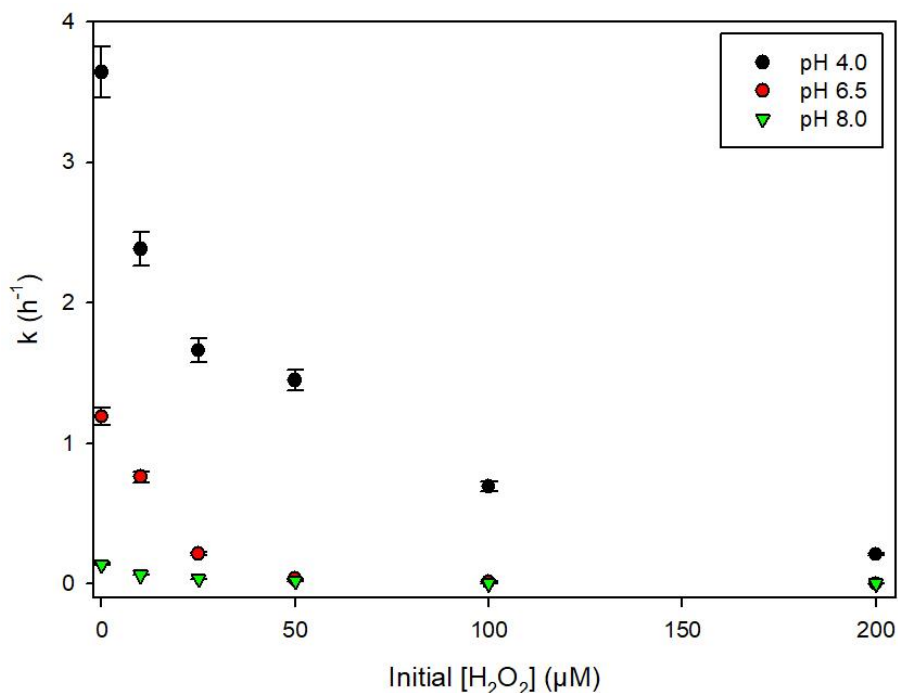
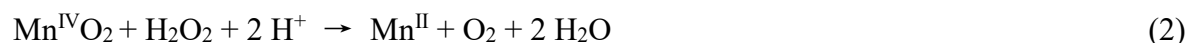


Figure 2. Removal rate constants (h^{-1}) of BPA as a function of H_2O_2 dose at three pH values (4, 6.5 and 8). Experimental conditions: $[\text{AB}] = 345 \mu\text{M}$, $[\text{BPA}] = 25 \mu\text{M}$, $[\text{H}_2\text{O}_2] = 0 - 200 \mu\text{M}$. $\text{H}_2\text{O}_2/\text{MnO}_2$ ratio = 0 - 0.6, room temperature. The relative experimental error lied at 5 %.

As for BPA, it is previously reported that hydrogen peroxide can also reduce Mn(IV) to Mn(III) and then Mn(II) as follows [47,48]:



To check this possibility under our experimental conditions, the reductive dissolution of MnO_2 in presence of various amounts of H_2O_2 was monitored at three pH values (Figure 3). In both Eq. 1 and Eq. 2, protons are directly involved in the oxidation of BPA as well as the reductive dissolution of MnO_2 . In the absence of H_2O_2 , dissolved Mn(II) was only detected at pH 4, while it was below the detection limit at pH 6.5 or 8. Increasing H_2O_2 concentration from 50 μM to 200 μM enhanced the amount of dissolved Mn(II), at the three investigated pH values. At each pH value, the amount of dissolved Mn(II) increased first, reached a maximum and then decreased. This two-step behavior is consistent with the H_2O_2 decomposition over time, where the complete decomposition of H_2O_2 observed after approximately 15 min of reaction time coincides with the peak observed for dissolved Mn(II) generation (Figure S3). This behavior

also suggests that the production of Mn(II) via H₂O₂-induced reduction of MnO₂ is faster than the Mn(II) adsorption onto birnessite. Once the added H₂O₂ is fully decomposed, the generated dissolved Mn(II) will in turn sorb onto MnO₂ surfaces.

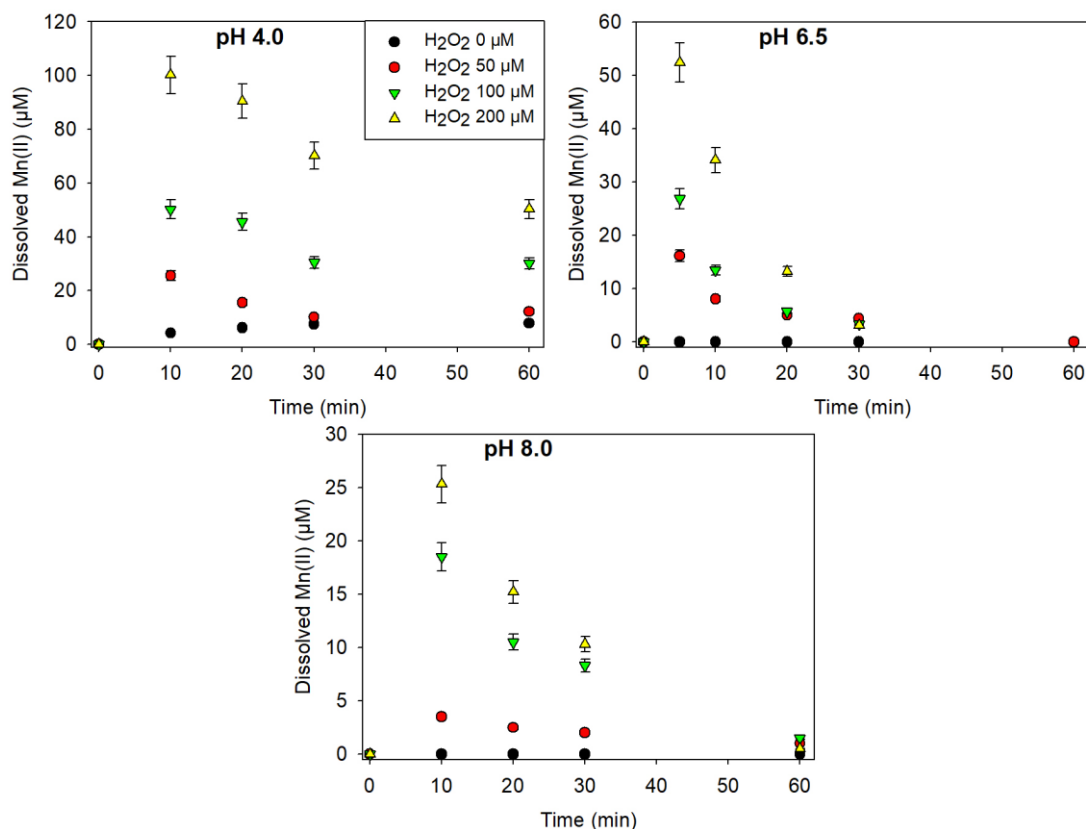


Figure 3. Mn(II) formation under different H₂O₂ concentrations and pH 4.0, 6.5 and 8.0.

Experimental conditions: [AB] = 345 µM and [BPA] = 25 µM. H₂O₂/MnO₂ ratio = 0 - 0.6, room temperature. The relative experimental error lied at 7 % for Mn(II).

Because higher pH implies more Mn(II) binding [49–51], greater amounts of Mn(II) were observed at low pH values (Figure 3). When a further addition of H₂O₂ is made after total decomposition of the initial amount (*e.g.* after 15 min at pH 4), the amount of generated Mn(II) increased again and reached almost twice the first measured amount within approximately 15 min. This suggests that the reductive dissolution of MnO₂ by H₂O₂ is a fast process, as compared to the reaction between MnO₂ and BPA.

To check whether Eq.1 and Eq.2 may occur simultaneously during the heterogeneous reactions with MnO₂, we compare the standard potential of involved reactions at the working pH range.

MnO₂ has standard (reduction) potential varying from 0.99 to 0.76 V when the pH rises from 4 to 8 for MnO₂ + 4 H⁺ + 2 e⁻ → Mn^{II} + 2 H₂O. This value is higher than the standard oxidation potential of O₂/H₂O₂ (O₂ + 2 H⁺ + 2e⁻ → H₂O₂ 0.68 V vs. NHE) or of BPA which varies between 0.75 V and 0.52 V in the pH range 4-8 [52–54]. Since the latter redox couples have comparable oxidation potential, reactions (Eq. 1) and (Eq. 2) could simultaneously take place. Assuming that these reactions obey pseudo-first order kinetic equation because MnO₂ is considered in excess, the reaction rate depends on the concentration of reactants (*i.e.* H₂O₂ or BPA). When the H₂O₂ amount increases, the reaction 2 should become much faster than the reaction 1. This was experimentally shown in Figures 1 and 3 and Figure S2, where both reactions Eq. 1 and Eq. 2 occurred simultaneously until complete inhibition of Eq. 1 at the highest H₂O₂ amount (200 μM). Though H₂O₂ was full decomposed after 15 min of reaction time (Figure S2), the suppressive effect on the birnessite reactivity was still observed over 24 h of reaction time (Figure 1). This was confirmed by carrying out sequentially the reactions (Eq. 2) and (Eq. 1). Indeed, suppression of BPA removal capacity was also observed when MnO₂ and H₂O₂ were allowed to react first (*i.e.* pre-equilibration step of 30 min) until total decomposition of H₂O₂ before addition of BPA (Figure S6). Therefore, the H₂O₂-mediated reduction of MnO₂ (Eq. 2) considerably affects the surface reactivity of birnessite and its ability to remove BPA. This reductive dissolution generates Mn(II) ions which will in turn bind to MnO₂ surfaces and then be oxidized into higher valence Mn:



This oxidation reaction may be made possible by the residual H₂O₂ and/or generated O₂ (through Eq. 2), which is pH-dependent. The contribution of O₂ from ambient air is excluded since reactivity assessment tests investigated under aerobic vs anaerobic conditions showed similar behavior in term of BPA removal.

It is worth noting that strong aggregation of MnO₂ particles and then fast sedimentation was observed upon addition of H₂O₂. This phenomenon can be ascribed to charge neutralization (*i.e.* surface charge switch from negative to positive) upon Mn(II) ions binding to negatively charged MnO₂ surfaces, as previously reported [55]. Furthermore, disproportionation

/comproportionation reaction (Eq. 4) may occur within the MnO₂, *i.e.* Mn^{II} exchanges electrons with Mn(IV) to form two Mn(III) centers and, conversely, two Mn(III) centers can disproportionate to form Mn(II) and Mn(IV) centers [12,32,35,51,56]:



Since this reaction is pH-dependent, we have measured the average oxidation state (AOS) of birnessite over the whole investigated pH range (4-8). The AOS of samples reacted with BPA (25 μM) alone only slightly decreased from 3.98 to 3.90 (± 0.02). However, partial reduction of MnO₂ upon addition of 200 μM of H₂O₂ dropped down the AOS to 3.74 (± 0.04) at pH 4 and 6.5, and 3.61 (± 0.04) at pH 8. This decrease suggests that percentages of Mn(III) or Mn(II) or both are relatively higher at the end of reaction with respect to the initial sample. The formation of Mn(III) was further confirmed by the detection of Mn(III)-pyrophosphate complex at 480 nm, Mn(III) being stabilized through ligand-binding complexes [57]. The effect of H₂O₂ on the structure of birnessite will be discussed in the following section.

Collectively, these results suggest that the H₂O₂ induced reduction of MnO₂ is an effective process, and the fast generation of Mn(II) is key for suppressed oxidative capacity of MnO₂ towards BPA. To confirm the impact of Mn(II) on the reactivity of MnO₂, BPA removal kinetics were investigated in Mn(II)-amended birnessite suspensions in the following section.

3.2. Effects of Mn(II) on the removal capacity of MnO₂

The initial rate constants of BPA removal sharply decreased with increasing in dissolved Mn(II) amount at pH 4 and 6.5, while at pH 8 it increased first between 0 and 10 μM but later decreased with increasing in initial Mn(II) amount (Figure 4). It is previously reported that the adsorption of cations such as Ca(II) or Mg(II) may change the surface charge from negative to positive by exchange of H⁺ on the MnO₂ surface [58,59]. Similarly, the Mn(II) adsorption should lead to a decrease in the negative surface charge, thereby altering the binding capacity of MnO₂. When the Mn(II) amount further increases, we speculate a competition between BPA and Mn(II) to bind at reactive sites of MnO₂ during the first kinetic phase, as recently observed for quinolones [43].

As for H₂O₂, dissolved Mn(II) displayed suppressive effects on the removal rate of BPA and the rate constants over the whole Mn(II) concentration range (10 - 100 μM) exhibited the same order, pH 4 > pH 6.5 > pH 8 (Figure 4). In addition to the comproportionation reaction that is pH-dependent, the decrease in the oxidative ability of MnO₂ in the presence of dissolved Mn(II) may result from competition of compound and Mn(II) to interact with reactive surface sites. The strong binding of Mn(II) to MnO₂ surfaces suggests competition of BPA and Mn(II) for surface sites, which is pH dependent [33,45]. Adsorption tests showed that 100 μM of Mn(II) were completely removed at both pH 6.5 and 8 (i.e. dissolved Mn(II) was below the detection limit), while 70 % of the added Mn(II) was removed at pH 4.

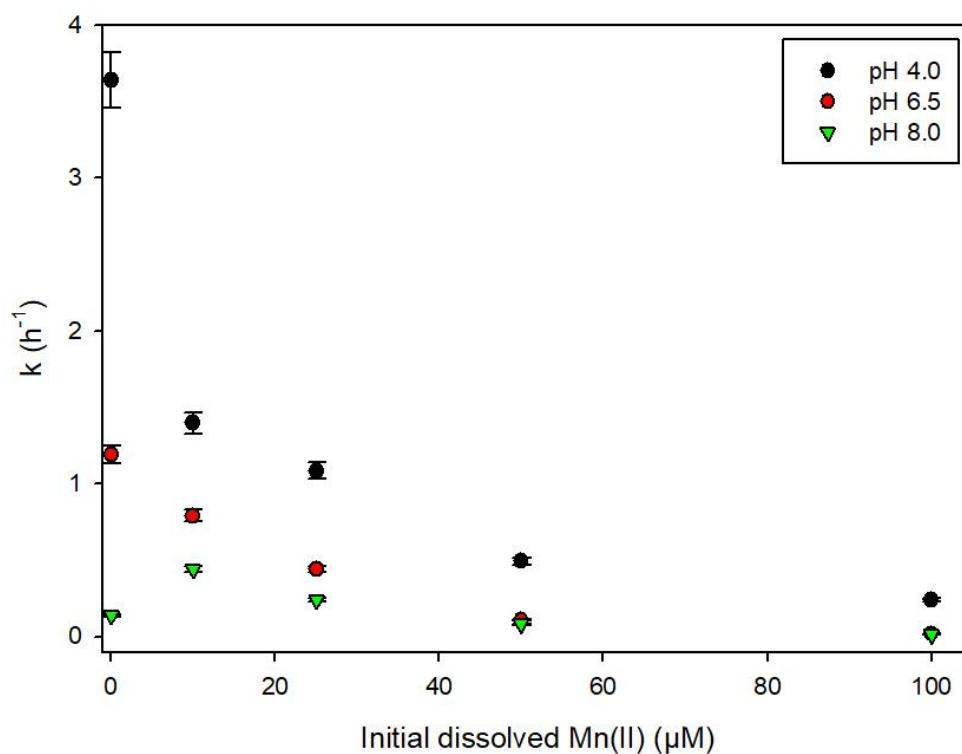


Figure 4. Removal rate constants (h⁻¹) of BPA as a function of Mn(II) concentration at three pH values (4, 6.5 and 8). Experimental conditions: [AB] = 345 μM, [BPA] = 25 μM, [Mn(II)] = 0 - 100 μM, room temperature. The relative experimental error lied at 5 %.

To check the affinity of birnessite for Mn(II) binding, sorption isotherms were determined at three pH values (4, 6.5 and 8) under aerobic conditions (Figure S7). It should be noted that Mn(II) removal under oxic conditions is expected to be higher than under anoxic conditions, especially at alkaline pH values, which has been attributed to surface-catalyzed oxidation of

Mn(II) by molecular oxygen [49,50]. Here, only aerobic conditions were tested, since the aim of these sorption isotherms is to assess the Mn(II) affinity under oxidizing conditions imposed by the presence of H₂O₂. As expected, Mn(II) binding to MnO₂ surfaces increased with pH increasing. Sorption isotherms showed different shape depending on pH value across the Mn(II) concentration range. At pH 4 a typical L-shape with a plateau was observed, while the removal amount continuously increased with Mn(II) concentration at higher pH values. This high binding of Mn(II) at high pH value could cause Mn(III) enrichment in MnO₂ surfaces [49,50]. Some studies have shown that at high Mn(II)/Mn(IV) ratio and pH > 7.5, dissolved Mn(II) can interact with hexagonal birnessite and then transfer electron to lattice Mn(IV) producing Mn(III) [49,50]. The buildup of Mn(III) will induce changes in mineral structure and composition by converting birnessite into lower-valence Mn phases. XRD analysis conducted on samples reacted with 100 μM of dissolved Mn(II) (Mn(II)/MnO₂ molar ratio = 0.3) showed no notable transformation of MnO₂ over the investigated pH range (Figure 5). However, titration experiments showed that addition of 100 μM of dissolved Mn(II) dropped down the AOS of MnO₂ from 3.98 to 3.60 (±0.05) at pH 4 and 6.5, and 3.50 (±0.05) at pH 8, suggesting more Mn(III) or Mn(II) at the end of reaction with respect to the initial sample. *A recent work showed that* birnessite transformation into triclinic birnessite and/or 4 × 4 tunneled Mn oxide may occur at low Mn(II)/MnO₂ ratios (0.09 and 0.13), while secondary phases such as MnOOH and Mn₃O₄ can be generated at high Mn(II)/MnO₂ ratios (0.5 and 1) [60]. In our XRD patterns, broad bands (hump) have appeared between 12° and 22° and between 25° and 35° in the samples reacted with Mn(II) (Mn(II)/MnO₂ molar ratio = 0.3) or H₂O₂ (H₂O₂/MnO₂ molar ratio = 0.6), suggesting changes in the structure or ordering of the birnessite mineral sheets (Figure 5). We also observed these broad bands in the XRD pattern of synthetic Mn(III)-rich birnessite sample (see Figure 5). This is consistent with previous studies, which suggested that Mn^{III} formation can be made in edge-sharing complexes on MnO₂ edge sites or around vacancy sites in octahedral layers of MnO₂ [5]. In addition, a small peak near 20° only present in the patterns of samples reacted at pH 8 would suggest the presence of feitknechtite (β-MnOOH), as previously reported [49].

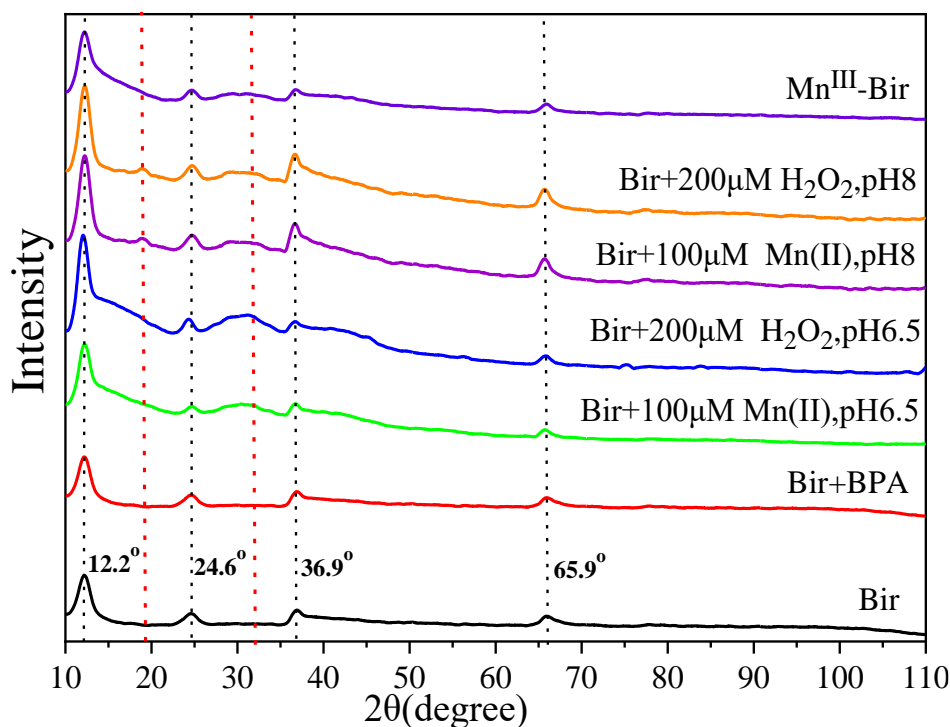


Figure 5. XRD patterns of birnessite before and after reaction in the presence of H_2O_2 or Mn(II) (two pH values, 24 h of reaction time), and of Mn(III) rich Birnessite. The black dashed lines indicate the peaks of acid birnessite, while the red dashed lines indicate broad bands appeared in reacted samples. Experimental conditions: $[\text{AB}] = 345 \mu\text{M}$ and $[\text{BPA}] = 25 \mu\text{M}$. $\text{H}_2\text{O}_2/\text{MnO}_2$ ratio = 0.6. $\text{Mn(II)}/\text{MnO}_2$ ratio = 0.3. The solid was characterized using X-ray powder diffraction (XRD) with a Bruker AXS D8 Advance diffractometer (θ - 2θ Bragg-Brentano geometry) using monochromated $\text{Cu K}\alpha_1$ (1.54\AA) radiation.

3.3. Synergistic effects of anions and H_2O_2 on the oxidative activity of MnO_2

To check whether the suppression of reactivity at environmental relevant concentrations of H_2O_2 can persist in presence of naturally occurring compounds, the initial rate constants k (h^{-1}) of BPA removal were determined at pH 6.5 in presence of silicate, nitrate and phosphate, commonly found in natural systems (Figure 6). At $0 \mu\text{M}$ of H_2O_2 , the presence of $100 \mu\text{M}$ of anions did not significantly influence the removal rate of BPA, probably because of weaker interactions of these anionic ligands with MnO_2 surfaces under the experimental conditions of this study (pH 6.5, $100 \mu\text{M}$ of anion, $345 \mu\text{M}$ of MnO_2). However, significant decrease in kinetic rate constants was observed in presence of silicate and phosphate when H_2O_2 was added

in the reaction medium ($\text{H}_2\text{O}_2/\text{MnO}_2$ molar ratio between 0.03 and 0.3), while no impact on the reactivity was observed in presence of nitrate (Figure 6). These results can be explained if the Mn(II) generated through H_2O_2 -induced reduction of MnO_2 renders the MnO_2 surfaces more able to bind anionic ligands, thereby altering the surface reactivity towards BPA.

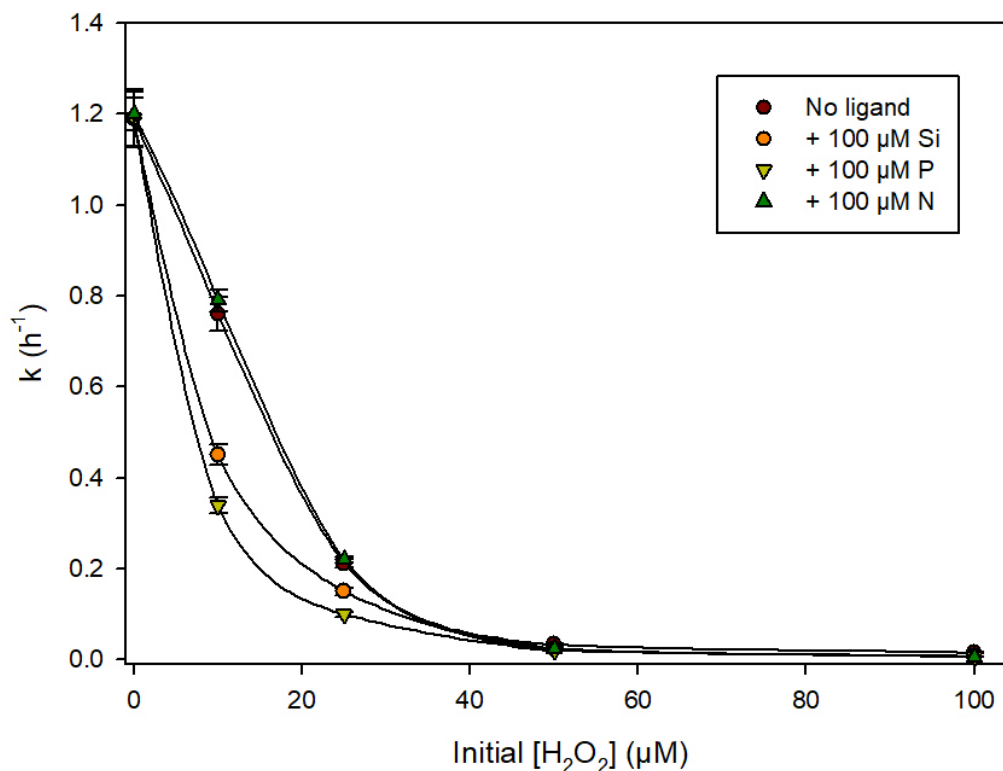


Figure 6. Removal rate constants (h^{-1}) of BPA as a function of H_2O_2 dose in absence or presence of silicate (Si), nitrate (N) or phosphate (P): Experimental conditions: pH 6.5, $[\text{AB}] = 345 \mu\text{M}$, $[\text{BPA}] = 25 \mu\text{M}$; $[\text{Na}_2\text{SiO}_3] = 100 \mu\text{M}$; $[\text{NaNO}_3] = 100 \mu\text{M}$; $[\text{NaH}_2\text{PO}_4] = 100 \mu\text{M}$. $\text{H}_2\text{O}_2/\text{MnO}_2$ ratio = 0 - 0.3, room temperature. The relative experimental error lied at 5 %.

It was previously reported that unlike nitrate, silicate or phosphate may interact with MnO_2 through hydrogen bonding or formation of outer-sphere complexes with surface hydroxyl groups of MnO_2 [59–62]. On the other hand, previous studies reported that the presence of dissolved silicate may decrease the oxidation rate constants of MnO_2 toward chlorinated compounds [63,64]. They have attributed the decrease in MnO_2 reactivity to the surface-bound silicate but none of them have provided adsorption data of silicate onto MnO_2 . In the present work, we showed that silicate or phosphate has a very low affinity to the negatively charged

MnO₂ surfaces under our experimental conditions, but the presence of 100 μM of Mn(II) significantly enhanced their adsorption amounts onto MnO₂ (Figure S8). This increased adsorption might be due to the changes in both the surface charge of MnO₂ and the solution speciation of anionic ligands in the presence of divalent cations such as Mn(II). Indeed, the ligand speciation may be modified, since different coordination modes of aqueous complexes of phosphate with Mn(II) ions have been previously reported [65]. However, no precipitation is possible under our experimental conditions due to the low degree of saturation, resulting from the very low aqueous concentration of ligand and complete removal of dissolved Mn(II) by adsorption ($\log K_s \text{ Mn(II)/phosphate} = -27.07$) [66]. Furthermore, Mn(II) binding should lead to a decrease in the negative surface charge, thereby enhancing ability to bind anions through electrostatic interactions [55,58,59]. Therefore, the MnO₂-bound Mn(II) system could adsorb more effectively anions such as phosphate or silicate through cation bridging, as recently reported for humic acid [55]. This surface-Mn(II)-ligand ternary complex *may* act as a barrier to electron transfer between BPA and Mn(IV) sites, thereby altering reactivity of MnO₂ surfaces. It should be noted that the decomposition of H₂O₂ (200 μM) was found to be similar in presence or absence of silicate or phosphate (100 μM) (Figure S9). Previous works have investigated the catalytic activity of manganese oxides for hydrogen peroxide decomposition and generation of reactive oxygen species in the context of environmental remediation studies [29–31]. Despite silicate adsorption on MnO₂ surfaces was found negligible, there was an inhibition effect on the H₂O₂ decomposition rate over the investigated silicate concentration range (0 to 1.5 mM) [30,67]. Although these works have used different experimental conditions (*e.g.* much higher concentration of ligands or H₂O₂), and different MnO₂ types, the present findings call for in-depth consideration of the combined/synergistic effects that the cations and anions co-presents in the reaction medium may have on the MnO₂ reactivity. Overall, these findings suggest that Mn(II) generation through H₂O₂-mediated reduction may alter both adsorption and redox transformation of environmental compounds.

4. Conclusions

Photochemical and dark production of H_2O_2 make it ubiquitous not only in oceanic and atmospheric systems but also in the subsurface environment. Here, we have notably demonstrated that environmental levels of hydrogen peroxide can induce reductive dissolution of MnO_2 into Mn(II) , thereby affecting the surface reactivity of MnO_2 . As the H_2O_2 decomposition is a fast process, the generated dissolved Mn(II) binds to MnO_2 surfaces, altering further interactions with co-existing organic compounds. This may result from competition of organic compound and Mn(II) to interact with reactive surface sites and/or aqueous complexation with Mn(II) . The presence of silicate or phosphate at concentrations comparable to those encountered in natural waters further decreased the reactivity of MnO_2 in presence of H_2O_2 . Birnessite-bound Mn(II) adsorbed more effectively anionic ligands such as phosphate or silicate and thus reducing interactions with BPA at a range of environmentally relevant pH values. These findings suggest that naturally occurring anions and H_2O_2 may have synergetic effects on the reactivity of nanostructured birnessite-type manganese oxide. As manganese oxides can break down high molecular weight humic substances into lower molecular weight organic molecules and/or stabilize dissolved organic carbon, these findings call for in-depth consideration of the impacts of environmental levels of H_2O_2 and co-existing anions on the global carbon cycle. Furthermore, the widespread presence of H_2O_2 in surface and ground water systems and associated impacts on the redox-active minerals should be considered in contaminant fate and transport assessment.

Acknowledgments

This work was supported by the Institut Universitaire de France, the Region Council of Auvergne Rhône-Alpes and the CNRS. We gratefully acknowledge the Chinese Scholarship Council of PR China for providing financial support for Daqing Jia and Qinzhi Li.

Reference

- [1] J.E. Post, Manganese oxide minerals: Crystal structures and economic and environmental significance, *Proceedings of the National Academy of Sciences*. 96 (1999) 3447–3454. <https://doi.org/10.1073/pnas.96.7.3447>.
- [2] Y. Wang, S. Benkaddour, F.F. Marafatto, J. Peña, Diffusion- and pH-Dependent Reactivity of Layer-Type MnO₂: Reactions at Particle Edges versus Vacancy Sites, *Environmental Science and Technology*. 52 (2018) 3476–3485. <https://doi.org/10.1021/acs.est.7b05820>.
- [3] N. Birkner, A. Navrotsky, Thermodynamics of manganese oxides: Sodium, potassium, and calcium birnessite and cryptomelane, *Proceedings of the National Academy of Sciences of the United States of America*. 114 (2017) E1046–E1053. <https://doi.org/10.1073/pnas.1620427114>.
- [4] S. Wick, J. Peña, A. Voegelin, Thallium Sorption onto Manganese Oxides, *Environmental Science and Technology*. 53 (2019) 13168–13178. <https://doi.org/10.1021/acs.est.9b04454>.
- [5] B.J. Lafferty, M. Ginder-Vogel, M. Zhu, K.J.T. Livi, D.L. Sparks, Arsenite Oxidation by a Poorly Crystalline Manganese-Oxide. 2. Results from X-ray Absorption Spectroscopy and X-ray Diffraction, *Environmental Science and Technology*. 44 (2010) 8467–8472. <https://doi.org/10.1021/es102016c>.
- [6] C.K. Remucal, M. Ginder-Vogel, A critical review of the reactivity of manganese oxides with organic contaminants, *Environmental Science: Processes & Impacts*. 16 (2014) 1247. <https://doi.org/10.1039/c3em00703k>.
- [7] R. Pokharel, Q. Li, L. Zhou, K. Hanna, Water Flow and Dissolved Mn^{II} Alter Transformation of Pipemidic Acid by Manganese Oxide, *Environmental Science and Technology*. 54 (2020) 8051–8060. <https://doi.org/10.1021/acs.est.0c01474>.
- [8] J. Huang, H. Zhang, Redox reactions of iron and manganese oxides in complex systems, *Frontiers of Environmental Science & Engineering*. 14 (2020) 76. <https://doi.org/10.1007/s11783-020-1255-8>.
- [9] A.N. Ricko, A.W. Psoras, J.D. Sivey, Reductive transformations of dichloroacetamide safeners: effects of agrochemical co-formulants and iron oxide + manganese oxide binary-

mineral systems, *Environmental Science: Processes & Impacts*. 22 (2020) 2104–2116. <https://doi.org/10.1039/D0EM00331J>.

[10] M. Villalobos, B. Lanson, A. Manceau, B. Toner, G. Sposito, Structural model for the biogenic Mn oxide produced by *Pseudomonas putida*, *American Mineralogist*. 91 (2006) 489–502. <https://doi.org/10.2138/am.2006.1925>.

[11] S.M. Webb, B.M. Tebo, J.R. Bargar, Structural characterization of biogenic Mn oxides produced in seawater by the marine bacillus sp. strain SG-1, *American Mineralogist*. 90 (2005) 1342–1357. <https://doi.org/10.2138/am.2005.1669>.

[12] M. Zhu, M. Ginder-Vogel, S.J. Parikh, X.-H. Feng, D.L. Sparks, Cation Effects on the Layer Structure of Biogenic Mn-Oxides, *Environmental Science and Technology*. 44 (2010) 4465–4471. <https://doi.org/10.1021/es1009955>.

[13] M. Villalobos, B. Toner, J. Bargar, G. Sposito, Characterization of the manganese oxide produced by *pseudomonas putida* strain MnB1, *Geochimica et Cosmochimica Acta*. 67 (2003) 2649–2662. [https://doi.org/10.1016/S0016-7037\(03\)00217-5](https://doi.org/10.1016/S0016-7037(03)00217-5).

[14] W.J. Cooper, D.R.S. Lean, Hydrogen peroxide concentration in a northern lake: photochemical formation and diel variability, *Environmental Science and Technology*. 23 (1989) 1425–1428. <https://doi.org/10.1021/es00069a017>.

[15] R.G. Zika, J.W. Moffett, R.G. Petasne, W.J. Cooper, E.S. Saltzman, Spatial and temporal variations of hydrogen peroxide in Gulf of Mexico waters, *Geochimica et Cosmochimica Acta*. 49 (1985) 1173–1184. [https://doi.org/10.1016/0016-7037\(85\)90008-0](https://doi.org/10.1016/0016-7037(85)90008-0).

[16] B. González-Flecha, B. Demple, Homeostatic regulation of intracellular hydrogen peroxide concentration in aerobically growing *Escherichia coli*, *Journal of Bacteriology*. 179 (1997) 382–388. <https://doi.org/10.1128/jb.179.2.382-388.1997>.

[17] F. Guillén, A.T. Martínez, M.J. Martínez, Production of hydrogen peroxide by aryl-alcohol oxidase from the ligninolytic fungus *Pleurotus eryngii*, *Applied Microbiology and Biotechnology*. 32 (1990) 465–469. <https://doi.org/10.1007/BF00903784>.

- [18] S. Garg, A.L. Rose, T.D. Waite, Photochemical production of superoxide and hydrogen peroxide from natural organic matter, *Geochimica et Cosmochimica Acta*. 75 (2011) 4310–4320. <https://doi.org/10.1016/j.gca.2011.05.014>.
- [19] J.W. Moffett, O.C. Zajiriou, An investigation of hydrogen peroxide chemistry in surface waters of Vineyard Sound with $\text{H}_2^{18}\text{O}_2$ and $^{18}\text{O}_2$, *Limnology and Oceanography*. 35 (1990) 1221–1229. <https://doi.org/10.4319/lo.1990.35.6.1221>.
- [20] K.L. Roe, R.J. Schneider, C.M. Hansel, B.M. Voelker, Measurement of dark, particle-generated superoxide and hydrogen peroxide production and decay in the subtropical and temperate North Pacific Ocean, *Deep Sea Research Part I: Oceanographic Research Papers*. 107 (2016) 59–69. <https://doi.org/10.1016/j.dsr.2015.10.012>.
- [21] W.J. Cooper, J.K. Moegling, R.J. Kieber, J.J. Kiddle, A chemiluminescence method for the analysis of H_2O_2 in natural waters, *Marine Chemistry*. 70 (2000) 191–200. [https://doi.org/10.1016/S0304-4203\(00\)00025-6](https://doi.org/10.1016/S0304-4203(00)00025-6).
- [22] X. Yuan, P.S. Nico, X. Huang, T. Liu, C. Ulrich, K.H. Williams, J.A. Davis, Production of Hydrogen Peroxide in Groundwater at Rifle, Colorado, *Environmental Science and Technology*. 51 (2017) 7881–7891. <https://doi.org/10.1021/acs.est.6b04803>.
- [23] P. Liao, K. Yu, Y. Lu, P. Wang, Y. Liang, Z. Shi, Extensive dark production of hydroxyl radicals from oxygenation of polluted river sediments, *Chemical Engineering Journal*. 368 (2019) 700–709. <https://doi.org/10.1016/j.cej.2019.03.018>.
- [24] E. Kim, Y. Liu, C.J. Baker, R. Owens, S. Xiao, W.E. Bentley, G.F. Payne, Redox-Cycling and H_2O_2 Generation by Fabricated Catecholic Films in the Absence of Enzymes, *Biomacromolecules*. 12 (2011) 880–888. <https://doi.org/10.1021/bm101499a>.
- [25] S.E. Page, G.W. Kling, M. Sander, K.H. Harrold, J.R. Logan, K. McNeill, R.M. Cory, Dark Formation of Hydroxyl Radical in Arctic Soil and Surface Waters, *Environmental Science and Technology*. 47 (2013) 12860–12867. <https://doi.org/10.1021/es4033265>.
- [26] J.D. Begg, M. Zavarin, A.B. Kersting, Plutonium desorption from mineral surfaces at environmental concentrations of hydrogen peroxide, *Environmental Science and Technology*. 48 (2014) 6201–6210. <https://doi.org/10.1021/es500984w>.

- [27] H.-P. Li, C.M. Yeager, R. Brinkmeyer, S. Zhang, Y.-F. Ho, C. Xu, W.L. Jones, K.A. Schwehr, S. Ootosaka, K.A. Roberts, D.I. Kaplan, P.H. Santschi, Bacterial Production of Organic Acids Enhances H₂O₂-Dependent Iodide Oxidation, *Environmental Science and Technology*. 46 (2012) 4837–4844. <https://doi.org/10.1021/es203683v>.
- [28] M. Amme, W. Bors, C. Michel, K. Stettmaier, G. Rasmussen, M. Betti, Effects of Fe(II) and Hydrogen Peroxide Interaction upon Dissolving UO₂ under Geologic Repository Conditions, *Environmental Science and Technology*. 39 (2005) 221–229. <https://doi.org/10.1021/es040034x>.
- [29] R.J. Watts, J. Sarasa, F.J. Loge, A.L. Teel, Oxidative and Reductive Pathways in Manganese-Catalyzed Fenton's Reactions, *Journal of Environmental Engineering*. 131 (2005) 158–164. [https://doi.org/10.1061/\(ASCE\)0733-9372\(2005\)131:1\(158\)](https://doi.org/10.1061/(ASCE)0733-9372(2005)131:1(158)).
- [30] A.L.-T. Pham, F.M. Doyle, D.L. Sedlak, Inhibitory Effect of Dissolved Silica on H₂O₂ Decomposition by Iron(III) and Manganese(IV) Oxides: Implications for H₂O₂-Based In Situ Chemical Oxidation, *Environmental Science and Technology*. 46 (2012) 1055–1062. <https://doi.org/10.1021/es203612d>.
- [31] M. Kamagate, M. Pasturel, M. Brigante, K. Hanna, Mineralization Enhancement of Pharmaceutical Contaminants by Radical-Based Oxidation Promoted by Oxide-Bound Metal Ions, *Environmental Science and Technology*. 54 (2020) 476–485. <https://doi.org/10.1021/acs.est.9b04542>.
- [32] S. Balgooyen, P.J. Alaimo, C.K. Remucal, M. Ginder-Vogel, Structural Transformation of MnO₂ during the Oxidation of Bisphenol A, *Environmental Science and Technology*. 51 (2017) 6053–6062. <https://doi.org/10.1021/acs.est.6b05904>.
- [33] K. Lin, W. Liu, J. Gan, Oxidative Removal of Bisphenol A by Manganese Dioxide: Efficacy, Products, and Pathways, *Environmental Science and Technology*. 43 (2009) 3860–3864. <https://doi.org/10.1021/es900235f>.
- [34] J. Huang, S. Zhong, Y. Dai, C.-C. Liu, H. Zhang, Effect of MnO₂ Phase Structure on the Oxidative Reactivity toward Bisphenol A Degradation, *Environmental Science and Technology*. 52 (2018) 11309–11318. <https://doi.org/10.1021/acs.est.8b03383>.

- [35] S. Balgooyen, G. Campagnola, C.K. Remucal, M. Ginder-Vogel, Impact of bisphenol A influent concentration and reaction time on MnO₂ transformation in a stirred flow reactor, *Environmental Science: Processes & Impacts*. 21 (2019) 19–27. <https://doi.org/10.1039/C8EM00451J>.
- [36] R.M. McKenzie, The synthesis of birnessite, cryptomelane, and some other oxides and hydroxides of manganese, *Mineralogical Magazine*. 38 (1971) 493–502. <https://doi.org/10.1180/minmag.1971.038.296.12>.
- [37] Q. Sun, P.-X. Cui, T.-T. Fan, S. Wu, M. Zhu, M.E. Alves, D.-M. Zhou, Y.-J. Wang, Effects of Fe(II) on Cd(II) immobilization by Mn(III)-rich δ -MnO₂, *Chemical Engineering Journal*. 353 (2018) 167–175. <https://doi.org/10.1016/j.cej.2018.07.120>.
- [38] A.A. Simanova, K.D. Kwon, S.E. Bone, J.R. Bargar, K. Refson, G. Sposito, J. Peña, Probing the sorption reactivity of the edge surfaces in birnessite nanoparticles using nickel(II), *Geochimica et Cosmochimica Acta*. 164 (2015) 191–204. <https://doi.org/10.1016/j.gca.2015.04.050>.
- [39] Y. Wu, M. Passananti, M. Brigante, W. Dong, G. Mailhot, Fe(III)–EDDS complex in Fenton and photo-Fenton processes: from the radical formation to the degradation of a target compound, *Environmental Science and Pollution Research*. 21 (2014) 12154–12162. <https://doi.org/10.1007/s11356-014-2945-1>.
- [40] T. Charbouillot, M. Brigante, G. Mailhot, P.R. Maddigapu, C. Minero, D. Vione, Performance and selectivity of the terephthalic acid probe for OH as a function of temperature, pH and composition of atmospherically relevant aqueous media, *Journal of Photochemistry and Photobiology A: Chemistry*. 222 (2011) 70–76. <https://doi.org/10.1016/j.jphotochem.2011.05.003>.
- [41] J.B. Mullin, J.P. Riley, The colorimetric determination of silicate with special reference to sea and natural waters, *Analytica Chimica Acta*. 12 (1955) 162–176. [https://doi.org/10.1016/S0003-2670\(00\)87825-3](https://doi.org/10.1016/S0003-2670(00)87825-3).
- [42] V. Ruiz-Calero, M.T. Galceran, Ion chromatographic separations of phosphorus species: a review, *Talanta*. 66 (2005) 376–410. <https://doi.org/10.1016/j.talanta.2005.01.027>.

- [43] Q. Li, R. Pokharel, L. Zhou, M. Pasturel, K. Hanna, Coupled effects of Mn(II), pH and anionic ligands on the reactivity of nanostructured birnessite, *Environmental Science: Nano*. 7 (2020) 4022–4031. <https://doi.org/10.1039/D0EN01046D>.
- [44] J. Im, C.W. Prevatte, S.R. Campagna, F.E. Löffler, Identification of 4-Hydroxycumyl Alcohol As the Major MnO₂-Mediated Bisphenol A Transformation Product and Evaluation of Its Environmental Fate, *Environmental Science and Technology*. 49 (2015) 6214–6221. <https://doi.org/10.1021/acs.est.5b00372>.
- [45] H. Zhang, W.-R. Chen, C.-H. Huang, Kinetic Modeling of Oxidation of Antibacterial Agents by Manganese Oxide, *Environmental Science and Technology*. 42 (2008) 5548–5554. <https://doi.org/10.1021/es703143g>.
- [46] W. Stumm, J.J. Morgan, *Aquatic Chemistry: Chemical Equilibria and Rates in Natural Waters*, John Wiley & Sons, 2012.
- [47] S. Baral, C. Lume-Pereira, E. Janata, A. Henglein, Chemistry of colloidal manganese dioxide. 2. Reaction with superoxide anion (O²⁻) and hydrogen peroxide (pulse radiolysis and stop flow studies), *The Journal of Physical Chemistry*. 89 (1985) 5779–5783. <https://doi.org/10.1021/j100272a041>.
- [48] D.B. Broughton, R.L. Wentworth, Mechanism of Decomposition of Hydrogen Peroxide Solutions with Manganese Dioxide. I, *Journal of the American Chemical Society*. 69 (1947) 741–744. <https://doi.org/10.1021/ja01196a003>.
- [49] J.P. Lefkowitz, A.A. Rouff, E.J. Elzinga, Influence of pH on the Reductive Transformation of Birnessite by Aqueous Mn(II), *Environmental Science and Technology*. 47 (2013) 10364–10371. <https://doi.org/10.1021/es402108d>.
- [50] E.J. Elzinga, Reductive Transformation of Birnessite by Aqueous Mn(II), *Environmental Science and Technology*. 45 (2011) 6366–6372. <https://doi.org/10.1021/es2013038>.
- [51] Q. Wang, P. Yang, M. Zhu, Structural Transformation of Birnessite by Fulvic Acid under Anoxic Conditions, *Environmental Science and Technology*. 52 (2018) 1844–1853. <https://doi.org/10.1021/acs.est.7b04379>.

- [52] H. Yin, Y. Zhou, J. Xu, S. Ai, L. Cui, L. Zhu, Amperometric biosensor based on tyrosinase immobilized onto multiwalled carbon nanotubes-cobalt phthalocyanine-silk fibroin film and its application to determine bisphenol A, *Analytica Chimica Acta*. 659 (2010) 144–150. <https://doi.org/10.1016/j.aca.2009.11.051>.
- [53] H. Yin, Y. Zhou, L. Cui, X. Liu, S. Ai, L. Zhu, Electrochemical oxidation behavior of bisphenol A at surfactant/layered double hydroxide modified glassy carbon electrode and its determination, *Journal of Solid State Electrochemistry*. 15 (2011) 167–173. <https://doi.org/10.1007/s10008-010-1089-6>.
- [54] Ş. Ulubay Karabiberoglu, Sensitive Voltammetric Determination of Bisphenol A Based on a Glassy Carbon Electrode Modified with Copper Oxide-Zinc Oxide Decorated on Graphene Oxide, *Electroanalysis*. 31 (2019) 91–102. <https://doi.org/10.1002/elan.201800415>.
- [55] H. Cheng, T. Yang, J. Jiang, X. Lu, P. Wang, J. Ma, Mn^{2+} effect on manganese oxides (MnOx) nanoparticles aggregation in solution: Chemical adsorption and cation bridging, *Environmental Pollution*. 267 (2020) 115561. <https://doi.org/10.1016/j.envpol.2020.115561>.
- [56] H. Zhao, M. Zhu, W. Li, E.J. Elzinga, M. Villalobos, F. Liu, J. Zhang, X. Feng, D.L. Sparks, Redox Reactions between Mn(II) and Hexagonal Birnessite Change Its Layer Symmetry, *Environmental Science and Technology*. 50 (2016) 1750–1758. <https://doi.org/10.1021/acs.est.5b04436>.
- [57] S.M. Webb, G.J. Dick, J.R. Bargar, B.M. Tebo, Evidence for the presence of Mn(III) intermediates in the bacterial oxidation of Mn(II), *Proceedings of the National Academy of Sciences*. 102 (2005) 5558–5563. <https://doi.org/10.1073/pnas.0409119102>.
- [58] T. Takamatsu, M. Kawashima, M. Koyama, The role of Mn^{2+} -rich hydrous manganese oxide in the accumulation of arsenic in lake sediments, *Water Research*. 19 (1985) 1029–1032. [https://doi.org/10.1016/0043-1354\(85\)90372-0](https://doi.org/10.1016/0043-1354(85)90372-0).
- [59] W. Yao, F.J. Millero, Adsorption of Phosphate on Manganese Dioxide in Seawater, *Environmental Science and Technology*. 30 (1996) 536–541. <https://doi.org/10.1021/es950290x>.

- [60] P. Yang, K. Wen, K.A. Beyer, W. Xu, Q. Wang, D. Ma, J. Wu, M. Zhu, Inhibition of Oxyanions on Redox-driven Transformation of Layered Manganese Oxides, *Environmental Science and Technology*. 55 (2021) 3419–3429. <https://doi.org/10.1021/acs.est.0c06310>.
- [61] S. Mustafa, M.I. Zaman, S. Khan, pH effect on phosphate sorption by crystalline MnO₂, *Journal of Colloid and Interface Science*. 301 (2006) 370–375. <https://doi.org/10.1016/j.jcis.2006.05.020>.
- [62] L.S. Balistrieri, T.T. Chao, Adsorption of selenium by amorphous iron oxyhydroxide and manganese dioxide, *Geochimica et Cosmochimica Acta*. 54 (1990) 739–751. [https://doi.org/10.1016/0016-7037\(90\)90369-V](https://doi.org/10.1016/0016-7037(90)90369-V).
- [63] S. Tadjale, H. Zhang, Impact of Interactions between Metal Oxides to Oxidative Reactivity of Manganese Dioxide, *Environmental Science and Technology*. 46 (2012) 2764–2771. <https://doi.org/10.1021/es204294c>.
- [64] M. Yu, X. He, B. Xi, Y. Xiong, Z. Wang, D. Sheng, L. Zhu, X. Mao, Dissolved Silicate Enhances the Oxidation of Chlorophenols by Permanganate: Important Role of Silicate-Stabilized MnO₂ Colloids, *Environmental Science and Technology*. 54 (2020) 10279–10288. <https://doi.org/10.1021/acs.est.0c00826>.
- [65] C.V.K. Sharma, C.C. Chusuei, R. Clérac, T. Möller, K.R. Dunbar, A. Clearfield, Magnetic Property Studies of Manganese–Phosphate Complexes, *Inorganic Chemistry*. 42 (2003) 8300–8308. <https://doi.org/10.1021/ic0300520>.
- [66] G. Friedl, B. Wehrli, A. Manceau, Solid phases in the cycling of manganese in eutrophic lakes: New insights from EXAFS spectroscopy, *Geochimica et Cosmochimica Acta*. 61 (1997) 275–290. [https://doi.org/10.1016/S0016-7037\(96\)00316-X](https://doi.org/10.1016/S0016-7037(96)00316-X).
- [67] K. Hanna, Comment on “Inhibitory Effect of Dissolved Silica on H₂O₂ Decomposition by Iron(III) and Manganese(IV) Oxides: Implications for H₂O₂-Based In Situ Chemical Oxidation,” *Environmental Science and Technology*. 46 (2012) 3591–3592. <https://doi.org/10.1021/es3002103>.

Supplementary Materials

Acid birnessite synthesis. Acid birnessite (AB) was prepared following the procedures of McKenzie [1]. 166 mL of concentrated HCl was added dropwise to 2.5 L of 0.4 M KMnO₄. The suspension was stirred vigorously and kept at 90 °C during the HCl addition. The reaction was continued at 90 °C for a further 10 min. Then, the obtained slurry was stirred vigorously at room temperature for 15 h. The precipitate was collected by centrifugation, washed with ultrapure water repeatedly until the conductivity was close to 0.6 μS cm⁻¹. The suspensions were stored in polypropylene containers at 4 °C for further use.

Preparation of Mn(III)-rich birnessite. Mn(III)-rich MnO₂ was synthesized according to previous published methods [2,3]. Briefly, about 2 g of acid birnessite was incubated with 80 mL of 10 mM HEPES and 10 mM NaCl solutions at pH 6.5 ± 0.05 at a temperature of 25 °C for 48h. The precipitate was collected by centrifugation and washed with ultrapure water.

Oxalic acid-permanganate back-titration method. 0.1 g of the acid birnessite was dissolved in 2.5 mL of 0.5 M H₂C₂O₄ and 5 mL of 1 M H₂SO₄ to reduce all highly charged manganese ions to Mn(II). After all samples to be dissolved, the excess C₂O₄²⁻ was back titrated with standardized 0.02 M KMnO₄ solution at 75–85 °C until the color of solution turned into reddish and lasted for 30 seconds without fading, to obtain the oxidation number of Mn. Then, 0.1 g of the acid birnessite sample was dissolved in 20 mL 0.25 M hydroxylamine hydrochloride and diluted to 2 L with ultrapure water. AAS was used to determine the total Mn content, and the Mn content of the synthesized acid birnessite is 51.42 (± 2.6) wt%. Then, according to the titration result and total Mn content, the AOS of acid birnessite was calculated. Triplicates were performed for each sample and the mean AOS value can be calculated.

$$\text{AOS} = 2 + 54.94 * \frac{n(\text{ the oxidation number,mol })}{m(\text{ the total Mn content,g})}$$

Hydroxyl radical detection method. Potential generation of hydroxyl radical was monitored by using a fluorescence method using terephthalic acid (TA) as a probe [4]. The detection mechanism is that nonfluorescence TA reacts with hydroxyl radical to generate fluorescent 2-hydroxyterephthalic acid which can be measured at 425 nm under the excitation of 320 nm. Specifically, in this work, 345 μM of acid birnessite was mixed with TA (1 mM) and H₂O₂ (200

μM) in the 100mL ultrapure water. At different time interval, 2 mL of sample was withdrawn and detected by a fluorescence spectrophotometer (Varian Cary Eclipse, USA). The limit of detection for hydroxyl radicals using fluorescence method was in the low nano-molar range.

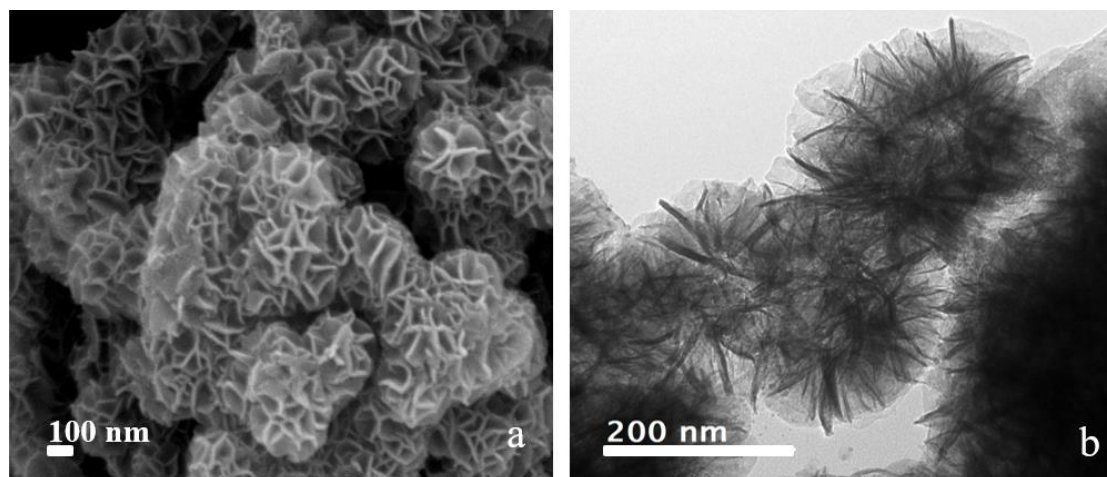


Figure S1. SEM (a) and TEM (b) images of the synthesized acid birnessite.

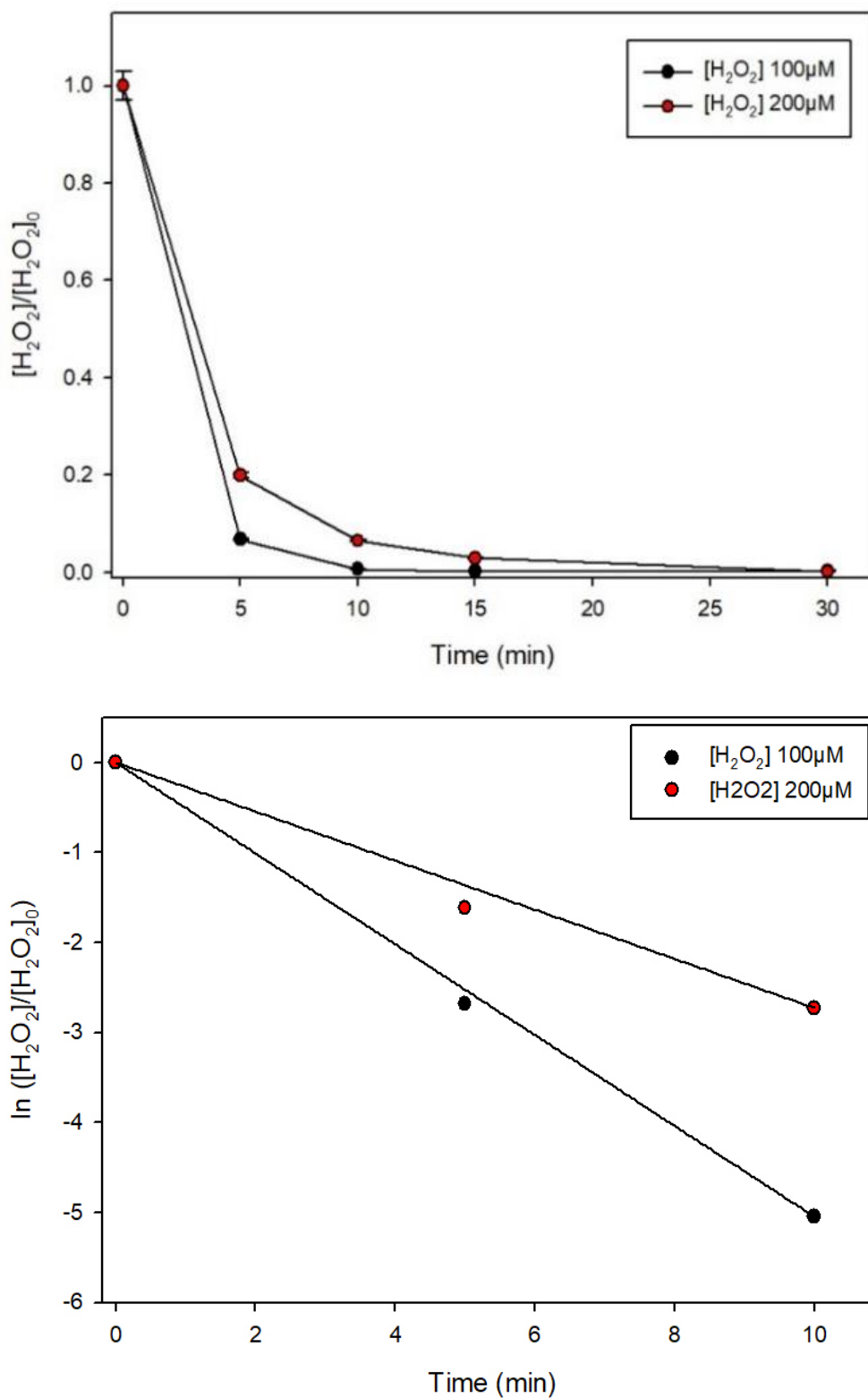


Figure S2. H_2O_2 decomposition versus time with two H_2O_2 concentrations and linear regression of $\ln [\text{H}_2\text{O}_2] / [\text{H}_2\text{O}_2]_0$ versus time. Experimental conditions: $[\text{AB}] = 345 \mu\text{M}$, $[\text{H}_2\text{O}_2] = 100$ and $200 \mu\text{M}$, $\text{pH} = 6.5$. $\text{H}_2\text{O}_2/\text{MnO}_2$ ratio = 0.3 and 0.6.

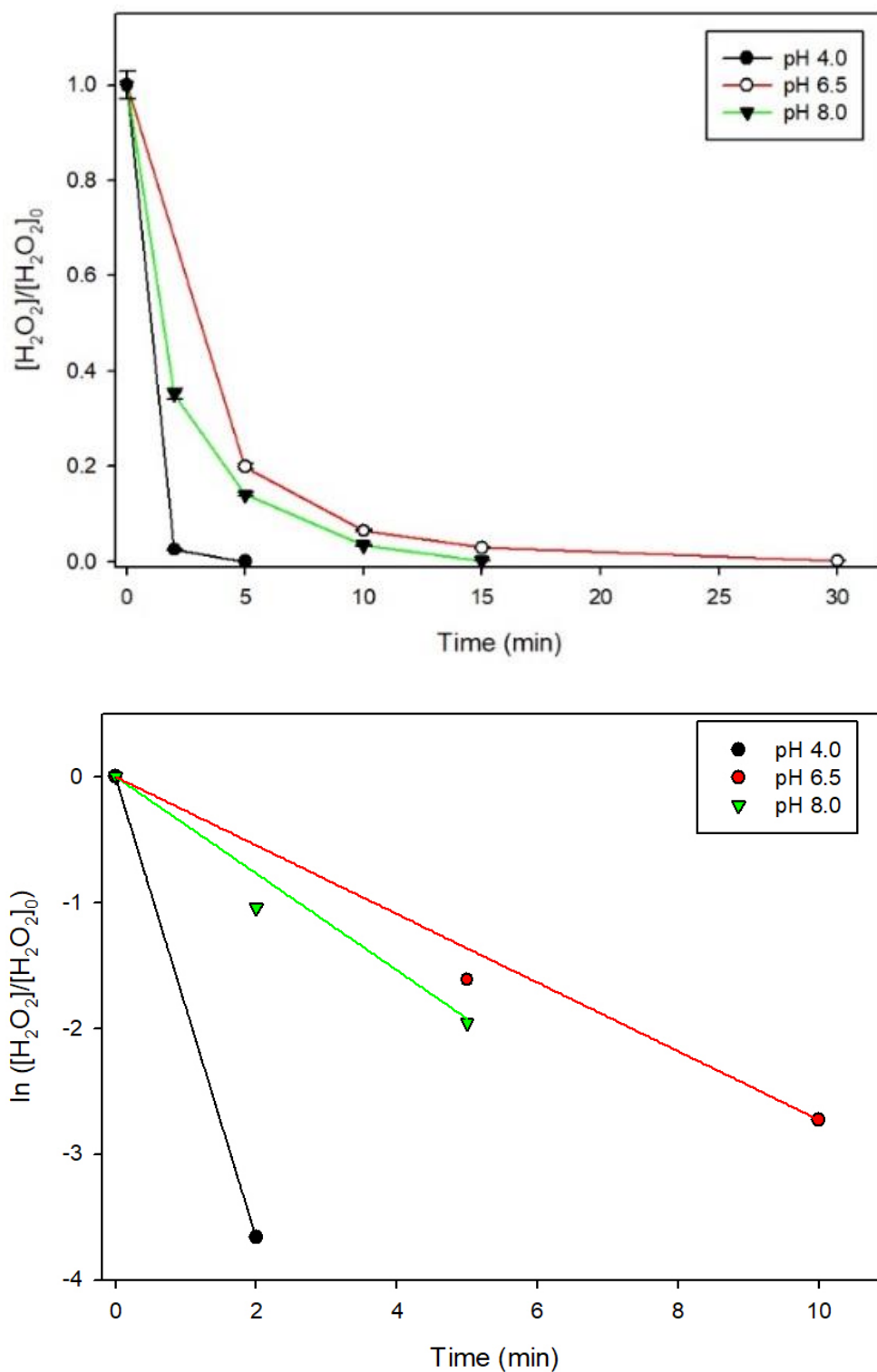


Figure S3. H_2O_2 decomposition vs time at pH 4, 6.5 and 8, and linear regression of $\ln [H_2O_2] / [H_2O_2]_0$ versus time. Experimental conditions: $[H_2O_2] = 200 \mu M$; $[AB] = 345 \mu M$; $[BPA] = 25 \mu M$. H_2O_2/MnO_2 ratio = 0.6.

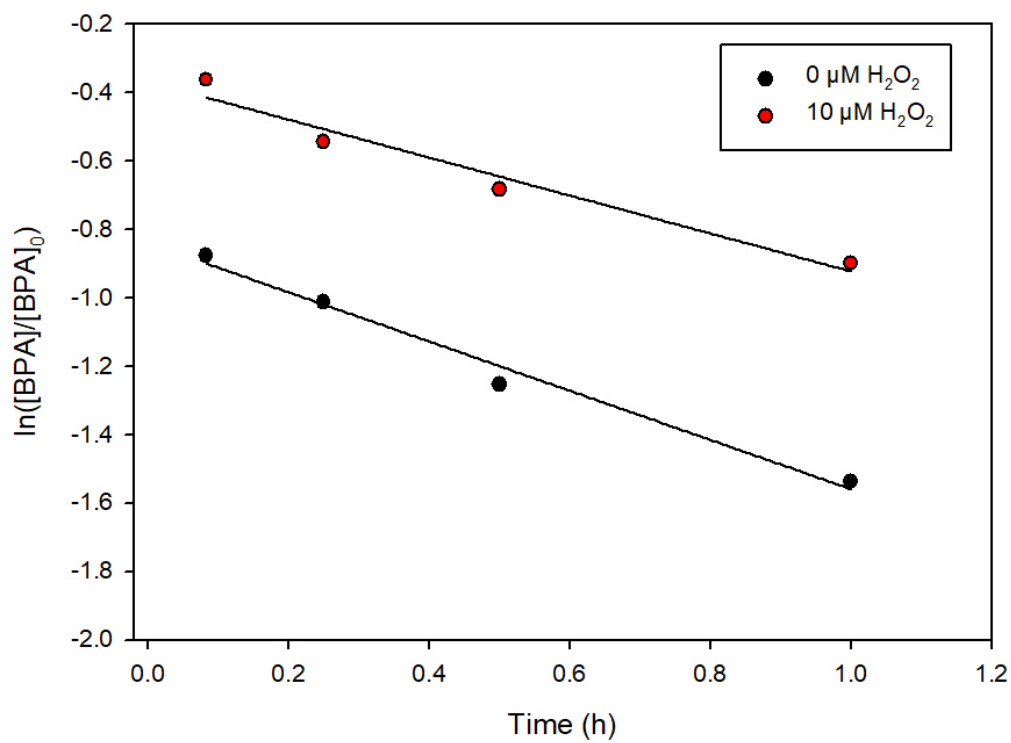


Figure S4. Linear regression of $\ln [BPA] / [BPA]_0$ versus time. Experimental conditions: pH 6.5, $[AB] = 345 \mu\text{M}$, $[BPA] = 25 \mu\text{M}$. $\text{H}_2\text{O}_2/\text{MnO}_2$ ratio 0 and 0.03.

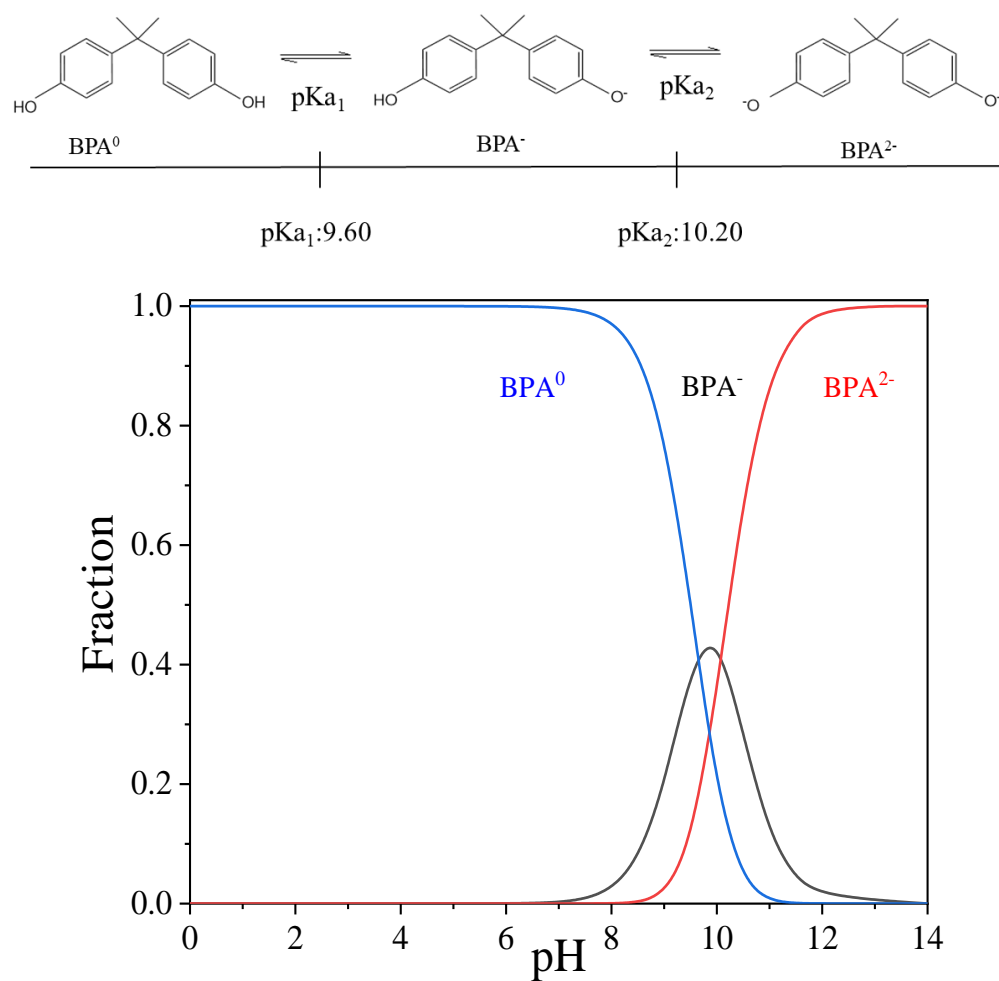


Figure S5. Chemical speciation of BPA vs pH. Ionic strength: 10 mM NaCl. pK_{as} of BPA (pK_{a,1} = 9.60 and pK_{a,2} = 10.20) at infinite dilution were obtained from conditional pK_a values and the Davies equation.

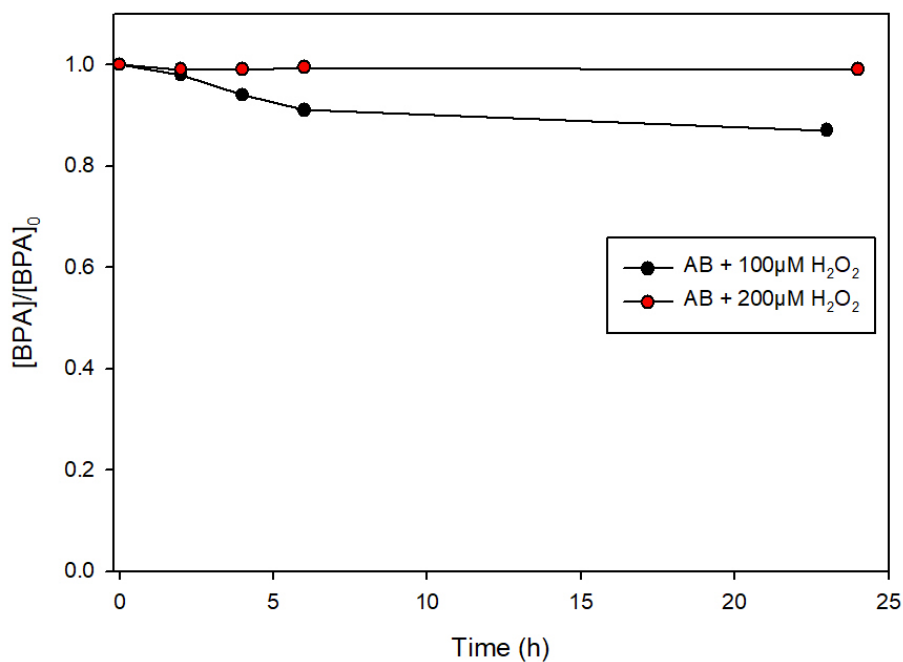


Figure S6. Effect of pre-equilibration H₂O₂/MnO₂ on the BPA removal. Experimental conditions: [AB] = 345 µM, [BPA] = 25 µM.

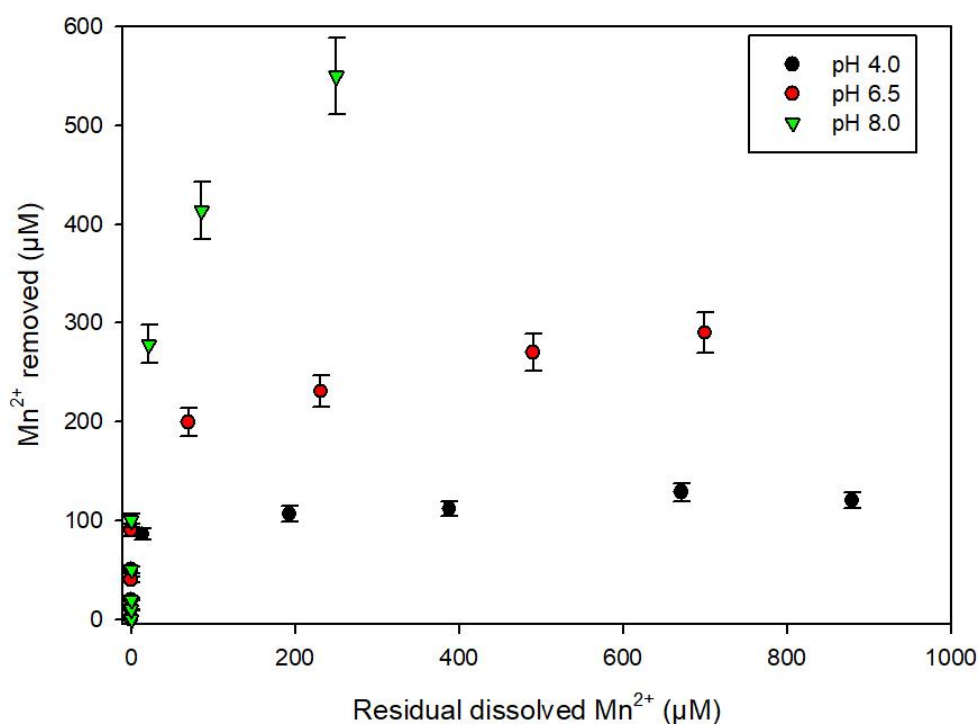


Figure S7. Mn(II)-birnessite sorption isotherms at three pH values. Experimental conditions: [AB] = 345 µM; T = 20 ± 1°C; reaction time = 48 h; aerobic conditions.

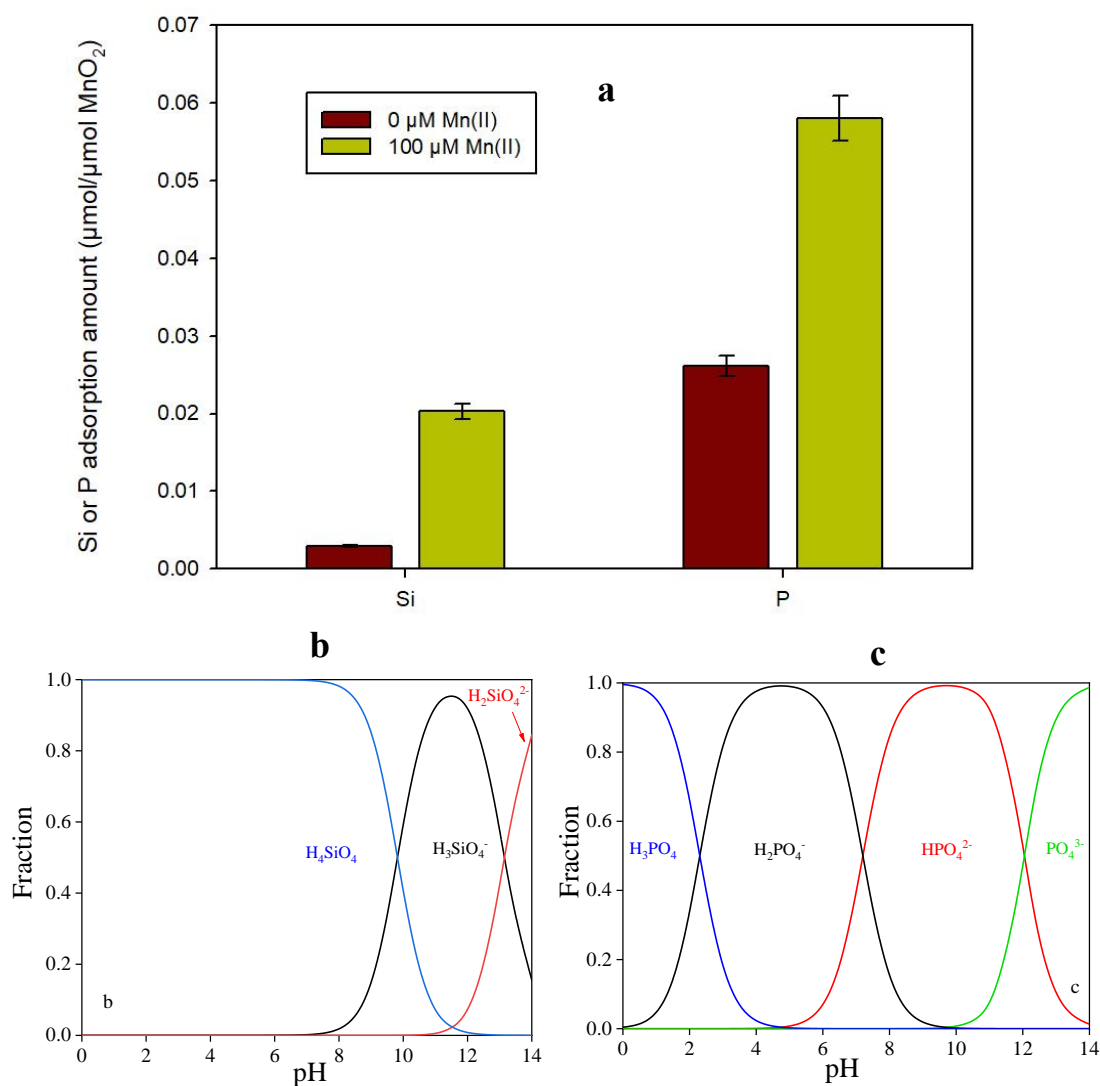


Figure S8. (a) Adsorption of Si or P at pH 6.5 in presence or absence of dissolved Mn(II). Chemical speciation of (b) silicates Si (Na_2SiO_3) and (c) phosphates P (NaH_2PO_4) versus pH. pK_{as} of silicate ($\text{pK}_{\text{a},1} = 9.82$ and $\text{pK}_{\text{a},2} = 13.45$) and phosphate ($\text{pK}_{\text{a},1} = 2.12$, $\text{pK}_{\text{a},2} = 7.21$ and $\text{pK}_{\text{a},3} = 12.31$) at infinite dilution were obtained from conditional pK_{a} values and the Davies equation. Experimental conditions: $[\text{AB}] = 345 \mu\text{M}$; $[\text{Mn(II)}] = 100 \mu\text{M}$; $[\text{Na}_2\text{SiO}_3] = 100 \mu\text{M}$; $[\text{NaH}_2\text{PO}_4] = 100 \mu\text{M}$; reaction time = 24 h.

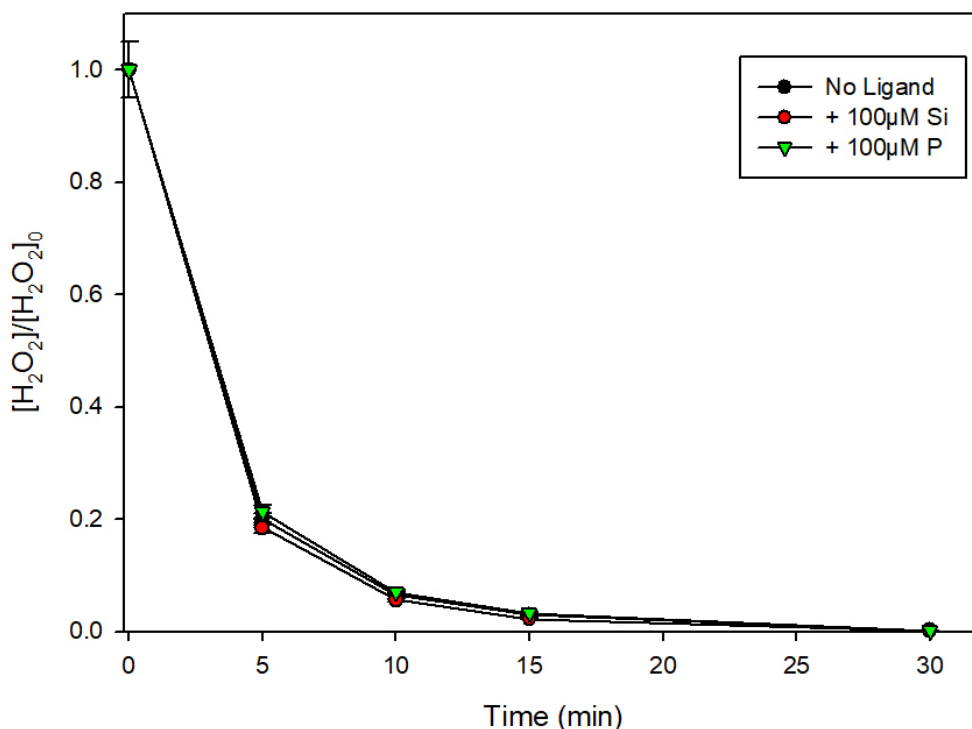


Figure S9. Decomposition of H_2O_2 (200 μM) versus time in presence or absence of silicate or phosphate (100 μM).

Reference

- [1] R. M. McKenzie, The synthesis of birnessite, cryptomelane, and some other oxides and hydroxides of manganese, *Mineralogical Magazine*, 1971, 38, 493-502.
- [2] Q. Sun, P. X. Cui, T. T. Fan, S. Wu, M. Zhu, M. E. Alves, D. M. Zhou and Y. J. Wang, Effects of Fe (II) on Cd (II) immobilization by Mn(III)-rich $\delta\text{-MnO}_2$, *Chemical Engineer Journal*, 2018, 353, 167-175.
- [3] A. A. Simanova, K. D. Kwon, S. E. Bone, J. R. Bargar, K. Refson, G. Sposito and J. Peña, Probing the sorption reactivity of the edge surfaces in birnessite nanoparticles using nickel (II), *Geochimica Cosmochimica Acta*, 2015, 164, 191-204.
- [4] T. Charbouillot, M. Brigante, G. Mailhot, P. R. Maddigapu, C. Minero and D. Vione, Performance and selectivity of the terephthalic acid probe for OH as a function of temperature, pH and composition of atmospherically relevant aqueous media, *Journal of Photochemistry and Photobiology A: Chemistry*, 2011, 222, 70-76

Chapter IV

**Trivalent manganese oxides activation of peroxydisulfate
and peroxymonosulfate for organic pollutants degradation
in water**

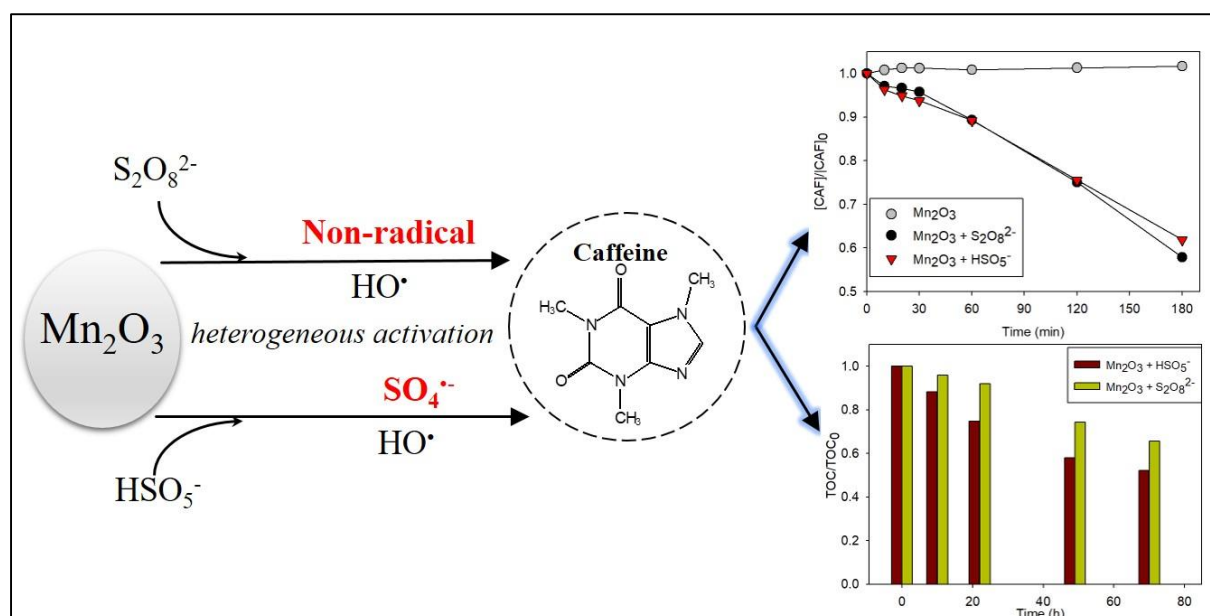
Motivation

The key role of trivalent manganese species in promoting sulfate radical-based advanced oxidation processes (SR-AOPs) has been reported. For example, Huang et al. indicated the efficient degradation of bisphenol A by crystalline MnO_2 in the presence of PMS was positively correlated to the amount of Mn(III). The investigation of PDS and PMS activation by Mn(III) oxides was also reported. For instance, Saputra et al. demonstrated that Mn_2O_3 compared with MnO , Mn_3O_4 , and MnO_2 showed the highest reactivity in PMS activation for phenol degradation. He et al. suggested that nanowires MnOOH have higher activity on PMS activation for 2,4-dichlorophenol oxidation as compared with multi-branches and nanorods MnOOH . Although the excellent performance of Mn(III) in radical precursors activation has been well highlighted in the previous literature, the activation mechanism of PDS and PMS by Mn(III) oxides (such as Mn_2O_3 and manganite) is not clear. Moreover, some important influence factors for the reactivity of Mn_2O_3 such as solution pH were not investigated. The comparison of PMS activation mechanism by different Mn(III) oxides was not reported. Furthermore, most of former investigations were conducted in the pure water, the efficiency of Mn(III) oxides + PDS/PMS system in the practical wastewater was not evaluated.

Considering the above-mentioned questions, the degradation of organic pollutants in water by Mn(III) oxides activated PDS and PMS were investigated. In the Chapter IV, the results of my study are divided into two parts. In the part 1, the caffeine degradation using PDS and PMS in the presence of Mn_2O_3 was investigated. In the part 2, the removal of estrogenic compounds in water by manganite-activated PMS was studied.

Part 1

Caffeine degradation using peroxydisulfate and peroxymonosulfate in the presence of Mn_2O_3 . Efficiency, reactive species formation and application in sewage treatment plant water



Published journal: Journal of Cleaner Production

Accepted date: 6th November 2021

1. Introduction

Advanced oxidation processes (AOPs) constitute a promising technology for the remediation of environmental compartments [1]. AOPs are efficient in the removal of harmful and persistent organic pollutants in water due to the generation of strongly reactive species [2]. Hydroxyl radical (HO^\bullet) belongs to the reactive oxygen species (ROS) and has a high oxidation potential ($E^0 = 2.73 \text{ V vs NHE}$) [3]. Similarly, the reactive sulfur species (RSS) such as sulfate radical ($\text{SO}_4^{\bullet-}$) ($E^0 = 2.6 \text{ V vs NHE}$) have also caught the attention of the scientific community due to their efficient oxidation abilities [4]. Generation of ROS and RSS is usually performed through the activation of radical precursors by the catalytic processes, such as direct photolysis [5], homogeneous metal ions activation [6], and heterogeneous metal oxides catalysis [7]. The metal oxides-based heterogeneous AOPs represent one of the most investigated strategies for organic pollutants removal in the laboratory and pilot scales [8]. Among various metal oxides, iron oxides are by far the most studied metal oxides for reactive radicals generation in water [9]. However, other metal oxides such as manganese oxides (MnO_x) are gaining stronger interests due to their versatile oxidation states (II, III, IV, and VII) [10].

Among the different MnO_x , manganese dioxide (MnO_2) has attracted increasing attention due to its good oxidative and catalytic performance for the elimination of pollutants [11]. For instance, Zhou et al. indicated the efficient degradation of 4-nitrophenol by α - and δ - MnO_2 activated PMS through the generation of $\text{SO}_4^{\bullet-}$ and HO^\bullet [12]. Zhu et al. demonstrated the rapid removal of bisphenol A (BPA) in the β - MnO_2 /PS system due to the formation of singlet oxygen ($^1\text{O}_2$) [13]. Moreover, the influence factors for the good catalytic and oxidative performance of various MnO_2 were investigated by Huang et al., and the results showed that the efficient oxidation of pollutants by MnO_2 with or without oxidants was attributed to the occurrence of Mn(III) on the surface of MnO_2 [14,15]. Therefore, it is believed that the presence of Mn(III) species in MnO_x can improve the activation efficiency of PS/PMS. Given the above, the direct activation of PS/PMS by Mn(III) oxides was investigated by previous studies. For example, Xu et al. reported the efficient elimination of p-chloroaniline in the γ - MnOOH /PS system through the formation of active intermediates between γ - MnOOH and PS [16]. Wang et al. indicated

the good reactivity of octahedral Mn_3O_4 on PMS activation for ciprofloxacin degradation due to the presence of high contents of Mn(III), Mn(IV) and hydroxyl groups (-OH) [17]. Moreover, the degradation of organic pollutants by PMS using synthesized Mn_2O_3 as the catalyst was also reported. For instance, Saputra et al. indicated that Mn_2O_3 compared with MnO, Mn_3O_4 , MnO_2 showed the highest reactivity in PMS activation for phenol degradation due to the formation of both $\text{SO}_4^{\cdot-}$ and $\text{SO}_5^{\cdot-}$ radicals [18]. The effect of Mn_2O_3 structures on PMS activation was also investigated by Saputra et al., and the results showed cubic- Mn_2O_3 has higher PMS catalysis efficiency due to its high surface area and surface atoms arrangement [19]. These experiments demonstrated well the effect of Mn oxidation states and catalyst structures on the activation of PMS. However, the catalytic mechanism of Mn_2O_3 on PMS is not clear, and some important influence factors for the reactivity of Mn_2O_3 such as solution pH were not investigated. Furthermore, Khan et al. investigated the activation of PS using synthesized Mn_2O_3 and MnO_2 for the degradation of phenol in solution [20]. The results showed that phenol was efficiently removed in A- Mn_2O_3 /PS system due to the generation of singlet oxygen ($^1\text{O}_2$). Although the authors adopted different experimental methods to identify the generated reactive species and investigated various influence parameters for the reactivity of A- Mn_2O_3 /PS system, it should be noted that the experiments were conducted in the acidic environment (pH~3.2). Moreover, since different reactive species were generated in γ - MnOOH /PS system under different solution pH [21], thus it is reasonable to deduce that the type of generated reactive species in the Mn_2O_3 /PS system can be influenced by solution pH. However, the authors only studied the generated reactive species in the acidic solution. Therefore, it is meaningful to investigate the mechanism of PS/PMS activation by Mn_2O_3 in the near-neutral solution and evaluate the suitability of the Mn_2O_3 activated PS/PMS system in real polluted waters. Caffeine (CAF) was used as a model of organic contaminants since its adverse effects on aquatic organisms and human beings [22]. Moreover, CAF as the emerging contaminant has been widely detected in different water matrices at concentrations ranging from ng/L to $\mu\text{g/L}$ [23].

In this work, we investigated and compared the ability of Mn_2O_3 to activate PS and PMS under different experimental conditions, i.e. pH, Mn_2O_3 dosage, and radical precursor concentrations.

Reactive radical species and non-radical pathways were identified and their contribution to the pollutant removal was quantified using chemical scavenging experiments, electron paramagnetic resonance spectroscopy (EPR) and X-ray photoelectron spectroscopy (XPS). Moreover, the CAF degradation pathway, main degradation products and mineralization efficiency were reported. Finally, the ability of both systems was compared in real sewage treatment plant water, where 80 % of CAF degradation was obtained by the proposed method after 20 hours.

2. Materials and Methods

2.1. Chemicals

All chemicals were reagent-grade (see Text S1 in Supplementary Materials) and used as received. Ultrapure water (Millipore, resistivity 18.2 M Ω cm) was used in the preparation of all solutions.

2.2. Catalyst characterization

The purity of the used Mn₂O₃ sample (Sigma-Aldrich) was confirmed by powder X-ray diffraction (XRD) (Figure S1). The average oxidation state (AOS) of Mn after reaction was obtained using X-ray photoelectron spectroscopy (XPS). The analysis conditions of XRD and XPS were presented in Text S2.

2.3. Experimental procedures

The chemical reactions were performed in a borosilicate brown bottle in which 100 mL of solution was kept at room temperature (298 \pm 2 K) under stirring (700 rpm) to ensure homogeneity. 25 μ M of CAF was added to the 100 mL reaction solution containing a certain concentration of Mn₂O₃, then a predetermined amount of oxidants (*i.e.* H₂O₂, PS, PMS, and HSO₃⁻) was added to start the reaction. The solution pH was fixed by adding 0.1 M sodium hydroxide and perchloric acid. 2 mL of samples were withdrawn at the predetermined interval times and were filtered (0.20 μ m PTFE filter) to remove Mn₂O₃ particles. The reaction was

stopped by the addition of 100 μL of methanol (HPLC grade, Sigma-Aldrich) and then the samples were analyzed by HPLC.

To determine the involvement of reactive radical species leading to the degradation of CAF, a kinetic competition study was performed using different radical scavengers such as *tert*-butanol (TBA) and 2-Propanol (2-Pr) to quench hydroxyl radical (HO^\bullet) and sulfate radical ($\text{SO}_4^{\bullet-}$) [24,25]. Furfuryl alcohol (FFA) was used to trap singlet oxygen ($^1\text{O}_2$) [26]. The contribution of main radical species to the degradation of CAF was estimated considering the second-order rate constants between the selected radicals and quenchers or CAF (see Table S1). The quenching efficiency was determined as $C_1 \times k_1 / (C_1 \times k_1 + C_2 \times k_2)$. Where C_1 was the initial concentration of organic scavengers and k_1 was the second-order rate constant with selected oxidant species (i.e. HO^\bullet , $\text{SO}_4^{\bullet-}$, or $^1\text{O}_2$), C_2 and k_2 were the concentration of CAF and reactivity constant with the oxidant species.

Sewage treatment plant water (STPW) was collected in December 2019 from the urban treatment plant named “3 rivières” in Clermont-Ferrand and used after 0.45 μm filtration using PTFE filter. The main physicochemical characteristics are reported in Table S2.

2.4. Chemical analysis and kinetics

CAF concentration was determined by a high-performance liquid chromatography system (HPLC, Alliance 2695 Waters) equipped with a photodiode array detector (DAD) and C18 column (Agilent Eclipse XDB, $250 \times 4.6 \text{ mm}$, 5 μm of particle size). The mobile phase was a mixture of acetonitrile (ACN) and milli-q water acidified with 0.1 % phosphoric acid in gradient eluent mode ($V_{\text{ACN}}/V_{\text{water}}$ from 20/80 to 70/30 in 6 min). The flow rate was set at 0.8 mL min^{-1} and the detection wavelength of CAF was fixed at 272 nm. The pseudo-first-order rate constant of CAF (k'_{CAF}) was determined from the slope of $\ln(C/C_0)$ vs time plot, where C_0 and C are the concentration of CAF at time 0 and t respectively. The error bars associated to the degradation constant data represent 3σ , derived from the scattering of the experimental data around the fit curves (intra-series variability).

To investigate the mineralization of CAF, total organic carbon (TOC) analysis (TOC-L CPH CN200, SHIMADZU) was performed.

PS and PMS concentrations were measured using a modified spectrophotometric method [27]. Briefly, 100 μL of PS or PMS sample was first transferred into 5 mL of the mixture of potassium iodide (KI, Sigma-Aldrich) and sodium bicarbonate (NaHCO_3 , Sigma-Aldrich) to generate iodine (I_2). Then, I_2 further reacted with iodide (I^-) leading to the formation of complex (I_3^-). Finally, I_3^- was detected using a Varian Cary 3 UV-visible spectrophotometer (Abs at 351 nm) and quantified using a calibration curve.

The identification of radicals was performed by electron paramagnetic resonance spectroscopy (EPR). The X-band cw-EPR spectra (modulation frequency of 100 kHz) were monitored at 293 K with the EMX*plus* spectrometer (Bruker) equipped with the High Sensitivity Probe-head (Bruker) in the small quartz flat cell (Wilmad-LabGlass, WG 808-Q) using 5,5-dimethyl-1-pyrroline *N*-oxide (DMPO, Sigma-Aldrich) and 2,2,6,6-tetramethyl-4-piperidinol (TEMP, Sigma-Aldrich) as the spin trapping agents. Typically, 375 μL of sample was withdrawn and immediately mixed with 125 μL of DMPO (100 mM) or TEMP (100 mM), then the mixture was transferred into an EPR quartz capillary tube (0.5 mm, 100 mm) for measurement. The EPR spectrometer settings were as follows: microwave frequency, ~ 9.87 GHz; microwave power, ~ 6.87 mW; center field, ~ 352.7 mT; sweep width, 20 mT; sweep time, 30 s; sample *g*-factors, 2.0; modulation amplitude, 1.0 G. The experimental EPR spectra were analyzed by the WinEPR software (Bruker) and the calculations of spin-Hamiltonian parameters and relative concentrations of individual DMPO-adducts were performed with the EasySpin toolbox working on MatLab[®] platform [28].

The identification of CAF transformation intermediates was obtained by an LC-MS system coupled with an ESI ion source (MSD VL). The column was a Phenomenex Kinetex C18 column (2.6 $\mu\text{m} \times 100 \text{ \AA}$; 100 \times 2.1 mm) using an initial gradient of 5% ACN and 95% water acidified with 1% formic acid (Sigma-Aldrich), followed by a linear gradient to 95% ACN within 15 min and kept constant during 10 min. The flow rate was 0.2 mL min^{-1} and the injection volume of 10 μL .

3. Results and discussion

3.1. Reactivity of Mn_2O_3 with PS and PMS

The reactivity of Mn_2O_3 with different radical precursors (i.e. H_2O_2 , PS, PMS, and HSO_3^-) was investigated. As shown in Figure 1, the CAF degradation was observed only in the Mn_2O_3 activated PS and PMS (5 mM) systems. Up to 40% of removal extent was observed after 3 h of reaction time in the unbuffered solutions. Although the solution pH dropped to 5.5 ± 0.2 and 2.7 ± 0.2 with the addition of PS and PMS, the purpose of checking the reactivity of Mn_2O_3 with PS and PMS was achieved (Table S3). Moreover, blank and adsorption tests showed that CAF removal by adsorption on Mn_2O_3 or direct oxidation by radical precursors was negligible whatever the investigated pH (Figure S2 and S3).

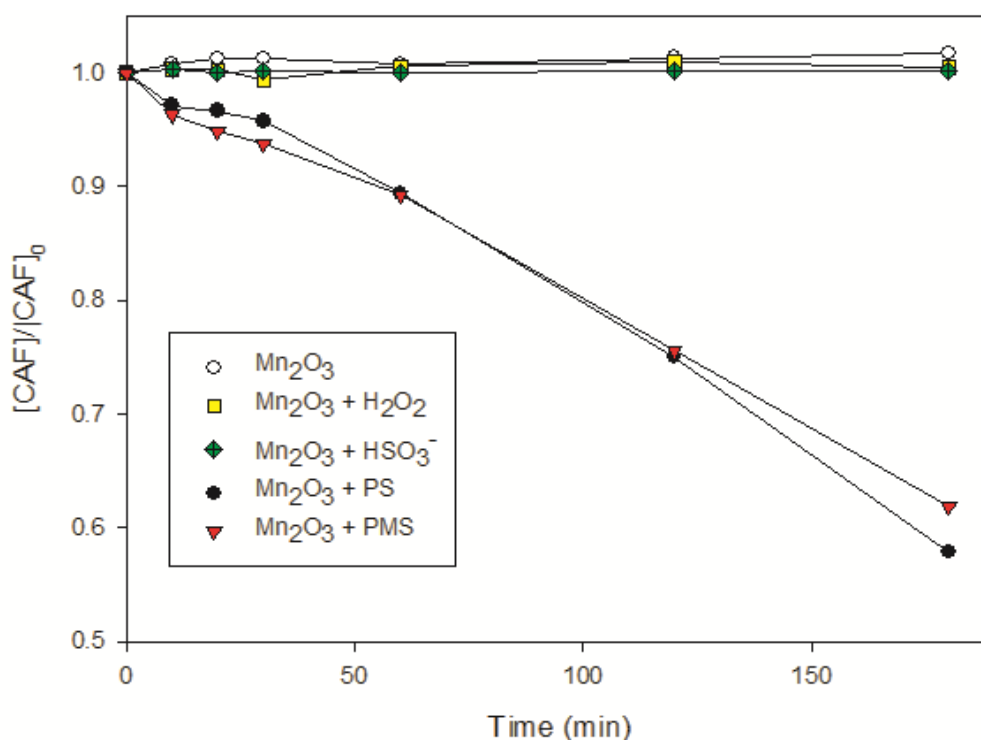


Figure 1. CAF (25 μM) degradation in the presence of 0.4 g L^{-1} of Mn_2O_3 and different oxidants at 5 mM, natural pH (see Table S3), and $T = 298 \text{ K}$.

The formation of radical species and their relative contribution to the CAF degradation were determined by chemical scavenging and EPR experiments. Before starting the scavenging tests, suitable concentrations of scavengers were determined through the calculation of scavenging efficiency with reactive oxygen species (ROS). As shown in Table S4, in the presence of 10

mM of TBA, 10 mM of 2-Pr and 1 mM of FFA, a scavenging efficiency of 97.4, 93.2 and 99.4 % of the corresponding ROS was achieved. Thus, the proposed scavenger concentration was enough to inhibit almost the whole radical reactions. In addition, to verify if the degradation of CAF was originated from the heterogeneous reaction between PS/PMS and Mn_2O_3 , the leaching of Mn^{2+} in Mn_2O_3 activated PS/PMS reactions and the homogeneous activation of PS/PMS by Mn^{2+} were studied. As shown in Figure S4. A negligible Mn^{2+} concentration ($\sim 1 \mu\text{M}$) was determined when 0.4 g L^{-1} of Mn_2O_3 was suspended in solution. Moreover, the degradation efficiency of CAF in the Mn^{2+} activated PS/PMS system was far lower than Mn_2O_3 , even the employed concentration of Mn^{2+} was 10-1000 times higher than leached Mn^{2+} . Thus, the removal of CAF was attributed to the activation of PS/PMS by Mn_2O_3 .

3.1.1 Reactivity of Mn_2O_3 with PS

In the system of $\text{Mn}_2\text{O}_3/\text{PS}$, only a negligible effect of TBA and 2-Pr was observed indicating that HO^\bullet and $\text{SO}_4^{\bullet-}$ were not the main radical species involving in the CAF degradation (Figure 2A). However, in the presence of 1 mM of FFA, the CAF degradation constant (k'_{CAF}) dropped from $2.4 \times 10^{-3} \text{ min}^{-1}$ to $2.6 \times 10^{-5} \text{ min}^{-1}$, corresponding to 99% of inhibition after 8 h (Figure S5). The inhibition of CAF degradation in the presence of FFA can be due to the quenching of $^1\text{O}_2$. To identify whether $^1\text{O}_2$ was generated in the $\text{Mn}_2\text{O}_3/\text{PS}$ system, the EPR experiments were conducted using TEMP as the spin trapping agent and no signal corresponding to the formation of TEMPO was observed (Figure S6), thus indicating the inhibition of CAF degradation by FFA was not related to the scavenging of $^1\text{O}_2$. Other reasons can explain the inhibition of CAF by FFA, such as the scavenging of HO^\bullet , the increased PS consumption, and the occupied reactive sites on the Mn_2O_3 surface [16,26,29]. The scavenging of HO^\bullet was excluded since CAF degradation was not inhibited in the presence of TBA (Figure 2A) while CAF removal was completely suppressed after the simultaneous addition of 2-Pr and FFA (Figure S7). Moreover, the PS decomposition due to the reactivity with FFA was negligible (Figure S8) compared to the reactivity in the presence of PMS [29]. Therefore, the inhibition of CAF degradation in presence of FFA was attributed to the adsorption of FFA on the surface of Mn_2O_3 and competing

with PS ions for the active sites. The results are in agreement with previous studies which reported FFA can affect the surface properties of catalysts [16,30].

Therefore, a non-radical mechanism of PS activation is proposed and it generally includes the generation of $^1\text{O}_2$ (as mentioned just above, this hypothesis is excluded), the surface-activated PS species, or the electron transfer process [31]. It is worth noting that the electron transfer mechanism in PS activation usually happens when carbon-based materials were used as catalysts [32]. Therefore, the removal of CAF in the $\text{Mn}_2\text{O}_3/\text{PS}$ system was attributed to the formation of Mn_2O_3 surface-activated PS. The result is in agreement with previous studies which indicated no $^1\text{O}_2$ was generated but the active intermediates formed between PS and catalyst were responsible for the degradation of pollutants [16,21].

To better understand the role of PS, the concentration of PS in different systems was monitored (Figure 2B). The depletion of PS by CAF alone was negligible, whereas a small amount of PS was consumed by Mn_2O_3 in the absence of CAF. This result indicates that PS was absorbed on the active sites present on the surface of Mn_2O_3 . CAF as an electron donor leads to the increased consumption of activated PS since in the $\text{Mn}_2\text{O}_3/\text{PS}$ system the depletion of PS was enhanced. The non-radical mechanism of PS activation was further verified through the measurement of the Mn oxidation state in the $\text{Mn}_2\text{O}_3/\text{PS}$ system. The average oxidation state (AOS) of samples was calculated from the binding energy difference (ΔE) of Mn 3s doublet splitting as following: $\text{AOS} = 8.956 - 1.126 \times \Delta E$ [33]. Figure S9 shows that the AOS of Mn_2O_3 did not change after reaction with PS (AOS ~ 3.00), indicating the activation of PS by Mn_2O_3 was a non-radical catalytic process.

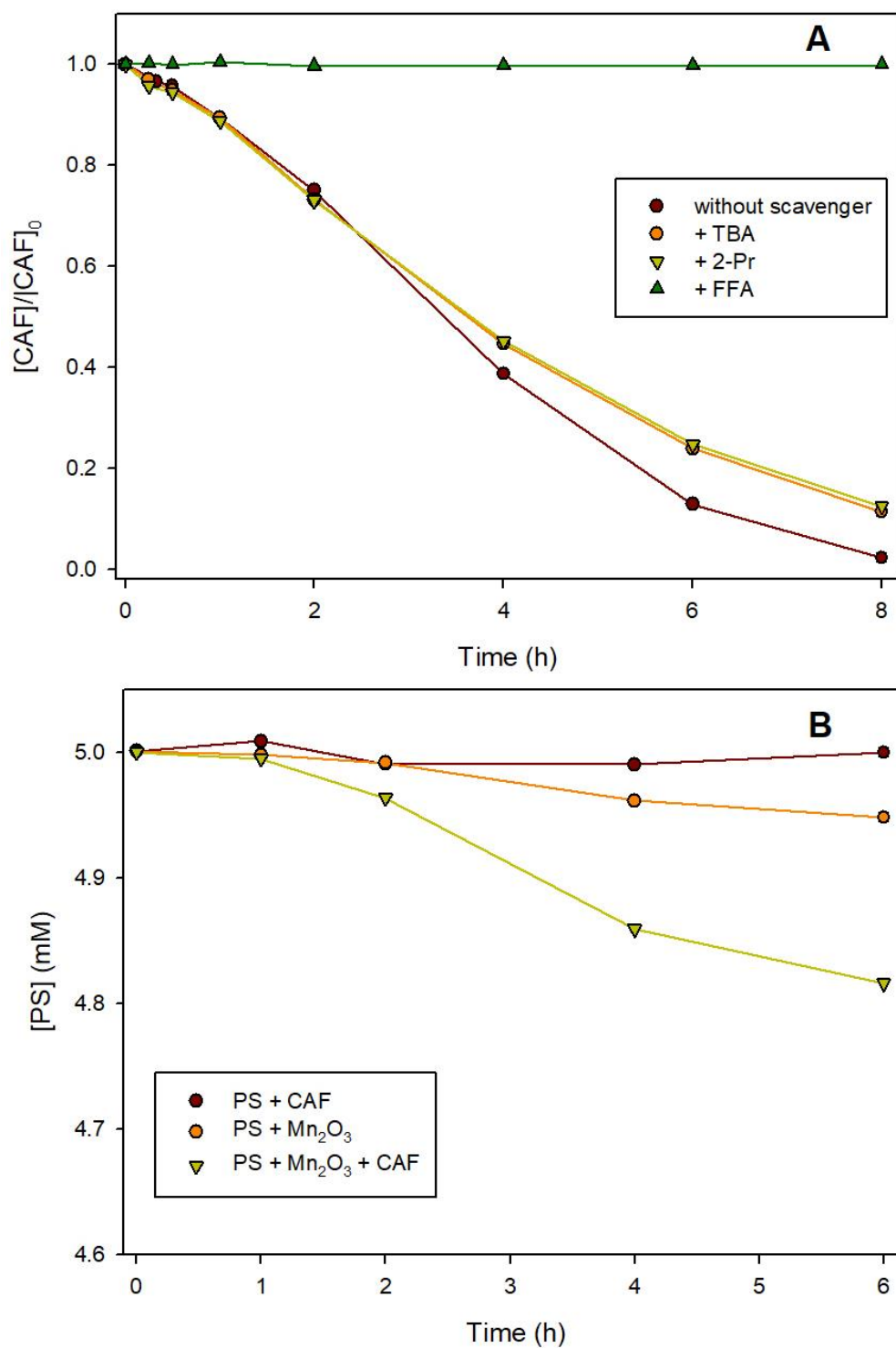


Figure 2. Determination of ROS species for CAF oxidation in Mn₂O₃/PS. **A:** CAF degradation by Mn₂O₃ with PS in the presence of different radical scavengers ($[TBA]_0 = [2\text{-Pr}]_0 = 10 \text{ mM}$, $[FFA]_0 = 1 \text{ mM}$). **B:** PS decomposition in different processes. $[Mn_2O_3]_0 = 0.4 \text{ g L}^{-1}$, $[CAF]_0 = 25 \text{ }\mu\text{M}$, $[PS]_0 = 5 \text{ mM}$, The pH of solution was 5.0 and $T = 298 \text{ K}$.

3.1.2 Reactivity of Mn₂O₃ with PMS

In the PMS-containing system, the presence of TBA and 2-Pr decreased the k'_{CAF} from $6.5 \times 10^{-3} \text{ min}^{-1}$ to $4.0 \times 10^{-3} \text{ min}^{-1}$ and $7.0 \times 10^{-4} \text{ min}^{-1}$, respectively (Figure 3A and Figure S10) indicating the predominant role of $\text{SO}_4^{\bullet-}$ compared to HO^{\bullet} . PMS can react with both $\equiv\text{Mn}^{\text{III}}$ (Eq. 1) and $\equiv\text{Mn}^{\text{IV}}$ (Eq. 2) leading to the formation of $\text{SO}_4^{\bullet-}$ and $\text{SO}_5^{\bullet-}$ [34]. Moreover, $\text{SO}_5^{\bullet-}$ self-reaction in water can lead to the formation of $\text{SO}_4^{\bullet-}$ (Eq. 3) [35]. Formation of HO^{\bullet} occurs through $\text{SO}_4^{\bullet-}$ reaction with water and hydroxide, although the latter reaction is only relevant in alkaline solution (Eqs. 4 and 5) [36]. The generation of $\text{SO}_4^{\bullet-}$ and HO^{\bullet} was further identified by EPR experiments. As shown in Figure 3B, the EPR spectrum represents a superposition of two individual signals (according to the results of the best simulation fit), including the nine-line signal of 5,5-dimethyl-2-oxo-pyrroline-1-oxyl ($^{\bullet}\text{DMPO-X}$) with the characteristic spin-Hamiltonian parameters ($a_{\text{N}} = 0.732 \text{ mT}$, $a_{\text{H}^{\gamma}}(2\text{H}) = 0.406 \text{ mT}$; $g = 2.0070 \pm 0.0001$), which is often produced by over-oxidation of DMPO in the presence of reactive oxygen species (*e.g.* HO^{\bullet} or $^1\text{O}_2$) [37]. The second signal is characterized by the hyperfine coupling constants ($a_{\text{N}} = 1.373 \text{ mT}$, $a_{\text{H}^{\beta}} = 1.019 \text{ mT}$, $a_{\text{H}^{\gamma}} = 0.135 \text{ mT}$, $a_{\text{H}^{\delta}} = 0.073 \text{ mT}$), which correlate well with $^{\bullet}\text{DMPO-SO}_4^{\bullet-}$ spin-adduct with limited stability in aqueous media [38].



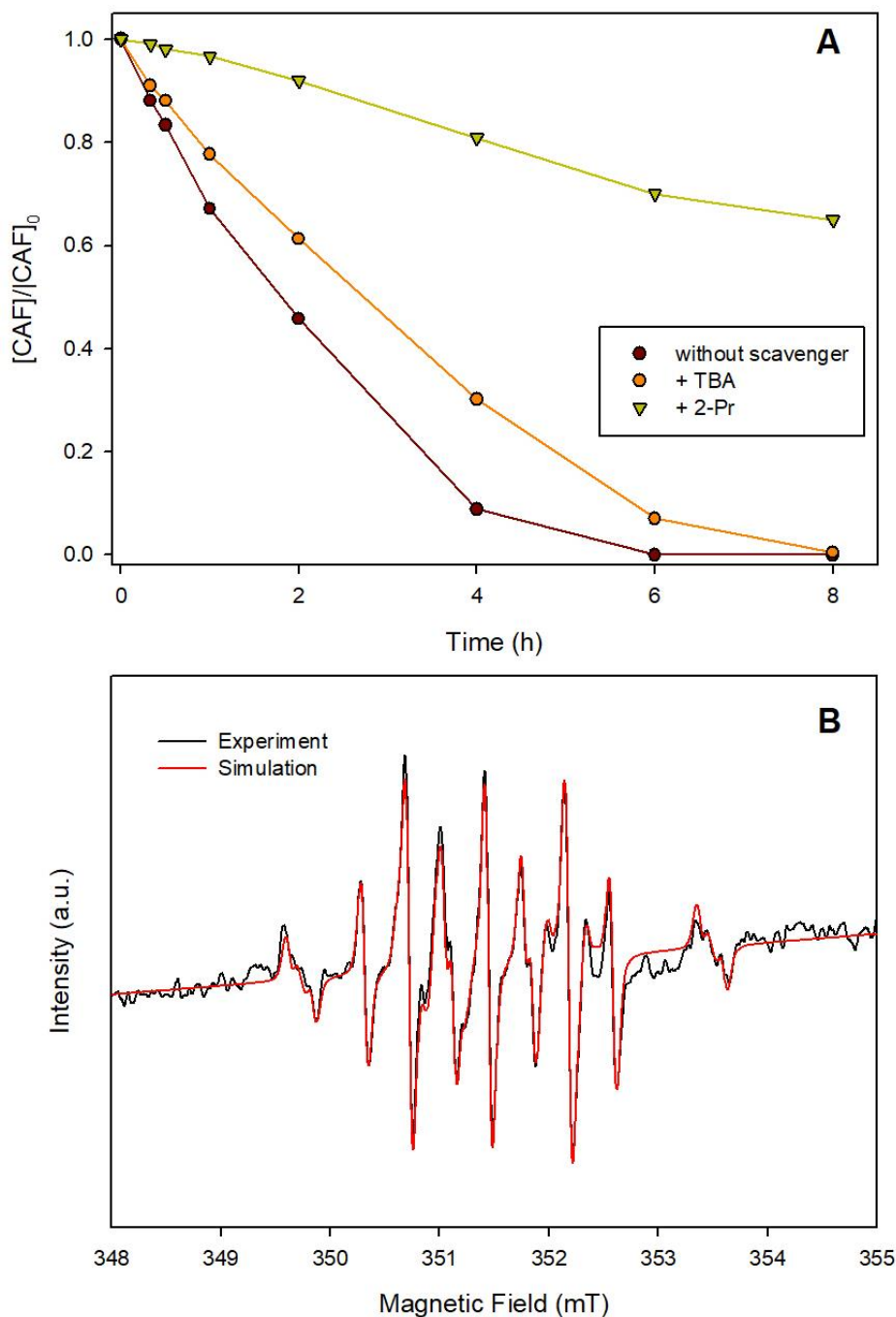


Figure 3. Determination of reactive radical species for CAF degradation in $\text{Mn}_2\text{O}_3/\text{PMS}$ system. **A:** Quenching tests of CAF degradation in the process of $\text{Mn}_2\text{O}_3 + \text{PMS}$ with various radical scavengers ($[\text{TBA}]_0 = [\text{2-Pr}]_0 = 10 \text{ mM}$). **B:** The normalized experimental (black line) and simulated (red line) EPR spectra measured in the suspension of $\text{PMS}/\text{Mn}_2\text{O}_3/\text{DMPO}/\text{water}$ ($[\text{DMPO}]_0 = 25 \text{ mM}$). $[\text{Mn}_2\text{O}_3]_0 = 0.4 \text{ g L}^{-1}$, $[\text{CAF}]_0 = 25 \text{ }\mu\text{M}$, $[\text{PMS}]_0 = 5 \text{ mM}$, the pH of solution was 5.0 and $T = 298 \text{ K}$.

Since the addition of FFA exhibited a strong inhibition effect (~ 85%) on CAF degradation (Figure S11A), thus, to verify whether the generated $\cdot\text{DMPO-X}$ was derived from the reaction with $^1\text{O}_2$, the EPR experiment was further performed. As shown in Figure S11B, in the presence of 25 mM of TEMP, a typical TEMPO signal (three-line signal with 1:1:1 intensity ratio) was observed in the presence of PMS alone which can be attributed to the self-decomposition of PMS [39]. In $\text{Mn}_2\text{O}_3/\text{PMS}$ system, the TEMPO signal was approximately equal to the TEMPO intensity from PMS alone, indicating that no further $^1\text{O}_2$ was generated in the $\text{Mn}_2\text{O}_3/\text{PMS}$ system. Moreover, the addition of FFA in the $\text{Mn}_2\text{O}_3/\text{PMS}$ system also showed a negligible effect on the intensity of the TEMPO signal. Thus, the formation of $\cdot\text{DMPO-X}$ in the system of $\text{Mn}_2\text{O}_3/\text{PMS}$ cannot be contributed to $^1\text{O}_2$. On the other side, the generated $\text{HO}\cdot$ might be responsible for the formation of $\cdot\text{DMPO-X}$, consistent with the observations of Yang et al. [39]. The decomposition of PMS was further investigated. Figure S11C shows that PMS can be decomposed by FFA alone, and the depletion efficiency of PMS is higher than Mn_2O_3 , suggesting the inhibition of CAF degradation in presence of FFA might be also attributed to the increased consumption of PMS.

Besides, the AOS of Mn in the $\text{Mn}_2\text{O}_3/\text{PMS}$ system was measured, as shown in Figure S9C. The AOS of Mn_2O_3 was increased to 3.10 after reacting with PMS, suggesting the generation of Mn (IV). It is known that Mn (IV) can oxidize organic pollutants compounds through a heterogeneous electron transfer process [14], thus the non-radical degradation of CAF in the $\text{Mn}_2\text{O}_3/\text{PMS}$ system might be related to the formation of Mn (IV).

In summary, different activation mechanisms of PS and PMS by the same Mn_2O_3 were exhibited. In the $\text{Mn}_2\text{O}_3/\text{PS}$ system, the catalyst surface-activated PS molecules were the primary reactive species that are responsible for the degradation of pollutants. This can be attributed to the symmetric structure of PS which facilitates the contained O-O bonds binding to Mn_2O_3 surface through the substitution with surface hydroxyl groups (-OH) [13,16,40]. In comparison, the activation of PMS by Mn_2O_3 was mainly processed with the generation of radicals. It can be explained by the fact that the unsymmetric structure of PMS can be easier

activated by catalysts, the causes are in agreement with the results of previous research [41–43].

3.2. Effect of pH

The CAF removal by Mn_2O_3 -mediated activation of PS or PMS was also investigated over a wide range of initial pH (3–8) and degradation pseudo-first order rates were plotted versus pH (Figure 4). In the presence of PS, k'_{CAF} decreased from 4.7×10^{-3} to $2.6 \times 10^{-4} \text{ min}^{-1}$ from pH 3 to 8. It should be noted that the neutral form of CAF predominates over the investigated pH range ($\text{pK}_a = 10.4$). The greater efficiency observed at low pH might result from the favorable electrostatic interactions between positively charged Mn_2O_3 (PZC ~ 5.9) and PS [44]. The system $\text{Mn}_2\text{O}_3/\text{PMS}$ exhibited an improved k'_{CAF} with increasing the solution pH from $2.2 \times 10^{-3} \text{ min}^{-1}$ to $6.4 \times 10^{-3} \text{ min}^{-1}$, followed by a decrease to $2.4 \times 10^{-3} \text{ min}^{-1}$ (Figure 4). The low efficiency at low pH may come from the impact of H^+ concentration on the reactivity of $\text{SO}_4^{\cdot-}$, resulting in the low CAF degradation [45]. Since the oxidation potential of HO^{\cdot} is lower than $\text{SO}_4^{\cdot-}$ under alkaline environments, the transformation from $\text{SO}_4^{\cdot-}$ to HO^{\cdot} may explain the low efficiency at high pH values. To further explore this transformation process, the scavenging tests with the addition of TBA and 2-Pr were conducted under various initial solution pH (Figure S12). The contribution of HO^{\cdot} and $\text{SO}_4^{\cdot-}$ in the degradation of CAF was also assessed using Eq. S1 (Text S3). As shown in Figure S12D, the radical involvement percentage (RI) of HO^{\cdot} after 6 h of CAF degradation first decreased from 10% to 7% and then increased to 34% as the initial solution pH increased from 3 to 8. In the meanwhile, the RI percentage of $\text{SO}_4^{\cdot-}$ first increased from 55% to 63% and then decreased to 50%. The results fully and directly demonstrated the transformation between HO^{\cdot} and $\text{SO}_4^{\cdot-}$ with the change of solution pH. In summary, neutral or basic conditions are suitable for the activation of PMS by Mn_2O_3 , while PS activation by Mn_2O_3 was enhanced in acidic conditions only.

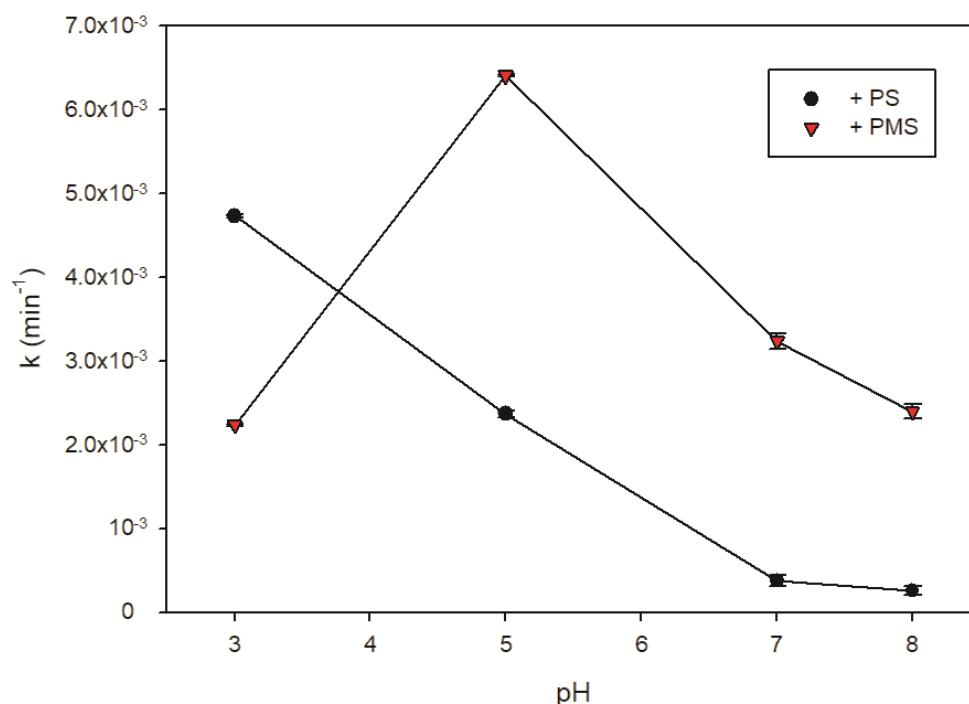


Figure 4. Degradation constant of CAF (k'_{CAF}) in the systems $Mn_2O_3 + PS$ and $Mn_2O_3 + PMS$ under different pH values. Experimental conditions are $[Mn_2O_3]_0 = 0.4 \text{ g L}^{-1}$, $[CAF]_0 = 25 \text{ }\mu\text{M}$, $[PS]_0 = [PMS]_0 = 5 \text{ mM}$, $T = 298 \text{ K}$.

3.3. Effects of Mn_2O_3 and oxidant dosages

The effect of Mn_2O_3 concentration on CAF degradation in presence of PS under initial solution pH 5 was then investigated (Figure 5A and Figure S13A). An increase of Mn_2O_3 dosage from 0.05 to 1.0 g L^{-1} led to an increase of k'_{CAF} from $5.4 \times 10^{-4} \text{ min}^{-1}$ to $4.6 \times 10^{-3} \text{ min}^{-1}$. Similarly, the removal of CAF by Mn_2O_3 activated PMS was increased with the increase in Mn_2O_3 concentration (Figure S13B). This effect can be attributed to the increase of the active surface area of Mn_2O_3 , leading to more active sites for radical precursor activation. It is worth noting that complete removal of CAF was obtained for $1.0 \text{ g L}^{-1} Mn_2O_3$ and 5 mM PMS after 2 h, while 8 h reaction time is required for the Mn_2O_3/PS system. The degradation of CAF (k'_{CAF}) by Mn_2O_3 (1.0 g L^{-1}) with PMS (5 mM) was $3.9 \times 10^{-2} \text{ min}^{-1}$, which results in an 8-fold increase compared to that in Mn_2O_3/PS system ($4.6 \times 10^{-3} \text{ min}^{-1}$). Figure 5B shows the increase of the k'_{CAF} from $1.6 \times 10^{-4} \text{ min}^{-1}$ to $4.7 \times 10^{-3} \text{ min}^{-1}$ with the increase of PS concentration from 1 to 10 mM. The effects of PMS concentration on CAF degradation in the presence of Mn_2O_3 (0.4

g L^{-1}) were similar, where an increase of k'_{CAF} from $3.5 \times 10^{-4} \text{ min}^{-1}$ to $8.5 \times 10^{-3} \text{ min}^{-1}$ with increasing PMS concentration from 1 to 10 mM. These enhanced degradations with the increase of radical precursor concentrations ($\leq 10 \text{ mM}$) can be attributed to the promotion of the number of reactive radicals as discussed in *section 3.1*.

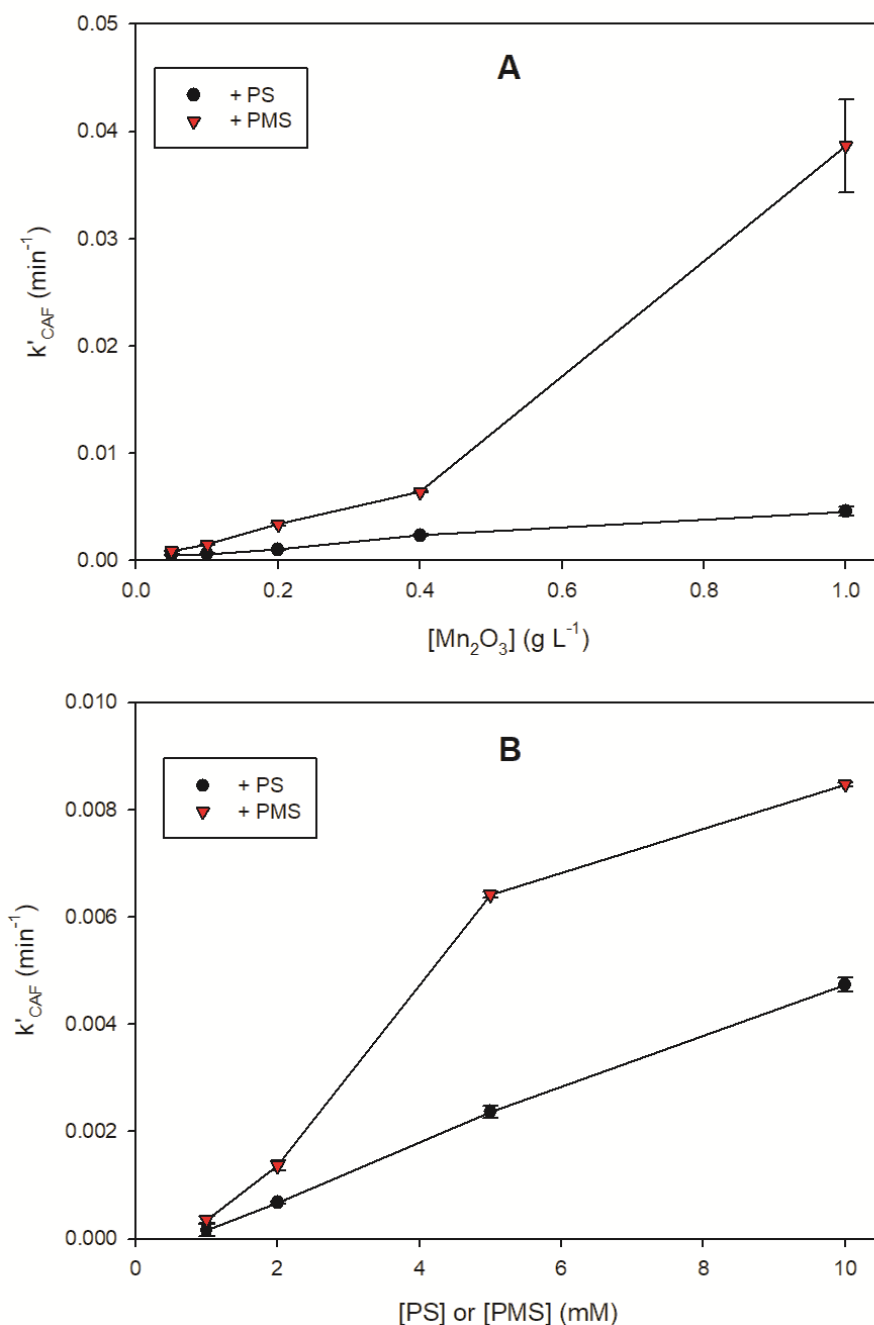


Figure 5. Degradation of CAF (k'_{CAF}) in the system Mn_2O_3 with PS and PMS. **A:** Effect of Mn_2O_3 concentration in the presence of 5 mM PS and PMS. **B:** Effect of PS and PMS concentrations using 0.4 g L^{-1} of Mn_2O_3 . Initial pH = 5.0, T = 298 K.

3.4. CAF degradation pathway and mineralization

The main transformation intermediates of CAF in Mn_2O_3 -activated PS and PMS systems were identified by LC-MS analysis. The experimental conditions were: $[\text{Mn}_2\text{O}_3]_0 = 0.4 \text{ g L}^{-1}$, $[\text{CAF}] = 25 \text{ }\mu\text{M}$ and $[\text{PS}] = [\text{PMS}]_0 = 5 \text{ mM}$, initial solution pH = 5.0 and analysis was performed after 2 hours of reaction. The molecular formulas, structures, retention time, and positive/negative molecular ions (m/z) of intermediates are summarized in Table S5, and the possible degradation pathways of CAF are shown in Figure 6. CAF was identified at $[\text{M}+\text{H}]^+ = 195.08 \text{ m/z}$. The first transformation step was the hydrogen abstraction (C8 position) and then water molecule addition generating an intermediate with a keto-enol equilibrium. Further oxidation steps lead to the formation of product P1 at $[\text{M}-\text{H}]^- = 228.19 \text{ m/z}$. Similar transformation processes in CAF oxidation were reported in the previous study [46,47]. Subsequently (pathway 1), the intermediate P2 ($[\text{M}+\text{H}]^+ = 202.15 \text{ m/z}$, $[\text{M}+\text{H}-\text{H}_2\text{O}]^+ = 184.13 \text{ m/z}$, and $[\text{M}-\text{H}]^- = 200.13 \text{ m/z}$) generated from the decarboxylation of P1 through the attack of radicals and followed by the addition of hydroxyl group was identified.

In pathway 2, the C=C bond of product P1 was attacked by radical species, opening the six-member ring and leading to the formation of two carbonyl groups (-C=O) on the carbon bonding with nitrogen [48,49]. Then the newly formed carbonyl groups might be further attacked by radicals and the C-N broke leading to the loss of nitrogen derivative (-N-CH₃-COOH) and formation of product P3 ($[\text{M}+\text{H}]^+ = 188.13 \text{ m/z}$, $[\text{M}+\text{H}-\text{H}_2\text{O}]^+ = 170.12 \text{ m/z}$ and $[\text{M}-\text{H}]^- = 186.11 \text{ m/z}$) [48]. The intermediate P4 at $[\text{M}+\text{H}]^+ = 174.11 \text{ m/z}$ and $[\text{M}-\text{H}]^- = 172.09 \text{ m/z}$ were further identified, which was originated from P3 through the demethylation process. It is worth noting that not all the intermediates (P1-P4) were observed in the Mn_2O_3 /PMS system and this can be explained by the different types of active radicals generated in Mn_2O_3 activated PS and PMS systems (see Table S5).

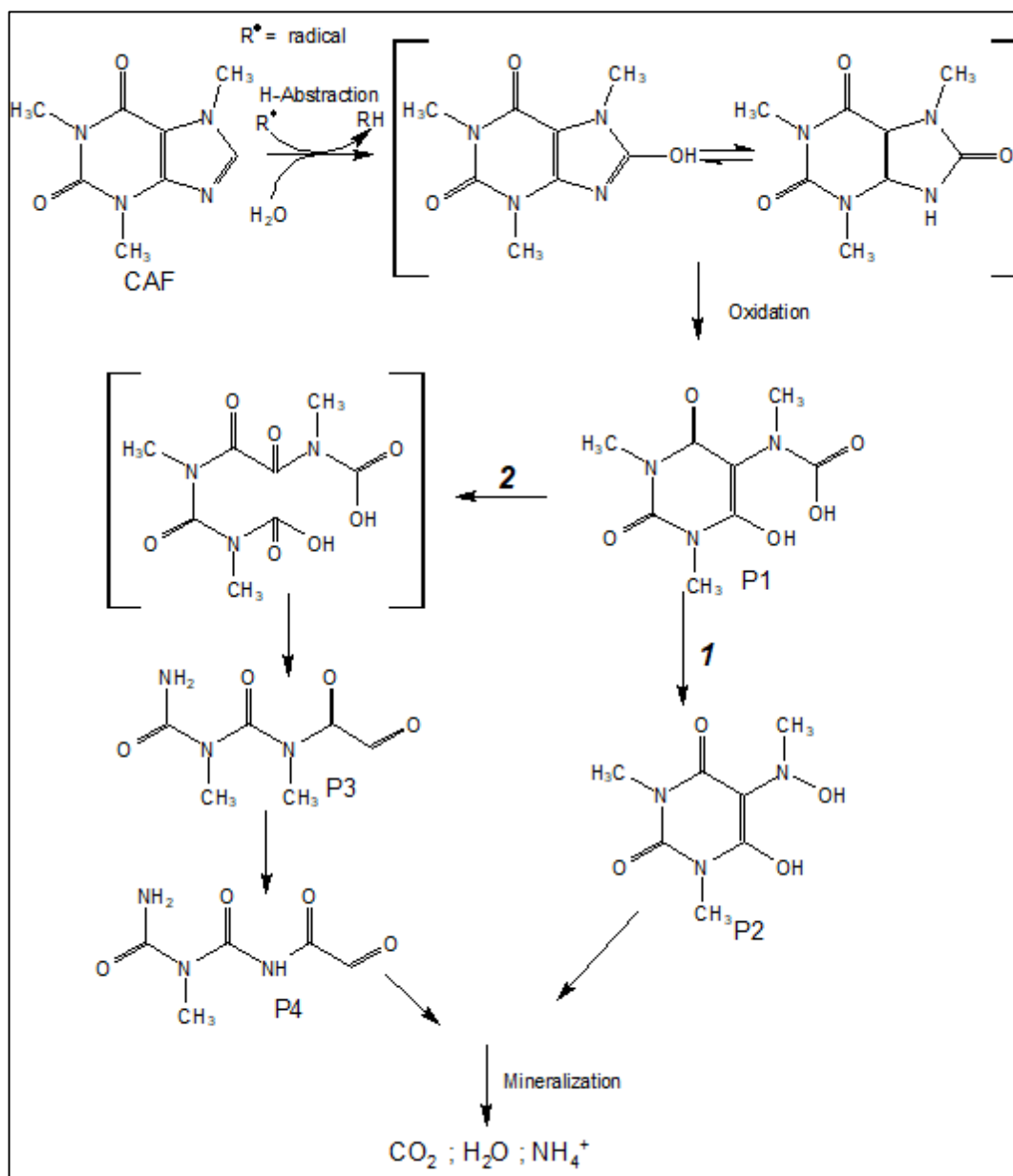


Figure 6. Proposed degradation pathways of CAF in Mn₂O₃-activated PS and PMS systems.

P2 and P4 were identified only in the presence of PS (see table S5).

The mineralization efficiency of Mn₂O₃ + PS and PMS systems was monitored by measuring TOC over reaction time. As shown in Figure 7, 34% and 48% of TOC degradation were reached in Mn₂O₃-activated PS and PMS system in 70 h, while complete removal of CAF was achieved before 8 h of reaction time (Figure S14). However, the oxidation process remains active for a long time, over 70 h, suggesting the long-term efficiency of the investigated process.

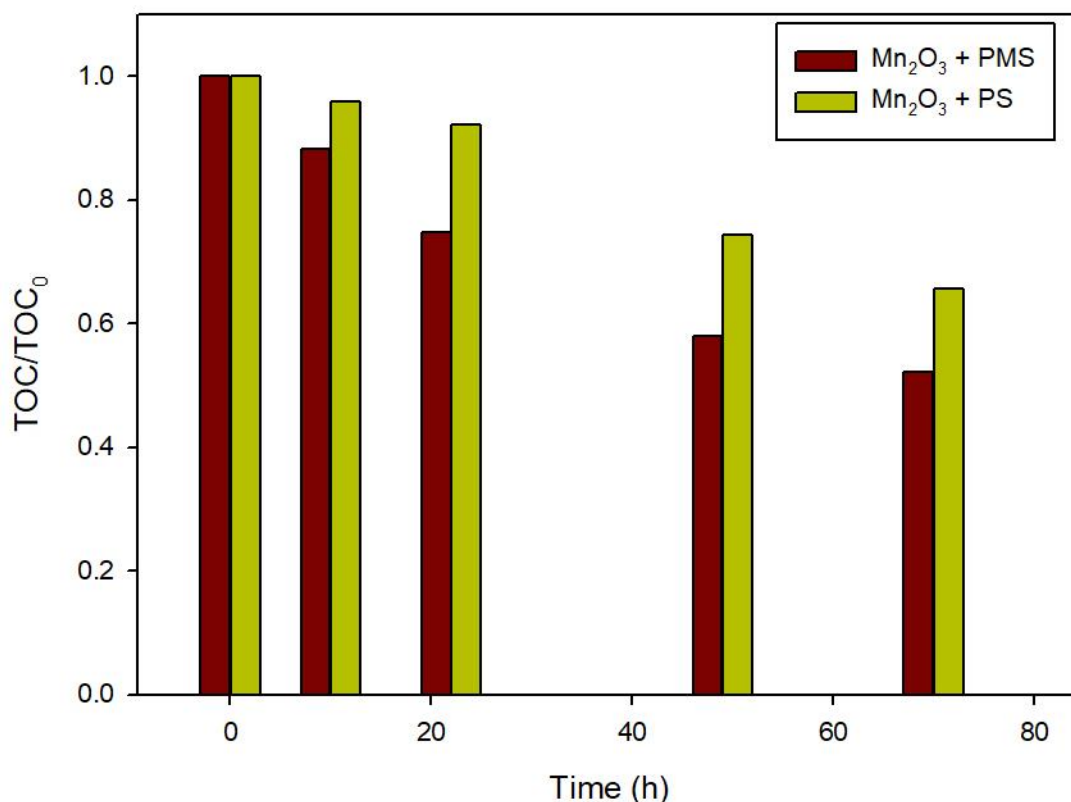


Figure 7. TOC decrease with time in Mn₂O₃-activated PS and PMS systems. Experimental conditions: [Mn₂O₃]₀ = 0.4 g L⁻¹, [CAF]₀ = 25 μM, [PS]₀ = [PMS]₀ = 5 mM, initial solution pH = 5.0, T = 25 ± 2 °C.

3.5. Degradation efficiency in sewage treatment plant waters (STPW)

To assess the performance and ability of Mn₂O₃ + PS and PMS to degrade CAF in the real water body, the degradation was evaluated in STPW (Total Organic Carbon (TOC) = 39.7 mg C L⁻¹, Inorganic Carbon (IC) = 4.5 mg C L⁻¹, pH = 8.1) and compared to milli-q water system using 0.4 and 1.0 g L⁻¹ of Mn₂O₃ (Figure S15). The degradation efficiency of CAF (DE) was determined from the percentage of CAF degraded after 20 hours of reaction and inhibition in STPW was observed in all experiments (Figure 8). Generally, this effect can be attributed to the radical scavenging ability of natural organic matter and inorganic carbon (i.e. hydrogen carbonate ions) of STPW that are recognized to be the main inhibitors of radicals in AOPs [15]. However, in Mn₂O₃/PS system, the main reactive species are the Mn₂O₃ surface-activated PS. The inhibition of CAF degradation in STPW was mainly attributed to the increased ionic strength [50].

The inhibition effect (IE) of STPW was determined as $IE = \left(1 - \frac{DE_{STPW}}{DE_{milli-q}}\right) \times 100$, in which DE_{STPW} and $DE_{milli-q}$ were the CAF degradation efficiencies in STPW and milli-q water after 20 hours. It is interesting to note that, in the presence of PS, about 95 % of inhibition was reported using two different Mn_2O_3 concentrations. The results verified again the non-radical mechanism in the Mn_2O_3/PS system and the formation of Mn_2O_3 surface-activated PS. However, a decrease of inhibition effect with the increase of Mn_2O_3 concentration was observed using PMS. The CAF degradation efficiency drops from 88.6 to 33.6 % (IE of 62%) when 0.4 g L^{-1} of Mn_2O_3 was used, while only 20% of inhibition in STPW was determined in the presence of 1.0 g L^{-1} . Increasing in the production of reactive species is expected when a higher amount of solid (higher exposed surface area) is used. This finding highlights the crucial role of Mn in promoting oxidation reactions and suggests that manganese-mediated advanced oxidation processes (Mn-AOPs) could be a promising process for wastewater treatment.

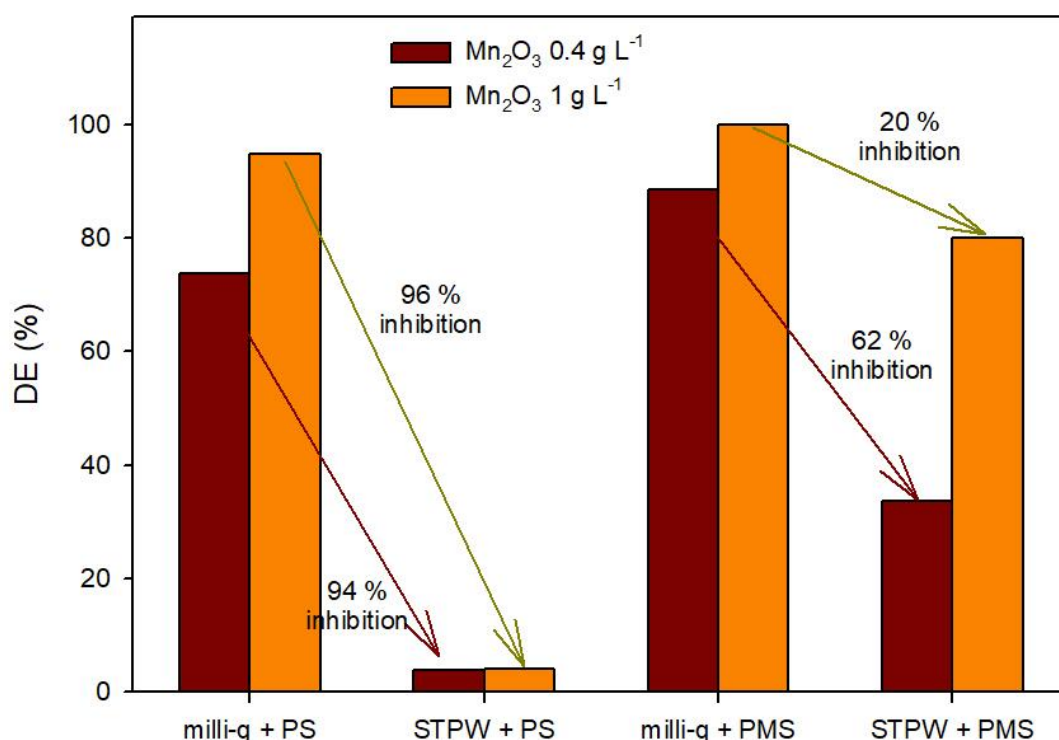


Figure 8. The degradation efficiency of CAF after 20 hours of reaction in milli-q and STP waters (STPW) using 0.4 and 1.0 g L^{-1} of Mn_2O_3 . PS and PMS concentrations were 5 mM and the pH of solutions was 8.0 ± 0.2 .

4. Conclusion

Mn₂O₃ exhibited higher activation capability for PS and PMS compared with H₂O₂ and HSO₃⁻. CAF degradation in the Mn₂O₃-activated PS and PMS was highly influenced by the initial solution pH. PS was efficiently activated by Mn₂O₃ under acidic pH, while under neutral or alkaline conditions, environmentally relevant pH values, higher degradation was observed using PMS. Chemical quenching and EPR experiments demonstrated that HO[•] and SO₄^{•-} were the main radicals generated in the system with PMS. In addition, a non-radical mechanism could contribute to the degradation of CAF in the Mn₂O₃/PS system. The degradation efficiency was tested in real STPW and, despite the inhibition of CAF degradation was observed due to the water constituents (mainly inorganic and organic carbon), the central role of Mn₂O₃ activation for highly reactive species formation was demonstrated in particular when PMS was used (about 80 % of CAF degradation was obtained in STPW after 20 hours). Comparison of obtained results in pure and real STPW indicates that a lower inhibition effect (20 %) was obtained using PMS compared to the PS system. Given the ability of Mn₂O₃ to activate PS and PMS, the manganese-based oxidation processes (Mn-AOPs) reactions can be considered as a promising treatment technology for the removal of organic pollutants in water.

Acknowledgments

This work was supported by the Region Council of Auvergne Rhône Alpes, the “Fédération des Recherches en Environnement” through the CPER “Environnement” founded by the Region Auvergne, the French government and the FEDER (European Community), PRC program CNRS/NSFC n°270437 and CAP 20–25 I-site project. The authors gratefully acknowledge financial support from China Scholarship Council provided to Daqing Jia (No, 201806920034) to study at the University Clermont Auvergne in Clermont-Ferrand, France. Vlasta Brezová is acknowledged for useful discussion on EPR spectra interpretation.

Reference

- [1] D.B. Miklos, C. Remy, M. Jekel, K.G. Linden, J.E. Drewes, U. Hübner, Evaluation of advanced oxidation processes for water and wastewater treatment – A critical review, *Water Research*. 139 (2018) 118–131. <https://doi.org/10.1016/j.watres.2018.03.042>.
- [2] Y. Deng, R. Zhao, Advanced Oxidation Processes (AOPs) in Wastewater Treatment, *Current Pollution Reports*. 1 (2015) 167–176. <https://doi.org/10.1007/s40726-015-0015-z>.
- [3] W. Dong, Y. Jin, K. Zhou, S.-P. Sun, Y. Li, X.D. Chen, Efficient degradation of pharmaceutical micropollutants in water and wastewater by Fe^{III}-NTA-catalyzed neutral photo-Fenton process, *Science of The Total Environment*. 688 (2019) 513–520. <https://doi.org/10.1016/j.scitotenv.2019.06.315>.
- [4] L. Sbardella, I. Velo Gala, J. Comas, S. Morera Carbonell, I. Rodríguez-Roda, W. Gernjak, Integrated assessment of sulfate-based AOPs for pharmaceutical active compound removal from wastewater, *Journal of Cleaner Production*. 260 (2020) 121014. <https://doi.org/10.1016/j.jclepro.2020.121014>.
- [5] A. Gabet, H. Métivier, C. de Brauer, G. Mailhot, M. Brigante, Hydrogen peroxide and persulfate activation using UVA-UVB radiation: Degradation of estrogenic compounds and application in sewage treatment plant waters, *Journal of Hazardous Materials*. 405 (2021) 124693. <https://doi.org/10.1016/j.jhazmat.2020.124693>.
- [6] Y. Jin, X. Wang, S.-P. Sun, W. Dong, Z. Wu, G. Bian, W.D. Wu, X.D. Chen, Hydroxyl and sulfate radicals formation in UVA/Fe^{III}-NTA/S₂O₈²⁻ system: Mechanism and effectiveness in carbamazepine degradation at initial neutral pH, *Chemical Engineering Journal*. 368 (2019) 541–552. <https://doi.org/10.1016/j.cej.2019.02.182>.
- [7] R. Yin, J. Sun, Y. Xiang, C. Shang, Recycling and reuse of rusted iron particles containing core-shell Fe-FeOOH for ibuprofen removal: Adsorption and persulfate-based advanced oxidation, *Journal of Cleaner Production*. 178 (2018) 441–448. <https://doi.org/10.1016/j.jclepro.2018.01.005>.
- [8] D. Jia, S.-P. Sun, Z. Wu, N. Wang, Y. Jin, W. Dong, X.D. Chen, Q. Ke, TCE degradation in groundwater by chelators-assisted Fenton-like reaction of magnetite: Sand columns

demonstration, *Journal of Hazardous Materials*. 346 (2018) 124–132. <https://doi.org/10.1016/j.jhazmat.2017.12.031>.

[9] Z. Pi, X. Li, D. Wang, Q. Xu, Z. Tao, X. Huang, F. Yao, Y. Wu, L. He, Q. Yang, Persulfate activation by oxidation biochar supported magnetite particles for tetracycline removal: Performance and degradation pathway, *Journal of Cleaner Production*. 235 (2019) 1103–1115. <https://doi.org/10.1016/j.jclepro.2019.07.037>.

[10] S. Zhong, H. Zhang, New insight into the reactivity of Mn(III) in bisulfite/permanganate for organic compounds oxidation: The catalytic role of bisulfite and oxygen, *Water Research*. 148 (2019) 198–207. <https://doi.org/10.1016/j.watres.2018.10.053>.

[11] M. Kamagate, M. Pasturel, M. Brigante, K. Hanna, Mineralization Enhancement of Pharmaceutical Contaminants by Radical-Based Oxidation Promoted by Oxide-Bound Metal Ions, *Environmental Science and Technology*. 54 (2020) 476–485. <https://doi.org/10.1021/acs.est.9b04542>.

[12] Z.-G. Zhou, H.-M. Du, Z. Dai, Y. Mu, L.-L. Tong, Q.-J. Xing, S.-S. Liu, Z. Ao, J.-P. Zou, Degradation of organic pollutants by peroxymonosulfate activated by MnO₂ with different crystalline structures: Catalytic performances and mechanisms, *Chemical Engineering Journal*. 374 (2019) 170–180. <https://doi.org/10.1016/j.cej.2019.05.170>.

[13] S. Zhu, X. Li, J. Kang, X. Duan, S. Wang, Persulfate Activation on Crystallographic Manganese Oxides: Mechanism of Singlet Oxygen Evolution for Nonradical Selective Degradation of Aqueous Contaminants, *Environmental Science and Technology*. 53 (2019) 307–315. <https://doi.org/10.1021/acs.est.8b04669>.

[14] J. Huang, Y. Dai, K. Singewald, C.-C. Liu, S. Saxena, H. Zhang, Effects of MnO₂ of different structures on activation of peroxymonosulfate for bisphenol A degradation under acidic conditions, *Chemical Engineering Journal*. 370 (2019) 906–915. <https://doi.org/10.1016/j.cej.2019.03.238>.

[15] J. Huang, S. Zhong, Y. Dai, C.-C. Liu, H. Zhang, Effect of MnO₂ Phase Structure on the Oxidative Reactivity toward Bisphenol A Degradation, *Environmental Science and Technology*. 52 (2018) 11309–11318. <https://doi.org/10.1021/acs.est.8b03383>.

- [16] X. Xu, Y. Zhang, S. Zhou, R. Huang, S. Huang, H. Kuang, X. Zeng, S. Zhao, Activation of persulfate by MnOOH: Degradation of organic compounds by nonradical mechanism, *Chemosphere*. 272 (2021) 129629. <https://doi.org/10.1016/j.chemosphere.2021.129629>.
- [17] F. Wang, M. Xiao, X. Ma, S. Wu, M. Ge, X. Yu, Insights into the transformations of Mn species for peroxymonosulfate activation by tuning the Mn₃O₄ shapes, *Chemical Engineering Journal*. 404 (2021) 127097. <https://doi.org/10.1016/j.cej.2020.127097>.
- [18] E. Saputra, S. Muhammad, H. Sun, H.-M. Ang, M.O. Tadé, S. Wang, Manganese oxides at different oxidation states for heterogeneous activation of peroxymonosulfate for phenol degradation in aqueous solutions, *Applied Catalysis B: Environmental*. 142–143 (2013) 729–735. <https://doi.org/10.1016/j.apcatb.2013.06.004>.
- [19] E. Saputra, S. Muhammad, H. Sun, H.-M. Ang, M.O. Tadé, S. Wang, Shape-controlled activation of peroxymonosulfate by single crystal α -Mn₂O₃ for catalytic phenol degradation in aqueous solution, *Applied Catalysis B: Environmental*. 154–155 (2014) 246–251. <https://doi.org/10.1016/j.apcatb.2014.02.026>.
- [20] A. Khan, K. Zhang, P. Sun, H. Pan, Y. Cheng, Y. Zhang, High performance of the α -Mn₂O₃ nanocatalyst for persulfate activation: Degradation process of organic contaminants via singlet oxygen, *Journal of Colloid and Interface Science*. 584 (2021) 885–899. <https://doi.org/10.1016/j.jcis.2020.10.021>.
- [21] Y. Li, L.-D. Liu, L. Liu, Y. Liu, H.-W. Zhang, X. Han, Efficient oxidation of phenol by persulfate using manganite as a catalyst, *Journal of Molecular Catalysis A: Chemical*. 411 (2016) 264–271. <https://doi.org/10.1016/j.molcata.2015.10.036>.
- [22] I.J. Buerge, T. Poiger, M.D. Müller, H.-R. Buser, Caffeine, an Anthropogenic Marker for Wastewater Contamination of Surface Waters, *Environmental Science and Technology*. 37 (2003) 691–700. <https://doi.org/10.1021/es020125z>.
- [23] S. Li, J. Wen, B. He, J. Wang, X. Hu, J. Liu, Occurrence of caffeine in the freshwater environment: Implications for ecopharmacovigilance, *Environmental Pollution*. 263 (2020) 114371. <https://doi.org/10.1016/j.envpol.2020.114371>.

- [24] G.V. Buxton, C.L. Greenstock, W.P. Helman, A.B. Ross, Critical Review of rate constants for reactions of hydrated electrons, hydrogen atoms and hydroxyl radicals ($\cdot\text{OH}/\cdot\text{O}^-$ in Aqueous Solution, *Journal of Physical and Chemical Reference Data*. 17 (1988) 513–886. <https://doi.org/10.1063/1.555805>.
- [25] C.L. Clifton, R.E. Huie, Rate constants for hydrogen abstraction reactions of the sulfate radical, SO_4^- . Alcohols, *International Journal of Chemical Kinetics*. 21 (1989) 677–687. <https://doi.org/10.1002/kin.550210807>.
- [26] E. Appiani, R. Ossola, D.E. Latch, P.R. Erickson, K. McNeill, Aqueous singlet oxygen reaction kinetics of furfuryl alcohol: effect of temperature, pH, and salt content, *Environmental Science: Processes and Impacts*. 19 (2017) 507–516. <https://doi.org/10.1039/C6EM00646A>.
- [27] S. Waclawek, K. Grübel, M. Černík, Simple spectrophotometric determination of monopersulfate, *Spectrochimica Acta Part A: Molecular and Biomolecular Spectroscopy*. 149 (2015) 928–933. <https://doi.org/10.1016/j.saa.2015.05.029>.
- [28] S. Stoll, A. Schweiger, EasySpin, a comprehensive software package for spectral simulation and analysis in EPR, *Journal of Magnetic Resonance*. 178 (2006) 42–55. <https://doi.org/10.1016/j.jmr.2005.08.013>.
- [29] Y. Yang, G. Banerjee, G.W. Brudvig, J.-H. Kim, J.J. Pignatello, Oxidation of Organic Compounds in Water by Unactivated Peroxymonosulfate, *Environmental Science and Technology*. 52 (2018) 5911–5919. <https://doi.org/10.1021/acs.est.8b00735>.
- [30] C. Guan, J. Jiang, S. Pang, C. Luo, J. Ma, Y. Zhou, Y. Yang, Oxidation Kinetics of Bromophenols by Nonradical Activation of Peroxydisulfate in the Presence of Carbon Nanotube and Formation of Brominated Polymeric Products, *Environmental Science and Technology*. 51 (2017) 10718–10728. <https://doi.org/10.1021/acs.est.7b02271>.
- [31] Y. Ding, X. Wang, L. Fu, X. Peng, C. Pan, Q. Mao, C. Wang, J. Yan, Nonradicals induced degradation of organic pollutants by peroxydisulfate (PDS) and peroxymonosulfate (PMS): Recent advances and perspective, *Science of The Total Environment*. (2020) 142794. <https://doi.org/10.1016/j.scitotenv.2020.142794>.

- [32] H. Lee, H.-J. Lee, J. Jeong, J. Lee, N.-B. Park, C. Lee, Activation of persulfates by carbon nanotubes: Oxidation of organic compounds by nonradical mechanism, *Chemical Engineering Journal*. 266 (2015) 28–33. <https://doi.org/10.1016/j.cej.2014.12.065>.
- [33] W. Yang, Y. Peng, Y. Wang, Y. Wang, H. Liu, Z. Su, W. Yang, J. Chen, W. Si, J. Li, Controllable redox-induced in-situ growth of MnO₂ over Mn₂O₃ for toluene oxidation: Active heterostructure interfaces, *Applied Catalysis B: Environmental*. 278 (2020) 119279. <https://doi.org/10.1016/j.apcatb.2020.119279>.
- [34] D. He, Y. Li, C. Lyu, L. Song, W. Feng, S. Zhang, New insights into MnOOH/peroxymonosulfate system for catalytic oxidation of 2,4-dichlorophenol: Morphology dependence and mechanisms, *Chemosphere*. 255 (2020) 126961. <https://doi.org/10.1016/j.chemosphere.2020.126961>.
- [35] A.N. Yermakov, B.M. Zhitomirsky, G.A. Poskrebyshv, D.M. Sozurakov, The branching ratio of peroxomonosulfate radicals (SO₅⁻) self-reaction aqueous solution, *The Journal of Physical Chemistry*. 97 (1993) 10712–10714. <https://doi.org/10.1021/j100143a031>.
- [36] E. Hayon, A. Treinin, J. Wilf, Electronic spectra, photochemistry, and autoxidation mechanism of the sulfite-bisulfite-pyrosulfite systems. SO₂⁻, SO₃⁻, SO₄⁻, and SO₅⁻ radicals, *Journal of the American Chemical Society*. 94 (1972) 47–57. <https://doi.org/10.1021/ja00756a009>.
- [37] J.M. Fontmorin, R.C. Burgos Castillo, W.Z. Tang, M. Sillanpää, Stability of 5,5-dimethyl-1-pyrroline-N-oxide as a spin-trap for quantification of hydroxyl radicals in processes based on Fenton reaction, *Water Research*. 99 (2016) 24–32. <https://doi.org/10.1016/j.watres.2016.04.053>.
- [38] G.R. Buettner, Spin Trapping: ESR parameters of spin adducts 1474 1528V, *Free Radical Biology and Medicine*. 3 (1987) 259–303. [https://doi.org/10.1016/S0891-5849\(87\)80033-3](https://doi.org/10.1016/S0891-5849(87)80033-3).
- [39] X. Yang, X. Wang, Y. Li, Z. Wu, W.D. Wu, X.D. Chen, J. Sun, S.-P. Sun, Z. Wang, A Bimetallic Fe–Mn Oxide-Activated Oxone for In Situ Chemical Oxidation (ISCO) of Trichloroethylene in Groundwater: Efficiency, Sustained Activity, and Mechanism

Investigation, *Environmental Science & Technology*. 54 (2020) 3714–3724. <https://doi.org/10.1021/acs.est.0c00151>.

[40] Z. Dong, Q. Zhang, B.-Y. Chen, J. Hong, Oxidation of bisphenol A by persulfate via Fe₃O₄- α -MnO₂ nanoflower-like catalyst: Mechanism and efficiency, *Chemical Engineering Journal*. 357 (2019) 337–347. <https://doi.org/10.1016/j.cej.2018.09.179>.

[41] G.P. Anipsitakis, D.D. Dionysiou, Radical Generation by the Interaction of Transition Metals with Common Oxidants, *Environmental Science & Technology*. 38 (2004) 3705–3712. <https://doi.org/10.1021/es035121o>.

[42] H. Lin, S. Li, B. Deng, W. Tan, R. Li, Y. Xu, H. Zhang, Degradation of bisphenol A by activating peroxymonosulfate with Mn_{0.6}Zn_{0.4}Fe₂O₄ fabricated from spent Zn-Mn alkaline batteries, *Chemical Engineering Journal*. 364 (2019) 541–551. <https://doi.org/10.1016/j.cej.2019.01.189>.

[43] H. Lin, J. Wu, H. Zhang, Degradation of clofibric acid in aqueous solution by an EC/Fe³⁺/PMS process, *Chemical Engineering Journal*. 244 (2014) 514–521. <https://doi.org/10.1016/j.cej.2014.01.099>.

[44] J.S. Salla, N. Padoin, S.M. Amorim, G. Li Puma, R.F.P.M. Moreira, Humic acids adsorption and decomposition on Mn₂O₃ and α -Al₂O₃ nanoparticles in aqueous suspensions in the presence of ozone, *Journal of Environmental Chemical Engineering*. 8 (2020) 102780. <https://doi.org/10.1016/j.jece.2018.11.025>.

[45] Y.-H. Huang, Y.-F. Huang, C. Huang, C.-Y. Chen, Efficient decolorization of azo dye Reactive Black B involving aromatic fragment degradation in buffered Co²⁺/PMS oxidative processes with a ppb level dosage of Co²⁺-catalyst, *Journal of Hazardous Materials*. 170 (2009) 1110–1118. <https://doi.org/10.1016/j.jhazmat.2009.05.091>.

[46] F. Qi, W. Chu, B. Xu, Catalytic degradation of caffeine in aqueous solutions by cobalt-MCM41 activation of peroxymonosulfate, *Applied Catalysis B: Environmental*. 134–135 (2013) 324–332. <https://doi.org/10.1016/j.apcatb.2013.01.038>.

- [47] K.-Y.A. Lin, B.-C. Chen, Efficient elimination of caffeine from water using Oxone activated by a magnetic and recyclable cobalt/carbon nanocomposite derived from ZIF-67, *Dalton Transactions*. 45 (2016) 3541–3551. <https://doi.org/10.1039/C5DT04277A>.
- [48] R. Rosal, A. Rodríguez, J.A. Perdígón-Melón, A. Petre, E. García-Calvo, M.J. Gómez, A. Agüera, A.R. Fernández-Alba, Degradation of caffeine and identification of the transformation products generated by ozonation, *Chemosphere*. 74 (2009) 825–831. <https://doi.org/10.1016/j.chemosphere.2008.10.010>.
- [49] J. Wang, Y. Sun, H. Jiang, J. Feng, Removal of caffeine from water by combining dielectric barrier discharge (DBD) plasma with goethite, *Journal of Saudi Chemical Society*. 21 (2017) 545–557. <https://doi.org/10.1016/j.jscs.2016.08.002>.
- [50] T. Zhang, Y. Chen, Y. Wang, J. Le Roux, Y. Yang, J.-P. Croué, Efficient Peroxydisulfate Activation Process Not Relying on Sulfate Radical Generation for Water Pollutant Degradation, *Environmental Science and Technology*. 48 (2014) 5868–5875. <https://doi.org/10.1021/es501218f>.

Supplementary Materials

Text S1. Chemicals. The reagents used in this study are as follows: Hydrogen peroxide (H_2O_2 , 30% in water), sodium persulfate (PS, $\text{Na}_2\text{S}_2\text{O}_8$, 99%), sodium bisulfite (NaHSO_3), manganese (II) chloride (MnCl_2 , 99%), potassium peroxymonosulfate (PMS) used in the form of OXONE[®] ($\text{KHSO}_5 \cdot 0.5\text{KHSO}_4 \cdot 0.5\text{K}_2\text{SO}_4$), phosphoric acid (H_3PO_4 , 88%), caffeine (CAF), sodium hydroxide (NaOH , 99%), perchloric acid (HClO_4 , 72%), 2-Propanol (99%) and furfuryl alcohol were purchased from Sigma-Aldrich Company, France. Acetonitrile solvent (HPLC grade) was obtained from the CARLO-ERBA-Reagents company. *tert*-butanol (99%) was purchased from Acros Organics.

Text S2. Catalyst characterization. The purity of the used Mn_2O_3 sample was confirmed by XRD. The XRD data were recorded with the monochromatized $\text{CuK}\alpha$ radiation on a Bruker AXS D8 Advance diffractometer (θ - 2θ Bragg-Brentano geometry) over the range of 10° - 100° 2θ at a step size of 0.02° . The average oxidation state (AOS) of Mn after the reaction was obtained using XPS (hemispherical electron energy analyzer OMICRON EA125, Germany). The data analysis, curve fitting, and quantification of the Mn XPS spectra were performed using XPSPEAK 4.1 software. The C 1s signal at 284.8 eV was taken as a reference for binding energy calibration.

Text S3. To evaluate the contribution of each radical to the CAF degradation, the radical involvement (RI) was determined as follows:

$$\text{RI (\%)} = \frac{P_{\text{scavenger}} - P_{\text{no scavenger}}}{1 - P_{\text{no scavenger}}} \times 100 \quad \text{S1}$$

Where $P_{\text{scavenger}}$ and $P_{\text{no scavenger}}$ are the percentage of CAF degradation with and without scavengers.

Table S1 Second-order rate constants (k'') of scavengers and CAF with different radical species.

Chemicals	$k''_{HO\cdot}$ ($M^{-1} s^{-1}$)	$k''_{SO_4^{\cdot-}}$ ($M^{-1} s^{-1}$)	$k''_{^1O_2}$ ($M^{-1} s^{-1}$)	Reference
<i>tert</i> -Butanol	6.0×10^8	8.4×10^5	NA	[1,2]
2-Propanol	1.9×10^9	8.2×10^7	NA	[1,2]
Furfuryl alcohol	1.5×10^{10}	NA	1.2×10^8	[3,4]
Caffeine	6.4×10^9	2.39×10^9	2.9×10^7	[5,6]

NA: not available.

Table S2 Physico-chemical properties of the sewage treatment plant water (STPW)

Parameter	Values
pH	8.5
TOC*	0.68 mM
IC*	2.53 mM
Cl ⁻	0.77 mM
NO ₃ ⁻	0.41 mM
SO ₄ ²⁻	0.29 mM
PO ₄ ³⁻	0.09 mM

*TOC: Total organic carbon; *IC: inorganic carbon.

Table S3 The initial (pH_{0h}) and final (pH_{3h}) pH values of different processes.

Reaction systems	pH_{0h}	pH_{3h}
Mn ₂ O ₃ + CAF	7.1	7.0
Mn ₂ O ₃ + H ₂ O ₂ + CAF	7.8	7.5
Mn ₂ O ₃ + HSO ₃ ⁻ + CAF	3.5	2.2
Mn ₂ O ₃ + PS + CAF	5.7	5.3
Mn ₂ O ₃ + PMS + CAF	2.7	2.6

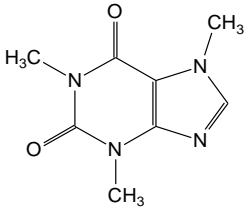
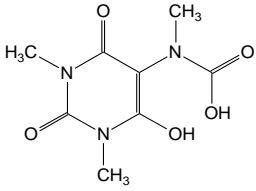
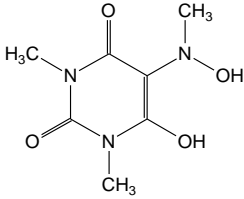
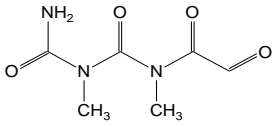
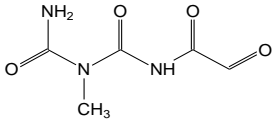
Table S4 Scavenging ratios between CAF and scavengers with ROS^a.

ROS	$C_1k_1 / (C_1k_1 + C_2k_2)$	% of radical reacting with scavenger
HO [•]	$[TBA]^c \times k_{HO^{\bullet},TBA} / ([TBA]^c \times k_{HO^{\bullet},TBA} + [CAF]^b \times k_{HO^{\bullet},CAF})$	97.4
SO ₄ ^{•-}	$[2-Pr]^d \times k_{SO_4^{\bullet-},2-Pr} / ([2-Pr]^d \times k_{SO_4^{\bullet-},2-Pr} + [CAF]^b \times k_{SO_4^{\bullet-},CAF})$	93.2
¹ O ₂	$[FFA]^e \times k_{^1O_2,FFA} / ([FFA]^e \times k_{^1O_2,FFA} + [CAF]^b \times k_{^1O_2,CAF})$	99.4

^aROS: Reactive Oxygen Species; 1 for scavengers and 2 for CAF;

^b[CAF]₀ = 25 μM; ^c[TBA]₀ = ^d[2-Pr]₀ = 10 mM; ^e[FFA]₀ = 1 mM;

Table S5 Degradation intermediates of CAF in Mn₂O₃-activated PS and PMS systems.

Compound	Molecular formula	Structure	R _T (min)	ESI (+)	ESI (-)	Mn ₂ O ₃ + PS	Mn ₂ O ₃ + PMS
CAF	C ₈ H ₁₀ N ₄ O ₂		2.19	195.0877		✓	✓
P1	C ₈ H ₁₁ N ₃ O ₅		4.53		228.1956	✓	✓
P2	C ₇ H ₁₁ N ₃ O ₄		3.02	202.1438 184.1333	200.1284	✓	
P3	C ₆ H ₉ N ₃ O ₄		2.54	188.1281 170.1176	186.1124	✓	✓
P4	C ₅ H ₇ N ₃ O ₄		2.0	174.1124 156.1019 128.1071	172.0969	✓	

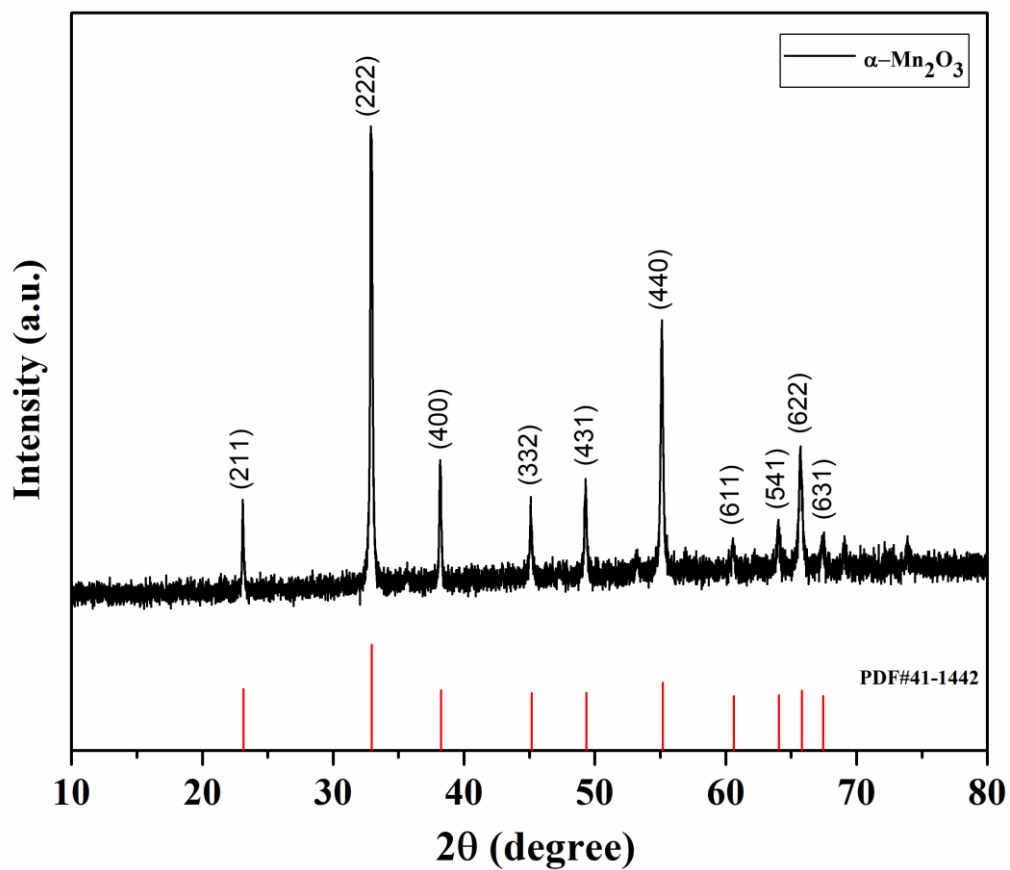


Figure S1. Powder XRD pattern of Mn_2O_3 used in the present study.

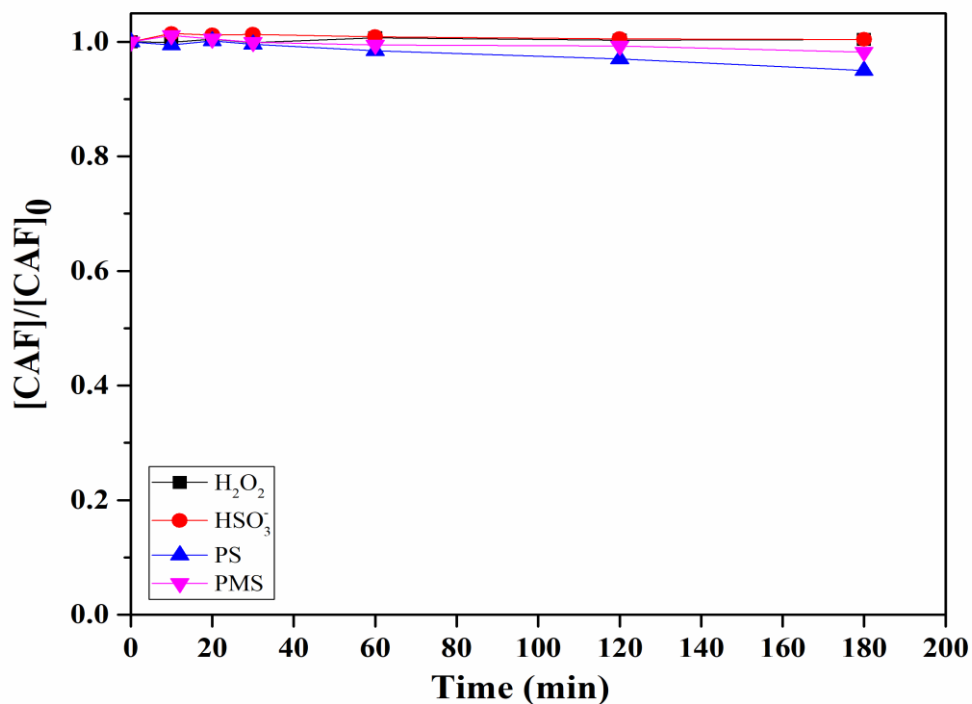


Figure S2. The changes in the relative concentration of CAF were monitored in the presence of 5 mM of H₂O₂, HSO₃⁻, PS, and PMS with the natural pH of 6.8, 4.0, 5.6, 2.7, respectively.

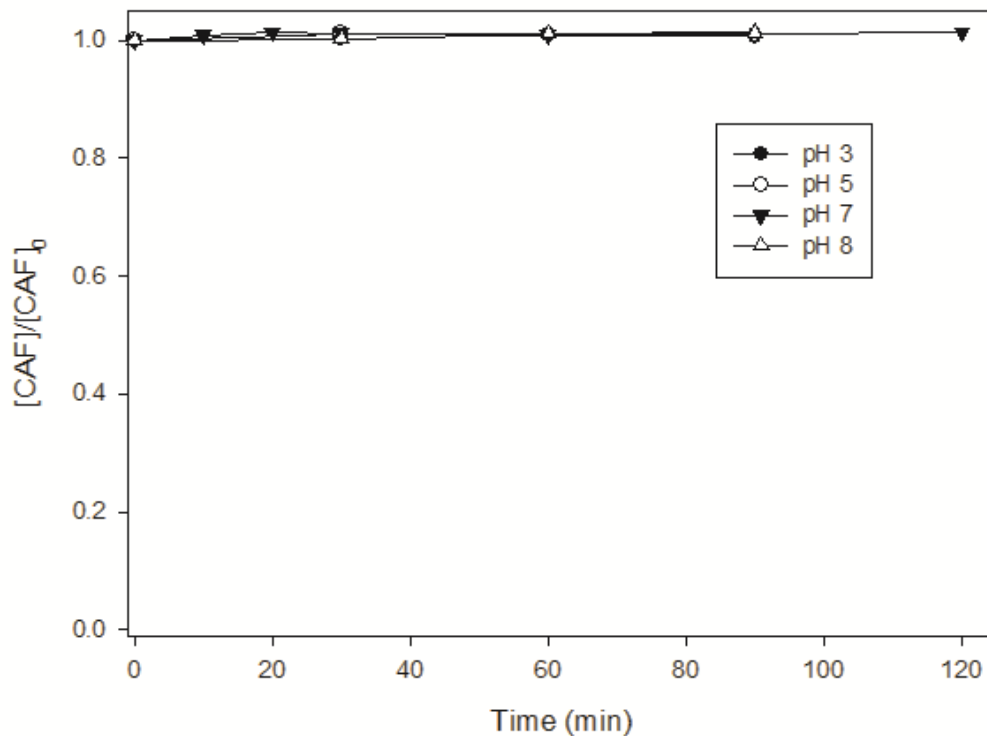


Figure S3. The changes in the relative concentration of CAF were monitored in the presence of Mn₂O₃ (0.4 g L⁻¹) under different initial pH values.

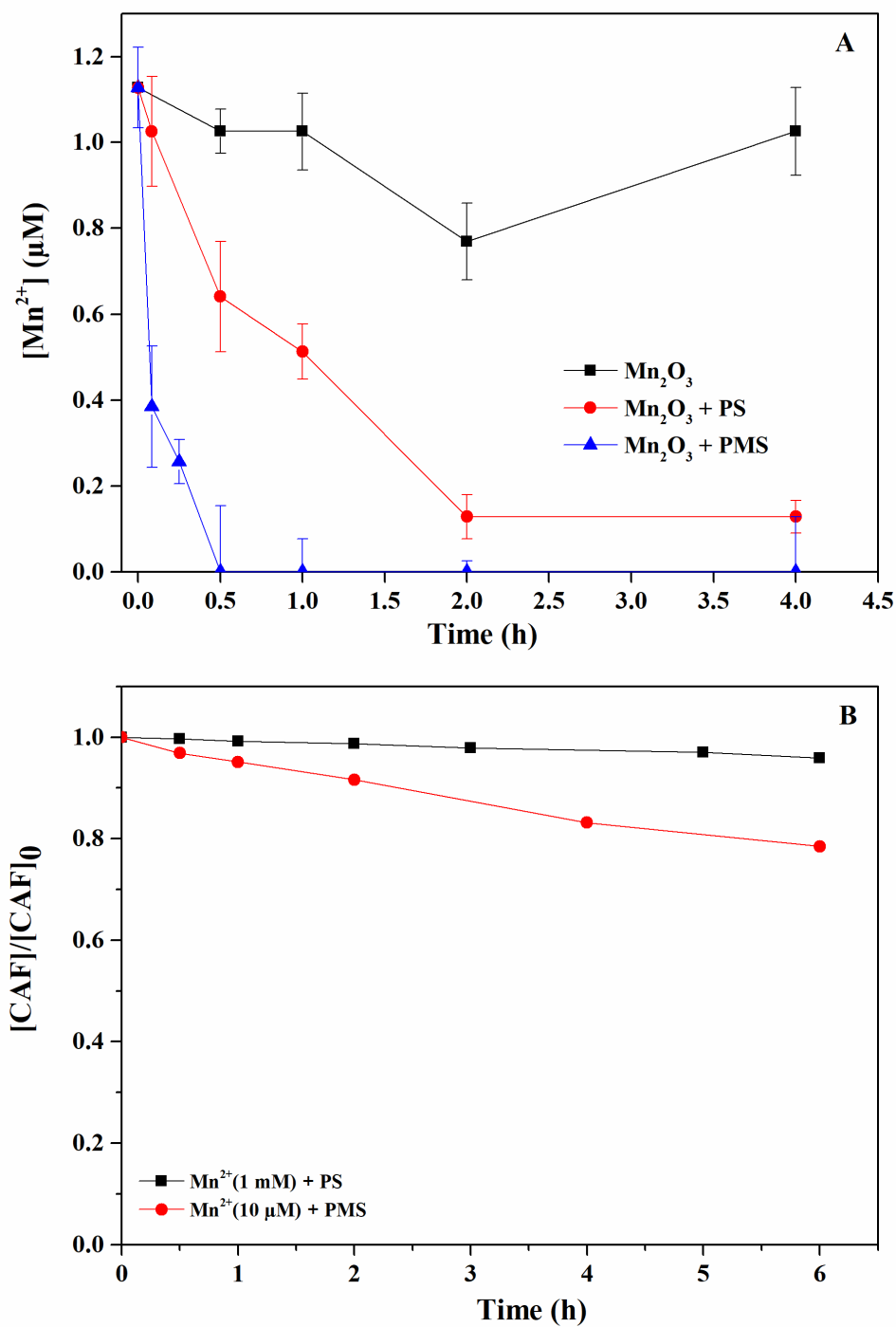


Figure S4. The leaching of Mn²⁺ in Mn₂O₃ (0.4 g L⁻¹) activated PS/PMS (5 mM) reactions (A) and the homogeneous activation of PS/PMS by Mn²⁺ (B). The pH of the solution was 5.0 and T = 25 ± 2 °C.

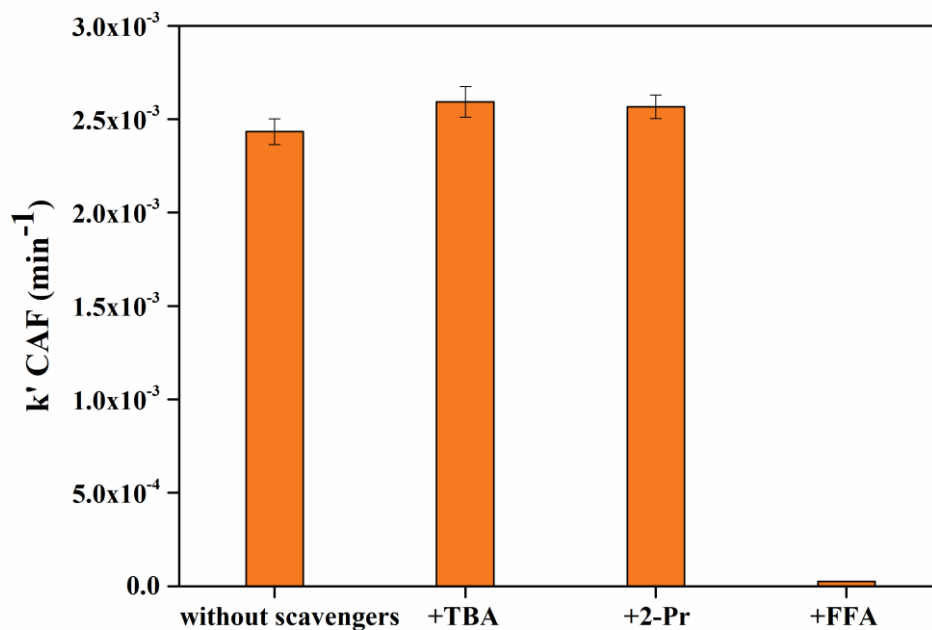


Figure S5. Kinetic values of CAF degradation by Mn_2O_3 with PS in the presence of different scavengers. Experimental conditions: $[\text{TBA}]_0 = [\text{2-Pr}]_0 = 10 \text{ mM}$, $[\text{FFA}]_0 = 1 \text{ mM}$, $[\text{Mn}_2\text{O}_3]_0 = 0.4 \text{ g L}^{-1}$, $[\text{CAF}]_0 = 25 \text{ }\mu\text{M}$, $[\text{PS}]_0 = 5 \text{ mM}$, The pH of solution was 5.0 and $T = 25 \pm 2 \text{ }^\circ\text{C}$.

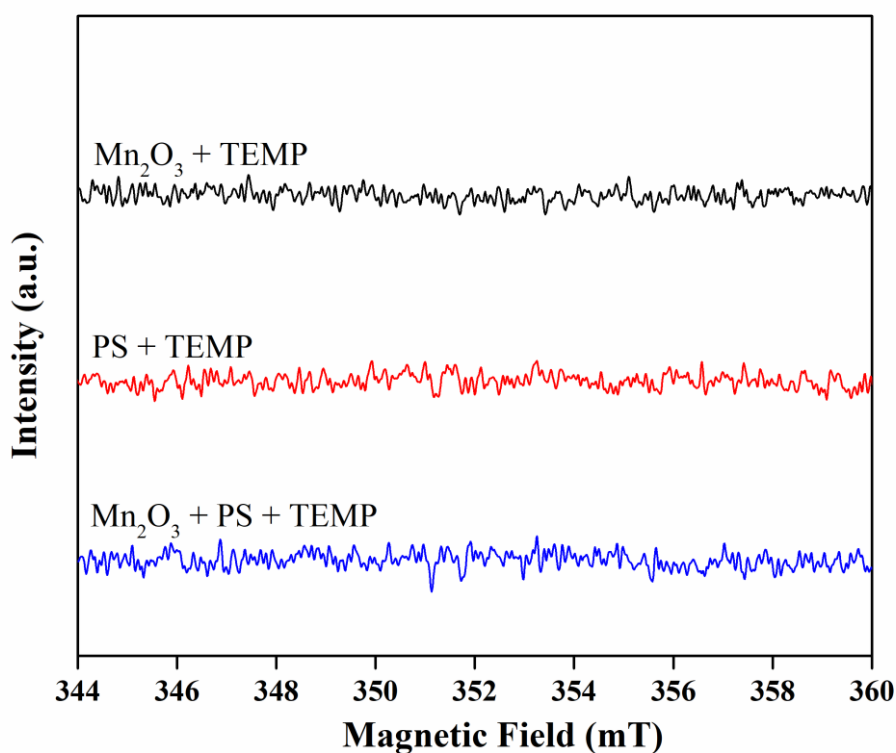


Figure S6. ERP spectra of different systems in the presence of TEMP. Experimental conditions: $[\text{Mn}_2\text{O}_3]_0 = 0.4 \text{ g L}^{-1}$, $[\text{PS}]_0 = 5 \text{ mM}$, $[\text{TEMP}]_0 = 25 \text{ mM}$.

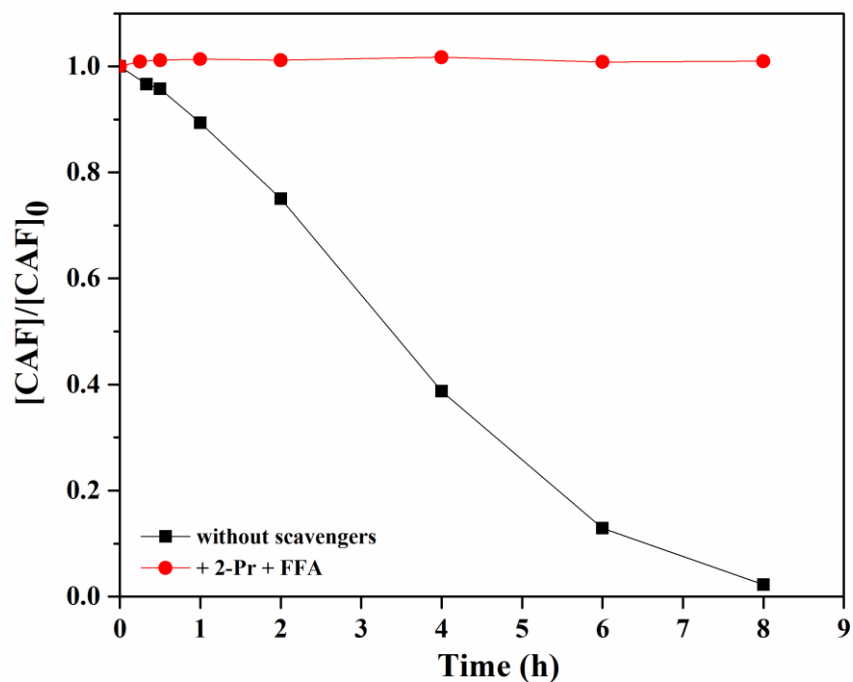


Figure S7. CAF degradation in the process of Mn_2O_3/PS with the addition of 2-Pr and FFA simultaneously. Experimental conditions: $[2-Pr]_0 = 10$ mM, $[FFA]_0 = 1$ mM, $[Mn_2O_3]_0 = 0.4$ g L^{-1} , $[CAF]_0 = 25$ μ M, $[PS]_0 = 5$ mM, The pH of solution was 5.0 and $T = 25 \pm 2$ $^{\circ}C$.

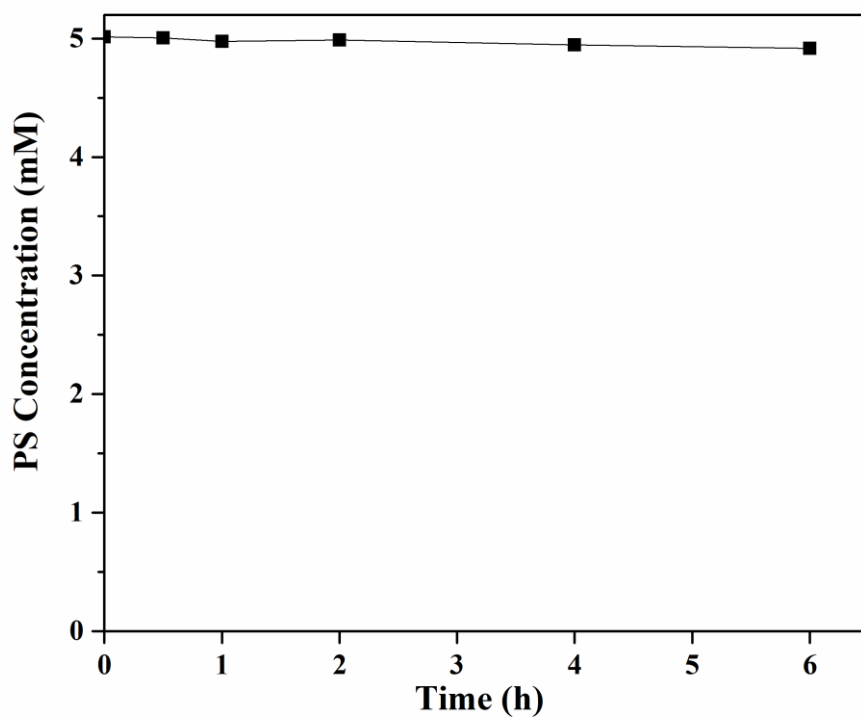


Figure S8. PS (5 mM) decomposition in the presence of 1 mM of FFA at solution pH 5.0.

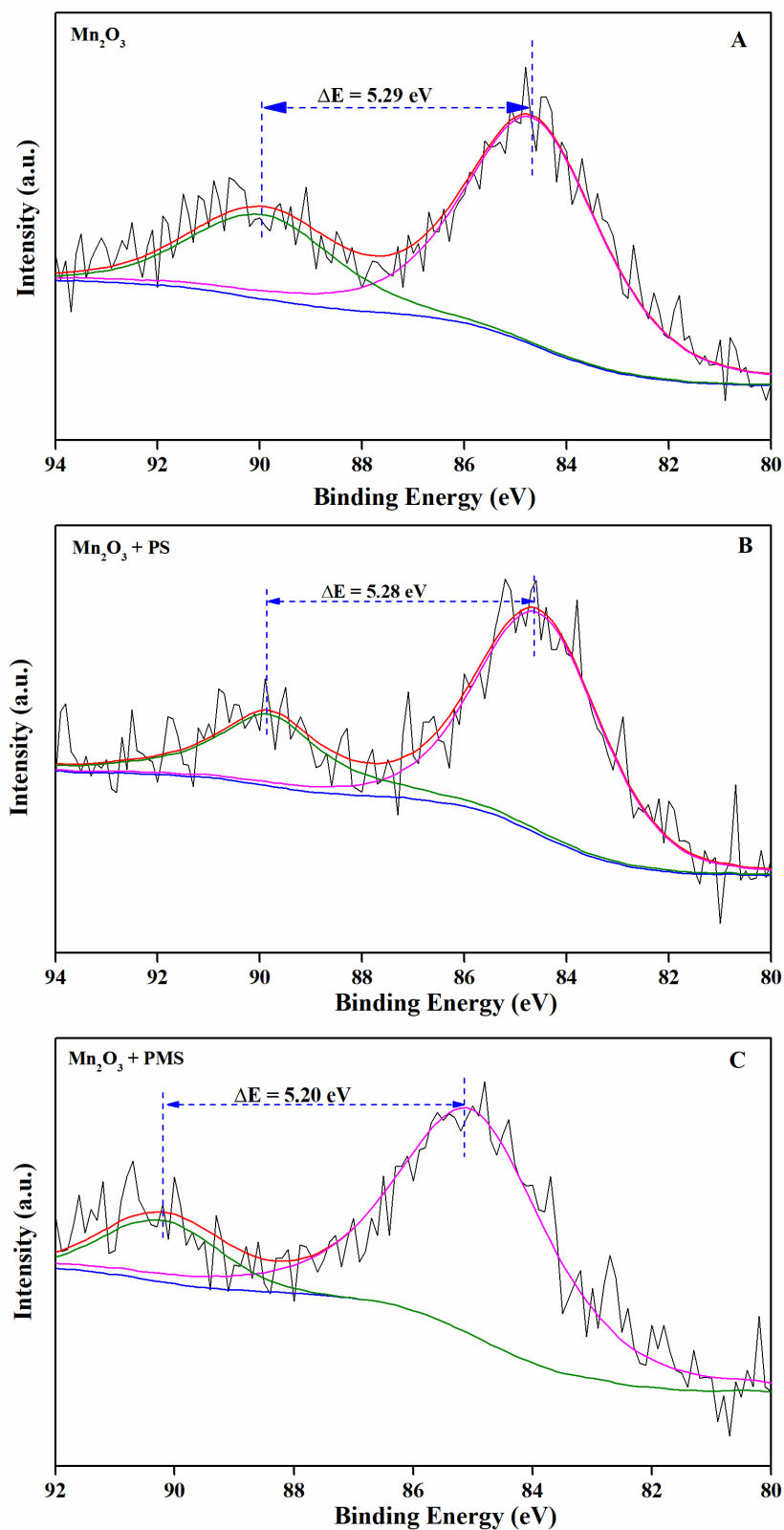


Figure S9. Fitting of XPS Mn 3s spectra of samples. (A) Mn_2O_3 ; (B) Mn_2O_3 with PS; (C) Mn_2O_3 with PMS. Experimental conditions: $[\text{Mn}_2\text{O}_3]_0 = 0.4 \text{ g L}^{-1}$, $[\text{PS}]_0 = [\text{PMS}]_0 = 5 \text{ mM}$, $\text{pH}_0 = 5$.

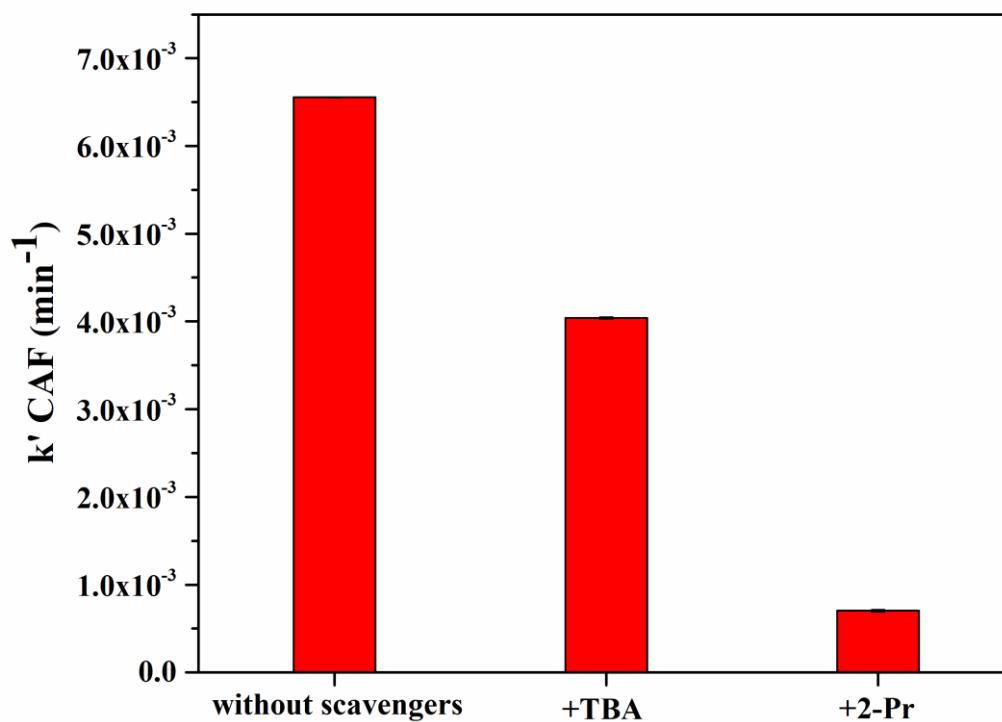


Figure S10. Kinetic values of CAF degradation by Mn_2O_3 with PMS in the presence of various scavengers. Experimental conditions: $[\text{TBA}]_0 = [\text{2-Pr}]_0 = 10 \text{ mM}$, $[\text{Mn}_2\text{O}_3]_0 = 0.4 \text{ g L}^{-1}$, $[\text{CAF}]_0 = 25 \text{ }\mu\text{M}$, $[\text{PMS}]_0 = 5 \text{ mM}$, The pH of solution was 5.0 and $T = 25 \pm 2 \text{ }^\circ\text{C}$.

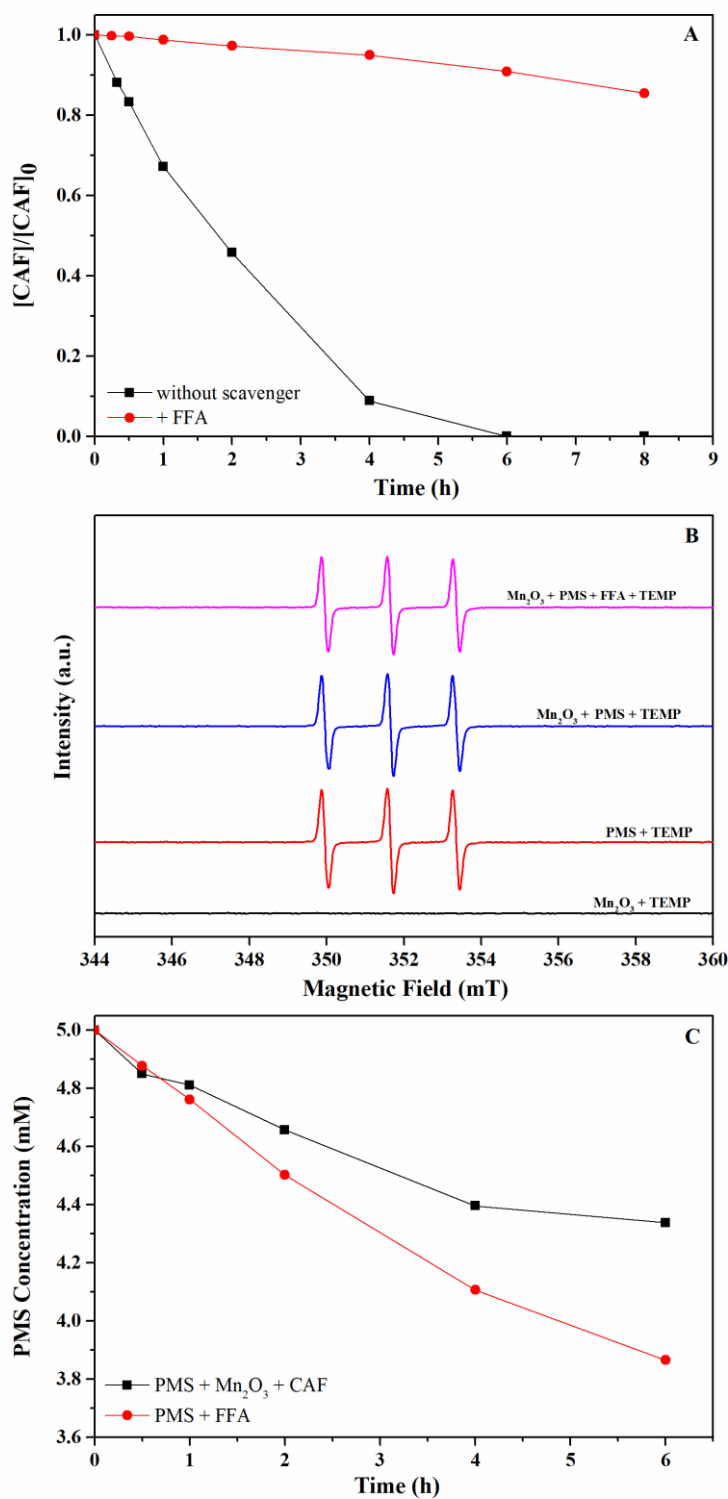


Figure S11. (A) the effect of FFA (1mM) on CAF degradation in Mn₂O₃/PMS system. (B) EPR signals of different systems in the presence of TEMP (25 mM). (C) PMS decomposition in the process of Mn₂O₃/PMS. Experimental conditions: $[Mn_2O_3]_0 = 0.4 \text{ g L}^{-1}$, $[CAF]_0 = 25 \text{ }\mu\text{M}$, $[PMS]_0 = 5 \text{ mM}$, The pH of solution was 5.0 and $T = 25 \pm 2 \text{ }^\circ\text{C}$.

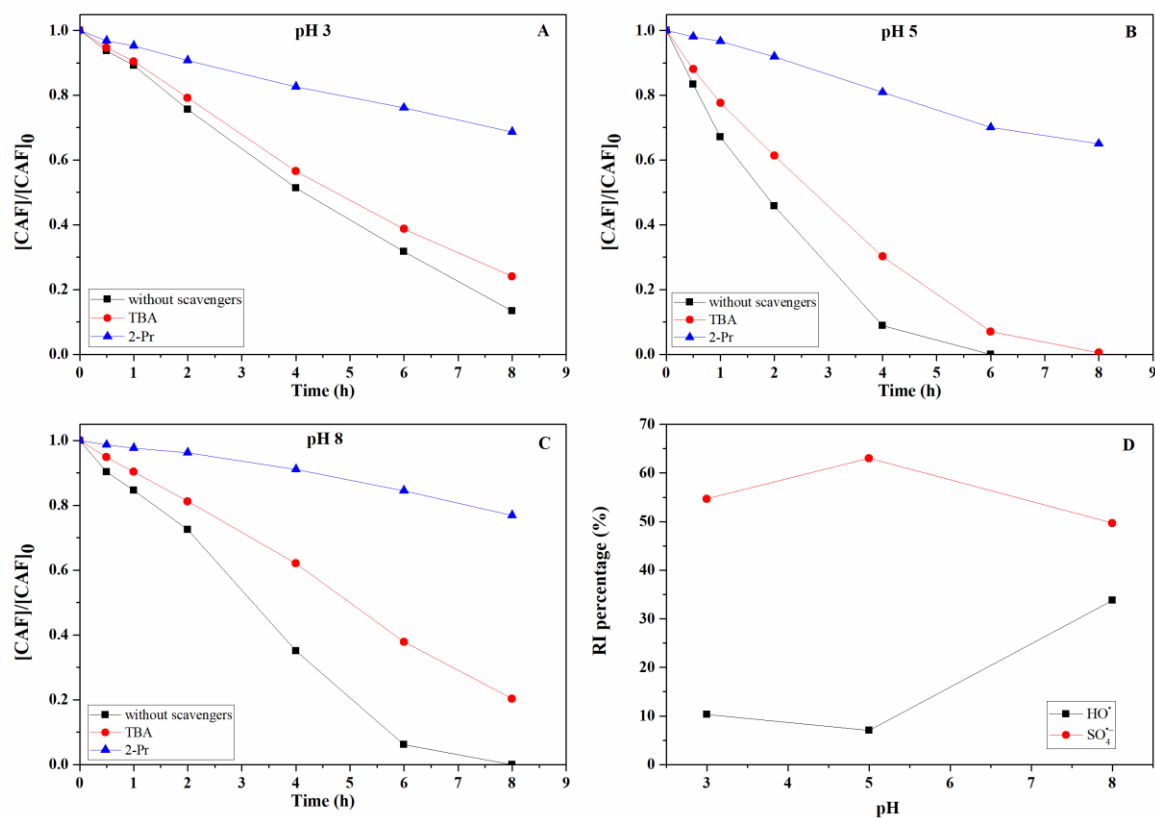


Figure S12. The changes of the RI percentages of HO^\bullet and $\text{SO}_4^{\bullet-}$ radicals in Mn_2O_3 (0.4 g L^{-1}) /PMS (5 mM) process under different initial pH values.

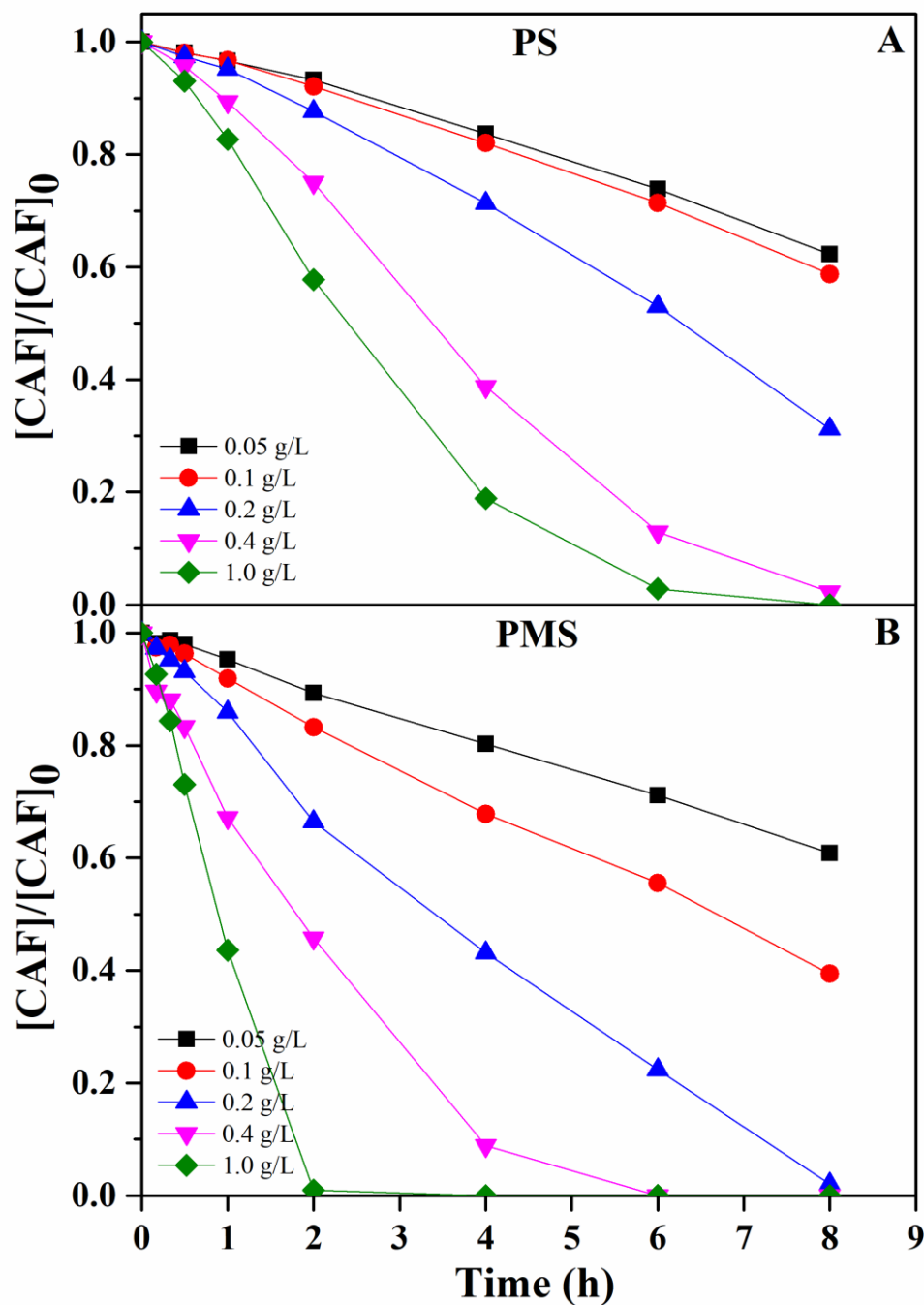


Figure S13. Effect of Mn_2O_3 loading on CAF degradation in the presence of 5 mM PS (A) and PMS (B). Experimental conditions: $[Mn_2O_3] = 0.05 - 1.0 \text{ g L}^{-1}$, $[CAF]_0 = 25 \mu\text{M}$, $[PS]_0 = [PMS]_0 = 5 \text{ mM}$, initial pH = 5.0, $T = 25 \pm 2 \text{ }^\circ\text{C}$.

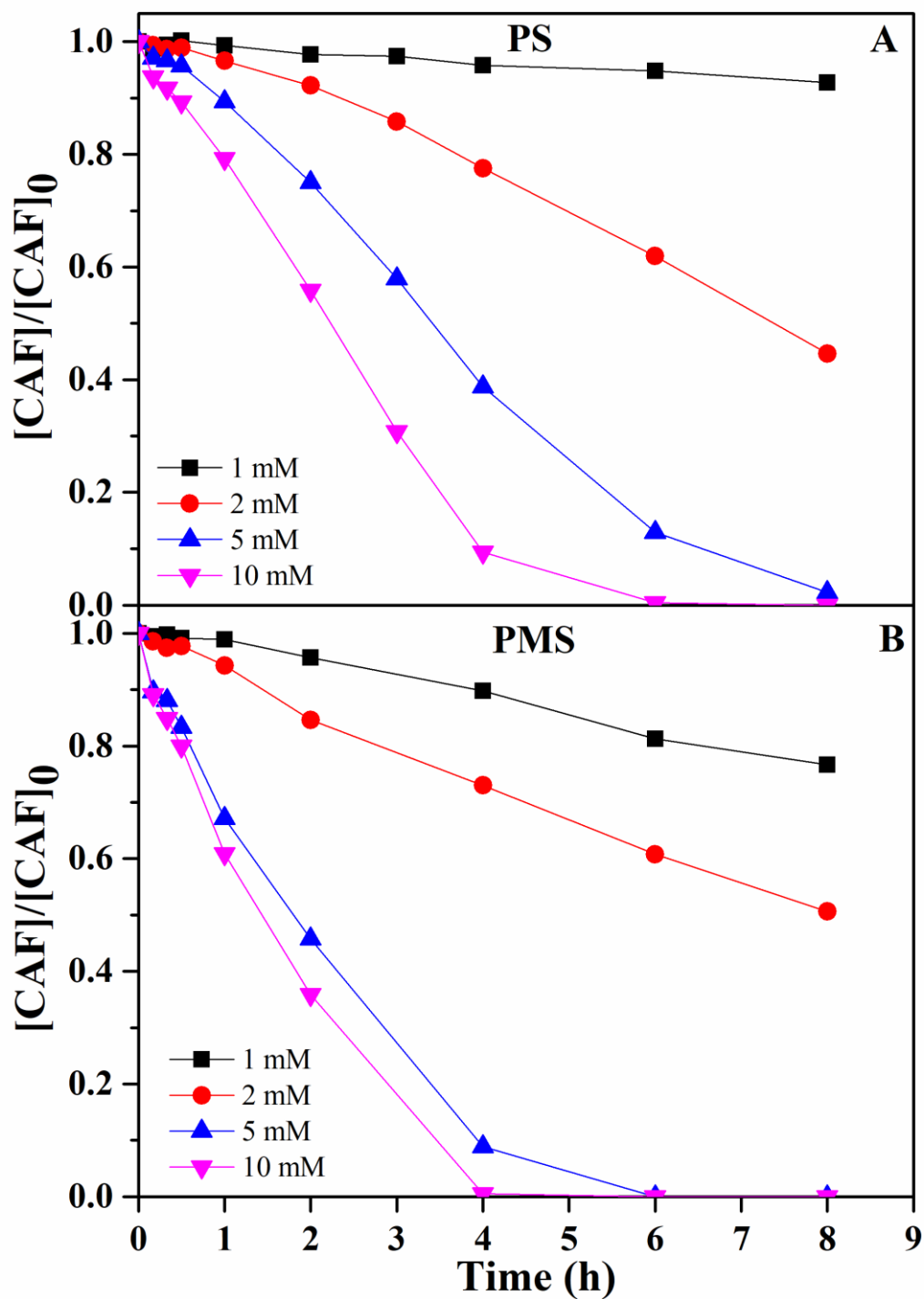


Figure S14. Effect of radical precursor concentrations on CAF degradation by Mn_2O_3 with PS (A) and Oxone (B). Experimental conditions: $[Mn_2O_3] = 0.4 \text{ g L}^{-1}$, $[CAF]_0 = 25 \text{ }\mu\text{M}$, $[PS]_0 = [PMS]_0 = 1 - 10 \text{ mM}$, initial pH = 5.0, $T = 25 \pm 2 \text{ }^\circ\text{C}$.

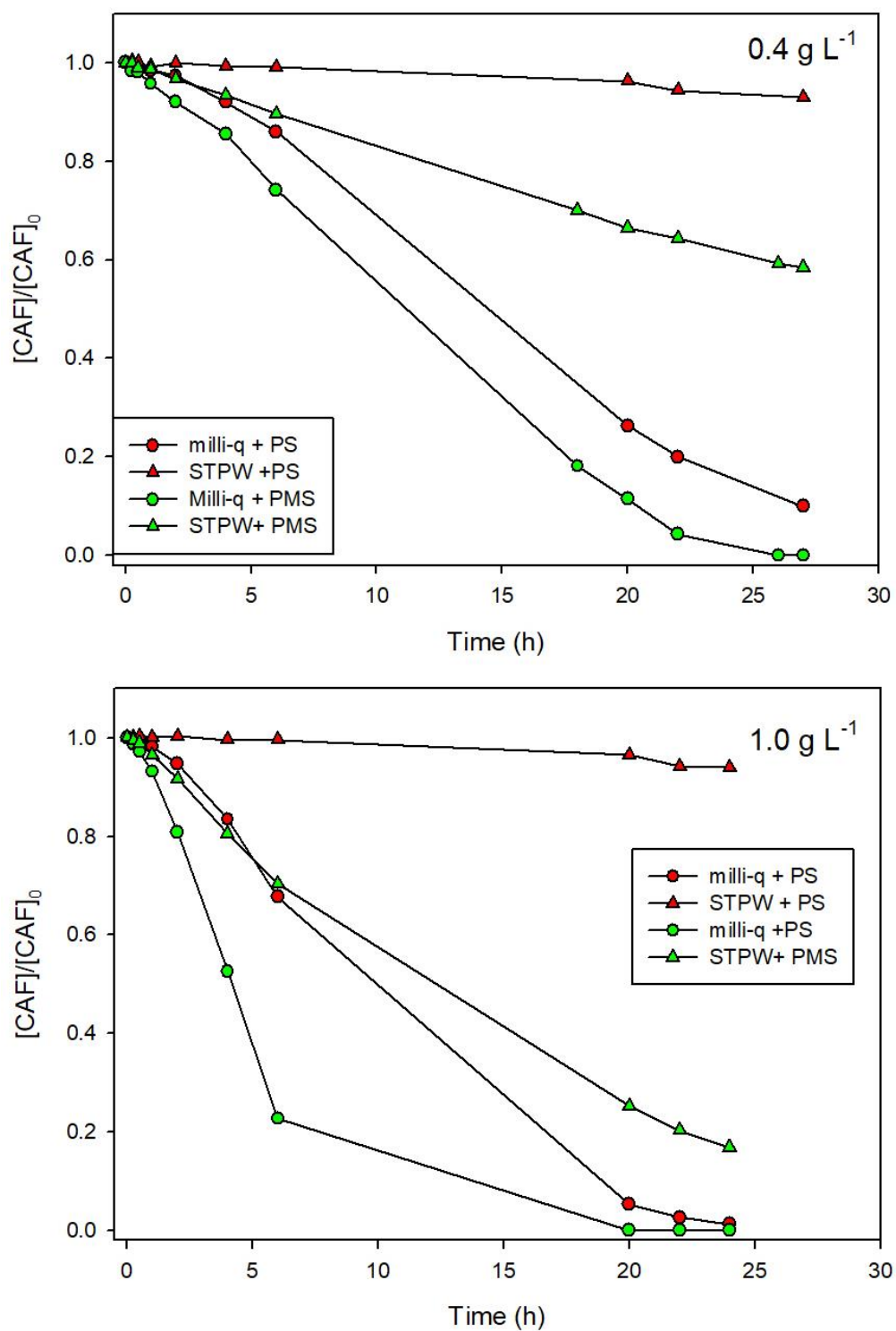


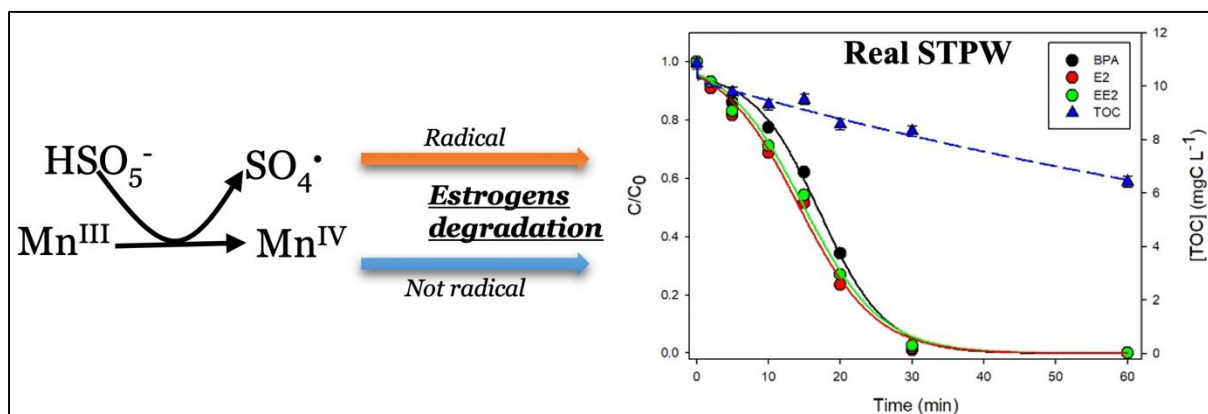
Figure S15. Degradation of CAF in milli-q (circles) and STP (triangles) waters using 5 mM of PS (red) and PMS (green) in the presence of Mn_2O_3 at 0.4 and 1.0 g L^{-1} . pH of solution was set to 8.0 ± 0.2 .

Reference

- [1] Buxton, G.V., Greenstock, C.L., Helman, W.P., Ross, A.B., 1988. Critical Review of rate constants for reactions of hydrated electrons, hydrogen atoms and hydroxyl radicals ($\cdot\text{OH}/\cdot\text{O}-$) in Aqueous Solution. *Journal of Physical and Chemical Reference Data*. 17, 513–886. <https://doi.org/10.1063/1.555805>
- [2] Clifton, C.L., Huie, R.E., 1989. Rate constants for hydrogen abstraction reactions of the sulfate radical, SO_4^- . Alcohols. *International Journal of Chemical Kinetics*. 21, 677–687. <https://doi.org/10.1002/kin.550210807>
- [3] Appiani, E., Ossola, R., Latch, D.E., Erickson, P.R., McNeill, K., 2017. Aqueous singlet oxygen reaction kinetics of furfuryl alcohol: effect of temperature, pH, and salt content. *Environmental Science: Processes & Impacts* 19, 507–516. <https://doi.org/10.1039/C6EM00646A>
- [4] Yang, Y., Banerjee, G., Brudvig, G.W., Kim, J.-H., Pignatello, J.J., 2018. Oxidation of Organic Compounds in Water by Unactivated Peroxymonosulfate. *Environmental Science and Technology*. 52, 5911–5919. <https://doi.org/10.1021/acs.est.8b00735>
- [5] Devasagayam, T.P., Kamat, J.P., Mohan, H., Kesavan, P.C., 1996. Caffeine as an antioxidant: inhibition of lipid peroxidation induced by reactive oxygen species. *Biochimica et Biophysica Acta*. 1282, 63–70. [https://doi.org/10.1016/0005-2736\(96\)00040-5](https://doi.org/10.1016/0005-2736(96)00040-5)
- [6] Nihemaiti, M., Miklos, D.B., Hübner, U., Linden, K.G., Drewes, J.E., Croué, J.-P., 2018. Removal of trace organic chemicals in wastewater effluent by UV/H₂O₂ and UV/PDS. *Water Research*. 145, 487–497. <https://doi.org/10.1016/j.watres.2018.08.052>

Part 2

Efficient removal of estrogenic compounds in water by Mn^{III} -activated peroxymonosulfate: mechanisms and application in sewage treatment plant water



Published journal: Environmental Pollution

Accepted date: 3th July, 2021

1. Introduction

Endocrine-disrupting chemicals (EDCs) affect the normal functioning of endogenous hormones [1]. EDCs consist of various types of chemicals such as natural and synthetic hormones, plasticizers, pesticides, and flame retardants [2]. With the development of industry and the pursuit of high-quality life of humans, the EDCs-containing products have been consumed in a large amount. Over the past 10 years, EDCs as a major concern of water quality have received extensive attention [3–5]. The regularly detected amount of EDCs in surface and drinking waters are up to ng/L while higher concentrations in municipal wastewater, an important source of anthropogenic pollution release into the environment, were also reported [3,6].

To decrease the concentration of EDCs in wastewater, different processes based on thermal and photochemical degradation were reported [7–9]. Advanced oxidation processes (AOPs) are innovative technologies used to improve the degradation of the recalcitrant pollutants based on the formation of highly oxidative species [7,8]. Reactive oxygen and sulfur species (ROS and RSS) with high oxidation potentials such as hydroxyl (HO^\bullet) and sulfate ($\text{SO}_4^{\bullet-}$) radicals are generated through photochemical or electron transfer reaction [10]. Such radicals are capable of inducing hazardous pollutants degradation till complete mineralization in water. Among the different AOPs systems, transition metal-based activation of radical precursors represents a low-energy cost and efficient process [11,12]. Iron (Fe) is one of the most used metal in homogeneous and heterogeneous applications and the redox cycle between Fe(II) and Fe(III) provide a very efficient system for activation of radical precursors and abatement of organic pollutant concentration in waters [13]. However, organic complexes such as aminopolycarboxylic are regularly used to improve the iron stability toward a large range of pH values [14,15].

Recently, other metals such as manganese (Mn) has been used for different water treatment applications. Mn is a promising metal due to its multiple oxidation states (+II, +III, +IV, +VII) and high oxidative and catalytic reactivity. Most of published reports have focused on manganese dioxide-based AOPs (MnO_2 -AOPs), to remove pollutants, such as phenol and 2,4-dichlorophenol, using MnO_2 activated peroxymonosulfate (PMS) or persulfate (PS) in water

[16,17]. Huang et al. (2019) investigated the effects of properties of MnO_2 such as crystal structure, morphology, and surface Mn oxidation states on PMS activation. They showed that the catalytic activity of MnO_2 is positively correlated with the surface Mn(III) content [18].

Other studies have used Mn(III) oxides as a mean to activate oxidants (e.g. PMS and PS) and then remove organic contaminants, such as $\alpha\text{-Mn}_2\text{O}_3$ [19] and MnOOH [20]. He et al. demonstrated that nanowires MnOOH have higher activity on PMS activation for 2,4-dichlorophenol oxidation as compared with multi-branches and nanorods MnOOH [21]. Moreover, Li et al. showed that sulfate and hydroxyl radicals can be generated from manganite-activated PS under pH 11 [22]. Although the good ability of Mn^{III} -oxides for PS or PMS activation has been investigated the underlying mechanisms of activation and generation of reactive species remain elusive. In addition, most of available data on the MnOOH/PMS activation process has been obtained in ultrapure water and very little is known about the application of this process in real wastewater. Therefore, the ability of $\gamma\text{-MnOOH}$ for PMS activation under real-world conditions for wastewater treatment merits investigation.

In the present study, we investigated the degradation of three EDCs (Bisphenol A (BPA), 17 β -estradiol (E2) and 17 α -ethynylestradiol (EE2)) using $\gamma\text{-MnOOH}$ -activated PMS process. We have combined radical scavenging approaches, EPR and XPS analyses, to determine the different activation and removal mechanisms (i.e. radical and non-radical pathways). Moreover, the influence of key parameters such as the initial concentration of $\gamma\text{-MnOOH}$ and PMS, and the impact of water inorganic constituents were also evaluated. Finally, the efficiency of the degradation system was evaluated in real sewage treatment plant water, collected from the “3 rivières” urban treatment plant in Clermont-Ferrand, France.

2. Material and Methods

2.1. Chemicals and reagents

Bisphenol A (BPA, 99%), 17 β -estradiol (E2, 98%), 17 α -ethynylestradiol (EE2, 98%), potassium peroxydisulfate (PMS, purchased in the form of $\text{KHSO}_5 \cdot 0.5\text{KHSO}_4 \cdot 0.5\text{K}_2\text{SO}_4$), sodium nitrite (NaNO_2 , 97%), sodium bicarbonate (NaHCO_3 , 99.7%), and sodium chloride

(NaCl, 99%) were purchased from Sigma-Aldrich Company, France. Sodium nitrate (NaNO_3 , 99%) was bought from Fluka. Manganese (II) chloride (MnCl_2) was purchased from Riedel-de Haen. HPLC grade acetonitrile solvent (ACN) was purchased from CARLO ERBA Reagents. Sodium hydroxide (NaOH , 99.9%) and perchloric acid (HClO_4 , 72%) which were used to adjust solution pH were purchased from Sigma-Aldrich. Ethanol (96%, VWR Chemicals), *t*-Butyl alcohol (TBA), and furfuryl alcohol (FFA) from Sigma-Aldrich were employed as radical and singlet oxygen scavengers. Ultrapure water (Millipore, resistivity 18.2 $\text{M}\Omega$ cm) was used in the preparation of all solutions. All chemicals were used as received without further purification.

2.2. γ -MnOOH synthesis and characterization

Manganite (γ -MnOOH) particles were synthesized as described by Yu and co-workers [23]. The nature of γ -MnOOH was confirmed by X-ray diffraction (XRD) and Transmission Electron Microscopy- Selective Area Electron Diffraction (TEM-SAED) using an accelerating voltage of 200 kV (TEM Jeol JEM 2100 HR) (Figure S1). TEM images of the as-prepared manganite display wire-like morphology with diameters of 20–40 nm, and the SAED pattern confirmed the nature of γ -MnOOH. For XPS analysis, 0.5 g/L of solid were put in contact with 5 mM of PMS with and without BPA (200 μM). After 1 h of reaction, the solution was centrifuged and water was withdrawn and the remaining water completely removed under the N_2 stream. Then, the solid particles were collected and analyzed in a UHV chamber (pressure 10^{-7} Pa) facilitated with an XPS system (hemispherical electron energy analyzer OMICRON EA125, Germany). Data analysis, curve fitting and quantification of the Mn XPS spectra were performed using CasaXPS software. The binding energy (BE) scale was referenced to the adventitious C1s peak at 284.8 eV. High-resolution XPS spectra were processed using Shirley background subtraction. After background subtraction, the spectra were smoothed and fitted by using of Gaussian-Lorentzian peak shape (70:30). For each sample, fitting parameters (FWHM, the full width at half maximum; H, the peak height; E, the peak position center) were adjusted to minimize the value of residual standard deviation (STD).

2.3. Real water matrix

The sewage treatment plant water (STPW) was collected from the urban treatment plant named “3 rivières” in Clermont-Ferrand, France in December 2019. Prior to use, the STP water was filtered using a syringe filter (CHROMAFIL® Xtra RC-45/25) and then use for experiments. The main physico-chemical parameters relevant to this study are reported in Table S1.

2.4. Experimental procedure

PMS was added to the solution containing selected EDCs and γ -MnOOH just before the reaction starts. All reactions were performed in a brown glass bottle (125 mL) at room temperature (293 ± 2 K) and under stirring to ensure homogeneity. Unless otherwise stated, experiments were performed at $\text{pH } 6.5 \pm 0.2$. For HPLC, 2 mL of solution were withdrawn at fixed interval times, filtered using 0.20 μM PTFE filter and the reaction was immediately quenched with the addition of 20% methanol (HPLC grade, Sigma-Aldrich). Samples were kept at 277 K and analysis was performed within 4 hours. Furthermore, to identify the generated radicals, EtOH, TBA and FFA were added to the solution before PMS addition and a kinetic approach based on the second-order rate constants and pseudo-first order decay determination was used to assess the radical species involvement.

2.5. Analytical methods

BPA, E2 and EE2 quantification during reactions was performed by high performance liquid chromatography (HPLC) equipped with a diode array detector (Waters 2475, USA). The injection volume was 50 μL and a flow rate of 1 mL min^{-1} with a mobile phase consisting of a mixture of water and ACN (50/50, v/v) were used. An Agilent Eclipse XDB C18 of 250 mm \times 4.6 mm \times 5 μm column was adapted as the analytic column. Under these conditions, the detection wavelength and retention time were: for BPA (277 nm) at 5.4 min, for E2 (280 nm) at 6.2 min, for EE2 (280 nm) at 7.3 min (Figure S2). To investigate the mineralization, the total organic carbon (TOC) analysis (TOC-L CPH CN200, Shimadzu) was performed.

The pseudo-first order decay of selected pollutant (k'_p) was determined from the slope of $\ln(C/C_0)$ vs reaction time as following: $\ln \frac{C}{C_0} = k'_p \times t$. Where C_0 and C are the initial and remaining concentrations in solution and t is the reaction time.

PMS was quantified using the iodometric titration in which generated I_3^- was quantified at 348 nm using a Cary 300 Varian Spectrophotometer [24]. Calibration was performed using different PMS concentrations and data are presented in the supplementary Materials (Figure S3). Briefly, 100 μ L of sample was withdrawn at different reaction times and added to 5 mL of a solution containing KI (0.6 M) and HCO_3^- (0.06 M). The Abs of solution at 348 nm was measured after 10 min of reaction and PMS concentration (C_{PMS} , (mM)) was determined as $C_{PMS} = \frac{V_{tot}}{V_{PMS}} \times \frac{Abs_{348\text{ nm}}}{0.5}$. Where V_{PMS} and V_{tot} are the volume of sample (100 μ L) and total volume (5.1 mL), 0.5 was the slope of the linear correlation between the PMS concentration and value of Abs at 348 nm.

The Atomic absorption spectroscopy (AAS, PerkinElmer) was employed to determine the concentration of dissolved Mn^{2+} in the aqueous solution. The procedure involved the filtration of the samples through a 0.2 μ m PTFE filter and the addition of 2% nitric acid (HNO_3 , 65%, Sigma-Aldrich) before detection. Mn^{2+} standard solution for AAS (TraceCERT[®], 1000 mg L⁻¹ Mn in 2% nitric acid, Sigma-Aldrich) was used for making the calibration curve of Mn^{2+} . The detection wavelength was set at 279.48 nm.

The identification of reactive oxygen species was performed on the electron paramagnetic resonance spectroscopy (EPR, Burker) using 5,5-dimethyl-1-pyrroline N-oxide (DMPO) as the spin trapping agents. Typically, 375 μ L of sample was withdrawn and immediately mixed with 125 μ L of DMPO (100 mM), then the mixture was transferred into an EPR quartz capillary tube (0.5 mm, 100 mm) for measurement. The EPR spectrometer settings were as follows: modulation frequency, \sim 100 kHz; microwave frequency, \sim 9.87 GHz; microwave power, \sim 6.87 mW; center field, \sim 352.7 mT; sweep width, 20 mT; sweep time, 30 s; sample g-factors, 2.0; modulation amplitude, 1.0 G.

3. Results and discussion

3.1. Effect of γ -MnOOH and PMS dosage

Preliminary experiments showed that no significant degradation was observed with PMS or γ -MnOOH, while efficient removal was reached when both γ -MnOOH and PMS were used simultaneously (Figure 1). In this system, BPA was completely removed after 2 h with an initial pseudo-first order degradation rate (k'_{BPA}) of $0.058 \pm 0.001 \text{ min}^{-1}$ showing that reactive species (such as $\text{SO}_4^{\cdot-}$ and HO^{\cdot}) may be generated through the reaction between γ -MnOOH and PMS in solution. Moreover, the adsorption of BPA on γ -MnOOH was negligible ($< 3 \%$) after 3 h of reaction.

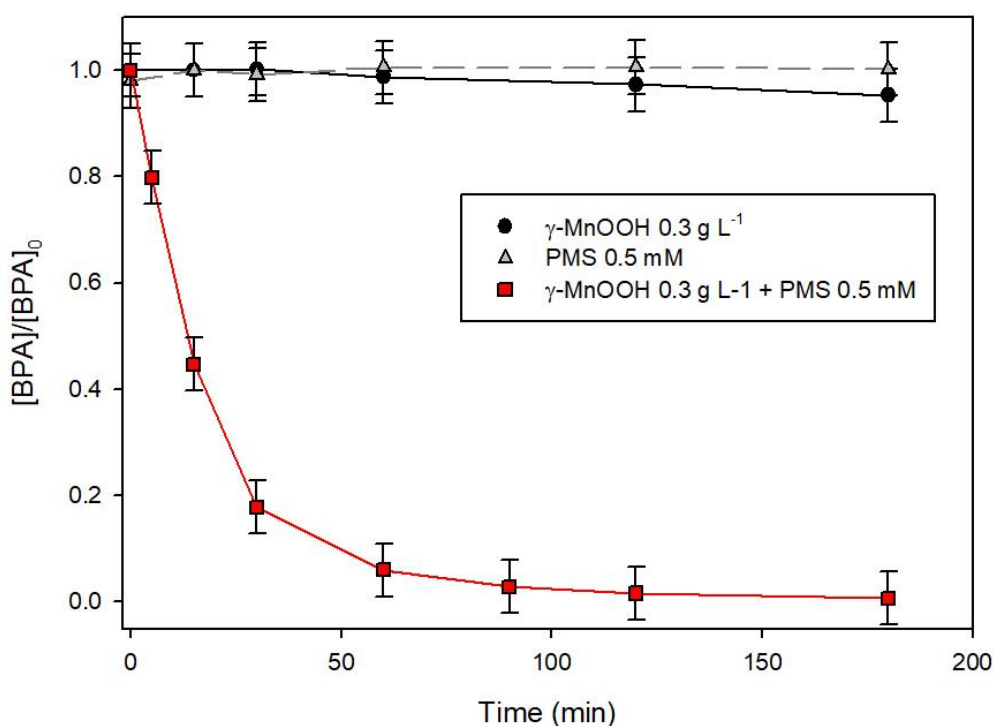


Figure 1. Degradation of BPA (25 μM) in the presence of γ -MnOOH (0.3 g L^{-1}) and PMS (0.5 mM) at pH 6.5.

When various concentrations of γ -MnOOH were used in the presence of 0.5 mM PMS (Figure 2A), a different trend can be observed. Increasing the γ -MnOOH concentration up to 0.1 g L^{-1} , faster degradation of BPA was determined and the corresponding kinetic rate constant of BPA degradation (k'_{BPA}) increased up to $0.163 \pm 0.001 \text{ min}^{-1}$. At higher γ -MnOOH concentrations, the BPA degradation decreased and almost no degradation was observed using 0.5 g L^{-1} of γ -

MnOOH. Similar trend was observed when different PMS concentrations were used in the presence of 0.1 g L⁻¹ of γ -MnOOH (Figure 2B). From 0 to 2 mM, k'_{BPA} increased almost linearly to $0.719 \pm 0.007 \text{ min}^{-1}$, while higher PMS concentrations inhibited the degradation. This behavior suggests that Mn(III)-oxide and PMS would scavenge the generated reactive species when they are used at high concentrations. This effect can be attributed to the quenching of excessive γ -MnOOH and PMS on the active species [25,26]. Thus, an optimal concentration of γ -MnOOH (0.1 g/L) and PMS (2 mM) was adopted for the followed study.

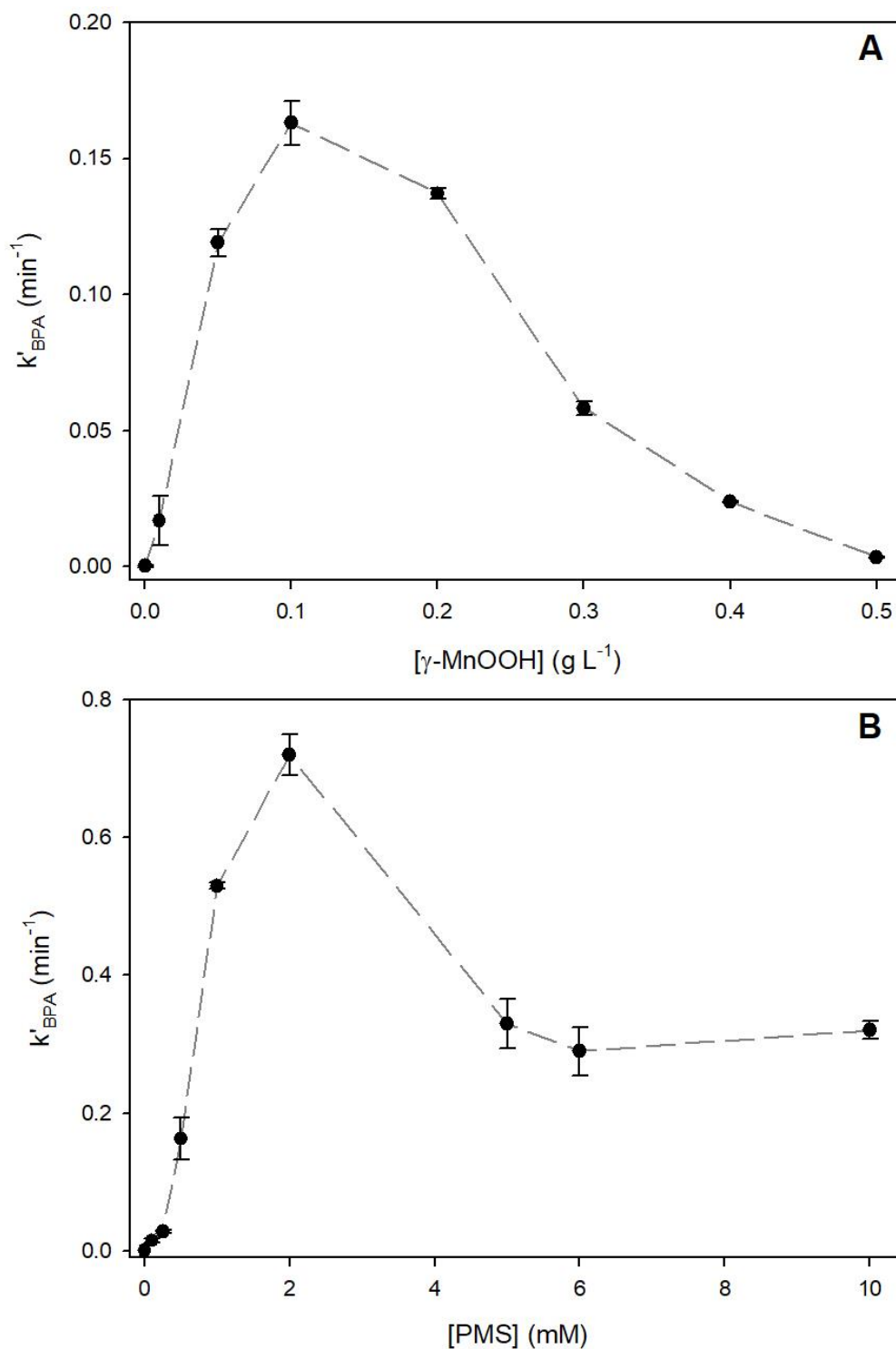


Figure 2. Pseudo-first order degradation rate of BPA using different $\gamma\text{-MnOOH}$ concentrations in the presence of 0.5 mM of PMS (A) and in the presence of $\gamma\text{-MnOOH}$ (0.1 g L^{-1}) and different PMS concentrations (B). Error bars are determined from the σ -level uncertainty of the data fit used to obtain k'_{BPA} .

3.2. Activation pathway and reactive species formation

In order to verify the generation of reactive species resulted from the activation of γ -MnOOH, the leaching of dissolved Mn^{2+} in γ -MnOOH/PMS system was measured, and the homogenous activation of PMS by Mn^{2+} was evaluated. The total amount of leached and adsorbed Mn^{2+} was determined at around 34 μ M after 30 min of reaction. However, a high amount of dissolved Mn^{2+} (100 μ M) can only remove about 20% of target compound in 1 h reaction (Figure S4). Therefore, the removal of BPA was mainly attributed to the heterogeneous activation of PMS by γ -MnOOH.

To identify the reactive species generated in the γ -MnOOH/PMS system, chemical scavenging tests and EPR experiments were conducted. Firstly, the generation of reactive oxidant species was investigated using different chemical quenchers. TBA was used as the HO^\bullet scavenger due to its higher selectivity toward HO^\bullet ($k_{TBA, HO^\bullet} = 6.0 \times 10^8 \text{ M}^{-1} \text{ s}^{-1}$) compared to $SO_4^{\bullet-}$ ($k_{TBA, SO_4^{\bullet-}} = 8.4 \times 10^5 \text{ M}^{-1} \text{ s}^{-1}$) [27]. Theoretically, the addition of 10 mM of TBA can suppress 96% of BPA degradation considering the reaction rate constants of TBA, PMS and BPA with HO^\bullet ($k_{PMS, HO^\bullet} = 1 \times 10^7 \text{ M}^{-1} \text{ s}^{-1}$ and $k_{BPA, HO^\bullet} = 8.6 \times 10^9 \text{ M}^{-1} \text{ s}^{-1}$) (Table S2) [28,29]. However, the k'_{BPA} was not inhibited when 10 mM of TBA were added to the solution, indicating that no HO^\bullet was generated in the system (Figure 3). Comparatively, using 10 mM of EtOH can efficiently quench both HO^\bullet and $SO_4^{\bullet-}$ radicals ($k_{EtOH, HO^\bullet} = 1.9 \times 10^9 \text{ M}^{-1} \text{ s}^{-1}$ and $k_{EtOH, SO_4^{\bullet-}} = 4.3 \times 10^7 \text{ M}^{-1} \text{ s}^{-1}$) [30,31]. The k'_{BPA} decreases to 40 % of the initial value (0.719 min^{-1}) showing that $SO_4^{\bullet-}$ are generated and contributed to the BPA degradation. Further increasing EtOH concentration up to 50 mM, the BPA degradation decreased to 39 %. The generation of reactive radicals were also confirmed by the EPR experiments using DMPO as the complexing agents. Figure S5 shows one clear seven-peaks signal was formed in the γ -MnOOH/PMS system. This multiplet peaks signal is recognized as the 5,5-dimethyl-2-oxo-pyrroline-1-oxyl (DMPOX) which can be generated by the overoxidizing of DMPO by reactive species such as HSO_5^- , HO^\bullet and $SO_4^{\bullet-}$ radicals. Since no HO^\bullet was generated in the reaction, and HSO_5^- has low reactivity to oxidize DMPO [32], the formation of DMPOX can be reasonably attributed to the reactivity of DMPO with $SO_4^{\bullet-}$ radicals.

Furthermore, under the adopted experimental conditions we can estimate that, considering only $\text{SO}_4^{\cdot-}$ involved during the degradation system, quenching of 78.5 and 94.8% of BPA degradation should be expected with the addition of 10 and 50 mM of EtOH (Table S2). However, this difference has not been observed in our experiments, which suggest the occurrence of other reactive species un-quenchable by the organic scavengers. Thus, one non-radical mechanism was assumed to be responsible for the degradation of the rest part of BPA. He et al. reported the generation of singlet oxygen ($^1\text{O}_2$) in the system of $\gamma\text{-MnOOH/PMS}$ [21]. To verify if $^1\text{O}_2$ was generated, the degradation of BPA was followed in the presence of 1 mM FFA as $^1\text{O}_2$ quencher ($k_{\text{FFA},^1\text{O}_2} = 1.2 \times 10^8 \text{ M}^{-1} \text{ s}^{-1}$) in addition to 50 mM of EtOH [33]. Since FFA has high reactivity with HO^{\cdot} ($k_{\text{FFA}, \text{HO}^{\cdot}} = 1.5 \times 10^{10} \text{ M}^{-1} \text{ s}^{-1}$) [34], the simultaneous addition of FFA and EtOH was planned to consume all the possible HO^{\cdot} radicals using EtOH, and then verify the inhibition of BPA degradation caused by FFA addition was only attributed to the generation of $^1\text{O}_2$. As reported in Figure 3, almost no effect was observed with the addition of FFA indicating that $^1\text{O}_2$ was not generated.

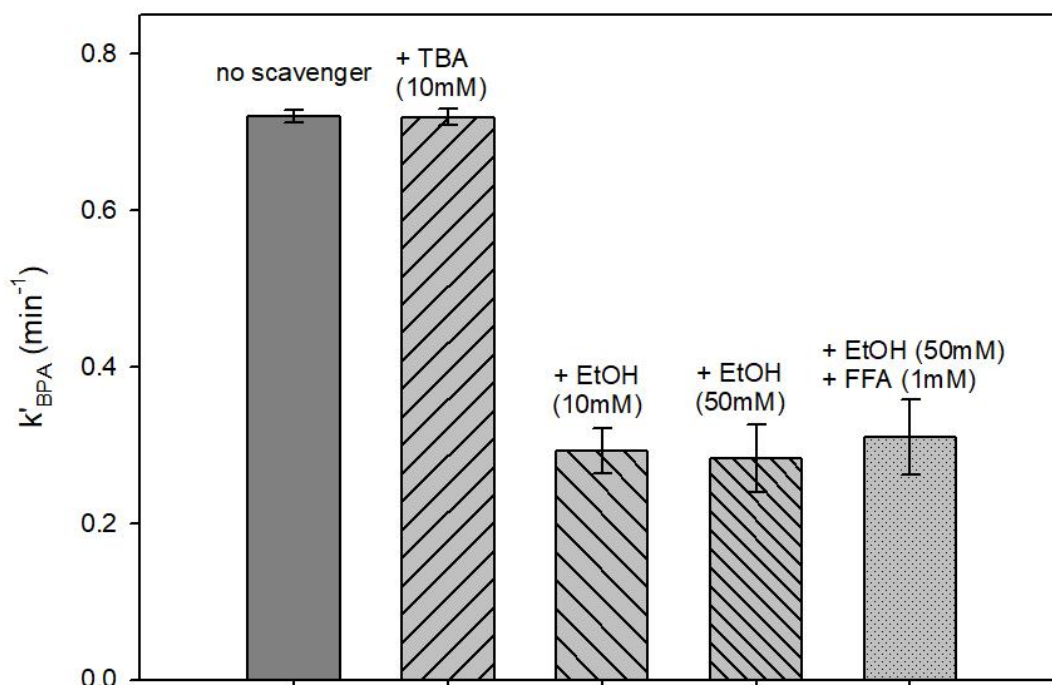


Figure 3. BPA degradation (k'_{BPA}) in the system $\gamma\text{-MnOOH } 0.1 \text{ g L}^{-1} + \text{PMS } 2 \text{ mM}$ in the absence and presence of different scavengers at pH 6.5. Error bars are determined from the σ -level uncertainty of the data fit used to obtain k'_{BPA} .

To further shed light on the non-radical mechanism in the γ -MnOOH/PMS system, more attention had been paid to the oxidation states of Mn species changing during the reaction. Since the direct oxidation of the organic compounds by Mn(IV) through electron transfer process has been widely reported [18,35], we can suppose that higher valence state Mn species (e.g. Mn^{IV}) can be formed, and thus contribute to the degradation of BPA. In order to get more insights on the redox process involving Mn species, XPS analysis of γ -MnOOH surfaces was performed during different reaction steps. The chemical oxidation state of Mn in the external layers was determined using the Mn 3s multiplet splitting method and the position and shape of the Mn 2p_{3/2} spectra (Figure 4) [36,37]. The peak position and relevant parameters from curve fitting of Mn 3s and Mn 2p_{3/2} high resolution spectra are listed in Table 1. The average oxidation state (AOS) of samples was calculated from the % of each Mn species from the fitting of Mn 2p_{3/2} spectra and from the binding energy difference of Mn 3s doublet splitting as following: $AOS = 8.956 - 1.126 \times \Delta E$ [25,26]. Using the multiplets fitting of the Mn 2p_{3/2} peaks, the percent contents of Mn(IV), Mn(III) and Mn(II) in the γ -MnOOH sample were 7%, 85% and 8%, respectively and AOS was 2.99. After reaction with PMS, the relative contents of Mn(IV), Mn(III) and Mn(II) changed and Mn(IV) percentage increased to 24.5 consistently with an increase of AOS up to 3.10. In the sample γ -MnOOH + PMS + BPA, Mn(II) percentage increased to 37% while Mn(IV) decreased to 9% with a decrease of AOS down to 2.72. AOS values were consistent with those determined from the fitting of Mn 3s multiplet splitting data (Table 1). The increase of Mn(IV) in the presence of PMS followed by a decrease when BPA was present in solution, suggests that freshly generated Mn(IV) may contribute to the degradation of BPA. Such a process, called metal-based oxidation, was previously indicated as relevant surface-mediated oxidation of organic pollutants in the presence of Mn(IV) oxides [38]. Huang et al. demonstrated the efficient oxidation of BPA by MnO₂ with different structures such as α -, β -, γ -, δ -MnO₂ with and without PMS [18,35]. Wang et al. reported the removal of BPA was due to a complex between amorphous MnO₂ and PMS [39].

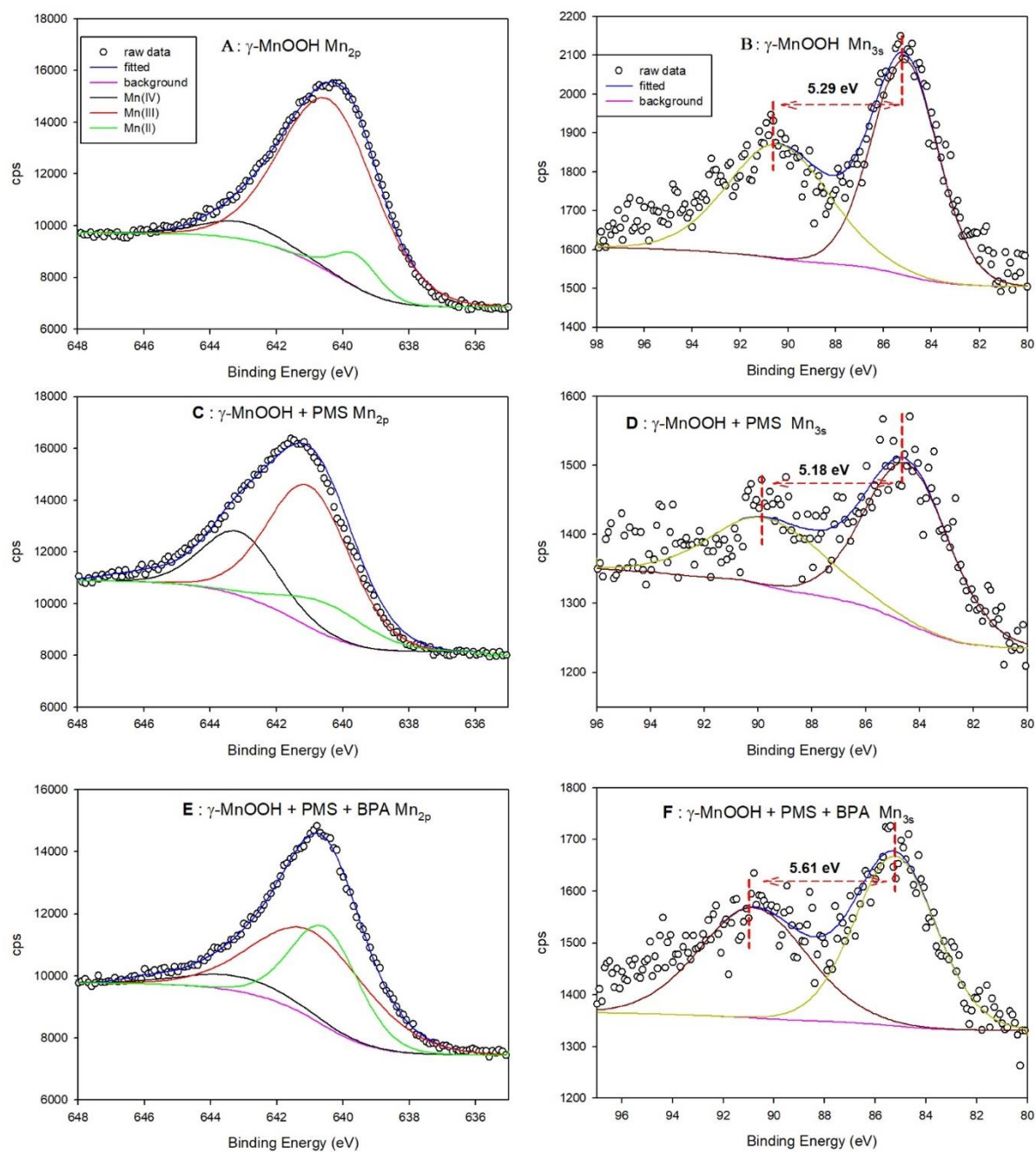
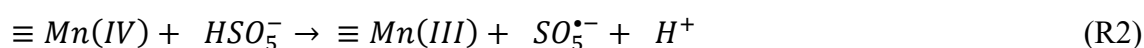
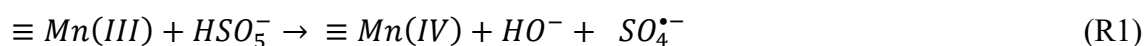


Figure 4. XPS Mn 2p and Mn 3s spectra of γ -MnOOH (A and B), γ -MnOOH + PMS (C and D) and γ -MnOOH + PMS + BPA (E and F) Initial conditions are [BPA] = 5 μ M, [γ -MnOOH] = 0.1 g L⁻¹ and [PMS] = 2 mM at pH 6.5.

Table 1. Parameters from curve fitting of Mn 3s and Mn 2p_{3/2} XPS spectra and average oxidation state.

Sample		γ -MnOOH	γ - MnOOH+PMS	γ - MnOOH+PMS+BPA	
Mn 2p	Mn(II)	BE (eV)	639.60	639.64	640.54
		%	8	14	37
	Mn(III)	BE (eV)	640.41	641.00	640.88
		%	85	61	54
	Mn(IV)	BE (eV)	643.10	642.85	643.18
		%	7	25	9
	AOS	2.99	3.10	2.72	
Mn 3s	Multiplet Splitting				
	(eV)		5.29	5.18	5.61
	AOS	3.00	3.12	2.64	

Collectively, quenching experiments and XPS analysis suggest that the first electron transfer reaction occurring between $\equiv\text{Mn(III)}$ and PMS on the surface of oxide led to the formation of $\equiv\text{Mn(IV)}$ and $\text{SO}_4^{\bullet-}$ (R1). $\text{SO}_4^{\bullet-}$ can oxidize BPA (R4) (Table S2) while Mn(IV) can further react with PMS leading to the formation of $\equiv\text{Mn(III)}$ and $\text{SO}_5^{\bullet-}$ (R2) or directly with BPA (R3). The involvement of $\text{SO}_5^{\bullet-}$ during the BPA degradation (R5) is reasonably considered less relevant due to the typical second-order rate constants between $\text{SO}_5^{\bullet-}$ and organic molecules ($10^4 - 10^6 \text{ M}^{-1} \text{ s}^{-1}$) [40].



3.3. Degradation and mineralization of BPA, E2 and EE2

Degradation and mineralization efficiencies of γ -MnOOH/PMS system were tested on BPA, E2 and EE2 mixing solution at pH 6.5. In Figure 5, the degradation of three EDCs (5 μ M each) and PMS (2 mM) consumption were followed during the reaction time in the presence of γ -MnOOH (0.1 g L⁻¹). Despite no degradation in the presence of γ -MnOOH alone and less than 10 % after 2 hours in the presence of PMS alone (Figure S6), almost complete degradation of three pollutants can be observed after 30 min. Degradation of BPA, E2 and EE2 follows a mono-exponential decay and after 30 min of reaction, \sim 100 μ M of PMS were consumed. We can then estimate an efficiency of degradation system considering the stoichiometric efficiency value (η) that is calculated as the ratio between degraded EDCs vs consumed PMS ($\eta = \frac{\Delta[EDCs]}{\Delta[PMS]}$). In the presence of 0.1 g L⁻¹ γ -MnOOH and 2 mM of PMS a value of $\eta = 15\%$ was determined at pH 6.5.

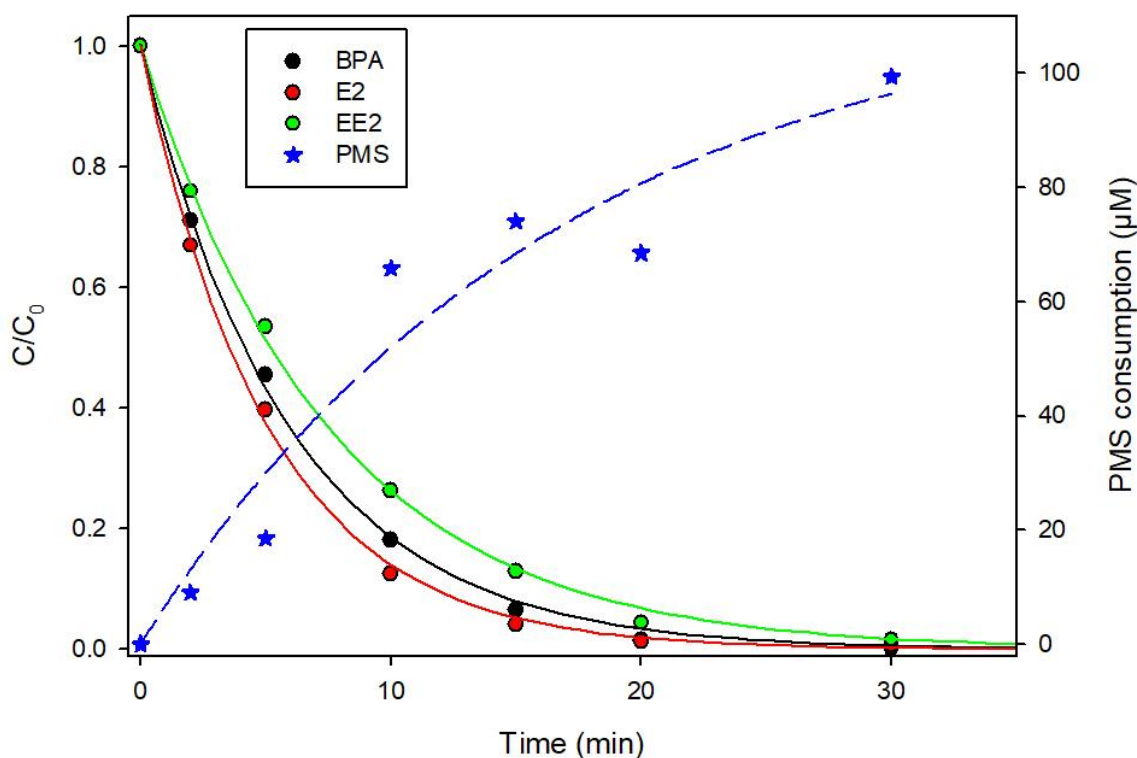


Figure 5. Degradation of BPA, E2 and EE2 in the system γ -MnOOH/PMS. The solid lines show the fit of data using a mono-exponential decay function. Blue points show the PMS consumption during the reaction. Initial conditions are [BPA] = [E2] = [EE2] = 5 μ M, [γ -MnOOH] = 0.1 g L⁻¹ and [PMS] = 2 mM at pH 6.5.

The reuse of γ -MnOOH is an important parameter with regard to the possible application in water treatment processes. For this purpose, the degradation efficiency (DE) for each EDCs after 30 min of reaction was tested for 3 cycles. For the recycling experiments, the solution containing mainly soluble products (PMS and EDCs degradation products) was completely removed from the reactor and a fresh solution containing PMS and EDCs at initial concentration was added again into the reactor containing γ -MnOOH. As shown in Figure 6, after three cycles of reuse, a reduction of EDCs degradation efficiency of about 20 % was observed indicating a good reusability of the oxidative system for EDCs removal. This effect can be explained considering the generation of $\equiv Mn(II)$ (R3) and slower formation of $\equiv Mn(III)$ through PMS reactivation (R6) [41].

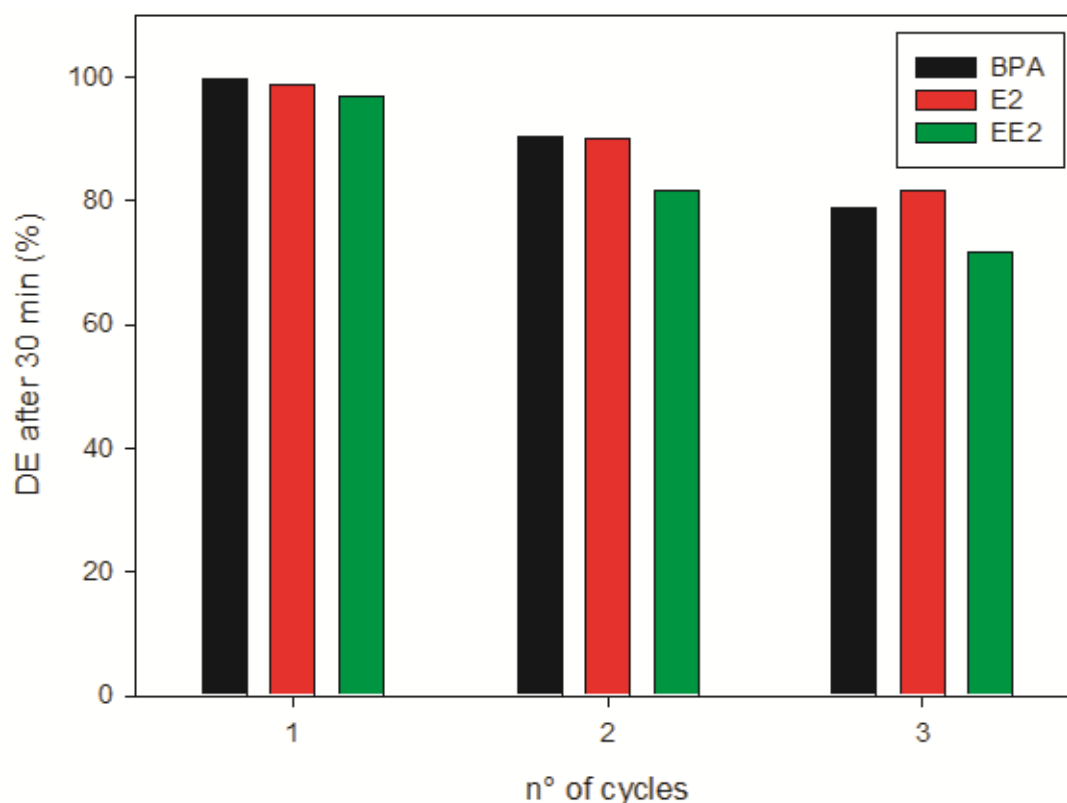
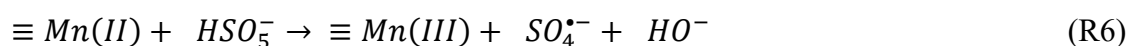


Figure 6. Reusability of γ -MnOOH over 3 cycles. Experimental conditions are: $[\gamma\text{-MnOOH}] = 0.1 \text{ g L}^{-1}$, $[\text{PMS}] = 2 \text{ mM}$, $[\text{BPA}] = [\text{E2}] = [\text{EE2}] = 5 \mu\text{M}$ and $\text{pH} = 6.5$.

3.4. Effect of inorganic ions

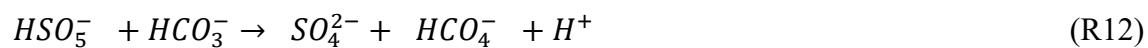
Inorganic anions are commonly detected in natural waters and they could affect the radical-mediated degradation efficiency of organic pollutants. In the γ -MnOOH / PMS system, the effect of chloride (Cl^-), bicarbonate (HCO_3^-), nitrite (NO_2^-) and nitrate (NO_3^-) anions was investigated and BPA, E2, and EE2 degradations were followed using 0.1 g L^{-1} of γ -MnOOH and 2 mM of PMS.

As illustrated in Figure 7A, increasing the concentration of Cl^- from 0 to 5 mM, the BPA, E2, and EE2 degradation rates slightly increased indicating a positive effect of Cl^- on the oxidation system. The results are in agreement with previous studies which indicated that improvement of organic pollutants degradation efficiency in the presence of Cl^- was attributed to the generation of reactive chlorine species such as Cl^\bullet and HOCl (R7 to R9) [42]. In fact, despite a different reactivity constant between Cl^\bullet and $\text{Cl}_2^{\bullet-}$ with organic compounds ($k_{\text{Cl}^\bullet} = 10^9 - 10^{10} \text{ M}^{-1} \text{ s}^{-1}$, $k_{\text{Cl}_2^{\bullet-}} = 10^7 - 10^8 \text{ M}^{-1} \text{ s}^{-1}$), their lower reactivity was partially counterbalanced by direct activation occurring in the presence of PMS leading to the formation of oxidant species such as HOCl as observed at high Cl^- concentration in absence of γ -MnOOH (R9) (Figure S7) [43].



Bicarbonate ions (HCO_3^-) are generally considered as interfering species during oxidative processes based on radical species generation due to their reactivity with radicals and generation of less oxidative species such as $\text{CO}_3^{\bullet-}$ [30,31]. However, a negligible impact on the EDCs degradation was observed with the addition of HCO_3^- (Figure 7B). Such effect can be explained considering that the inhibition effect on the sulfate radical reactivity (R10-R11) is counterbalanced by the direct activation of HCO_3^- by PMS leading to the formation of HCO_4^- as reported in Figure S7 (R12) [42].





The effect of nitrogen anions (NO_2^- and NO_3^-) on BPA, E2 and EE2 degradation were investigated, individually. As shown in Figure S8, no effect of both NO_2^- and NO_3^- on the degradation of the three EDCs was observed.

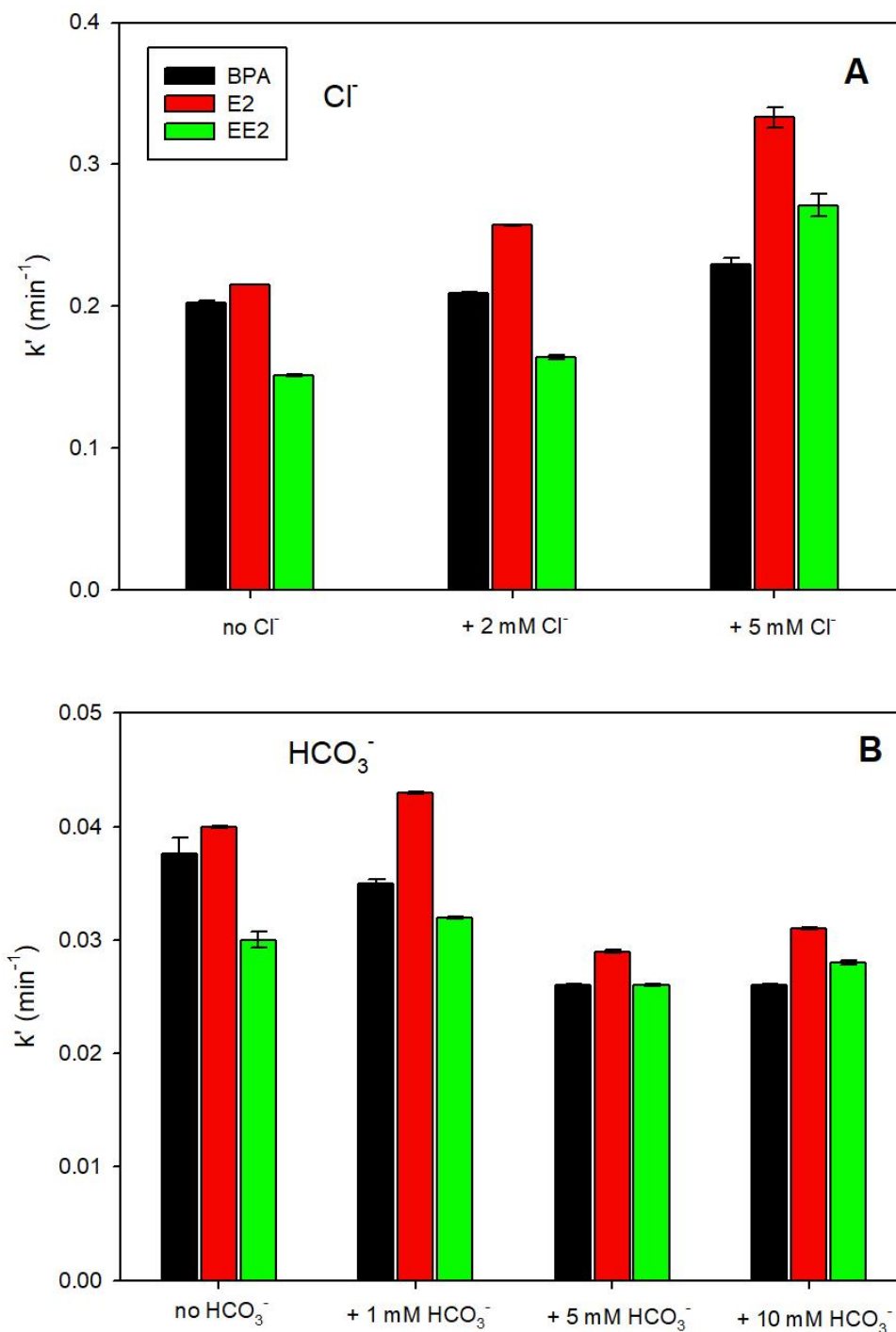


Figure 7. Effect of chloride ions (Cl^-) (A) and bicarbonate ions (HCO_3^-) (B) on the degradation of BPA, E2, and EE2 using $\gamma\text{-MnOOH/PMS}$ system. Experimental conditions are: $[\gamma\text{-MnOOH}] = 0.1 \text{ g L}^{-1}$, $[\text{PMS}] = 2 \text{ mM}$, $[\text{BPA}] = [\text{E2}] = [\text{EE2}] = 5 \mu\text{M}$, $\text{pH} = 6.5$ (for Cl^-) and $\text{pH} = 8.0$ (for HCO_3^-). Error bars are determined from the σ -level uncertainty of the data fit used to obtain k' of estrogens.

3.5. Efficiency in the real water matrix

To evaluate the efficiency of γ -MnOOH/PMS system in realistic conditions, the treatment of three EDCs in filtered sewage treatment plant water (STPW) was conducted. The initial TOC was determined to be 10.8 mgC L^{-1} (in which 2.8 mgC L^{-1} come from the addition of 3 EDCs). As expected, the removal rates and efficiencies of EDCs and TOC in STP water were slower in comparison with results in milli-Q water (Figure 8). This effect can be attributed to the organic matter and inorganic anions present in STP water, which can compete with degradation EDCs during the γ -MnOOH/PMS process. It is interesting to notice that EDCs initial degradation in STP water is lower during the first 15 min and rapidly increases to almost complete removal after 35-40 min. 18 % of TOC removal was also observed after 30 min of reaction and TOC removal continues after EDCs degradation with a rate of $0.067 \pm 0.007 \text{ mgC min}^{-1}$.

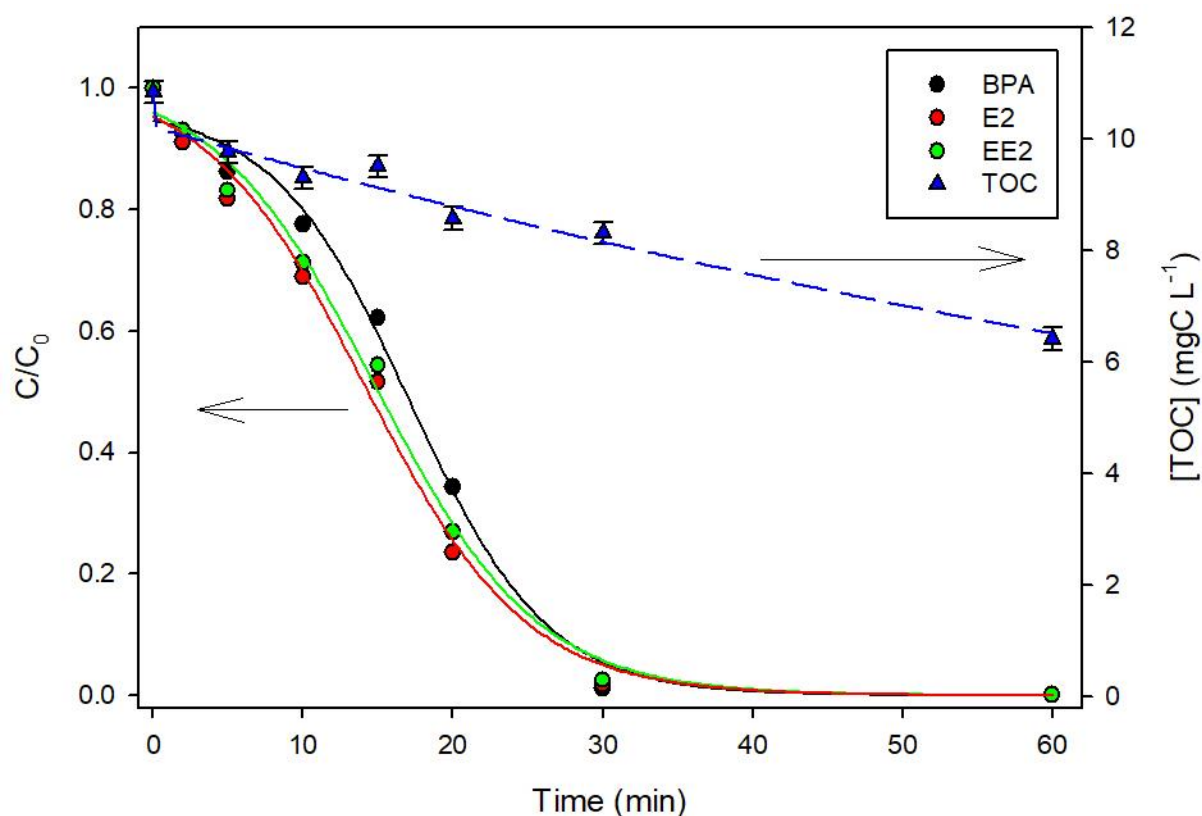


Figure 8. BPA, E2 and EE2 degradation by γ -MnOOH/PMS system in STPW and TOC removal. Experimental conditions are: $[\gamma\text{-MnOOH}] = 0.1 \text{ g L}^{-1}$, $[\text{PMS}] = 2 \text{ mM}$, $[\text{BPA}] = [\text{E2}] = [\text{EE2}] = 5 \mu\text{M}$, and $\text{pH} = 6.5$. Error bars on TOC analysis was 0.2 mgC L^{-1} .

4. Conclusion

In this work, the degradation of three estrogens: BPA, E2 and EE2 was performed using manganite (γ -MnOOH) in the presence of peroxymonosulfate ions (PMS). The rapid degradation in water was attributed to the generation of sulfate radical and the direct oxidation mediated by Mn(IV). In fact, about 60% of estrogens degradation was attributed to the generation of sulfate radical, while ~ 40 % to the direct oxidation mediated by Mn(IV). The effect of inorganic ions at environmentally relevant concentrations showed only limited inhibition effect on EDCs degradation in ultrapure water and real sewage treatment plant water, indicating that the γ -MnOOH/PMS system can be applied for real wastewater treatment. The Mn(III)/(IV) cycle represents the main reaction step leading to the formation of sulfate radical but also mediated Mn(IV) species have high oxidation ability toward the removal of selected pollutants. These results have strong implications for the development of Mn-mediated oxidation processes in wastewater remediation technologies.

Acknowledgements

We gratefully acknowledge the Chinese Scholarship Council of PR China for providing financial support for Daqing Jia. This work was supported by the Institut Universitaire de France, the Region Council of Auvergne Rhône-Alpes and the CNRS.

Reference

- [1] X. Zhou, Z. Yang, Z. Luo, H. Li, G. Chen, Endocrine disrupting chemicals in wild freshwater fishes: Species, tissues, sizes and human health risks, *Environmental Pollution*. 244 (2019) 462–468. <https://doi.org/10.1016/j.envpol.2018.10.026>.
- [2] C. Yang, G. Song, W. Lim, Effects of endocrine disrupting chemicals in pigs, *Environmental Pollution*. 263 (2020) 114505. <https://doi.org/10.1016/j.envpol.2020.114505>.
- [3] M. Adeel, X. Song, Y. Wang, D. Francis, Y. Yang, Environmental impact of estrogens on human, animal and plant life: A critical review, *Environment International*. 99 (2017) 107–119. <https://doi.org/10.1016/j.envint.2016.12.010>.

- [4] S.M. Havens, C.J. Hedman, J.D.C. Hemming, M.G. Mieritz, M.M. Shafer, J.J. Schauer, Occurrence of estrogens, androgens and progestogens and estrogenic activity in surface water runoff from beef and dairy manure amended crop fields, *Science of The Total Environment*. 710 (2020) 136247. <https://doi.org/10.1016/j.scitotenv.2019.136247>.
- [5] C.L.S. Vilela, J.P. Bassin, R.S. Peixoto, Water contamination by endocrine disruptors: Impacts, microbiological aspects and trends for environmental protection, *Environmental Pollution*. 235 (2018) 546–559. <https://doi.org/10.1016/j.envpol.2017.12.098>.
- [6] K. Lei, C.-Y. Lin, Y. Zhu, W. Chen, H.-Y. Pan, Z. Sun, A. Sweetman, Q. Zhang, M.-C. He, Estrogens in municipal wastewater and receiving waters in the Beijing-Tianjin-Hebei region, China: Occurrence and risk assessment of mixtures, *Journal of Hazardous Materials*. 389 (2020) 121891. <https://doi.org/10.1016/j.jhazmat.2019.121891>.
- [7] M. Gmurek, M. Olak-Kucharczyk, S. Ledakowicz, Photochemical decomposition of endocrine disrupting compounds – A review, *Chemical Engineering Journal*. 310 (2017) 437–456. <https://doi.org/10.1016/j.cej.2016.05.014>.
- [8] A. Gabet, H. Métivier, C. de Brauer, G. Mailhot, M. Brigante, Hydrogen peroxide and persulfate activation using UVA-UVB radiation: Degradation of estrogenic compounds and application in sewage treatment plant waters, *Journal of Hazardous Materials*. 405 (2021) 124693. <https://doi.org/10.1016/j.jhazmat.2020.124693>.
- [9] F.P. Chaves, G. Gomes, A. Della-Flora, A. Dallegrave, C. Sirtori, E.M. Saggiaro, D.M. Bila, Comparative endocrine disrupting compound removal from real wastewater by UV/Cl and UV/H₂O₂: Effect of pH, estrogenic activity, transformation products and toxicity, *Science of The Total Environment*. 746 (2020) 141041. <https://doi.org/10.1016/j.scitotenv.2020.141041>.
- [10] S. Gligorovski, R. Streckowski, S. Barbati, D. Vione, Environmental Implications of Hydroxyl Radicals (\bullet OH), *Chemical Reviews*. 115 (2015) 13051–13092. <https://doi.org/10.1021/cr500310b>.
- [11] Z. Xiong, Y. Jiang, Z. Wu, G. Yao, B. Lai, Synthesis strategies and emerging mechanisms of metal-organic frameworks for sulfate radical-based advanced oxidation process: A review, *Chemical Engineering Journal*. (2020) 127863. <https://doi.org/10.1016/j.cej.2020.127863>.

- [12] J. Wang, S. Wang, Activation of persulfate (PS) and peroxymonosulfate (PMS) and application for the degradation of emerging contaminants, *Chemical Engineering Journal*. 334 (2018) 1502–1517. <https://doi.org/10.1016/j.cej.2017.11.059>.
- [13] H. Kusic, I. Peternel, S. Ukic, N. Koprivanac, T. Bolanca, S. Papic, A.L. Bozic, Modeling of iron activated persulfate oxidation treating reactive azo dye in water matrix, *Chemical Engineering Journal*. 172 (2011) 109–121. <https://doi.org/10.1016/j.cej.2011.05.076>.
- [14] O. Abida, G. Mailhot, M. Litter, M. Bolte, Impact of iron-complex (Fe(III)–NTA) on photoinduced degradation of 4-chlorophenol in aqueous solution, *Photochemical & Photobiological Sciences*. 5 (2006) 395–402. <https://doi.org/10.1039/B518211E>.
- [15] W. Huang, M. Brigante, F. Wu, C. Mousty, K. Hanna, G. Mailhot, Assessment of the Fe(III)–EDDS Complex in Fenton-Like Processes: From the Radical Formation to the Degradation of Bisphenol A, *Environmental Science & Technology*. 47 (2013) 1952–1959. <https://doi.org/10.1021/es304502y>.
- [16] Y. Wang, S. Indrawirawan, X. Duan, H. Sun, H.M. Ang, M.O. Tadé, S. Wang, New insights into heterogeneous generation and evolution processes of sulfate radicals for phenol degradation over one-dimensional α -MnO₂ nanostructures, *Chemical Engineering Journal*. 266 (2015) 12–20. <https://doi.org/10.1016/j.cej.2014.12.066>.
- [17] Y. Zhao, Y. Zhao, R. Zhou, Y. Mao, W. Tang, H. Ren, Insights into the degradation of 2,4-dichlorophenol in aqueous solution by α -MnO₂ nanowire activated persulfate: catalytic performance and kinetic modeling, *RSC Advance*. 6 (2016) 35441–35448. <https://doi.org/10.1039/C6RA00008H>.
- [18] J. Huang, Y. Dai, K. Singewald, C.-C. Liu, S. Saxena, H. Zhang, Effects of MnO₂ of different structures on activation of peroxymonosulfate for bisphenol A degradation under acidic conditions, *Chemical Engineering Journal*. 370 (2019) 906–915. <https://doi.org/10.1016/j.cej.2019.03.238>.
- [19] E. Saputra, S. Muhammad, H. Sun, H.-M. Ang, M.O. Tadé, S. Wang, Shape-controlled activation of peroxymonosulfate by single crystal α -Mn₂O₃ for catalytic phenol degradation in

aqueous solution, *Applied Catalysis B: Environmental*. 154–155 (2014) 246–251. <https://doi.org/10.1016/j.apcatb.2014.02.026>.

[20] X. Xu, Y. Zhang, S. Zhou, R. Huang, S. Huang, H. Kuang, X. Zeng, S. Zhao, Activation of persulfate by MnOOH: Degradation of organic compounds by nonradical mechanism, *Chemosphere*. 272 (2021) 129629. <https://doi.org/10.1016/j.chemosphere.2021.129629>.

[21] D. He, Y. Li, C. Lyu, L. Song, W. Feng, S. Zhang, New insights into MnOOH/peroxymonosulfate system for catalytic oxidation of 2,4-dichlorophenol: Morphology dependence and mechanisms, *Chemosphere*. 255 (2020) 126961. <https://doi.org/10.1016/j.chemosphere.2020.126961>.

[22] Y. Li, L.-D. Liu, L. Liu, Y. Liu, H.-W. Zhang, X. Han, Efficient oxidation of phenol by persulfate using manganite as a catalyst, *Journal of Molecular Catalysis A: Chemical*. 411 (2016) 264–271. <https://doi.org/10.1016/j.molcata.2015.10.036>.

[23] C. Yu, J.-F. Boily, A. Shchukarev, H. Drake, Z. Song, K.J. Hogmalm, M.E. Åström, A cryogenic XPS study of Ce fixation on nanosized manganite and vernadite: Interfacial reactions and effects of fulvic acid complexation, *Chemical Geology*. 483 (2018) 304–311. <https://doi.org/10.1016/j.chemgeo.2018.02.033>.

[24] S. Waclawek, K. Grübel, M. Cernik, Simple spectrophotometric determination of monopersulfate, *Spectrochimica Acta Part A Molecular and Biomolecular Spectroscopy*. 149 (2015). <https://doi.org/10.1016/j.saa.2015.05.029>.

[25] N. Wang, D. Jia, Y. Jin, S.-P. Sun, Q. Ke, Enhanced Fenton-like degradation of TCE in sand suspensions with magnetite by NTA/EDTA at circumneutral pH, *Environmental Science and Pollution Research*. 24 (2017) 17598–17605. <https://doi.org/10.1007/s11356-017-9387-5>.

[26] H. Zhang, X. Wang, Y. Li, K. Zuo, C. Lyu, A novel MnOOH coated nylon membrane for efficient removal of 2,4-dichlorophenol through peroxymonosulfate activation, *Journal of Hazardous Materials*. 414 (2021) 125526. <https://doi.org/10.1016/j.jhazmat.2021.125526>.

[27] Y. Yuan, T. Luo, J. Xu, J. Li, F. Wu, M. Brigante, G. Mailhot, Enhanced oxidation of aniline using Fe(III)-S(IV) system: Role of different oxysulfur radicals, *Chemical Engineering Journal*. 362 (2019) 183–189. <https://doi.org/10.1016/j.cej.2019.01.010>.

- [28] P. Maruthamuthu, P. Neta, Radiolytic chain decomposition of peroxomonophosphoric and peroxomonosulfuric acids, *Journal of Physical Chemistry*. 81 (1977) 937–940.
- [29] W. Huang, A. Bianco, M. Brigante, G. Mailhot, UVA-UVB activation of hydrogen peroxide and persulfate for advanced oxidation processes: Efficiency, mechanism and effect of various water constituents, *Journal of Hazardous Materials*. 347 (2018) 279–287.
- [30] G.V. Buxton, C.L. Greenstock, W.P. Helman, A.B. Ross, Critical review of rate constants for reactions of hydrated electrons, hydrogen atoms and hydroxyl radicals ($\cdot\text{OH}/\cdot\text{O}^-$ in aqueous solution, *Journal of Physical and Chemical Reference Data*. 17 (1988) 513–886.
- [31] C.L. Clifton, R.E. Huie, Rate constants for hydrogen abstraction reactions of the sulfate radical, SO_4^- . Alcohols, *International Journal of Chemical Kinetics*. 21 (1989) 677–687. <https://doi.org/10.1002/kin.550210807>.
- [32] X. Yang, X. Wang, Y. Li, Z. Wu, W.D. Wu, X.D. Chen, J. Sun, S.-P. Sun, Z. Wang, A Bimetallic Fe–Mn Oxide-Activated Oxone for In Situ Chemical Oxidation (ISCO) of Trichloroethylene in Groundwater: Efficiency, Sustained Activity, and Mechanism Investigation, *Environmental Science and Technology*. 54 (2020) 3714–3724. <https://doi.org/10.1021/acs.est.0c00151>.
- [33] W.R. Haag, J. Hoigne', E. Gassman, A. Braun, Singlet oxygen in surface waters — Part I: Furfuryl alcohol as a trapping agent, *Chemosphere*. 13 (1984) 631–640. [https://doi.org/10.1016/0045-6535\(84\)90199-1](https://doi.org/10.1016/0045-6535(84)90199-1).
- [34] Y. Yang, G. Banerjee, G.W. Brudvig, J.-H. Kim, J.J. Pignatello, Oxidation of Organic Compounds in Water by Unactivated Peroxymonosulfate, *Environmental Science and Technology*. 52 (2018) 5911–5919. <https://doi.org/10.1021/acs.est.8b00735>.
- [35] J. Huang, S. Zhong, Y. Dai, C.-C. Liu, H. Zhang, Effect of MnO_2 Phase Structure on the Oxidative Reactivity toward Bisphenol A Degradation, *Environmental Science and Technology*. 52 (2018) 11309–11318. <https://doi.org/10.1021/acs.est.8b03383>.
- [36] S. Ardizzone, C.L. Bianchi, D. Tirelli, Mn_3O_4 and $\gamma\text{-MnOOH}$ powders, preparation, phase composition and XPS characterisation, *Colloids and Surfaces A: Physicochemical and Engineering Aspects*. 134 (1998) 305–312. [https://doi.org/10.1016/S0927-7757\(97\)00219-7](https://doi.org/10.1016/S0927-7757(97)00219-7).

- [37] E.S. Ilton, J.E. Post, P.J. Heaney, F.T. Ling, S.N. Kerisit, XPS determination of Mn oxidation states in Mn (hydr)oxides, *Applied Surface Science* (1985). 366 (2016) 475–485. <https://doi.org/10.1016/j.apsusc.2015.12.159>.
- [38] M. Kamagate, M. Pasturel, M. Brigante, K. Hanna, Mineralization Enhancement of Pharmaceutical Contaminants by Radical-Based Oxidation Promoted by Oxide-Bound Metal Ions, *Environmental Science and Technology*. 54 (2020) 476–485. <https://doi.org/10.1021/acs.est.9b04542>.
- [39] L. Wang, J. Jiang, S.-Y. Pang, Y. Zhou, J. Li, S. Sun, Y. Gao, C. Jiang, Oxidation of bisphenol A by nonradical activation of peroxymonosulfate in the presence of amorphous manganese dioxide, *Chemical Engineering Journal*. 352 (2018) 1004–1013. <https://doi.org/10.1016/j.cej.2018.07.103>.
- [40] R.E. Huie, P. Neta, One-electron redox reactions in aqueous solutions of sulfite with hydroquinone and other hydroxyphenols, *The Journal of Physical Chemistry*. 89 (1985) 3918–3921. <https://doi.org/10.1021/j100264a032>.
- [41] Y. Gao, Y. Zhou, S.-Y. Pang, J. Jiang, Y.-M. Shen, Y. Song, J.-B. Duan, Q. Guo, Enhanced peroxymonosulfate activation via complexed Mn(II): A novel non-radical oxidation mechanism involving manganese intermediates, *Water Research*. 193 (2021) 116856. <https://doi.org/10.1016/j.watres.2021.116856>.
- [42] J. Wang, S. Wang, Effect of inorganic anions on the performance of advanced oxidation processes for degradation of organic contaminants, *Chemical Engineering Journal*. 411 (2021) 128392. <https://doi.org/10.1016/j.cej.2020.128392>.
- [43] G. Lente, J. Kalmár, Z. Baranyai, A. Kun, I. Kék, D. Bajusz, M. Takács, L. Veres, I. Fábíán, One- Versus Two-Electron Oxidation with Peroxomonosulfate Ion: Reactions with Iron(II), Vanadium(IV), Halide Ions, and Photoreaction with Cerium(III), *Inorganic Chemistry*. 48 (2009) 1763–1773. <https://doi.org/10.1021/ic801569k>.

Supplementary Material**Table S1.** Characteristics of the sewage treatment plant water (STPW).

Parameters	Values
pH	8.5
TOC*	8.2 mgC L ⁻¹
IC*	30.35 mgC L ⁻¹
Cl ⁻	0.77 mM
NO ₃ ⁻	0.41 mM
SO ₄ ²⁻	0.29 mM
PO ₄ ³⁻	0.09 mM

*TOC: Total organic carbon; *IC: inorganic carbon.

Table S2. Radical reactivity (%) of each chemical species determined from the second order rate constants from literature [1-3] and initial concentrations.

Radical species	Concentrations	Second order rate constants (M ⁻¹ s ⁻¹)	Calculated pseudo-first order constant (s ⁻¹)	Radical reactivity (%)
SO₄^{•-}	PMS (2 mM)	$k_{PMS,SO_4^{•-}} < 1 \times 10^5$	200	< 0.1
	TBA (10 mM)	$k_{TBA,SO_4^{•-}} = 8.4 \times 10^5$	8.4×10^3	6.6
	BPA (25 μM)	$k_{BPA,SO_4^{•-}} = 4.7 \times 10^9$	1.18×10^5	93
SO₄^{•-}	PMS (2 mM)	$k_{PMS,SO_4^{•-}} < 1 \times 10^5$	200	< 0.1
	EtOH (10 mM)	$k_{EtOH,SO_4^{•-}} = 4.3 \times 10^7$	4.3×10^5	78.5
	BPA (25 μM)	$k_{BPA,SO_4^{•-}} = 4.7 \times 10^9$	1.18×10^5	21.5
SO₄^{•-}	PMS (2 mM)	$k_{PMS,SO_4^{•-}} < 1 \times 10^5$	200	< 0.1
	EtOH (50 mM)	$k_{EtOH,SO_4^{•-}} = 4.3 \times 10^7$	2.15×10^6	94.8
	BPA (25 μM)	$k_{BPA,SO_4^{•-}} = 4.7 \times 10^9$	1.18×10^5	5.2
HO[•]	PMS (2 mM)	$k_{PMS,HO^{\bullet}} = 1.7 \times 10^7$	3.4×10^4	0.5
	TBA (10 mM)	$k_{TBA,HO^{\bullet}} = 6.0 \times 10^8$	6.0×10^6	96
	BPA (25 μM)	$k_{BPA,HO^{\bullet}} = 8.6 \times 10^9$	2.15×10^5	3.4
HO[•]	PMS (2 mM)	$k_{PMS,HO^{\bullet}} = 1.7 \times 10^7$	3.4×10^4	< 0.1
	EtOH (10 mM)	$k_{EtOH,HO^{\bullet}} = 1.9 \times 10^9$	1.9×10^7	98.7
	BPA (25 μM)	$k_{BPA,HO^{\bullet}} = 8.6 \times 10^9$	2.15×10^5	1.1

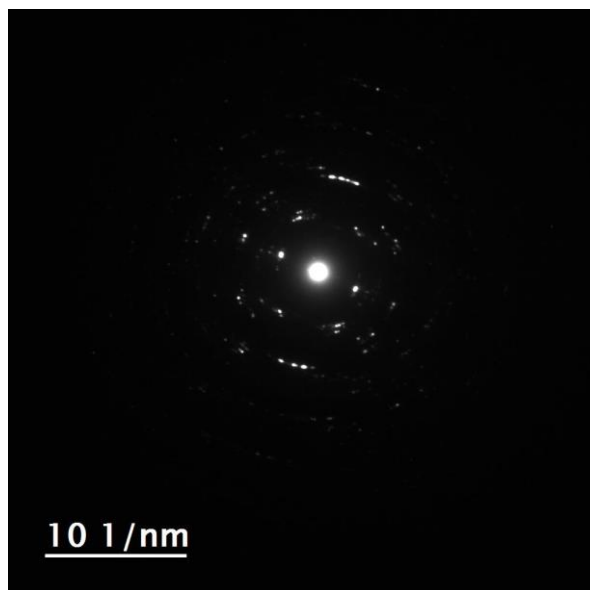
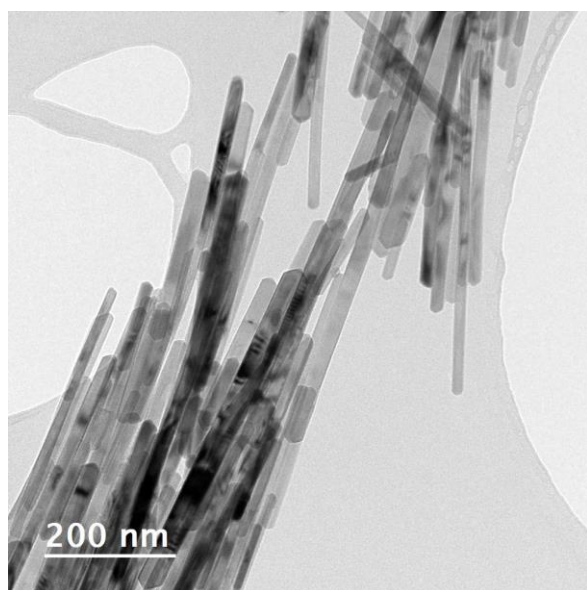
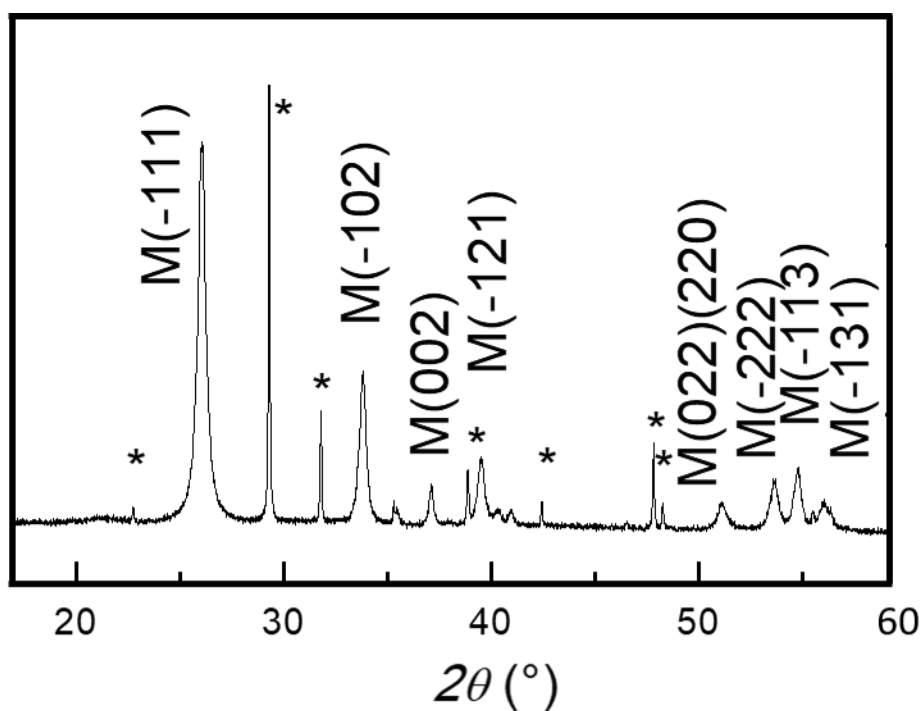


Figure S1. XRD patterns of $\gamma\text{-MnOOH}$. $\gamma\text{-MnOOH}$ indexed with the manganite structure (* indicates an XRD contribution from the stored salt NaNO_3 of manganite suspension). For clarity, only the main Bragg peaks are indexed. TEM image of the as-synthesized manganite (MnOOH) nanowires. SAED pattern. Structure of $\gamma\text{-MnOOH}$ confirmed by the electronic diffraction diagrams. Interreticular distances: 3,472 Å (111); 2,466 Å (002) ; 2,244 Å (121).

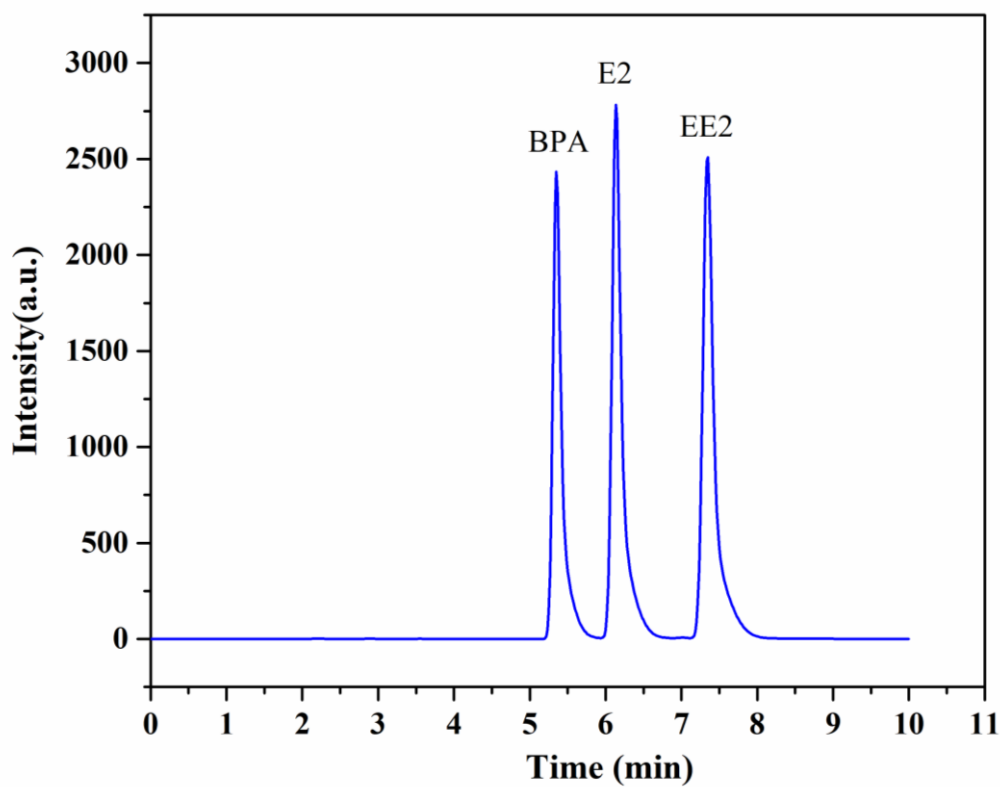


Figure S2. HPLC-fluorescence chromatography of 5 μ M BPA, E2 and EE2.

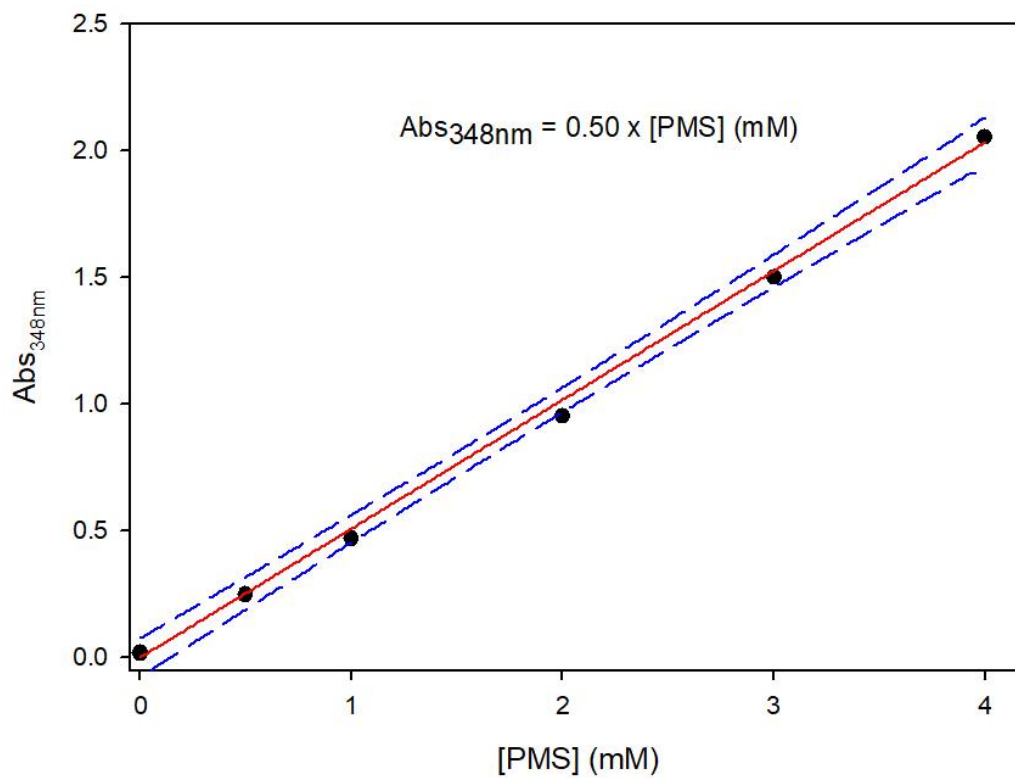


Figure S3. Calibration curve of PMS quantification using iodometric titration.

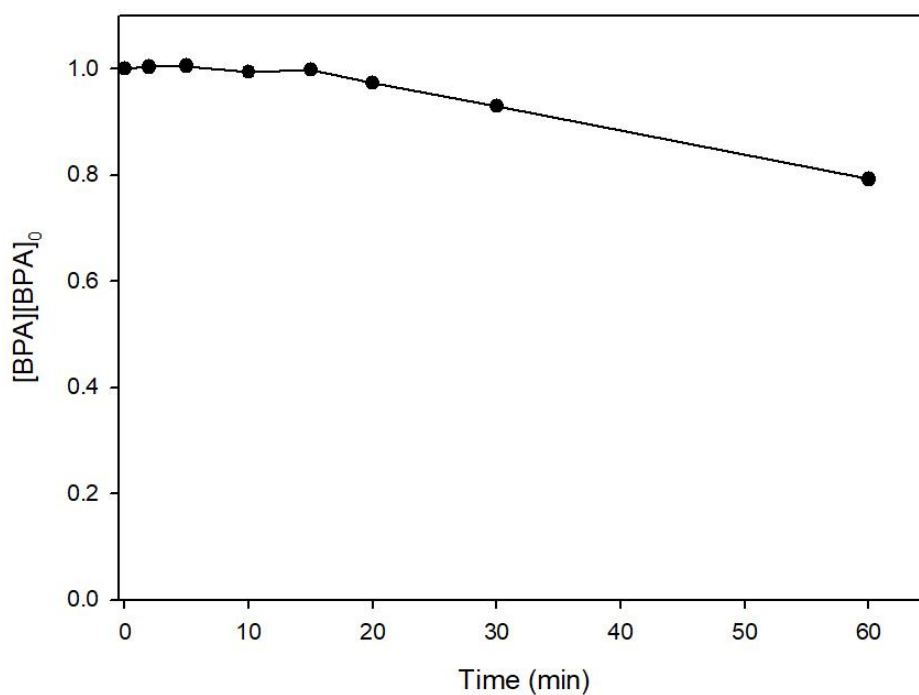


Figure S4. 25 μM BPA degradation in the presence of Mn^{2+} (100 μM) and PMS (2 mM) at pH 6.5.

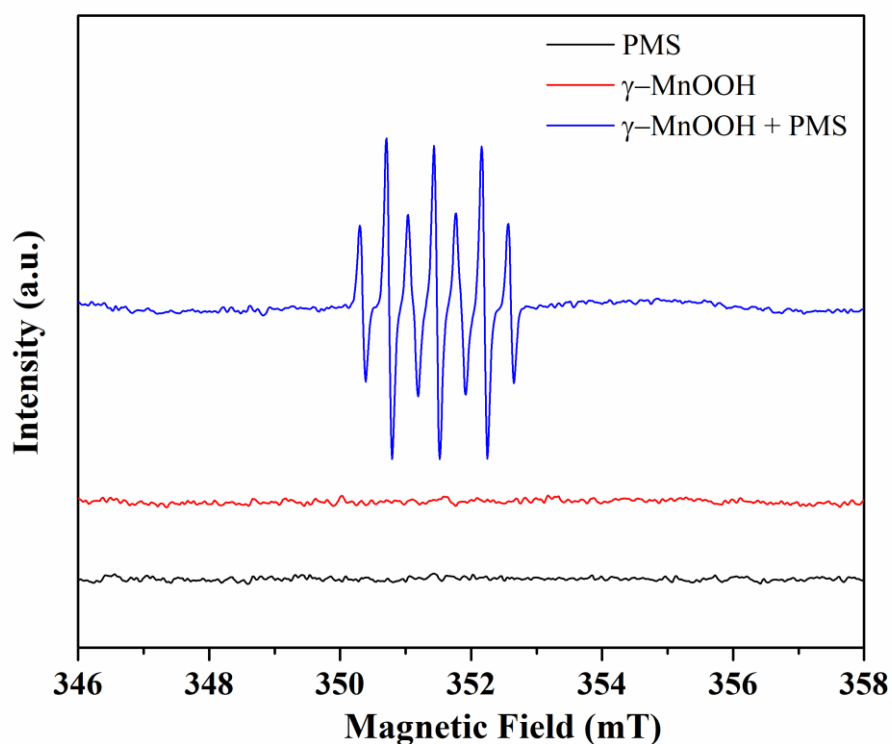


Figure S5. ERP spectra of different systems in the presence of DMPO. Experimental conditions: $[\gamma\text{-MnOOH}]_0 = 0.1 \text{ g L}^{-1}$, $[\text{PMS}]_0 = 2 \text{ mM}$, $[\text{DMPO}]_0 = 25 \text{ mM}$.

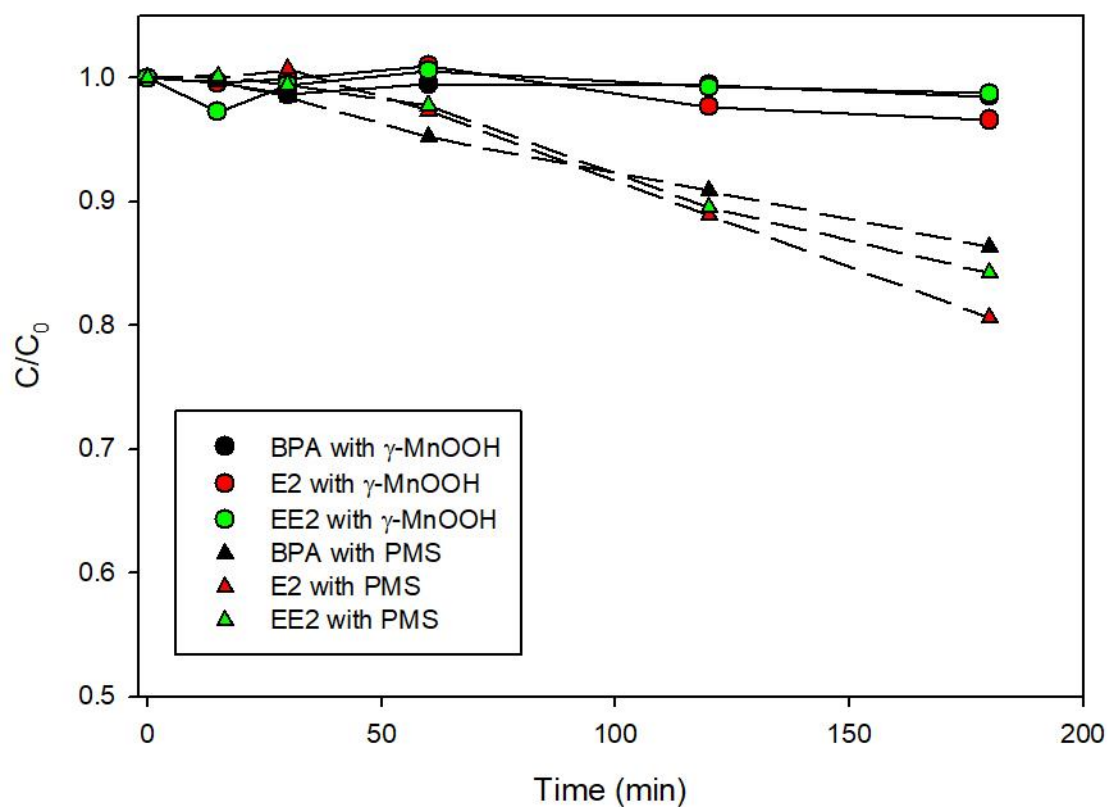


Figure S6. BPA, E2, and EE2 (5 μ M) degradation in the presence of 0.1 g/L γ -MnOOH and 2 mM PMS at pH 6.5.

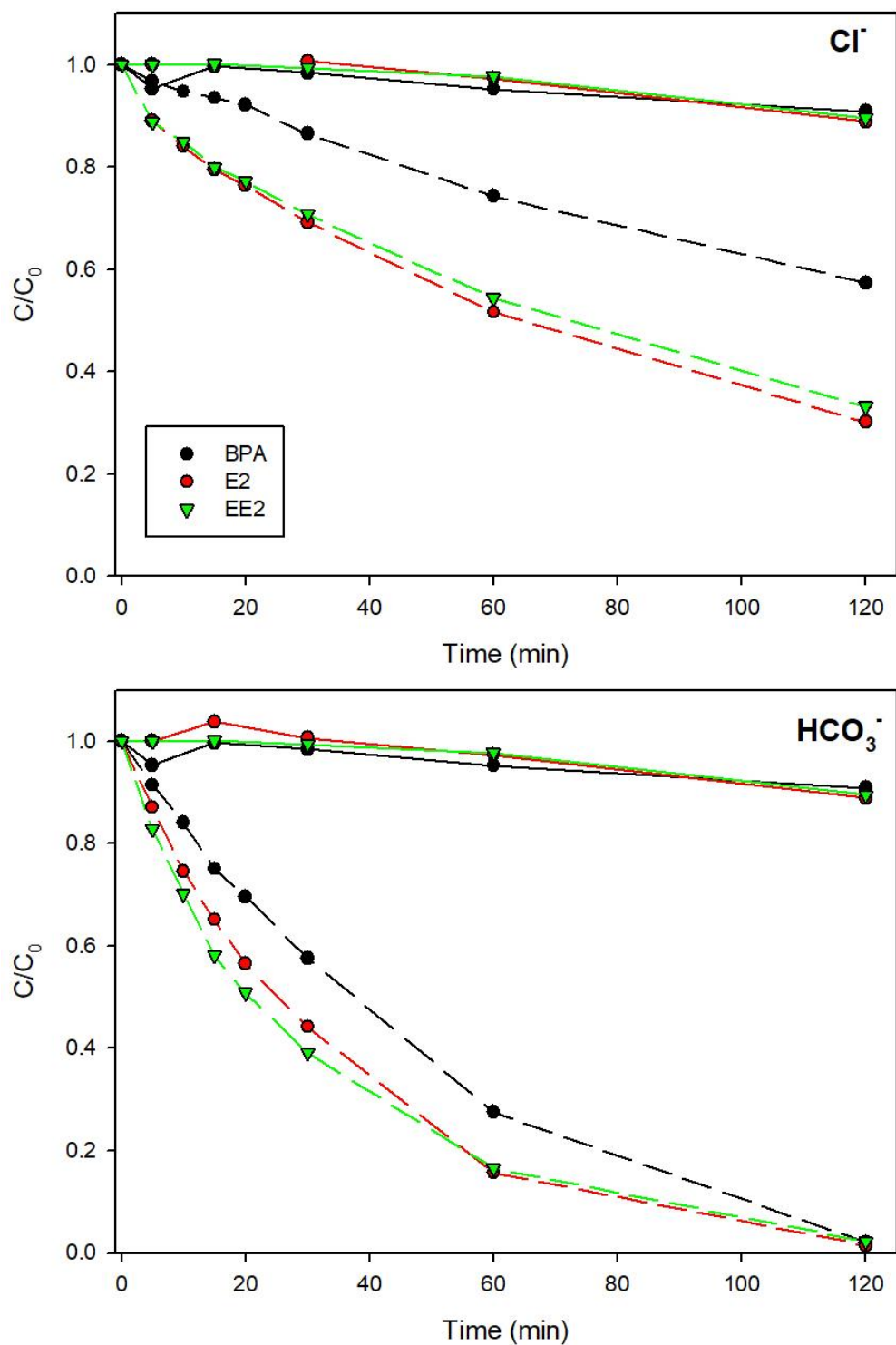


Figure S7. BPA, E2, and EE2 degradation in the presence of PMS without (solid line) and with (dashed lines) and Cl⁻ or HCO₃⁻. Experimental conditions are: [PMS] = 2mM, [BPA] = [E2] = [EE2] = 5 μM, [NaCl] = 2 mM, [NaHCO₃] = 5 mM and pH = 6.5.

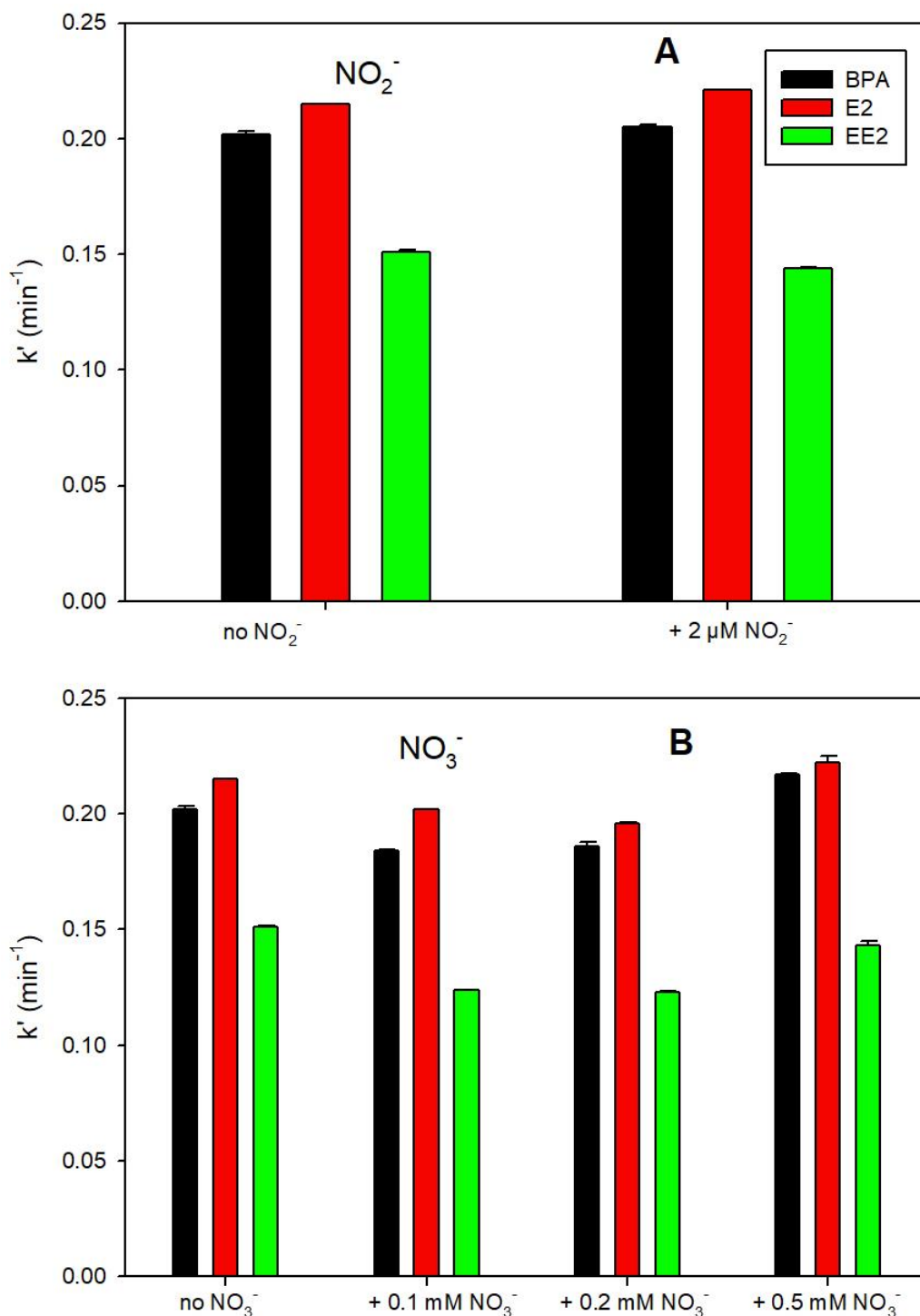


Figure S8. Effect of NO_2^- (A) and NO_3^- (B) on the degradation of BPA, E2, and EE2 using γ -MnOOH/PMS system. Experimental conditions are: $[\gamma\text{-MnOOH}] = 0.1 \text{ g L}^{-1}$, $[\text{PMS}] = 2 \text{ mM}$, $[\text{BPA}] = [\text{E2}] = [\text{EE2}] = 5 \mu\text{M}$, $\text{pH} = 6.5$. Error bars are determined from the σ -level uncertainty of the data fit used to obtain k' of estrogens.

Reference

- [1] G.V. Buxton, C.L. Greenstock, W.P. Helman, A.B. Ross, Critical review of rate constants for reactions of hydrated electrons, hydrogen atoms and hydroxyl radicals ($\cdot\text{OH}/\cdot\text{O}^-$) in aqueous solution, *Journal of Physical and Chemical Reference Data*. 17 (1988) 513–886.
- [2] C.L. Clifton, R.E. Huie, Rate constants for hydrogen abstraction reactions of the sulfate radical, SO_4^- . Alcohols, *International Journal of Chemical Kinetics*. 21 (1989) 677–687. <https://doi.org/10.1002/kin.550210807>.
- [3] W. Huang, A. Bianco, M. Brigante, G. Mailhot, UVA-UVB activation of hydrogen peroxide and persulfate for advanced oxidation processes: Efficiency, mechanism and effect of various water constituents, *Journal of Hazardous Materials*. 347 (2018) 279–287.

Chapter V

General conclusion and outlook

During this PhD, we have investigated the ability of various manganese oxides used to degrade the organic pollutants in water. The activation mechanism of radical precursors (such as H_2O_2 , PDS, and PMS) by Mn(III/IV) oxides was investigated. Different influence factors (such as solution pH, catalysts and oxidants dosages, presence of inorganic anions) on the oxidative and catalytic activity of Mn(III/IV) oxides were studied. Moreover, the application of PDS or PMS activated by Mn(III) oxides system in the sewage treatment plant (STP) water was also evaluated.

In the first part of this dissertation, the impacts of environmental levels of hydrogen peroxide and oxyanions on the redox activity of MnO_2 particles were investigated. We have notably demonstrated that environmental levels of hydrogen peroxide can induce reductive dissolution of MnO_2 into Mn(II), thereby affecting the surface reactivity of MnO_2 . As the H_2O_2 decomposition is a fast process, the generated dissolved Mn(II) binds to MnO_2 surfaces, altering further interactions with co-existing organic compounds. This may result from competition of organic compound and Mn(II) to interact with reactive surface sites and/or aqueous complexation with Mn(II). The presence of silicate or phosphate at concentrations comparable to those encountered in natural waters further decreased the reactivity of MnO_2 in presence of H_2O_2 . Birnessite-bound Mn(II) adsorbed more effectively anionic ligands such as phosphate or silicate and thus reducing interactions with BPA at a range of environmentally relevant pH values. These findings suggest that naturally occurring anions and H_2O_2 may have synergetic effects on the reactivity of nanostructured birnessite-type manganese oxide. As manganese oxides can break down high molecular weight humic substances into lower molecular weight organic molecules and/or stabilize dissolved organic carbon, these findings call for in-depth consideration of the impacts of environmental levels of H_2O_2 and co-existing anions on the global carbon cycle. Furthermore, the widespread presence of H_2O_2 in surface and ground water

systems and associated impacts on the redox-active minerals should be considered in contaminant fate and transport assessment.

In the second part of this dissertation, the removal of caffeine (CAF) in water using PDS or PMS in the presence of Mn_2O_3 was investigated. Mn_2O_3 exhibited higher activation capability for PDS and PMS compared with H_2O_2 and HSO_3^- . Moreover, the degradation of CAF in the Mn_2O_3 -activated PDS or PMS system was highly influenced by the initial solution pH. PDS was efficiently activated by Mn_2O_3 under acidic pH, while under neutral or alkaline conditions, environmentally relevant pH values, higher degradation was observed using PMS. Chemical quenching and EPR experiments demonstrated that HO^\bullet and $\text{SO}_4^{\bullet-}$ were the main radicals generated in the system with PMS. In addition, a non-radical mechanism could contribute to the degradation of CAF in the Mn_2O_3 /PDS system. The degradation efficiency was tested in the real STP water, and despite the inhibition of CAF degradation was observed due to the water constituents (mainly inorganic and organic carbon), the central role of Mn_2O_3 activation for highly reactive species formation was demonstrated in particular when PMS was used (about 80 % of CAF degradation was obtained in STP water after 20 hours). Comparison of obtained results in pure and real STP waters indicates that a lower inhibition effect (20 %) was obtained using PMS compared to the PDS system. Given the ability of Mn_2O_3 to activate PDS and PMS, the manganese-based oxidation processes (Mn-AOPs) reactions can be considered as a promising treatment technology for the removal of organic pollutants in water.

In the third part of this dissertation, the degradation of three estrogens: BPA, E2 and EE2 was performed using manganite ($\gamma\text{-MnOOH}$) in the presence of peroxymonosulfate ions (PMS). The rapid degradation in water was attributed to the generation of sulfate radical and the direct oxidation mediated by Mn(IV). In fact, about 60% of estrogens degradation was attributed to the generation of sulfate radical, while ~ 40 % to the direct oxidation mediated by Mn(IV). The effect of inorganic ions at environmentally relevant concentrations showed only limited inhibition effect on EDCs degradation in ultrapure water and real sewage treatment plant water, indicating that the $\gamma\text{-MnOOH}$ /PMS system can be applied for real wastewater treatment. The Mn(III)/(IV) cycle represents the main reaction step leading to the formation of sulfate radical

but also mediated Mn(IV) species which have high oxidation ability toward the removal of selected pollutants. These results have strong implications for the development of Mn-mediated oxidation processes in wastewater remediation technologies.

Given the fruitful results, some future outlooks are proposed.

(1) Introducing the ultraviolet light (UV) into the homogeneous Mn-mediated AOPs. For example, Mn(II) can activate radical precursors to generate radicals and high-valent Mn species such as Mn(V). The presence of UV light can assist the recycle of Mn from Mn(V) to Mn(II), which resulting in the improvement of degradation efficiency of organic pollutants.

(2) Synthesizing the Mn containing-composites. The synthesis of bimetallic Fe-Mn oxides has been reported. However, the activation mechanism of radical precursors by Fe-Mn oxides was not clear. Moreover, in addition to the synthesizing of Fe-Mn oxides, there are many other transition metals (such as Co, Cu) that can be used to produce composites with Mn. Furthermore, the synthesis of Mn containing photocatalytic materials also can be one good option for the degradation of organic pollutants in water.

(3) Introducing chelators into homogeneous and heterogeneous Mn-mediated AOPs. Mn(III) plays an important role in the oxidative and catalytic reactivity of MnO₂. However, the stability of Mn(III) in solution is weak. The presence of chelators can complex Mn(III) species leading to the increase of pollutant degradation efficiency.

(4) The application of Mn-mediated AOPs is not restrict to the removal of organic pollutants in wastewater. The system can be used for the removal of recalcitrant contaminants in groundwater and soil as well. Moreover, the combining of Mn-mediated AOPs with other water treatment technologies (such as membrane technology) will provide new solutions for the elimination of pollutants in sewage and remediation of groundwater and soil.